Stellingen behorende bij het proefschrift Propositions with the Ph. D. Dissertation

Time Dependent Behaviour of High Strength Concrete

door

Ningxu Han

Delft, 25 november 1996

- Tegenwoordig moeten chemische en minerale toevoegingen eerder als onmisbare bestanddelen van beton worden beschouwd, dan als minderwaardige tweederangs toevoegingen.
 - Nowadays, chemical and mineral admixtures have to be considered as indispensable components in concrete, rather than as discriminated second class additives.
- 2. Indien twee hoge sterkte betonmengsels dezelfde cementmatrix hebben, is de sterkte van de toeslag bepalend voor de sterkte van het beton, omdat de scheuren door de toeslagkorrels lopen. Sterkere toeslagkorrels hebben echter ook een sterkere vervormingsverhinderende werking ten aanzien van de krimp van de matrix, zodat het beton met de sterkste (en stijfste) toeslagkorrels de laagste E-modulus.

In high strength concretes with the same cement matrix, the aggregate strength governs the concrete strength, because the cracks propagate through the aggregate particles. However, stronger aggregates have also a stronger restraining effect on the shrinkage of the matrix, so that the concrete with the strongest and stiffest aggregates has the lowest E-modulus.

- Naast de hydratatie van cement is silicaatpolymerisatie, veroorzaakt door belasten, een andere belangrijke bijdrage aan de veroudering van beton. Silicaatpolymerisatie vergroot de kristalliniteit van de ruimte in de tussenlaag tussen de korrels en bijgevolg wordt de onderlinge binding tussen de korrels vergroot.
 - In addition to the hydration of cement, silicate polymerization induced by loading is another important contribution to the ageing of concrete. Silicate polymerization increases the crystallinity of the interlayer space, and, consequently improves the interparticle bonding.
- 4. Water in beton speelt een belangrijke rol wat betreft het tijdsafhankelijke gedrag van beton. In het uiterste geval, wanneer er weinig of geen water in het beton is, zal er weinig of geen tijdsafhankelijke vervorming optreden.
 - Water in concrete plays a dominant role as far as the time dependent behaviour of concrete is concerned. At an extreme, if there is little or no water in the concrete, there will be little, if any, time dependent deformation.
- 5. Vergelijkbaar met de grotere bijdrage van de treksterkte van de matrix en het grensvlakoppervlak aan de druksterkte van beton dan aan de treksterkte van beton, is de bijdrage van het Stefan-Effect aan de gevoeligheid voor de vervormingssnelheid onder drukbelasting groter dan onder trekbelasting.

Similar to the larger contribution of the tensile strength of the matrix and the interface area to the compressive strength of the concrete rather than to the tensile strength of concrete, the contribution of the Stefan Effect to the strain rate sensitivity in compression is larger than in tension.

6. Hoge sterkte beton behoort absoluut tot de groep hoogwaardige betonsoorten. Hoogwaardig beton hoeft echter niet noodzakelijkerwijs een hoge sterkte te hebben.

High strength concrete definitely belongs to the group of high performance concretes. However, high performance concrete does not necessarily have the high strength.

7. De effecten van vervormingssnelheid en vervormingsgradiënt op het gedrag van beton kunnen niet los van elkaar worden gezien. Zij hebben een logisch verband. In een constructie, zoals in de drukzone van een balk van gewapend beton, veroorzaakt de vervormingsgradiënt ongelijke vervormingssnelheden in de verschillende vezels, hetgeen resulteert in een verschillende gegeneraliseerde spanning-vervorming relatie.

The effects of strain rate and strain gradient on the behaviour of concrete can not be separated. They have some logical relations. In a structure, like in the compression zone of a reinforced concrete beam, the strain gradient causes very different strain rates in different fibres, resulting in a different overall stress-strain relationship.

8. Wat betreft de tijdsafhankelijke vervorming van beton is het verstandig om eerder de kruipcompliantie toe te passen dan de kruipcoëfficiënt om de arbitraire grens tussen elastische en kruipvervorming te vermijden.

Concerning the time-dependent deformation of concrete it is wise to use the creep compliance rather than the creep coefficient in order to avoid an arbitrary demarcation between elastic strain and creep strain.

9. Om de kans op innovatie in de bouwindustrie te vergroten is het absoluut noodzakelijk de samenwerking tussen de ontwerper en de constructeur te stimuleren omdat de eerste geen financiële drijfveer heeft om nieuwe technologiën toe te passen, terwijl de laatste het vermogen heeft om nieuwe technologiën in te brengen, maar gedwongen is om te werken zoals het ontwerp voorschrijft.

To improve the conditions for innovation in the construction industry it is absolutely necessary to encourage a co-operation between designer and constructor, because the former does not have a financial incentive to utilize new technologies, while the latter does have the ability to introduce new technologies, but is obliged to work as designed.

10. De natuur is ongetwijfeld spitsvondiger en complexer dan ons huidige wetenschappelijke model toelaat, terwijl onze wetenschappelijke methoden om de natuur te beheersen in vergelijking primitief zijn en, op de lange duur, niet doeltreffend.

Nature is infinitely more subtle and complex than our current scientific model admits, while our scientific methods of controlling nature are by comparison primitive and, in long term, usually ineffective.

Richard Milton, "Forbidden Science", p. 205, Fourth Estate, London (1994)

- 11. Het maken van beton is net als koken. Met precies dezelfde ingrediënten is de kwaliteit van het eten sterk afhankelijk van de kok.
 - Making concrete is just like cooking. With exactly the same ingredients the quality of the food strongly depends on the cook.
- 12. Wanneer men spreekt over mensenrechten in een ontwikkelingsland, moet men niet vergeten wat Bertold Brecht heeft gezegd: 'Het eten komt eerst, dan de moraal' [The threepenny opera (1928) proloog].

When you are talking about human rights in a developing country, do not forget what Bertolt Brecht said: 'Food comes first, then moral' [The Threepenny Opera (1928) prologue].

13. Een cultuurschok is wat optreedt wanneer een reiziger zich plotseling op een plaats bevindt waar ja nee betekent, waar over een 'vaste prijs' onderhandeld kan worden, waar wachten in een buitenkantoor geen reden is voor belediging, en waar lachen ergernis kan betekenen.

Culture shock is what happens when a traveller suddenly finds himself in a place where yes may mean no, where a 'fixed price' is negotiable, where to be kept waiting in an outer office is no cause for insult, where laughter may signify anger.

Alvin Toffler, "Future Shock", Ch. 1 (1970)

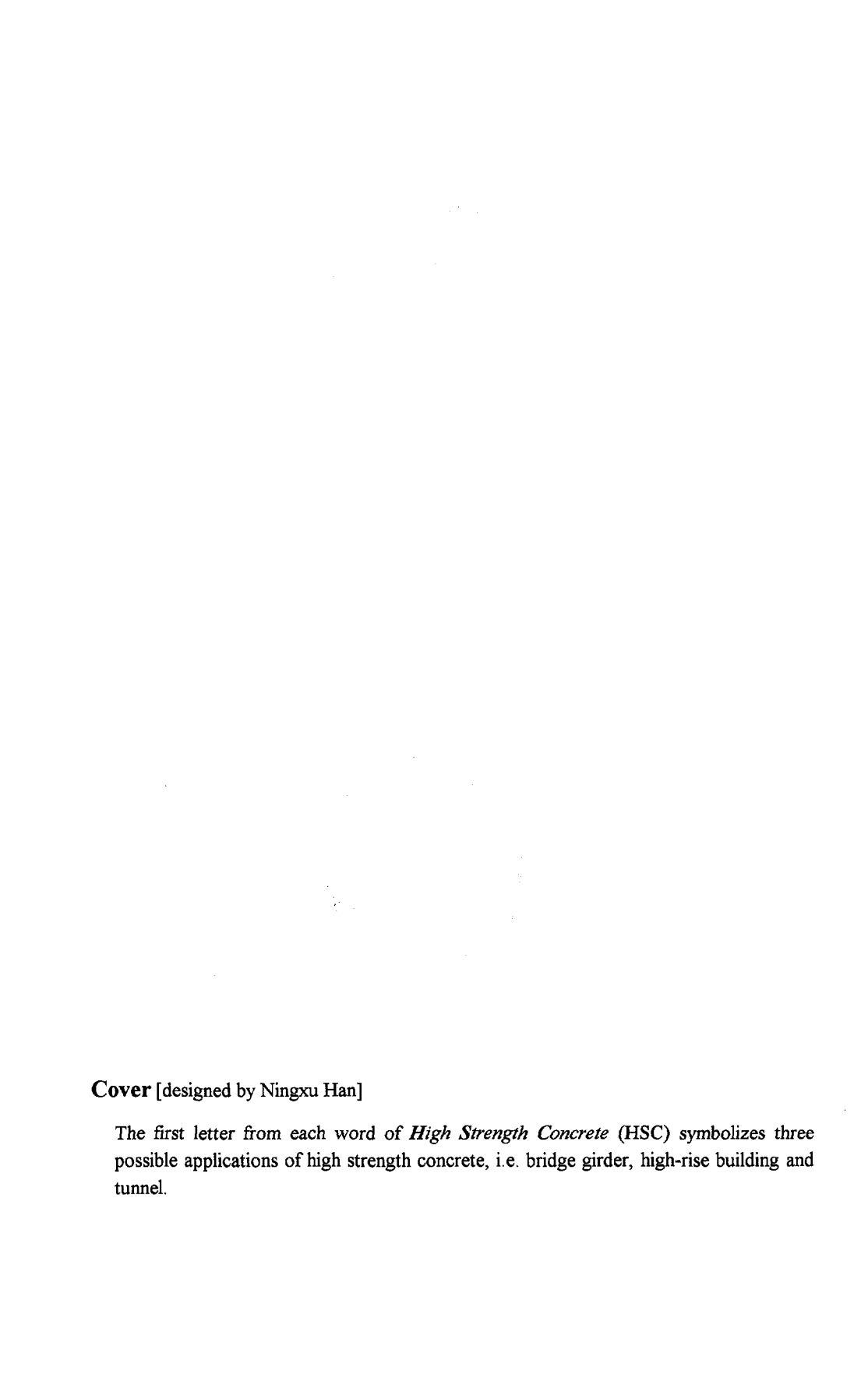
14. In de Chinese cultuur is het zeer moeilijk, zo niet onmogelijk, om tegen iemand direct 'nee' te zeggen.

In the Chinese culture, it is very difficult to directly say 'No' to somebody, if not impossible.

672747 3191330

TR diss 2844

Time Dependent Behaviour of High Strength Concrete



Time Dependent Behaviour of High Strength Concrete

PROEFSCHRIFT

ter verkrijging van de graad van doctor
aan de Technische Universiteit Delft,
op gezag van de Rector Magnificus Prof. ir. K. F. Wakker,
in het openbaar te verdedigen ten overstaan van een commissie,
door het College van Dekanen aangewezen,
op maandag 25 november 1996 te 16:00 uur



door

Ningxu Han

Bachelor of Science, Tongji University, Shanghai, China geboren te Ningxia, China

Dit proefschrift is goedgekeurd door de promotor:

Prof. dr. ir. J. C. Walraven

Samenstelling promotiecommissie:

Rector Magnificus, voorzitter

Prof. dr. ir. J. C. Walraven, promotor

Prof. ir. H. W. Bennenk

Prof. dr. ir. R. de Borst

Prof. dr. ir. Ch. F. Hendriks

Prof. dr. ir. L. Taerwe

Prof. ir. Ch. J. Vos.

Technische Universiteit Delft

Technische Universiteit Delft

Technische Universiteit Eindhoven

Technische Universiteit Delft Technische Universiteit Delft

Universiteit Gent

Technische Universiteit Delft

Published and distributed by:

Delft University Press

Mekelweg 4

2628 CD Delft

The Netherlands

Telephone

+31 15 2783254

Fax

+31 15 2781661

CIP-DATA KONINKLIJKE BIBLIOTHEEK, DEN HAAG

Han, Ningxu

Time Dependent Behaviour of High Strength Concrete / Ningxu Han. - Delft : Delft University Press. - Ill.

Thesis Delft University of Technology. - With ref. - With summary in Dutch.

ISBN 90-407-1398-7

NUGI 841

Subject headings: Time dependent /High Strength Concrete/Rate sensitivity/Creep

Copyright [©] 1996 by Ningxu Han

All rights reserved. No part of the material protected by this copyright notice may be reproduced or utilized in any form or by any means, electronic or mechanical, including photocopying, recording or by any information storage and retrieval system, without permission from the publisher: Delft University Press, Mekelweg 4, 2628 CD Delft, The Netherlands.

Printed in The Netherlands



Acknowledgment

This thesis describes the results of my research work in the past several years, which was carried out in the Stevin Laboratory, Faculty of Civil Engineering, Delft University of Technology, the Netherlands. The research work would be not successfully completed without the help and support of many people and organizations. I would like to express my sincere gratitude to all of them.

First of all, I would like to thank Prof. dr. ir. J. C. Walraven for creating such an opportunity for me to study in the Stevin Laboratory and for his wonderful supervising, continuous support, fruitful discussion and stimulation. This thesis would not have been written without his patient guidance, advice and criticism.

I am very grateful to SPOB, MEBIN, CUR (the Dutch Centre for Civil Engineering, Research, Codes and Specifications) and BFBN (the Dutch Prestress and Prefabrication Industry) for their financial support.

The author is indebted to Mr. A. van Rhijn, Mr. F. J. P. Schilperoort, Mr. G. W. Nagtegaal and Mr. E. Horweg for their substantial assistance during the experimental program.

My deepest gratitude is extended to ir. J. J. M. Gulikers, my colleague and former roommate, for the translation of the summary and prepositions of this thesis into Dutch and his continuous help during my staying in the Netherlands.

Words can not express my appreciation to my wife Lan for her love, patience, understanding and encouragement during my research.

Table of contents

ACKNOWLEDGEMENT	vii
TABLE OF CONTENTS	ix
SYMBOLS AND ABBREVIATIONS	xvii
CHAPTER 1 INTRODUCTION	1
1.1 BACKGROUND	1
1.1.1 Nature of the problem	1
1.1.2 Significance for the engineering practice	
1.1.3 Significance of high strength concrete	3
1.2 AIM, SCOPE AND METHOD OF THE RESEARCH	4
1.2.1 Aim	4
1.2.2 Scope	
1.2.3 Method of the research	5
1.3 OUTLINE OF THE THESIS	7
CHAPTER 2 CLASSIFICATION OF TIME-DEPENDENT BEHAVIOUR OF HSC	9
2.1 Introduction	9
2.2 CLASSIFICATION OF EXTERNAL ACTIONS	10

2.3 CLASSIFICATION OF DEFORMATIONS	12
2.4 CLASSIFICATION OF THE AGEING EFFECT	15
CHAPTER 3 RATE SENSITIVITY OF CONCRETE	17
3.1 INFLUENCE OF STRAIN RATE IN CENTRIC COMPRESSION	17
3.1.1 Influence of the curing condition	18
Concluding remarks	
3.1.2 Influence of the age of the concrete at loading	
Concluding remarks	
3.1.3 Influence of strength of concrete	
Concluding Remarks	
3.1.4 Influence of method to control strain (or stress) rate	<i>27</i>
3.1.5 Summary	30
3.2 INFLUENCE OF STRAIN GRADIENT IN COMPRESSION	30
Concluding Remarks	36
3.3 MODELLING OF THE INFLUENCE OF THE STRAIN RATE AND THE STRAIN GRADIENT	37
Equilibrium condition:	
Plane sections remain plane:	40
Stress-strain relationship in flexure:	
3.4 INFLUENCE OF STRAIN RATE (OR STRESS RATE) IN TENSION	43
3.5 REMARKS ON THE BASIS OF THE LITERATURE STUDY	53
CHAPTER 4 CREEP OF CONCRETE IN COMPRESSION	55
4.1 Introduction	55
4.2 CREEP OF NORMAL STRENGTH CONCRETE IN COMPRESSION	56
4.2.1 Factors affecting creep	56
4.2.1.1 The influence of concrete composition on creep	
4.2.1.2 The influence of water/cement ratio on creep	
4.2.1.3 The influence of stress/strength ratio on creep	
4.2.1.4 The influence of the age at application of the load on the creep deformation	
4.2.1.5 The influence of development of microcracks on the creep deformation	60
4.2.1.6 The influence of relative humidity on the creep deformation	
4.2.1.7 The influence of temperature on the creep deformation	61
4.2.2 Mechanism of creep	62
4.2.2.1 Plastic flow theories	62

4.2.2.2 Viscous flow theories	63
4.2.2.3 Seepage theories	
4.2.2.4 Contribution of microcracking to creep	64
4.2.3 Models to predict creep	64
4.2.3.1 Models of microstructure	
4.2.3.2 Generalization of practical models for predicting creep.	
The product model (ageing model)	
The summation model (rate of flow model or improved Dischinger model)	
4.2.3.3 CEB-FIP Model Code 1990	69
Basic model	
Creep coefficient	
Effect of type of cement and curing temperature Effect of high stresses	
4.2.3.4 American Concrete Institute (ACI 209), 1992.	
4.2.3.4 American Concrete Institute (ACI 209), 1992	
Ambient relative humidity γ_{RH}	
Average thickness of member γ_{ai}	
Factors for concrete composition γ_s , γ_ρ , and γ_a	74
4.2.4 Comparison of linear creep prediction models.	
Constant stress	
Decreasing stress but increasing time dependent strain	
Decreasing stress and decreasing time dependent strain	
Relaxation	75
4.2.5 A non-linear model for creep prediction	76
2 Charles on LICC at a Manager and an experience	==
.3 CREEP OF HSC AT A NORMAL AGE IN COMPRESSION	78
4.3.1 New features of high strength concrete	78
Cement paste	
Cement paste-aggregate interface	79
4.3.2 Creep behaviour of high strength concrete	80
4.3.3 Models for predicting creep of high strength concrete	
4.3.3.1 CEB-FIP Model Code 1990	
4.3.3.2 Modifications of CEB-FIP Model Code 1990	
4.3.3.3 Bazant-Panula model (modification)	
4.3.3.4 AFREM model	86
.4 CREEP OF CONCRETE AT EARLY AGES IN COMPRESSION	87
4.4.1 Properties of concrete at early ages	87
4.4.1.1 Degree of hydration	
4.4.1.2 Development of strength	
4.4.1.3 Practical models for predicting the strength development of concrete	
CEB-FIP Model Code 1990 [CEB-FIP (1991)]	92
Model from American Concrete Institute	94

Table of contents

Model from AFREM	94
4.4.2 Creep of concrete at early ages	
4.4.3 Models to predict the creep of concrete at early ages	
4.4.3.1 Model of Byfors (1980)	97
4.4.3.2 CEB-FIP Model Code 1990	
4.4.3.3 Model of the American Concrete Institute	
4.4.3.4 Model of AFREM	
CHAPTER 5 DESCRIPTION OF EXPERIMENTAL PROGRAM	99
5.1 INTRODUCTION	99
5.1.1 Aim of the experimental program	99
5.1.2 Scope of the experimental program	100
Rate sensitivity tests	
High sustained loading tests	
Tests on creep at normal ages	
Tests on creep at early ages	
5.1.3 Identification of the tests	103
5.2 MATERIALS AND PREPARATION OF THE SPECIMENS.	108
5.2.1 Mix proportions	108
5.2.1.1 Mix proportions for high strength concrete	108
5.2.1.2 Mix proportions for normal strength concrete	108
5.2.2 Moulds, casting and curing	108
5.2.2.1 Preparation of the moulds	108
5.2.2.2 Mixing procedure	
Mixing procedure for the high strength concrete	
Mixing procedure for the normal strength concrete	109
5.2.2.3 Curing	
Curing conditions for the test series R, S and C _n	
Curing conditions for the test series C_e and C_n	
5.2.3 Preparation of the specimens	
5.2.3.1 Specimens for the test series R in compression	
5.2.3.2 Specimens for the test series R in tension	
5.2.3.3 Specimens for the test series S, C _n and C _e	110
5.3 MEASUREMENTS AND TEST PROCEDURES	110
5.3.1 Loading and deformation measurements	110
5.3.1.1 Loading measurements	110
5.3.1.2 Deformation measurements	112
Measurements in test series R in centric compression	112
Measurements for the remaining tests in the series R and S in compression	112

Measurements in test series R in eccentric tension Measurements in test series C_n . Measurements in test series C_e . Measurements in control tests	114 114
5.3.2 Test procedures	
5.3.2.1 Test procedure in the series R	
5.3.2.2 Test procedure in the series S	
5.3.2.3 Test procedure in the series C _n	
5.3.2.4 Test procedure in the series C _e	117
5.4 TEST RESULTS	117
5.4.1 General	117
5.4.2 Control tests	117
5.4.3 Test results in series R.	118
5.4.3.1 Centric compression	118
5.4.3.2 Centric tension (including softening)	118
5.4.3.3 Eccentric compression and tension	119
5.4.4 Test results in series S	120
5.4.5 Test results in the series C_n and C_e	121
5.4.5.1 Creep under a constant sustained or stepwise increased stress	
5.4.5.2 Creep under a decreasing stress (recovery)	121
CHAPTER 6 EXPERIMENTAL RESEARCH AND ANALYSIS - STRAIN RATE	
CHAPTER 6 EXPERIMENTAL RESEARCH AND ANALYSIS - STRAIN RATE	123
CHAPTER 6 EXPERIMENTAL RESEARCH AND ANALYSIS - STRAIN RATE SENSITIVITY	1 23 123
CHAPTER 6 EXPERIMENTAL RESEARCH AND ANALYSIS - STRAIN RATE SENSITIVITY	123 123
CHAPTER 6 EXPERIMENTAL RESEARCH AND ANALYSIS - STRAIN RATE SENSITIVITY	123 123 124
CHAPTER 6 EXPERIMENTAL RESEARCH AND ANALYSIS - STRAIN RATE SENSITIVITY 6.1 INTRODUCTION 6.2 AN EXPLANATION FOR THE STRAIN RATE SENSITIVITY 6.2.1 Material structure of concrete and classification of water.	123 123 124 124 125
CHAPTER 6 EXPERIMENTAL RESEARCH AND ANALYSIS - STRAIN RATE SENSITIVITY 6.1 INTRODUCTION 6.2 AN EXPLANATION FOR THE STRAIN RATE SENSITIVITY 6.2.1 Material structure of concrete and classification of water 6.2.2 Assumed mechanism of rate sensitivity of concrete	123 123 124 125 126
CHAPTER 6 EXPERIMENTAL RESEARCH AND ANALYSIS - STRAIN RATE SENSITIVITY 6.1 INTRODUCTION 6.2 AN EXPLANATION FOR THE STRAIN RATE SENSITIVITY 6.2.1 Material structure of concrete and classification of water. 6.2.2 Assumed mechanism of rate sensitivity of concrete 6.3 INFLUENCE OF THE STRAIN RATE ON THE BEHAVIOUR IN CENTRIC COMPRESSION. 6.3.1 The failure mode of concrete in compression.	123 124 124 125 126
CHAPTER 6 EXPERIMENTAL RESEARCH AND ANALYSIS - STRAIN RATE SENSITIVITY 6.1 INTRODUCTION 6.2 AN EXPLANATION FOR THE STRAIN RATE SENSITIVITY 6.2.1 Material structure of concrete and classification of water. 6.2.2 Assumed mechanism of rate sensitivity of concrete 6.3 INFLUENCE OF THE STRAIN RATE ON THE BEHAVIOUR IN CENTRIC COMPRESSION 6.3.1 The failure mode of concrete in compression. 6.3.2 Stress-strain relationships	123 124 125 126 127 128
CHAPTER 6 EXPERIMENTAL RESEARCH AND ANALYSIS - STRAIN RATE SENSITIVITY 6.1 INTRODUCTION 6.2 AN EXPLANATION FOR THE STRAIN RATE SENSITIVITY 6.2.1 Material structure of concrete and classification of water. 6.2.2 Assumed mechanism of rate sensitivity of concrete 6.3 INFLUENCE OF THE STRAIN RATE ON THE BEHAVIOUR IN CENTRIC COMPRESSION. 6.3.1 The failure mode of concrete in compression. 6.3.2 Stress-strain relationships. 6.3.3 The strength (peak stress) in compression.	123 124 125 126 127 128 132
CHAPTER 6 EXPERIMENTAL RESEARCH AND ANALYSIS - STRAIN RATE SENSITIVITY 6.1 INTRODUCTION 6.2 AN EXPLANATION FOR THE STRAIN RATE SENSITIVITY 6.2.1 Material structure of concrete and classification of water 6.2.2 Assumed mechanism of rate sensitivity of concrete 6.3 INFLUENCE OF THE STRAIN RATE ON THE BEHAVIOUR IN CENTRIC COMPRESSION 6.3.1 The failure mode of concrete in compression 6.3.2 Stress-strain relationships 6.3.3 The strength (peak stress) in compression 6.3.4 Initial modulus of elasticity.	123 124 124 125 126 127 128 132
CHAPTER 6 EXPERIMENTAL RESEARCH AND ANALYSIS - STRAIN RATE SENSITIVITY 6.1 INTRODUCTION 6.2 AN EXPLANATION FOR THE STRAIN RATE SENSITIVITY 6.2.1 Material structure of concrete and classification of water. 6.2.2 Assumed mechanism of rate sensitivity of concrete 6.3 INFLUENCE OF THE STRAIN RATE ON THE BEHAVIOUR IN CENTRIC COMPRESSION. 6.3.1 The failure mode of concrete in compression. 6.3.2 Stress-strain relationships. 6.3.3 The strength (peak stress) in compression. 6.3.4 Initial modulus of elasticity. 6.3.5 Initial Poisson's ratio.	123 124 125 126 127 128 133
CHAPTER 6 EXPERIMENTAL RESEARCH AND ANALYSIS - STRAIN RATE SENSITIVITY 6.1 INTRODUCTION 6.2 AN EXPLANATION FOR THE STRAIN RATE SENSITIVITY 6.2.1 Material structure of concrete and classification of water 6.2.2 Assumed mechanism of rate sensitivity of concrete 6.3 INFLUENCE OF THE STRAIN RATE ON THE BEHAVIOUR IN CENTRIC COMPRESSION 6.3.1 The failure mode of concrete in compression 6.3.2 Stress-strain relationships 6.3.3 The strength (peak stress) in compression 6.3.4 Initial modulus of elasticity.	123 124 124 125 126 127 128 132 135 135

6.4 INFLUENCES OF STRAIN GRADIENTS ON THE BEHAVIOUR IN ECCENTRIC COMPRESSION	139
6.4.1 General experimental observations	. 140
6.4.2 Description of the compressive damage zone model	. 141
6.4.2.1 Failure hypothesis	141
6.4.2.2 Model description	142
6.4.2.3 Material parameters	
The parameter k	
6.4.3 Compressive strain gradients	
6.4.3.1 Extra assumptions	
6.4.3.2 CDZ model for eccentric load	150
6.4.3.3 Effect of the strain rate	152
6.4.4 Numerical study of the eccentrically loaded prisms	. 154
6.4.4.1 Numerical model	154
6.4.4.2 Numerical simulations	
6.4.5 Evaluations of the stress-strain relations in two extended codes for HSC	. 159
6.4.6 Concluding remarks	. 161
6.5 THE INFLUENCE OF STRAIN RATE AND STRAIN GRADIENT ON THE BEHAVIOUR IN CENTRIC AND ECCENTRIC TENSION	162
6.5.1 Influence of the strain rate on the tensile peak stress	. 162
6.5.2 Influence of the strain rate on the tensile deformation	. 164
6.5.3 Influence of the strain rate and the strain gradient on the tensile behaviour	. 165
6.5.4 The influence of the strain rate on the fracture energy	166
6.5.5 Concluding remarks	168
CHAPTER 7 EXPERIMENTAL RESEARCH AND ANALYSIS - CREEP AND	
SHRINKAGE OF HSC	171
7.1 INTRODUCTION	171
7.2 DEVELOPMENT OF STRENGTH AND E-MODULUS OF HSC	172
7.3 SHRINKAGE OF HSC	175
7.4 CREEP OF HSC	178
7.4.1 Creep of HSC under a constant sustained load applied at an age of 28 days	. 178
7.4.1.1 Load-related strain, creep strain and creep coefficient	178
7.4.1.2. Comparisons of test results with three creep prediction approaches	181

7.4.2 Creep of HSC under variable stresses applied at various ages starting from a of 28 days	ın age 181
7.4.2.1 Load-related strain	181
7.4.2.2 Comparison of test results with three existing formulations on the basis of the assu	
of the principle of superposition	
7.4.3.1 Load related strain, creep strain and creep coefficient	
7.4.3.2 Comparisons of test results with three creep prediction approaches	
7.5 CREEP RECOVERY OF HSC	
7.5.1 Creep recovery of HSC totally unloaded in one step	193
7.5.2 Creep recovery of HSC unloaded in a step-wise way	200
7.6 CONCLUDING REMARKS	203
CHAPTER 8 A MODIFIED SHRINKAGE AND CREEP MODEL	205
8.1 INTRODUCTION	205
8.2 THE SHRINKAGE AND CREEP OF CONCRETE	206
8.2.1 Development of strength and E-modulus with time	206
8.2.2 Shrinkage	209
8.2.3 Linear creep	211
8.2.4 Stress dependent strain and the principle of superposition	214
8.2.5 Non-linear creep	214
8.3 VERIFICATION OF THE MODIFIED SHRINKAGE AND CREEP FORMULATIONS	215
8.3.1 The development of strength and E-modulus	215
8.3.2 Shrinkage of HSC	217
8.3.3 Load-related strain and total strain	219
8.3.3.1 Load-related strain and total strain under a constant sustained stress	219
8.3.3.2 Load-related strain under variable stresses	
8.3.4 Creep recovery	
8.3.4.1 Creep recovery of HSC totally unloaded in one step	
8.3.4.2 Creep recovery of HSC unloaded in a step-wise method	
8.4 CONCLUDING REMARKS	232
CHAPTER 9 SUMMARY	235

Table of contents

REFERENCES	241
APPENDIX A GENERAL OVERVIEW OF THE RESEARCH PROGRAM	257
APPENDIX B MIX PROPORTIONS OF HSC AND NSC	263
APPENDIX C EXPERIMENTAL SET-UP	265
APPENDIX D RESULTS OF STANDARD REFERENCE TESTS	269
APPENDIX E TEST RESULTS OF ALL SERIES	279
APPENDIX F RESULTS OF EXPERIMENTAL ANALYSIS	297
SAMENVATTING	311
CURRICULUM VITAE	317

Symbols and abbreviations

1 Symbols

α	a parameter varying according to the type of cement used
	or a shape factor in Eq. (6.11)
α	a constant used in Eq. (4.76)
α_1, α_2	parameters considering the influence of the development of strength on the creep properties of concrete, see Eq. (8.27) and Eq. (8.28)
$lpha_{\sigma}$	a constant taken as 1.5
α_a	the air content
α_E	a constant taken as $2.15 \times 10^4 \text{ N/mm}^2$
α_i	the average stress level in the time interval (t_{i+1}, t_i)
α_k	the stress-strength ratio in the spring H_k , i.e. $\sigma_k f_k$
α_m	the stress-strength ratio in the spring H_m , i.e. σ_m/f_m
α_m^*	the highest stress level in the history in the spring H_m
B	a constant used in Eq. (4.76)
$\beta(f_{cm})$	the coefficient considering the influence of the strength of concrete on creep
$\beta(t_0)$	a monotonically decreasing ageing function
$\beta(t_0, \gamma_a)$	a parameter to consider the effects of time at which the load is applied and the type of aggregate used in concrete on creep
$\beta_c(t, t_0)$	the coefficient describing the development of creep with time after loading

$\beta_{c, sus}(t, t_0)$	a coefficient which depends on the time under sustained loads $(t-t_0)$
$eta_{cc}(t)$	a function defining the ratio of a strength of concrete at a time t , $f_{cm}(t)$ to the 28 day strength f_{cm}
$\beta_{cs}(t)$	a parameter calculated according to Eq. (8.34)
$\beta_{\rm E}(t)$	a function defining the ratio of E-modulus at a time t , $E_{ci}(t)$ to the 28 day E-modulus E_{ci}
$oldsymbol{eta_{\!H}}$	a parameter calculated according to Eq. (8.32)
$oldsymbol{eta_{RH}}$	a coefficient considering the influence of the relative humidity on shrinkage
$\beta_s(t, t_{s0})$	the coefficient describing the development of shrinkage with time
$oldsymbol{eta_{sc}}$	a coefficient considering the type of cement used
$oldsymbol{eta_{sRH}}$	a parameter calculated according to Eq. (8.19)
$\beta_{ss}(t)$	a parameter calculated according to Eq. (8-16)
χ	the ratio of a strain to the strain at the peak stress
Δf	a constant taken as 8 N/mm ²
Δt_i	the number of days where a temperature $T(\Delta t_i)$ prevails
ε	the compressive strain outside the damage zone [see Eq. (6.1)]
$\mathcal{E}(t_0)$	the strain at the time of t_0
$\varepsilon(y)$	the strain distribution as a function of the distance from the neutral axis y
\mathcal{E}_0	the strain at the peak stress
$\varepsilon_{as}(t)$	autogeneous shrinkage of concrete at the time t
\mathcal{E}_c	the compressive strain
$\varepsilon_{c\sigma}(t, t_0)$	stress dependent strain at the time t , loaded at the time t_0
\mathcal{E}_{c0}	the compressive strain at the peak stress σ_{cmax} or at the peak load P_{max}
\mathcal{E}_{cc}	the strain at the near side fibre under an eccentric compressive load
\mathcal{E}_{cc0}	the strain at the near side fibre corresponding to the peak load P_{max}
\mathcal{E}_{cci}	the ith strain at the near side fibre measured from the test
\mathcal{E}_{ccu}	the ultimate strain at the near side fibre in an eccentric compression
\mathcal{E}_{cD}	the strain factor which decides the descending branch of the stress-strain curve [see Eqs. (3.29) and (3.30)]
\mathcal{E}_{ci}	the initial strain in a sustained compression
\mathcal{E}_{cl}	the longitudinal compressive strain

\mathcal{E}_{cl50}	the longitudinal compressive strain at a strain rate of $6.25 \times 10^{-6} \text{ s}^{-1}$
\mathcal{E}_{cl0}	the longitudinal compressive strain at the peak stress
$oldsymbol{arepsilon}_{cli}$	the initial longitudinal strain in a sustained compression
\mathcal{E}_{clu}	the ultimate longitudinal strain in a sustained compression
\mathcal{E}_{cr}	the creep of concrete
$\mathcal{E}_{cr, b}$	the basic creep of concrete
$\mathcal{E}_{cr, d}$	the drying creep of concrete
$\varepsilon_{cs}(t, t_{ms})$	total shrinkage of concrete at the time t , beginning to measure at the time t_{ms}
\mathcal{E}_{cso}	the notional shrinkage coefficient, see Eq. (8.13)
\mathcal{E}_{ct}	the strain at the far side fibre under an eccentric compressive load
\mathcal{E}_{ct0}	the strain at the far side fibre corresponding to the peak load P_{max}
\mathcal{E}_{cti}	the ith strain at the far side fibre measured from the test
\mathcal{E}_{ctr}	the transverse compressive strain
\mathcal{E}_{ctr0}	the transverse compressive strain at the peak stress
\mathcal{E}_{ctr50}	the transverse compressive strain at a strain rate of 6.25×10^{-6} s ⁻¹
\mathcal{E}_{ctri}	the initial transverse strain in a sustained compression
\mathcal{E}_{ctru}	the ultimate transverse strain in a sustained compression
\mathcal{E}_{ctu}	the ultimate strain at the far side fibre in an eccentric compression
\mathcal{E}_{cu}	the ultimate compressive strain
\mathcal{E}_d	the additional compressive strain after peak stress [see Eq. (6.1)]
$\varepsilon_{ds}(t, t_{s0})$	drying shrinkage of concrete at the time t , exposed to drying at the time t_{s0}
\mathcal{E}_{du}	the ultimate value of ε_d [see Eq. (6.32)]
\mathcal{E}_{ie}	the initial elastic strain in a creep test
\mathcal{E}_{irec}	the initial creep recovery
\mathcal{E}_k	the strain in the spring H_k
\mathcal{E}_{ku}	the ultimate strain in the spring H_k
\mathcal{E}_m	the strain in the spring H_m or the average compressive strain in Eq. (6.1)
\mathcal{E}_{mu}	the ultimate strain in the spring H_m
	or the mean compressive strain at failure [see Eq. (6.33)]
\mathcal{E}_{rec}	the creep recovery

$\varepsilon_s(f_{cm}, t_{s0})$	the shrinkage coefficient mainly depends on the strength of concrete, the time at which concrete is exposed to drying, the type of cement used, the
	type of aggregate used
$\varepsilon_{sh}(t)$	the shrinkage of a concrete at the time t
\mathcal{E}_t	the tensile strain
\mathcal{E}_{t0}	the tensile strain at the peak stress σ_{tmax} or at the peak load P_{tmax}
\mathcal{E}_{tc0}	the strain at the far side fibre corresponding to the peak tensile stress $P_{\textit{tmax}}$
\mathcal{E}_{tcu}	the ultimate strain at the far side fibre in an eccentric tension
\mathcal{E}_{tl0}	the strain at the peak tensile stress with a measuring length of 110 mm
\mathcal{E}_{tot}	the total strain including the load-related strain and the shrinkage
\mathcal{E}_{tsh0}	the strain at the peak tensile stress with a measuring length of 35 mm
\mathcal{E}_{tt0}	the strain at the near side fibre corresponding to the peak tensile stress $P_{\it tmax}$
\mathcal{E}_{ttu}	the ultimate strain at the near side fibre in an eccentric tension
\mathcal{E}_{tu}	the ultimate tensile strain
\mathcal{E}_{vmax}	the maximum volume strain in compression
$\Phi(t-t_0)$	a monotonically increasing function standing for the time development of creep with loading duration $(t-t_0)$
ϕ_{∞}	a constant taken as 2.35
$\phi_{\infty}(t_0)$	the ultimate creep coefficient [see Eq. (4.22)]
ϕ_0	the notional creep coefficient
$\phi_{0,k}$	the non-linear notional creep coefficient
$\phi_{28}(t,t_0)$	creep coefficient at the time t with respect to the 28-day initial elastic strain, loaded at the time t_0
$\phi_{bf}(t, t_0)$	the creep coefficient in terms of the basic creep proposed by Byfors (1980)
$\phi_{bf}(t-t_0)$	a correction factor which considers the loading duration in the creep coefficient proposed by Byfors (1980)
$\phi_{bf}(t_0)$	a correction factor which considers the age at application of the load in the creep coefficient proposed by Byfors (1980)
ϕ_{bj0}	the basic value of the creep coefficient according to Byfors (1980)
ϕ_{RH}	the coefficient considering the influence of relative humidity on creep
ϕ_{r0}	creep coefficient at the time t with respect to the initial elastic strain at the time t_0 , loaded at the time t_0

γ	the variation coefficient
$\Gamma(t)$ - $\Gamma(t_0)$	a function standing for the flow which is an irreversible part of the creep deformation
γ_{lpha}	a parameter considering the effect of air content
$\gamma_{ ho}$	a parameter considering the effect of the fine to total aggregate ratio
γ_a	a parameter defining the ratio between E_{ci} of a concrete with any type of aggregate and E_{ci} of a concrete with crushed gravel
Yat	a parameter considering the effect of the average thickness of a member
γc	a correction factor [see Eq. (4.23)]
Yla	a parameter considering the effect of the loading age
Y RH	a parameter considering the effect of the ambient relative humidity
γ_{ts}	the total safety factor
γ_s	a parameter considering the effect of the slump
η	a parameter calculated according to Eq. (8.15)
η_k	the modulus of viscosity of the dashpot N
9	the degree of hydration
\mathcal{G}_{cr}	the critical degree of hydration [see Eq. (4.67)]
$oldsymbol{arphi}_0$	the strain gradient at the peak compressive load P_{max} (rad/mm)
$arphi_d$	the final drying creep value [see Eq. (4.47)]
$oldsymbol{arphi}_d$	the final drying creep as a function of the delay of the start of loading after the start of drying [see Eq. (4.47)]
λ	a parameter calculated by using Eq. (4.40) or (4.41) on the basis of the case of either creep or relaxation
μ	Poisson's ratio in the initial stage
μ_k	a parameter calculated according to Eq. (4.37)
v	the production of ε_{cD} and ε_{c0}
0	properties such as peak stress, strain at the peak stress or E-modulus at any strain rate
$\mathcal{O}_{0.08}$	properties such as peak stress, strain at the peak stress or E-modulus at a strain rate of $0.08 \%/min$
$ heta_c$	a parameter calculated according to Eq. (8.33)
θ_k	the strain level in the spring H_k , i.e. $\theta_k = \varepsilon_k / \varepsilon_{ku}$

```
\theta_m
                  the strain level in the spring H_m, i.e. \theta_m = \varepsilon_m / \varepsilon_{mn}
                  a parameter calculated according to Eq. (8.21)
θ.
                  the fine to total aggregate ratio
\rho_a
                  the compressive stress (N/mm<sup>2</sup>)
\sigma_c
\sigma_c(t_0)
                  compressive stress applied at the time t_0 (N/mm<sup>2</sup>)
                  the stress at the near side fibre under an eccentric compressive load
\sigma_{cc}
                  the initial stress in a sustained compression (N/mm<sup>2</sup>)
\sigma_{ci}
                  the peak stress in compression (N/mm<sup>2</sup>)
\sigma_{cmax}
                  the stress at the far side fibre under an eccentric compressive load
\sigma_{ct}
                  the stress in the spring H_k
\sigma_k
                  the stress in the spring H_m
\sigma_m
                  the stress in the dashpot N
\sigma_n
                  the tensile stress (N/mm<sup>2</sup>)
\sigma_t
                  the peak stress in tension (N/mm<sup>2</sup>)
\sigma_{tmax}
                  the calculated tensile stress at the near side fibre in an eccentric tension on
\sigma_{ttc}
                  the basis of the linear stress distribution (N/mm<sup>2</sup>)
                  the tensile stress at the near side fibre in an eccentric tension on the basis of
\sigma_{ttm}
                  the measured neutral axis position x (N/mm<sup>2</sup>)
\sigma_{vms}
                  the compressive stress corresponding to \varepsilon_{vmax}
                  the time point at which the stress diverts from \sigma_c(t_0)
τ
                  the reduction factor due to the long-term loading
\tau_r
                  the ultimate value of the reduction factor \tau_r
\tau_{roo}
                  the shrinkage-square half-time which is proportional to the square of
\tau_{sh}
                  thickness of concrete
                  the creep rate factor, [see Eq. (4.36)]
ω
Ω
                  the time function calculated according to Eq. (4.43)
ξ
                  a parameter calculated according to Eq. (4.38)
\Psi(t-t_0)
                  a monotonically increasing function standing for delayed elasticity
5
                  a parameter calculated according to Eq. (4.39)
\mathcal{R}
                  the relative strength, \mathcal{R} = f_{cm}(t)/f_{cm} [see Eq. (4.70)]
                  a constant used in Eq. (3.4)
а
```

```
A
                 a parameter used in Eq. (3.31)
A_0
                 the air content used in Eq. (4.68)
a_1, \dots a_n
                 the parameters used in Eq. (3.17)
A_1, A_2, A_3
                 the constants used in Eq. (4.5)
                 a constant taken as 0.17 in Eq. (4.80)
a_{bf}
A_{r}
                 the cross-section of a member (mm<sup>2</sup>)
aı
                 a constant used in Eq. (4.47)
                 a constant used in Eq. (4.3)
A_{\circ}
                 a parameter used in the calculation of the function \beta_F(t)
a_{F}
                 a constant used in Eq. (4.70)
a_i
                 constants used in Eq. (4.71)
a_{i1}, a_{i2}
                 a coefficient used in Eq. (3.33)
A_{r}
                 a parameter used in the calculation of the function \beta_{cc}(t)
a_{st}
                 the parameters used in Eq. (3.32)
a_t, b_t, c_t
b
                 the width of a cross-section of a specimen
                 a parameter used in Eq. (4.48)
b_d
b_i
                 a constant used in Eq. (4.70)
b_n, b_n
                 constants used in Eq. (4.71)
B_r
                 a coefficient used in Eq. (3.33)
c
                 the cement content
C
                 the specific creep (MPa<sup>-1</sup>)
C_{\alpha}
                 a constant used in Eq. (4-1)
Ca
                 a correction coefficient
                 the nonlinearity factor in the spring H_k
C_k
                 the nonlinearity factor in the spring H_m
C_m
                 the specific creep recovery (MPa<sup>-1</sup>)
C_{rec}
                 the material factor for unloading
C_{u,m}
D
                 a parameter used in Eq. (3.31)
d
                 the height of a cross-section of a specimen
dε/dt
                 the strain rate (s<sup>-1</sup>)
(d\varepsilon)_i/dt
                 the initial strain rate in a sustained compression (s<sup>-1</sup>)
(d\varepsilon)_l/dt
                 the longitudinal strain rate (s<sup>-1</sup>)
```

```
the transverse strain rate (s<sup>-1</sup>)
(d\varepsilon)_t/dt
                  the initial transverse strain rate (s<sup>-1</sup>)
[(d\varepsilon)_t/dt]_i
dφ/dt
                  the strain gradient rate (rad/mm/s)
dh,/dt
                  the velocity of the relative displacement of the pore walls
ď
                  the depth of the damage zone [see Eq. (6.27)]
                  the eccentricity of a load
o
e/d
                  the ratio of the eccentricity to the height of a cross-section of a specimen
E_c
                  the modulus of elasticity of concrete (N/mm<sup>2</sup>)
                  the secant modulus in Eq. (6.28)
E_{c0}
E_{ci}
                  the modulus of elasticity of concrete at the age of 28 days (N/mm<sup>2</sup>)
E_c(t)
                  the modulus of elasticity of concrete at an age of t (N/mm<sup>2</sup>)
e_i
                  the distance from the neutral axis to the loading point
E_{k,0}
                  the modulus of elasticity for initial loading
E_{m,del}
                  the modulus of elasticity for unloading
E_{t}
                  the modulus of elasticity of concrete in tension (N/mm<sup>2</sup>)
                  the load carried by a single element [see Eq. (3.1)]
                  stresses at the different time for concretes with different w/c (see Fig. 4.2)
f_1, f_2, f_3, f_4
F
                  the total load carried by a specimen in uniaxial compression [see Eq. (3.1)]
f(y)
                  the stress distribution as a function of the distance from the neutral axis y
f_0
                  a constant used in Eq. (4.69)
f_c
                  cylinder strength of concrete (N/mm<sup>2</sup>)
                  the cube strength of concrete at an age of 28 days (N/mm<sup>2</sup>)
f_{cc28}
                  the design strength at an age of 28 days (N/mm<sup>2</sup>) [see Eqs. (6.38), (6.39)]
f_{cd}
f_{cD}
                  the strength factor which decides the descending branch of the stress-strain
                  curve [see Eq. (3.28)]
                  the characteristic strength at an age of 28 days (N/mm<sup>2</sup>)
f_{ck}
f_{cm}
                  a cylinder strength of concrete at an age of 28 days (N/mm<sup>2</sup>)
f_{cm}(t)
                  the cylinder strength of a concrete at an age of t (N/mm<sup>2</sup>)
                  a constant taken as 10 N/mm<sup>2</sup>
fomo
f_{cv28}
                  the prismatic strength of concrete at an age of 28 days (N/mm<sup>2</sup>)
f_{cp}(t_0)
                  the prismatic strength of concrete at the time of t_0 (N/mm<sup>2</sup>)
                  the strength of a concrete subjected to a strain rate de/dt
f_{cr}
                  the compressive strength of the spring H_k
f_k
```

f_m	the compressive strength of the spring H_m
$f_{cm, sus}(t, t_0)$	the mean compressive strength of the concrete at a time t when subjected to
	a sustained compressive stress at an age of loading $t_0 \le t$
F_p	the hydrostatic pressure (pore water pressure)
F_{st}	the opposing force created by the Stefan Effect
$f_t(t)$	the tensile strength of the concrete at an age of t (N/mm ²)
f_t	the tensile strength of a concrete (N/mm ²)
g_{ct}	a constant taken as 0.043
$G_{\!f}$	the fracture energy (N/m)
G^{l}	the energy per unit area perpendicular to the stress consumed in the shear band [see Eq. (6.2)]
h	the notional size of member (mm)
h_0	a constant taken as 100 mm
h_a	the average thickness of a member (mm)
h_p	the distance between the opposite walls of a pore
$J(t, t_0)$	the creep function or creep compliance (1/N/mm²)
\boldsymbol{k}	a constant which defines the stiffness of an element [see Eq. (3.2)]
	a material parameter in Eq. (6.4)
K	the number of data obtained from tests
k_{σ}	the stress-strength ratio at the time t_0 , $\sigma_c(t_0)/f_{cm}(t_0)$
k_h	a constant used in Eq. (4.67)
k^{l}	a parameter used in Eq. (6.29)
L	the length of a specimen
L^d	the length of a damage zone
l_{ch}	the characteristic length (fracture toughness) (mm)
M	the moment according to the neutral axis
M_{ci}	the moment calculated according to Eq. (3.16) for the ith set of data
m_e	a constant used in Eq. (4.4)
M_i	the <i>ith</i> moment calculated on the basis of P_i [see Eq. (3.18)]
m_v	a parameter used in Eq. (4.44)
$N(arepsilon_c)$	the number of elements carrying the load [see Eq. (3.1)]
n	the exponent of double power law [see Eq. (4.48)]
n_v	a parameter used in Eq. (4.44)

P	the load in an eccentric test
P_a	the probability of a given unstressed particle of gel to overcome the bond
P_{ci}	the load calculated according to Eq. (3.15) for the ith set of data
P_{cr}	the critical porosity of a paste (related to \mathcal{G}_{cr})
P_i	the ith load measured from the eccentric compressive tests
P_{max}	the maximum load-carrying capacity in an eccentric compression
P_p	the porosity of a paste
P_{tmax}	the maximum load-carrying capacity in an eccentric tension
Q	the total heat created by hydration
Q_0	a constant used in Eq. (4.4)
Q_a	the activation energy [see Eq. (4.1)]
r	a parameter proportional to the average distance between successive longitudinal cracks [see Eq. (6.5)]
R	the gas constant [see Eq. (4.1)]
RH	the relative humidity of the ambient environment (%)
RH_o	a constant taken as 100%
R_s	the reduction of the strength due to the long-term loading [see Eq. (3.8)]
s	a coefficient which depends on the type of cement used
$S_d(t, t_0)$	a function which gives the shape of drying creep curve
S_D	the ratio of f_{cD} to f_{cr}
S_{I}	the slump of a concrete (mm)
t	the age of concrete (days)
T	the absolute temperature
t^{\star}	the time to failure in a sustained tensile loading test (minutes)
$T(\Delta t_i)$	the temperature during the time period Δt_i (°C)
t_0	the age of concrete at which a load is applied (days)
T_{0}	a constant taken as 1 °C
$t_{0,T}$	the age of the concrete at application of the load adjusted by Eq. (4.18)
t_1	a constant taken as 1 day
$t_{1, T}$	a constant taken as 1 day
t_{ad}	the adjusted time according to the type of cement used (days)
$t_c(t)$	the calculated time according to the type of cement used and the age of concrete t , see Eq. (8.1) and Eq. (8.2), (days)

t_{c0}	the time in which the strain corresponding to the peak stress is reached
t_{cr}	the critical time at which 55% of the 28-day strength is reached (days)
t_{ms}	the age of concrete at which the measurement of shrinkage begins (days)
t_n	the time point at which the stress changes
t_{s0}	the age of concrete at which the concrete is exposed to drying (days)
T_{ν}	a parameter used in Eq. (4.44)
и	the perimeter of the member in contact with atmosphere (mm)
u_e	the increment of the activation energy
v/s	the volume to surface ratio (mm)
V_a	the activation volume [see Eq. (4.5)]
V_{sd}	the quantity of water adsorbed by the concrete when stored in water
w	the unit weight of concrete (kg/m³)
	or additional deformation in the fracture zone [see Eq. (6.1)]
W^c	the compressive fracture energy per unit volume [see Eq. (6.2)]
W^d	the total energy per unit volume consumed in the longitudinal tensile cracks [see Eq. (6.5)]
W^{el}	the elastic energy at peak stress [see Eq. (6.9)]
W ⁱⁿ	the energy per unit volume absorbed in the longitudinal cracks up to peak stress [see Eq. (6.2)]
w/c	the water to cement ratio
W_c	the vertical component of the sliding deformation along the shear band at failure [see Eq. (6.3)]
w_n	the quantity of bound water
W ^s	the energy per unit volume absorbed in the longitudinal cracks after peak stress [see Eq. (6.2)]
x	the distance between the neutral axis and the near side fibre
X_i	the difference between P_{ci} and P_i for the <i>ith</i> set of data
Y_i	the difference between M_{ci} and M_i divided by e_i for the <i>ith</i> set of data
Z	the least squares according to Eq. (3.20)

2 Abbreviations

ACI American Concrete Institute

AFREM French Chapter of RILEM

BFBN Bond van Fabrikanten van Betonprodukten in Nederland

C-H Calcium Hydroxide [Ca(OH)₂]

C-S-H Calcium Silicate Hydrates

CEA Concrete at Early Ages

CEB Comité Euro-International du Béton

cg HSC with the aggregate of crushed gravel

FE Finite Element

FIP Fédération Internationale de la Précontrainte

gr HSC with the aggregate of granite

HSC High Strength Concrete

ls HSC with the aggregate of limestone

LSC Longitudinal Strain-Rate Control

LVDT Linear Voltage Displacement Transducer

MC90 CEB-FIP Model Code 1990

MdMC90 Modified CEB-FIP Model Code 1990

MEBIN Maatschappij tot Exploitatie van Betonmortelbedrijven In Nederland

NR Normally Hardening Cement
NSC Normal Strength Concrete

PFE Preprogrammable Function Equipment

RILEM The International Union of Testing and Research Laboratories for Materials

and Structures

RS Rapidly Hardening High Strength Cement

SD Standard Deviation

SEM Scanning Electron Microscopy

SL Slowly Hardening Cement

TSC Transverse Strain-Rate Control

Chapter **1**Introduction

Concrete is a material with time-dependent properties. The behaviour of structural elements made of concrete varies with time under external actions. The nature of this phenomenon and its significance to the engineering practice are briefly described, with particular attention to high strength concrete. The aim and the scope of the research project are given. The outline of this thesis is shown at the end of this chapter.

1.1 Background

1.1.1 Nature of the problem

'Perhaps the most uncertain and least well understood aspect of the design of concrete structures is the prediction of time-dependent behaviour...', Gilbert (1988) said. This may look strange since research into the time-dependent properties of concrete and their effect on the behaviour of concrete structures has been carried out world-widely during the past 80 years. The fact that final concensus still has not been reached may be attributed to the complex nature of time-dependent behaviour of concrete.

Time-dependent behaviour of concrete is influenced both by internal and external forces. Concrete is a kind of ageing material, i.e. its properties develop with time due to the continuous chemical reaction of cement and water (hydration), which is influenced by temperature and relative humidity. In comparison with other important structural materials, such as steel, and plastics, concrete shows a strong ageing effect.

If concrete is subjected to external actions (such as a load, or changes in temperature or humidity), it will continuously deform for a very long period of time under normal service conditions. This time-dependent behaviour, which is caused by external influences

and was first discovered by Hatt in USA, is called creep [Neville et.al. (1983)]. Although other important structural materials also experience creep, there are some fundamental differences. Concrete creeps under conventional conditions, whereas other materials creep only under extreme conditions. For example, steel creeps at elevated temperatures, some rocks at high stresses.

As far as the material itself is concerned, concrete shows more complicated features than most other structural materials. Concrete, with its cement gel, crystalline products of hydration, water, unhydrated cement and aggregate is heterogeneous at virtually any level of observation. Furthermore, the properties of concrete are strongly affected by temperature and relative humidity, i.e. by the environment, which plays a dominant role as far as the time-dependent behaviour is considered.

1.1.2 Significance for the engineering practice

Time-dependent behaviour of concrete results in time-dependent behaviour of structural members. In members subjected to bending, time-dependent deformation may cause an increase of the curvature and a consequent increase in deflection. For a column, the time-dependent deformation results in an increase of the lateral deflection due to initial eccentricity, which may eventually lead to instability (buckling).

In prestressed concrete structures, in addition to causing increases in deflection, timedependent deformation causes shortening of the member and consequently shortening of the prestressing steel which leads to losses of the magnitude of the prestressing force.

Time-dependent behaviour of concrete includes also a reduction of the concrete strength under long term loading. This has a considerable significance for design and detailing. This refers to the design of members loaded in compression, bending and shear. It also plays an important role with regard to crack width control and minimum reinforcement.

For the construction industry, knowledge of the time-dependent properties of concrete becomes more and more important. This refers both to technical and economical considerations. Early formwork stripping, accelerating the construction process of slip formed structural members, shortening production cycles in the precasting industry and early prestressing of structural elements are examples. From the cases mentioned before, it can be seen that knowledge of the time-dependent behaviour of concrete is definitely indispensable.

In general, time-dependent properties of concrete significantly affect structural behaviour. In some respects, these effects are unfavourable, while in others, they are beneficial. On the one hand, time-dependent deformation causes losses of prestress and increase of deformations and deflections which may impair the serviceability of a structure. On the other hand, they can generate a favourable initial stress distribution which may be introduced intentionally by an imposed deformation (for example preflexed girders). The reduction of strength may further decrease the load-bearing capacity of a structure. Time-dependent deformation also can reduce undesirable stresses in the concrete caused by unintentionally imposed deformations such as support settlements, shrinkage and thermal gradients.

1.1.3 Significance of high strength concrete

Not only the development and application of high strength concrete (HSC) has significantly increased during the last years, also in research, more and more attention is paid toward differences in fundamental properties between HSC and normal strength concrete (NSC). HSC is characterized by superior properties such as a high compressive strength, an increased modulus of elasticity, and a high density (improved durability).

The material structure of HSC remarkably differs from that of NSC. HSC has a more discontinuous and closed pore structure, smaller pore sizes, and a more uniform pore distribution. This is, among others, a result of the addition of silica fume. The pozzolanic reaction of this material leads to a better bond between aggregate and cement matrix, whereas the microparticles have a filler function as well. The interface area between the matrix and the aggregate, which usually contains larger pores and more microcracks, becomes very compact by virtue of silica fume. Less flaws and pre-loading microcracks are found in HSC, possibly due to the difficulty of moisture exchange between the inside and the outside of the concrete, resulting in a smaller drying shrinkage. Furthermore, the stronger bond within the interface area also contributes to the reduction of number and size of microcracks.

It can be expected that changes in the microstructure of the material cause changes in properties like creep and shrinkage. To investigate of this is the aim of this thesis.

1.2 Aim, scope and method of the research

1.2.1 Aim

The main aim of this research program is to generally improve the knowledge of the time-dependent behaviour of HSC. On the basis of an experimental analysis, more information about several aspects of time-dependent properties of HSC is gained. The results are used to develop improved formulations for the time-dependent behaviour of HSC

1.2.2 Scope

The total research project comprises two parts: experimental analysis and theoretical modelling. In the experimental part, constant strain rate tests in compression and tension for both HSC and NSC are carried out. Besides, shrinkage and creep tests (including high sustained loading tests) in compression for HSC are conducted. A general overview of the research program is given in Fig. 1.1.

The time-dependent behaviour of both HSC and NSC are firstly studied by loading concrete with various strain rates and strain gradients. The strain rates adopted in these experiments range from loading to failure in a few minutes to loading to failure in a number of days. Both compression and tension tests are carried out. Not only centric loading, but also eccentric loading is carried out in combination with various strain rates. The observations in the experiments are qualitatively interpreted by means of a rate-sensitivity model. In this model, the pore structure and the moisture content inside the concrete play a very important role.

The time-dependent behaviour of HSC is furthermore investigated by subjecting concrete to a constant sustained stress. In these tests, the main parameters are the stress level and the age at application of the load; the load is applied at an age of 28 days, as well as at earlier ages. Additionally, various aggregates are used in the mixtures to study their influence on the time-dependent behaviour. Shrinkage and creep recovery is also included. Based on the experimental observations and analyses, modified formulations are proposed.

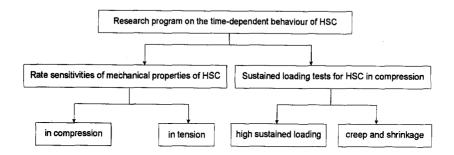


Fig. 1.1 A general view of the research program

1.2.3 Method of the research

The study of the time-dependent behaviour of HSC is carried out in four inter-related phases:

- Literature survey
- Experimental research program
- Theoretical modelling
- Evaluation

In the first phase, three comprehensive literature studies are carried out. These are: a general review of all aspects of HSC, a survey of the time-dependent behaviour of concrete, especially on the rate-sensitive aspect, and a literature review about creep and shrinkage of HSC and NSC at normal ages and at early ages.

In the second phase, a number of laboratory tests are carried out. The parameters which are investigated are shown in Fig. 1.2 and Fig. 1.3. Based on the experimental results, a comprehensive analysis is carried out.

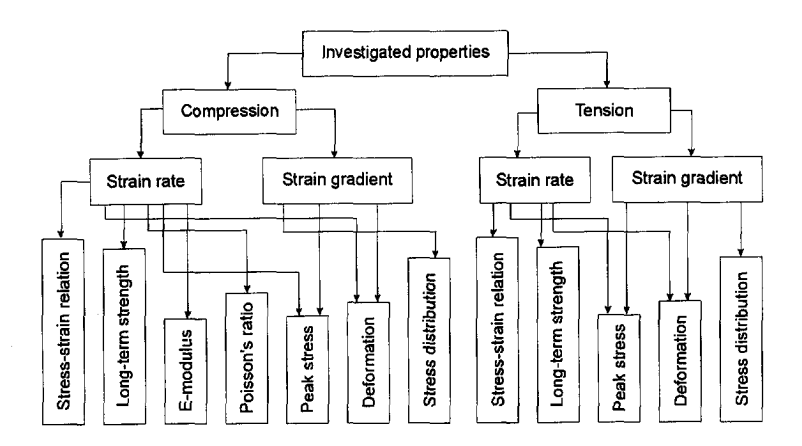


Fig. 1.2 Parameters considered in the rate-sensitivity tests.

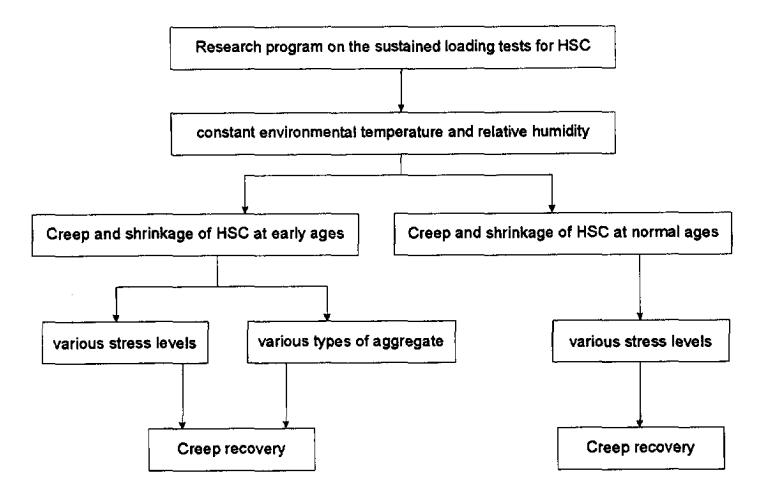


Fig. 1.3 Parameters considered in the sustained-loading tests.

In the third phase, on the basis of the experimental analysis, a description model is developed to explain the mechanism of time-dependent behaviour of concrete. On the basis of the Compressive Damage Zone (CDZ) model, a modified CDZ model including the effects of strain rate and strain gradient is developed. In combination with other factors, a modified formulation based on the CEB-FIP Model Code 1990 for predicting the time-dependent behaviour (creep and shrinkage) of HSC is proposed, which can be used to predict either linear time-dependent deformation or non-linear time-dependent deformation.

Finally, the proposed model is evaluated.

1.3 Outline of the thesis

This thesis starts with an introductory chapter, where the nature of the problem concerning the time-dependent behaviour of concrete is described. In combination with the application of HSC, the significance of this research to the engineering practice is briefly outlined. Afterwards, the aim, scope of this investigation, as well as the research approach adopted in this study are shown. Finally, the contents of this thesis are briefly summarized.

The classification and definition of three important aspects concerning the time-dependent properties of concrete are given in *chapter 2*: the external actions, the deformations of concrete and the ageing effects. With respect to the external actions, static and creep loads are considered. The total deformation under the external actions are divided into time-independent (elastic) strain, creep and load-independent strain (shrinkage). The contributions of the ageing effect to the development of the properties of concrete, in particular, to the strength and the E-modulus are taken into account.

A comprehensive literature survey of the behaviour of concrete subjected to various strain rates and strain gradients in both compression and tension is carried out in *chapter 3*. Various mechanical properties (such as strength, E-modulus, Poisson ratio, critical stress, long-term strength) under the influence of strain rate are discussed in detail. Additionally, the influence of the strain gradient on the behaviour of concrete is also reviewed. However, most of the papers reviewed here concern normal strength concrete, while those about high strength concrete rarely appear on the list of literature. Since the internal structure of high strength concrete is different from that of normal strength concrete, some remarks are also made as far as the rate sensitivity of high strength concrete is concerned.

In chapter 4, a literature survey about creep behaviour of concrete in compression is presented. The factors which have an influence on creep are briefly discussed. The up-to-date's knowledge on the creep mechanism and several viable predicting models are also surveyed. At a later stage of this literature study, attention is given as well to creep of young concrete. The survey is carried out for both normal and high strength concrete, whereas emphasis is placed on high strength concrete.

The details of the experimental program involved in this research project are described in *chapter 5*, which include the extent of the experimental research, the materials used, test set-up, measurements and test procedure. Finally, the arrangement of the experimental results is generalized.

In chapter 6, on the basis of the test data, a comprehensive experimental analysis is given, which mainly focuses on the influences of the strain rate as well as the strain gradient on the fundamental mechanical properties of high strength concrete and normal strength concrete (for comparison) in compression as well as in tension. The phenomena observed in the experiments are interpreted by referring to a proposed mechanism of the rate sensitivity of concrete, whereas the differences of the internal structure between high strength concrete and normal strength concrete are emphasised. In order to simulate the time-dependent behaviour of HSC under an eccentric loading, a model based on the idea of the Compressive Damage Zone (CDZ) is developed. Several parameters obtained from the centric loading tests are introduced in this model to simulate the influences of strain rates and strain gradients on the stress distributions in the compression zone. The calculated load-strain relations are compared with those from the centric compressive tests. Additionally, a case study is carried out by using two recently adopted Dutch and German Codes for HSC.

Chapter 7 presents a comprehensive experimental analysis, which mainly focuses on the influences of the age at application of the load, the stress level as well as the type of aggregate on the creep as well as creep recovery of high strength concrete in compression. The development of strength and E-modulus and the autogeneous shrinkage, which are believed to be significant as far as the time-dependent behaviour of HSC at early ages is concerned, are also discussed. The experimental results are compared with the predictions according to several existing formulations.

A modified shrinkage and creep formulation on the basis of the expression in the MC90 is derived in *chapter 8*. This formulation can be used to predict the development of strength and E-modulus of concrete with time. It can also be used to calculate the shrinkage and creep, either at early ages or at normal ages. Under the assumption of linear creep, the principle of superposition can be applied with these formulations in order to calculate the creep under variable stresses as well as the creep recovery. The non-linearity of creep is explicitly taken into account in this formulation. Evaluations are carried out on the basis of the experimental results.

Finally, the main conclusions of this research project are summarized in *chapter 9*.

References, mixture proportions and experimental data are attached at the end of this thesis.

Chapter 2

Classification of time-dependent behaviour of concrete

Three important aspects concerning the time-dependent behaviour of concrete are classified in this chapter: the external actions, the deformations of concrete and the ageing effects. With respect to the external actions, static and creep loads are considered. The total deformations under the external actions are divided into time-independent (elastic) strain, creep and load-independent strain (shrinkage). Since concrete is an ageing material, the contributions of the ageing effect to the development of properties of concrete, in particular to strength and E-modulus, have to be taken into consideration as the time-dependent behaviour of concrete is treated

2.1 Introduction

Concrete structures are subjected to a wide range of external actions during their service life. These external actions can be generally classified as time-independent and time-dependent actions. A typical time-independent action is the self-weight of the concrete. However, a large majority of actions are time-dependent, i.e. their magnitude and the way to influence the concrete structure vary with time. Typical examples are wind, earthquake, wave etc. Besides load the external actions also include the change of the environmental conditions, such as the temperature and relative humidity, which can impose actions on the structures.

In contrast, the response of concrete structures to these external actions also can be classified into two categories: time-independent and time-dependent deformation. Time-independent deformation represents the immediate reaction when the external action is imposed on the concrete structure. Its value does not change with time. Based on causes of

deformation, time-dependent response of concrete can be further divided into creep and shrinkage. Normally, creep is regarded as a load-induced deformation, whereas shrinkage is the deformation in the absence of an external load.

The third important time-dependent aspect of concrete is its ageing effect, i.e. its material structure and the response to the external action varies with time. The development of the mechanical properties of concrete is closely associated with the hydration process of cement with water. Since this process takes a very long time to finish, obviously, unlike other materials, such as steel, the contribution of the ageing effects further complicates the time-dependent behaviour of concrete.

In general, time-dependent behaviour of concrete can be treated with the following three classifications: type of external action, type of deformation and the ageing effect.

2.2 Classification of external actions

Real structures have to resist various external actions during their service life. The external actions normally include dynamic loading (wind, storm, earth quake, explosion, etc.), static loading (self-weight of structure, fixed equipment, etc.), as well as actions due to changes of the environmental conditions (temperature, relative humidity, etc.). Generally speaking, all those actions vary with time, except for the static loading. A wide range of loading conditions concerned in civil engineering are shown in Fig. 2.1.

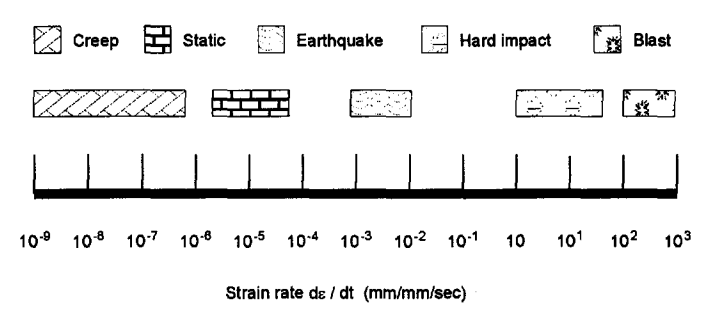


Fig. 2.1 Various external actions imposed on concrete structures in civil engineering.

On the basis of the rate of the action imposed on the structure, three situations can be distinguished: dynamic, static and creep. The dynamic loading has been a subject for research for several decades, and a number of reports can be referred for further investigation. There is no further consideration about dynamic loading in this thesis. In the range of static loading, the external action normally occurs in a relatively short time, and is

regarded as a time-independent action. For the creep loading, three possibilities can be distinguished: a constant loading rate, a constant strain rate and a sustained constant loading. The action versus time curves of these situations are shown in Fig. 2.2.

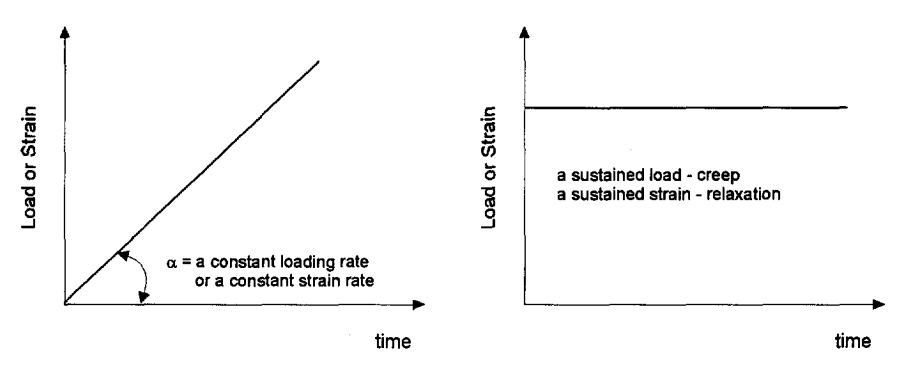


Fig. 2.2 Generalized two external actions versus time.

In practice, any real external action history can be simulated by using the above mentioned generalized situations. A simple example is shown in Fig. 2.3.

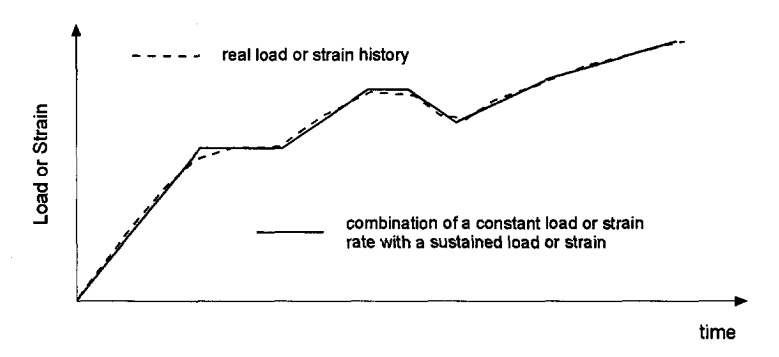


Fig. 2.3 An example of the simulation of real external action.

2.3 Classification of deformations

In general, the total deformation of concrete under the external action can be classified in load-dependent deformation, load independent deformation, time-dependent deformation and time-independent deformation.

The load-independent deformation is normally referred to as *shrinkage* and *swelling*, which take place due to movement of water from or to the ambient medium without the action of external loading. Shrinkage and swelling are time-dependent deformations. The total observed shrinkage at any time t, $\varepsilon_{cs}(t)$ consists of two components: *basic shrinkage* $\varepsilon_{as}(t)$ and *drying shrinkage* $\varepsilon_{ds}(t)$. The basic shrinkage is also known as autogenous or chemical shrinkage, which occurs without the loss of water to the environment. The load-independent time-dependent deformation is illustrated in Fig. 2.4.

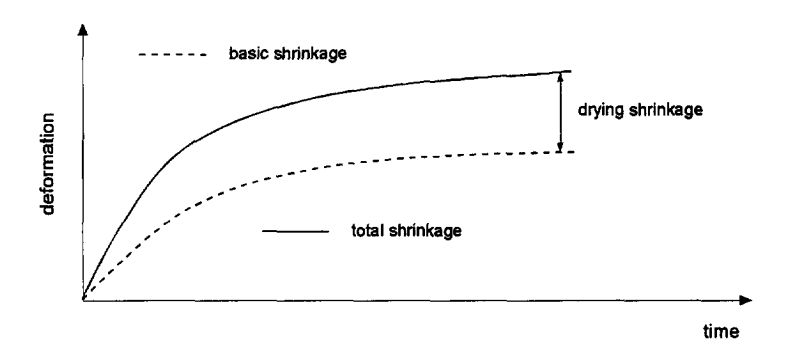


Fig. 2.4 Load-independent deformation of concrete.

The general deformation-time curve of concrete subjected to an external load is shown in Fig. 2.5. The deformation at zero time, instantaneous deformation ε_{ie} , includes an elastic part and an inelastic part. The latter is irrecoverable as the load is removed. The instantaneous deformation is regarded as a time-independent deformation. But, strictly speaking, it does depend on the time t_0 at which the load is applied, and the rate of application of the load. Only if t_0 is larger than a certain value and the rate of application of the load is restricted within a certain range, this part of the deformation can be treated as being time-independent, although, in practice, it is very difficult, if not impossible, to obtain it.

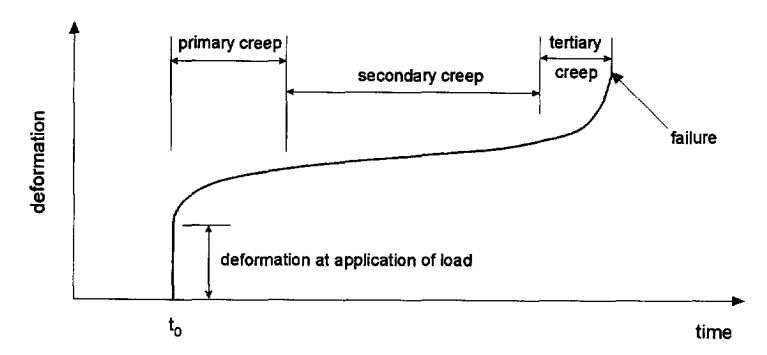


Fig. 2.5 Deformation-time curve of concrete subjected to creep.

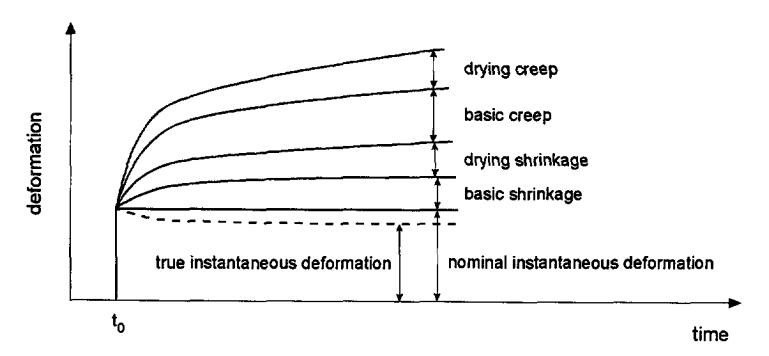


Fig. 2.6 Total strain of concrete under the external actions.

The time-dependent deformation of concrete under an external load is basically called creep ε_{cr} . In Fig. 2.5, it is indicated that this part of the deformation is divided into three stages, mainly depending on the loading level. In the primary area, creep develops very fast, but the rate of creep decreases. As a minimum creep rate appears, the deformation-time curve enters the secondary stage, which is also called stationary deformation. This part of the creep normally occurs when the concrete is subjected to working stresses between 25 to 50 per cent of the short-term strength of the concrete. The tertiary creep only occurs when a high stress is applied to the concrete. This will lead to failure of concrete.

Depending on the ambient humidity of the environment, the total creep of concrete may be further defined as the *basic creep* ($\varepsilon_{cr,b}$) and the *drying creep* ($\varepsilon_{cr,d}$). Basic creep is the creep occurring under conditions of no moisture exchange with the ambient medium. Under the conditions of drying, there is an additional component termed drying creep (or the Pickett effect after the investigator who first reported this phenomenon).

Shrinkage, instantaneous deformation and creep are expressed as strain (millimeter per millimeter). It is known that shrinkage and creep are not two independent phenomena. The effect of shrinkage on creep is in fact to increase the magnitude of creep. However, because of the simplicity, in this thesis, these two phenomena are considered to be additive, i.e. creep is the deformation in excess of shrinkage and instantaneous deformation. The total strain of concrete under the external actions is shown in Fig. 2.6.

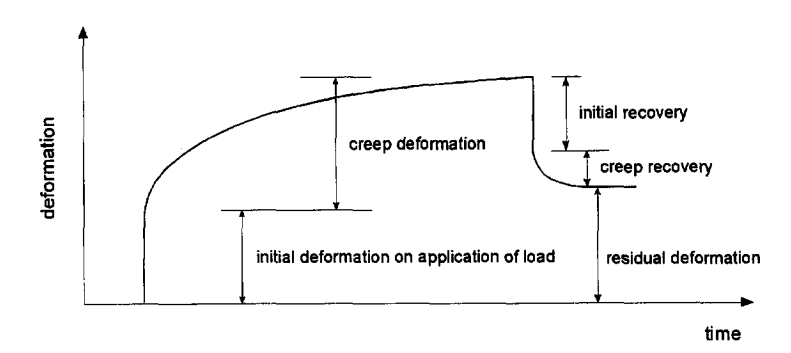


Fig. 2.7 Initial recovery and creep recovery at the time of removing the applied stress.

Normally, the creep deformation of concrete is compared with the elastic deformation. At any time t, the ratio of creep to the elastic strain loaded at the time t_0 is termed as the creep coefficient $\phi(t, t_0)$. The magnitude of creep per unit of stress is called the specific creep $C(t, t_0)$, which is expressed as the ratio of creep, $\varepsilon_{cr}(t, t_0)$, after loading at a time t_0 to the stress $\sigma_c(t_0)$. As shown in Fig. 2.6, the sum of the instantaneous deformation $\varepsilon_{ie}(t_0)$ and the creep $\varepsilon_{cr}(t, t_0)$ is termed as the stress-related strain $\varepsilon_{co}(t, t_0)$. The magnitude of the stress-related strain per unit of stress is called the creep function or the creep compliance, $J(t, t_0)$, which is expressed as the ratio of the stress-related strain $\varepsilon_{co}(t, t_0)$ to the stress $\sigma_c(t_0)$ applied at time t_0 .

When the stress is partly or totally removed, concrete undergoes an instantaneous recovery, which is called the *initial recovery*, ε_{irec} . The initial recovery is followed by a

time-dependent recovery, referred to in this thesis as creep recovery, ε_{rec} (see Fig. 2.7). The ratio of the creep recovery to the unit of the removed stress is termed as the specific creep recovery, C_{rec} .

2.4 Classification of the ageing effect

Concrete is an ageing material. Its properties develop with time. This development comes from the hydration of cement with water, which normally takes a long time to complete. In addition, this process is strongly influenced by the ambient temperature and relative humidity. Among other factors, it is believed that the type of cement used in the concrete, the temperature in the hydration process and the relative humidity play a very important role.

In this thesis, only two mechanical properties are taken into account, i.e. the strength and the E-modulus. With respect to the development of these two properties, two coefficients are used: $\beta_{cc}(t)$ is a coefficient to describe the ratio of the strength at any time t, $f_{cm}(t)$, to the strength at an age of 28 days, f_{cm} ; $\beta_{E}(t)$ is a coefficient to describe the ratio of the E-modulus at any time t, $E_{ci}(t)$, to the E-modulus at an age of 28 days, E_{ci} . These factors are believed to be very important as far as the time-dependent behaviour of concrete at early ages is concerned.

Chapter 3

Rate sensitivity of concrete

A literature survey of the behaviour of concrete subjected to various strain rates and strain gradients in both compression and tension is presented. The strain rate range is mostly limited to the region between the so called static and creep loading. Various mechanical properties (such as strength, deformation, E-modulus, Poisson ratio, critical stress, long-term strength) under the influence of strain rate are discussed in detail. Additionally, the influence of the strain gradient on the behaviour of concrete is also reviewed, where the key points are the stress distribution, the peak stress and the ultimate strain of the extreme fibre. The basic mechanism which causes the rate sensitivity is explored. Several mathematical models are presented, which have been developed to evaluate the stress-strain relationship in flexure. However, most of the papers reviewed here concern normal strength concrete, while those about high strength concrete rarely appear on the list of literature. Since the internal structure of high strength concrete is different from that of normal strength concrete, some remarks are also made as far as the rate sensitivity of high strength concrete is concerned.

3.1 Influence of strain rate in centric compression

The effect of strain rate on the mechanical behaviour of concrete in compression (especially on the compressive strength) has been a subject of extensive research over several decades. Some investigators [Spooner (1971), Dhir & Sangha (1972), Sparks & Menzies (1973)] found that the influence of the strain rate on the mechanical properties of concrete (such as strength) is very small, while others [Watstein (1953), Rüsch (1960), Rasch (1962), Spooner (1972)], indicated that the mechanical properties (such as strength) are strongly influenced by the strain rate. Since these research projects have been carried out under very different test conditions, apparently contradictory results were obtained.

The main factors that could have influenced the test results are the curing condition; the concrete strength; the age of the concrete at loading and the methods used to control the rate, which will be discussed in detail.

3.1.1 Influence of the curing condition

Nearly eight decades ago, Abrams (1917) reported his results regarding the strain rate sensitivity. He used concretes of three strengths (5.5, 12 and 19.6 MPa at 28 days) to investigate the effect of the strain rate on the mechanical properties for strain rates in the range between 8×10^{-6} s¹ and 2×10^{-4} s⁻¹. Cylindrical specimens with a diameter of 15.2 mm and a height of 30.5 mm were cured in a damp condition for 28 days. It was reported that the maximum reduction of the compressive strength, within the adopted strain rate range, was about 20%.

Jones & Richart (1936) carried out a research programme in order to study the strain rate effect on the behaviour of concrete. Cylinders (15.2 × 30.5 mm) with three strengths (14, 24 and 35 MPa) were tested under strain rates in the range between 1.0×10^{-5} s⁻¹ and 2 × 10^{-3} s⁻¹. All the specimens were cured in a moist condition during 28 days before testing. The results of this research indicated that the reduction of the peak stress due to the decrease of the strain rate in the range considered was about 15%.

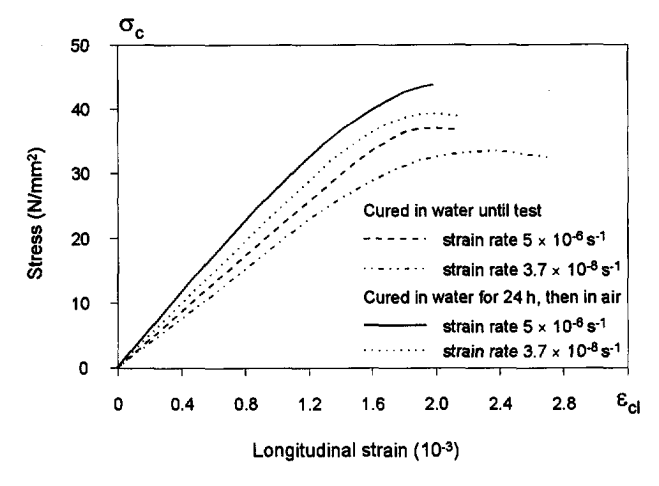


Fig. 3.1 Stress-strain relationships for two different strain rates on air-cured and on water-cured specimens [after Spooner (1971)].

Watstein (1953) studied the strain rate sensitivity by adopting various strain rates (from 1.0×10^{-6} to 10 s^{-1}) with two concretes having approximate compressive strengths of 17.2 MPa and 44.8 MPa at 28 days. 76.2×152.4 mm cylinders were moist-cured during 25 days and air-dried during three days (during which the specimens were also placed for 3 to 4 hours in an oven at 60°C) prior to testing. The decrease in strength for both concretes, for strain rates between 10^{-4} s^{-1} and 10^{-7} s^{-1} , was only 5%.

Spooner (1971) adopted two widely different curing regimes in order to show the influence of curing conditions on the rate sensitivity of concrete. $75 \times 75 \times 250$ mm prismatic specimens were used in his investigation. After demoulding, the specimens were either placed in water at 19 °C or left in the laboratory where the environment was controlled at 19 °C and 65% R.H. Tests were carried out after the concrete reached the age of about three months. Two strain rates $(5 \times 10^{-6} \text{ s}^{-1} \text{ and } 3.7 \times 10^{-8} \text{ s}^{-1})$ were used in this research project. The test results (see Fig. 3.1) show that in the air-cured condition the peak stress in the faster strain-rate test is not significantly different from that in the slower strain-rate test (about 4.2%), whereas in the water-cured condition the difference between the two strain rates amounts to about 12.4%. Additionally, the longitudinal strain corresponding to the peak stress is influenced in an opposite way (27.1% in the air-cured condition and 2.8% in the water-cured condition).

Table 3 I	Effect of strain	rate on the str	ength of concre	te lafter Dhir	and Sanaha (10	7211
lanie 3.1	Effect of strain	rate on the sir	engin of concre	ie ianei Dini	anu Sangna (19	1211

Strain rate	Compressive strength (N/mm²)						Stand.	
mm/mm/sec	Individual results						Mean	devi.
2.5 × 10 ⁻³	37.29	39.18	41.66	39.47	37.97	38.99	39.09	1.50
2.5 × 10 ⁻⁴	38.11	37.87	37.87	36.80	38.45	37.48	37.76	0.57
2.5 × 10 ⁻⁵	38.21	38.84	38.84	36.71	35.93	39.57	38.02	1.40
2.5 × 10 ⁻⁶	37.39	38.84	36.66	36.27	38.36	39.13	37.77	1.18
2.5 × 10 ⁻⁷	38.16	37.68	36.66	36.80	37.19	38.36	37.48	0.71
5.0 × 10 ⁻⁸	37.68	39.62	37.14	35.78	37.73	38.73	37.73	1.28

Dhir & Sangha (1972) investigated the effect of the strain rate by using 50×125 mm cylindrical specimens cored from 150 mm cubes. Twenty-four hours after casting, the cubes were removed from the steel moulds and stored in water, at 18 to 20° C, for 28 days. The cores were obtained by drilling into the direction of casting. The specimens were then stored in the laboratory atmosphere for a further 10 weeks before testing. Strain rates ranging from 5.0×10^{-8} s⁻¹ to 2.5×10^{-3} s⁻¹ were adopted. From the results of this

investigation (see Table 3.I) it can be seen that there is no reduction in strength for strain rates lower than 2.5×10^{-4} s⁻¹.

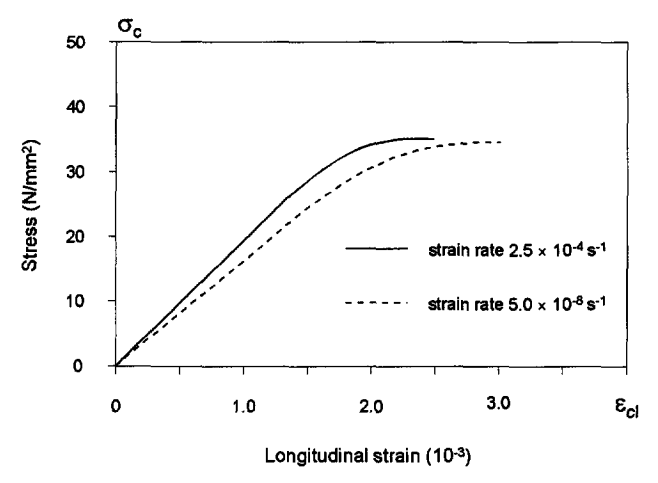


Fig. 3.2 Effect of strain rate on the relationship between stress and longitudinal strain [after Dhir and Sangha (1972)].

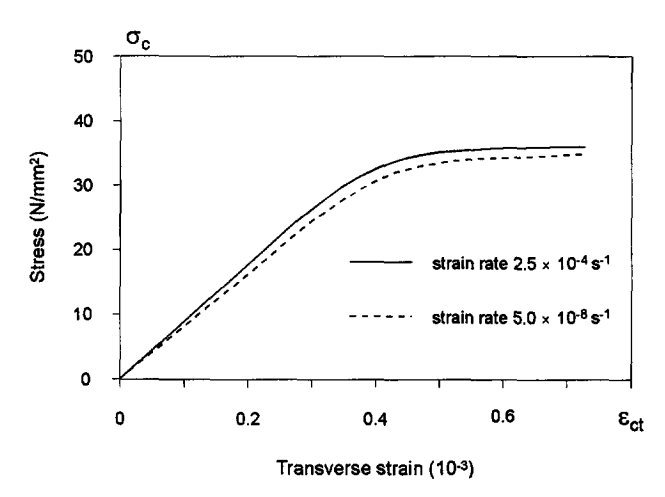


Fig. 3.3 Effect of strain rate on the relationship between stress and transverse strain [after Dhir and Sangha (1972)].

The comparison between the two extreme strain rates in this investigation is also shown in Fig. 3.2, from which it is clear that the peak stress is hardly influenced by the strain rate. The effect of the strain rate on mechanical properties was investigated as well in

this research program. In Fig. 3.3 the stress-transverse strain relationships for the two extreme strain rates are shown. It is seen that the transverse strain is less dependent on the strain rate than the longitudinal strain. For a certain stress level (25 MPa), the difference between the strains corresponding to the two extreme strain rates is 18.1% and 9.2 % for longitudinal and transverse strains, respectively.

The variation of Poisson's ratio as a function of the strain rate is also discussed by Dhir and Sangha (1972). From Fig. 3.4 it can be seen that Poisson's ratio increases with increasing strain rate. A possible physical explanation of this phenomenon is the following: at a lower strain rate, a greater degree of consolidation takes place and there is a smaller tendency to deform in the transverse direction, i.e. there will be a smaller tendency for matrix cracks to develop at lower strain rates. The E-modulus (Young's modulus) is also investigated by subjecting concrete to various strain rates. From Fig. 3.5 it can be seen that the reduction of E-modulus by decreasing the strain rate from 2.5×10^{-4} s⁻¹ to 5×10^{-8} s⁻¹ was 22%.

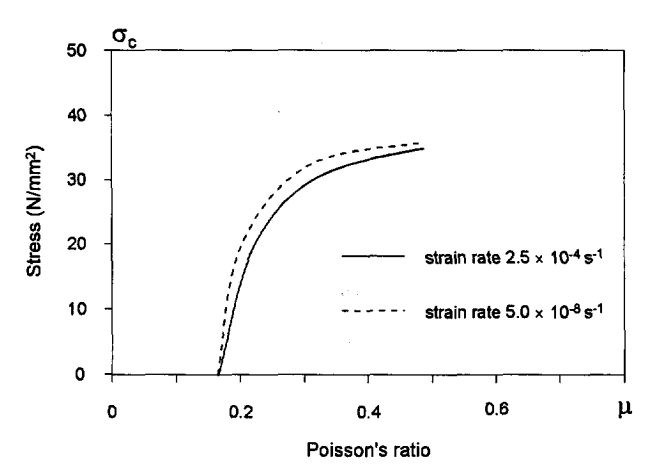


Fig. 3.4 Effect of strain rate on the relationship between stress and instantaneous Poisson's ratio [after Dhir and Sangha (1972)].

In addition to this, Dhir and Sangha (1972) have also conducted some tests, in which the specimens were moist-cured for 28 days, and subsequently put in an air-cured condition during two years before testing. Strain rates ranging from 1.0×10^{-7} s⁻¹ to 1.0×10^{-4} s⁻¹ were used. The test results indicated that the reduction in strength in this case was only 3%.

Sparks and Menzies (1973) carried out an investigation, which originally focused on the influence of the aggregates on the mechanical properties of the concrete. In this project constant loading rates in stead of constant strain rates were adopted. The specimens used in this investigation were $102 \times 102 \times 203$ mm prisms cast in steel moulds. After casting, the specimens were stored for 24 hours in a curing room with 100% relative humidity. They were then demoulded and stored in water at 18.3 °C for 7 days. Afterwards, they were placed in the test laboratory under a normal room curing condition. The test results (see Fig. 3.6) indicated that the sensitivity of the strength to the rate of loading appears to be related to the stiffness of the aggregate related to that of the matrix, changing from 4% (stiffer aggregate, softer matrix) to 16% (softer aggregate, stiffer matrix).

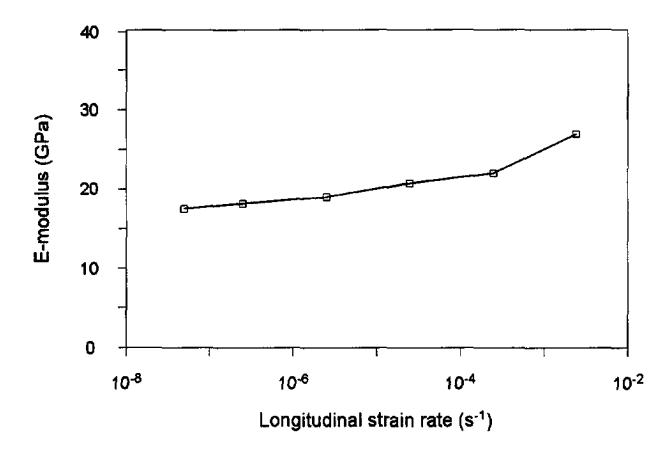


Fig. 3.5 Relationship between E-modulus of concrete and strain rate [after Dhir and Sangha (1972)].

Kaplan (1980) carried out a research program in order to investigate the rate sensitivity of concrete under various curing regimes, ages at testing and nominal concrete strengths. In this investigation, $40 \times 40 \times 160$ mm prismatic specimens were used in order to study the effect of different curing regimes on the strength/loading-rate relationship. The specimens were divided into three groups after removing from their moulds and were subjected to three different curing conditions: (1) in water at 18 ± 1 °C; at 100% R.H.; (2) in the humidity chamber at 18 ± 1 °C; (3) in normal laboratory conditions where the relative humidity was $75 \pm 8\%$ and the temperature was 18 ± 2 °C. After 28 days, the specimens kept in the humidity chamber and in the laboratory were immersed in water for 3 further days in order to bring the relative moisture content of all three groups to the same level. It was concluded that the saturated specimens showed up to about 40% increase in

strength, whereas specimens which had been dried did not show significant changes in strength for test which lasted anywhere between 1 second and 4 hours.

Harsh, Shen and Darwin (1990) performed a study concerning the rate-sensitivity of paste and mortar. The key point in their research is that the materials remained in a saturated condition. They found that the stress-strain response of cement paste and mortar is significantly sensitive to the strain rate. The strain rates range from 3×10^{-7} s⁻¹ to 3×10^{-1} s⁻¹. The test results indicate that the peak stress increases with about 15% with each order of magnitude increase in strain rate. The strain at peak stress at first decreases but then increases with an increase in strain rate. The results also clearly show that the E-moduli of cement paste and mortar increase significantly with each order of magnitude increase in strain rate. It further emphasizes that the mechanical behaviour of concrete in compression can not be considered without taking the influence of the strain rate in due consideration.

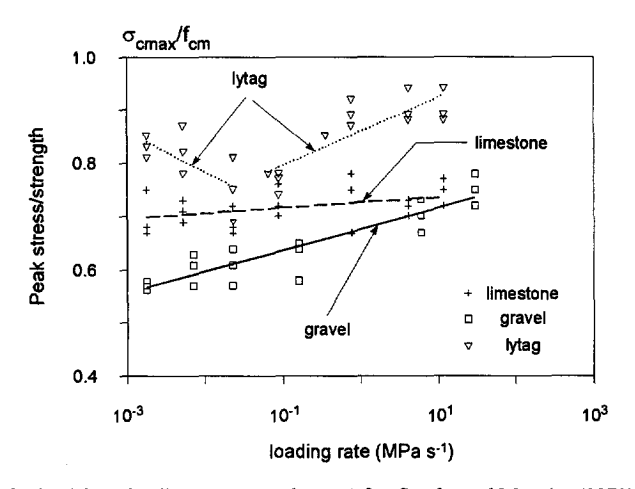


Fig. 3.6 Results obtained from loading rate control tests [after Sparks and Menzies (1973)].

Concluding remarks

According to the survey of literature, concerning the influence of the curing condition on the strain rate sensitivity of concrete, it may be concluded that, at a given age and strength, the effect of strain rate on the concrete strength decreases as the degree of aircuring increases. What is the reason that the curing regime can play such a dominant role as far as the strain rate effect is concerned? Kaplan (1980) tried to give an answer about this question. He pointed out that, when compressive stresses are applied to a concrete specimen, the pores and channels within the matrix will tend to close, thus causing the water to move within the specimen. This movement, because of viscosity, will be accompanied by a pressure gradient in the liquid phase. At higher rates of loading, this may give rise to a hydrostatic pressure in the pores. This, in turn, would delay the onset of excessive cracking within the solid phase and thereby increase the compressive strength. Based on this assumption, the phenomena observed in various investigations could be explained as follows: In the air-cured condition, more free water inside the specimen escapes during the curing period, thus less water is available at the moment of testing to produce pore-water pressure during the higher strain rate test, resulting in a relatively lower strength.

3.1.2 Influence of the age of the concrete at loading

The results of tests by Jones & Richart (1936), who tested concrete specimens, which were cured in a moist condition at ages of 7 days and 28 days, showed that, as the rate of loading increased from 0.007 to 7 N/mm² s⁻¹, the increase in strength was 20 and 25%, respectively.

Rasch (1962) conducted a systematic research programme which aimed at the study of the stress-strain relationship of concrete and its variability with time. In his tests, constant strain rates were adopted. The results of the tests which were carried out at two ages (56 days and 390 days) are compared in Fig. 3.7. It can be clearly seen that the reduction of the strength of the older concrete is larger than that of the younger concrete.

Spooner (1972) studied the stress-strain relationship of cement paste strained at two rates $(8.3 \times 10^{-7} \text{ s}^{-1} \text{ and } 8.3 \times 10^{-8} \text{ s}^{-1})$. The ages of the specimens at the beginning of the tests were 7, 14, 28, and 84 days. Three different water/cement ratio's (w/c = 0.35, 0.47, 0.59) were adopted. The test results (see table 3.II) clearly demonstrated the influence of age at testing on the rate sensitivity. The reduction of peak stress due to the change of strain rate is larger for older specimens than for younger specimens.

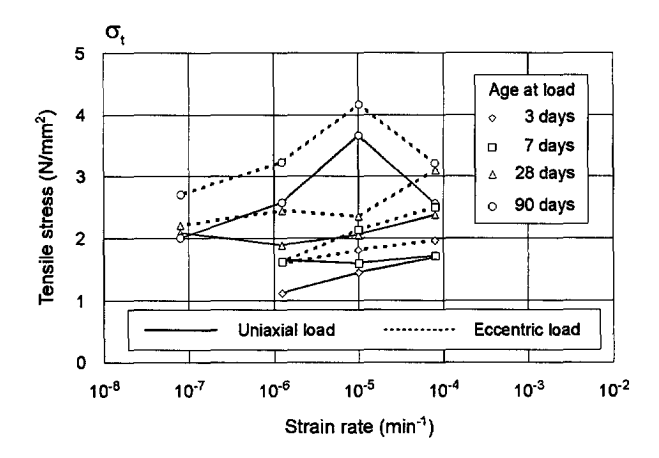


Fig. 3.7 The relationship between peak stress and strain rate for concrete tested at different ages [after Rasch (1962)].

Table 3.II Peak stress and corresponding strains for cement paste of various ages strained to failure at constant strain rates [after Spooner (1972)]

Water	Specimen aged								
cement	7 days		14 days		28 days		84 days		
ratio	σ _{cmax} (MPa)	ε _{σ0} (10 ⁻³)	σ _{cmex} (MPa)	ε _{σ0} (10 ⁻³)	σ _{cmax} (MPa)	ε _{c0} (10 ⁻³)	σ _{cmax} (MPa)	ε _{c0} (10 ⁻³)	
Strain rate 8.3 × 10 ⁻⁷ s ⁻¹									
0.35	41.5	5.545	46.0	4.300	52.7	5.000	67.2	5.400	
	40.4	5.150	50.0	5.575	58.7	6.480	66.4	5.750	
0.47	17.0	3.400	25.6	3.700	32.5	3.875	42.6	4.500	
0.47	18.4	4.250	26.2	3.825	32.9	4.025	38.2	4.025	
0.59	9.1	2.600	14.0	3.450	20.0	3.775	26.2	3.875	
0.59	10.1	2.915	15.5	3.200	19.6	4.820	25.4	3.960	
Strain rate 8.3 × 10 ⁻⁸ s ⁻¹									
0.35	41.1	8.655	49.0	8.825	53.5	7.375	60.5	6.835	
	36.7	5.915	48.5	8.325	54.5	7.125	62.0	7.700	
0.47	19.2	4.750	26.0	5.000	33.2	6.325	36.2	4.980	
	20.8	5.975	28.4	6.750	29.9	5.990	36.2	5.070	
0.59	9.9	4.660	15.5	5.000	18.0	5.350	22.4	5.025	
0.55	8.8	2.760	16.2	6.490	17.8	4.700	22.6	5.125	

Kaplan (1980) has also studied the effect of age on the rate sensitivity of concrete. The specimens were tested at ages of 3, 7 and 36 days. He pointed out that older specimens were more rate-sensitive than younger specimens (see Fig. 3.8)

Concluding remarks

The age at testing is one of the important factors which could influence the rate sensitivity of concrete. As the testing age increases, the internal pores and channels of concrete will be smaller due to continued hydration of cement and filling in the remaining voids, so that consequently higher pore-water pressures are to be expected.

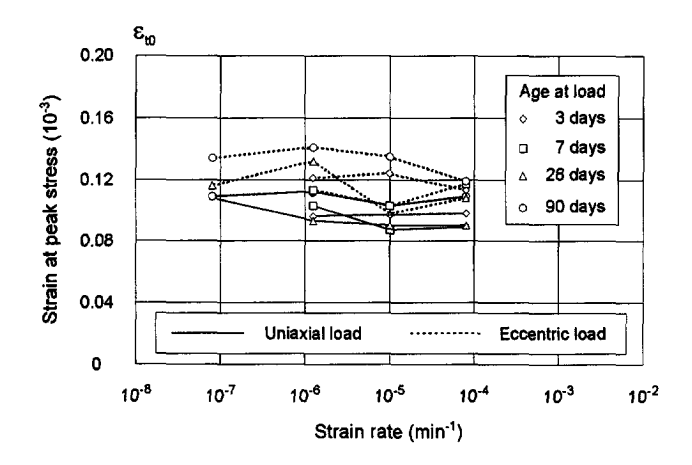


Fig. 3.8 The relationship between peak stress and loading rate for concrete specimens of different ages [after Kaplan (1980)].

3.1.3 Influence of strength of concrete

Two concretes of widely different compressive strengths tested at several strain rates which ranged from 10⁻⁶ to about 10 s⁻¹ (from static to dynamic loading) were adopted in the research of Watstein (1953). The cylindrical compressive strengths of the two concretes were 17.2 MPa and 44.8 MPa respectively. The results indicate that there is a slight increase in the effect of loading rate as the strength of concrete increases. Average ratios of the peak stresses at the highest rate and the lowest rate were 1.84 for concrete with lower strength and 1.85 for concrete with higher strength.

Rasch (1962) varied the concrete strength from 23 N/mm² to 59 N/mm² in his research on the effect of the strain rate. The results showed that the reduction in strength of concrete was 7.9% and 11% respectively as the strain rate decreased from 1.66×10^{-5} s⁻¹ to 1.66×10^{-9} s⁻¹

Dhir and Sangha (1972) reported that they have carried out a research programme to study the strain rate effect on two sandstone (also called 'natural stone'), having strengths of 73 and 115 N/mm². It was found that the reduction in strength as the loading time to failure increased from 10 min to 5 years was 6.5% and 22% respectively.

The investigation on the strain rate sensitivity carried out by Harsh, Shen and Darwin (1990) with saturated cement and mortar by using various water/cement ratios indicated that the strain rate sensitivity of the cement paste and the mortar seems to be independent of the strength. They pointed out that the main reason for the apparent controdiction is that the earlier studies that show a greater relative strength enhancement of lower strength concrete with increasing loading rate were performed under stress-control or at 'constant loading head speed' rather than strain-control. In either case, the strain rate will increase more near the peak stress for weaker concretes than for stronger concretes. Therefore, the weaker concretes were really subjected to a higher strain rate and should be expected to show more strength enhancement than stronger concretes.

Concluding Remarks

According to Mindess (1985) the principal parameters which determine the strength of concrete are total porosity, pore size distribution and the presence of flaws in concrete. Higher strength concrete normally can be symbolized as having a smaller total porosity, a more uniform pore size distribution and less flaws (such as air voids). Because of these reasons it is logical to predict that higher strength concrete will show a higher rate sensitivity than normal strength concrete due to higher pore-water pressure as the strain rate increases

3.1.4 Influence of method to control strain (or stress) rate

Besides the factors which could influence the rate-sensitivity of concrete, the contradictory results found by various researchers may be attributed to the variations of rate-control methods. In the test process various rate-control ways (such as loading rate control, longitudinal strain rate control or transverse strain rate control) could give different results. Therefore, some results of previous investigations carried out by different researchers are not comparable with each other. Since the stress-strain curve of concrete is non-linear, especially near the peak stress area, where the strain increases significantly while

stress nearly remains constant, constant loading rate control tests may result in higher strain rates near the peak stress area than constant strain rate control tests. In comparison with normal strength concrete, it is found that high strength concrete shows significantly smaller amounts of cracking at all stress levels, consequently resulting in relatively linear ascending part of the stress-strain curve [Carrasquillo, Slate and Nilson (1981); Ngab, Slate and Nilson (1981); Smadi and Slate (1989)]. Therefore, the difference between the two rate control methods is less as the strength of the concrete increases. There is the third possibility to control the strain rate in tests if the compressive strength of concrete is very high. Shah, Gokoz and Ansari (1981) pointed out that in order to gain a stable failure and a complete stress-strain curve, transverse strain control is needed. Because the change rates of longitudinal and transverse strains are different (depending on Poisson's ratio), diverse results could be expected as two rate control methods are adopted. As the stress level raises, the transverse strain increases faster than the longitudinal strain does. In the case of transverse strain rate control test, the corresponding longitudinal strain rate would be lower as the stress level approaches the peak stress. Accordingly, dissimilar results would be created. Differences are illustrated in Fig. 3.9 if various rate control methods are used.

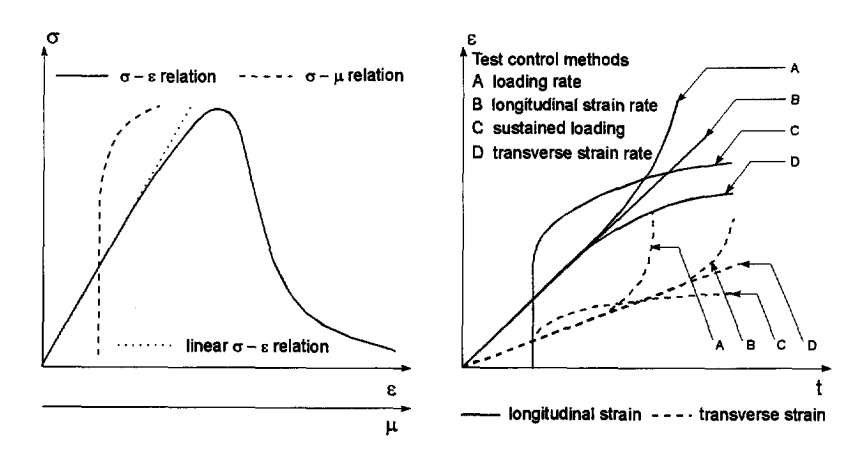


Fig. 3.9 Illustrations of the different responses of concrete with various test control methods [after Han (1992)].

In Fig. 3.9 there is another so-called sustained loading method which is world-widely adopted in creep tests. Rüsch (1960) indicated that this loading method is close to that in actual structures, where the load is applied relatively quickly and is then kept constant. In Fig. 3.10 Rüsch pointed out that for failure after a given period of time, sustained loads lead to somewhat lower failure loads than loads applied at constant strain rates. It is clear

that in the case of a sustained load the initial stress level is critical, since loaded concrete is normally subjected to two opposite effects. The strength reduction caused by a sustained load is counteracted by the strength increase with time. If the initial stress level is relatively lower (for example, less than 30% of the peak stress), the final strength obtained under a sustained loading (loaded to failure after the sustained loading period) is higher than that under the constant rate control loading. This beneficial effect is explained by Kaplan (1980) on the basis of a more homogeneous distribution of the water within the solid phase as well as by crystals positioning themselves in a more stable condition. Hughes and Ash (1970) attributed this factor to the closure of microcracks due to autogenous healing, particularly in concretes loaded at an early age. Coutinho (1977) suggested that increases in strength are due to forced hydration.

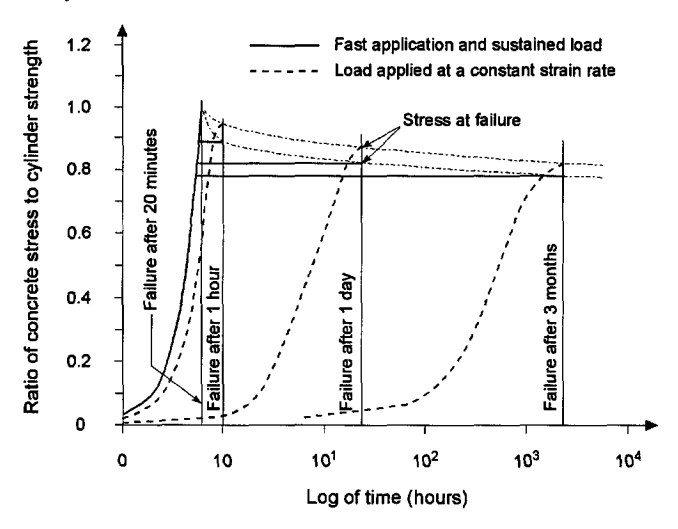


Fig. 3.10 Influence of type of loading on ultimate strength of concrete [after Rüsch (1960)].

As far as rate sensitivity is concerned, the way to control the rate plays a very important role. Since in different rate ranges the sensitivity of concrete to the rate is different, it is unjustified to make direct interpretations of testing results without considering the rate control method. However, the question about which way of loading control is more unfavourable is remaining open. According to Smadi, Slate and Nilson (1985) the long-term sustained strength of high strength concrete (59-69 MPa) is found to be higher than that of normal strength concrete (21-41 MPa), being about 80 to 85 percent of its short-term strength for high strength concrete and about 75 to 80 percent of its short-

term strength for normal strength concrete. Ngab, Nilson and Slate (1981) even indicated that the ratio of the sustained loading strength to the short-term strength is as high as 85 to 95 percent for high strength concrete (70 MPa). The effect of a high sustained load is related to internal microcracking.

3.1.5 Summary

The important factors which strongly influence the rate sensitivity of concrete such as curing conditions, strength of concrete, age at testing and rate control methods can be related to the internal structure of concrete, especially the moisture distribution inside the concrete. Free water, pore distribution and pore size may play a dominant role. However, initial flaws like microcracks are also very important. As the load is applied to the concrete, free water situated in the stressed regions tries to flow through the pore channels to the unstressed areas. Thus, the capability of flowing of free water is decisive for the rate sensitivity of the concrete. On the other hand, the pore water pressure also depends on the size of the pores. Smaller sizes of pores will create larger pore pressures. Generally speaking, the rate sensitivity of the concrete is a function of the pore size (also including flaw size), and the changing rate of size (various loading or strain rates). Hence, any parameter which affects the physical structure of the solid phase, such as curing conditions, age, growth and development of cracks will also affect the rate sensitivity. It is now worldwidely accepted that the internal structure of high strength concrete is fundamentally different from that of normal strength concrete. High strength concrete is regarded to be characterized by finer pore size, uniform pore distribution, less flaws and higher density. All these features could lead to a relatively increased difficulty of movement of free water inside the concrete, resulting in a larger sensitivity to the strain rate. That is the reason why more attention should be paid to this fundamental difference and why improved knowledge about this behaviour of high strength concrete is definitely needed.

3.2 Influence of strain gradient in compression

In concrete structures, most load-bearing elements (such as beams, columns, slabs) experience strain gradients. This fact was recognized already in the early days of application of concrete. However, up to now, the applicability of concrete properties obtained from centric compressive tests to situations where strain gradients prevail still remains questionable. During the last several decades, various research programs were carried out world-widely in order to fully understand the fundamental differences between uniform strain distribution and strain gradient. Most of this work focused on the development of a

new theory for flexure of concrete structures, especially in the period that the ultimate strength design method became popular around the world.

Hognestad, Hanson and McHenry (1955) conducted an investigation with the primary objective of developing a test method leading to an improved quantitative understanding of concrete stress distribution in flexure. They developed a test method in which a 127 × 203 mm unreinforced concrete sections were loaded with an eccentricity that was varied during each test. Furthermore, by numerical differentiation, the flexural stress-strain relationship of the concrete was determined from zero load to failure. A striking similarity was found between flexural stress-strain relations and those obtained in concentric compressive tests of cylinders. This led to the conclusion that the effect of the strain gradient on concrete behaviour was negligible.

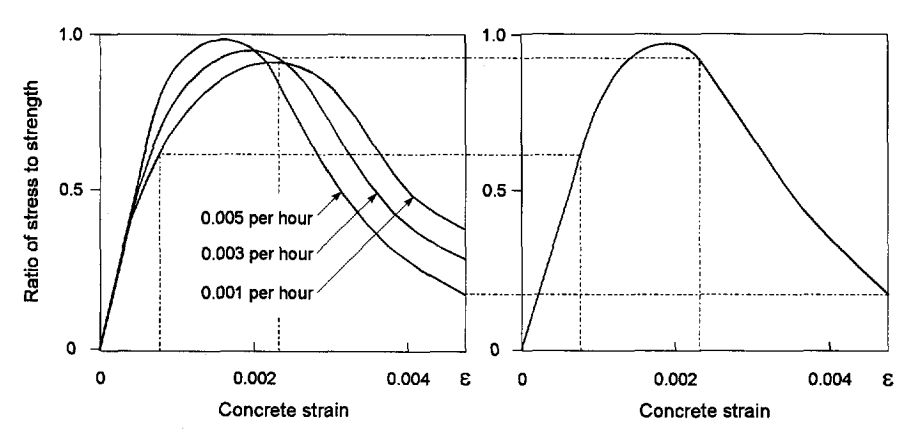


Fig. 3.11 Determination of stress-strain relationship in flexure (schematic only). Stress-strain curves for centric compression and various strain rates (left). Stress-strain relationship for eccentric compression after one hour of loading at constant strain rates [after Rüsch (1960)].

Based on the principle developed by Hognestad, Hanson and McHenry (1955), an apparatus was developed by Smith (1960) in order to determine the compressive stress-strain properties of concrete in flexure. He also developed a theoretical method which enables the distribution of the stress in the concrete to be determined across the section, without reference to the magnitude of the strain. The comparison was made between the theoretical strains and the experimental strains obtained during a test on a concrete prism. No big difference was found between these two cases, although the theoretical strains and experimental strains vary a little, which is explained by the author as a result of the

divergence from the basic assumptions of the theoretical analysis, in which creep is ignored and the concrete is assumed to be homogeneous and isotropic.

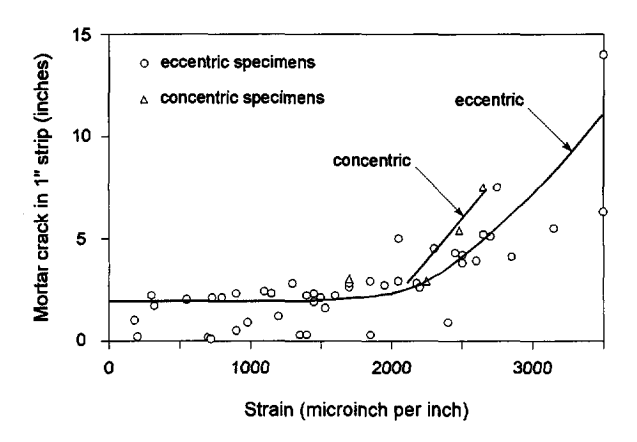


Fig. 3.12 The relationship between mortar cracking, strain and strain gradient [after Sturman, Shah and Winter (1965)].

Rasch (1962) advocated a method, which was also quoted by Rüsch (1960), based on the principle that in a compression zone of constant depth, whose extreme fibre is strained at a constant rate, every other element of the cross section is also subjected to a constant but different rate of strain. Its magnitude depends on the distance of the element from the neutral axis. If the strain of a particular element at any chosen time is known, its stress can be directly read from the stress-strain curve corresponding to its particular rate of strain. This stress-strain curve is obtained from the results of concentric tests carried out under that specific constant strain rate. In this way, the stress distribution over the entire cross-section can be found at any given time. The derivation of the stress-strain relationship in the concrete compression zone in flexure is schematically shown in Fig. 3.11. According to this concept, the differences between concrete behaviour in compression and flexure are due to the combined action of the strain gradient and the resulting strain rate variation.

In order to develop further understanding of the behaviour and failure mechanism of flexural members the influence of strain gradients on the microcracking phenomenon was studied by Sturman, Shah and Winter (1964, 1965) and Shah and Slate (1965). The stress-strain behaviour of plain concrete loaded concentrically and eccentrically was compared. It was found that the strain gradient retards microcracking, especially mortar cracking as

compared to cracking at the same strain in centric compression. It is pointed out that, if the strain gradient affects the microcracking, it is possible that the stress-strain relationship in eccentric compression may be different from that in concentric compression. In order to test this hypothesis based on the retarding effect of a strain gradient on the development of microcracking, the stress-strain relationship in eccentric compression was investigated by a combined experimental-analytical approach using statistical methods. The results of an extensive analysis indicated that the stress-strain curve, if a strain gradient exists, differs materially from that for concentric compression. The peak stress of a stress-strain curve in flexure occurs at a stress of about 20 percent larger than that in centric compression, while the strain under peak stress in flexure is about 50 percent higher than that in centric compression. The effect of the strain gradient on the microcracking and the stress-strain relationship is shown in Fig. 3.12 and 3.13, respectively.

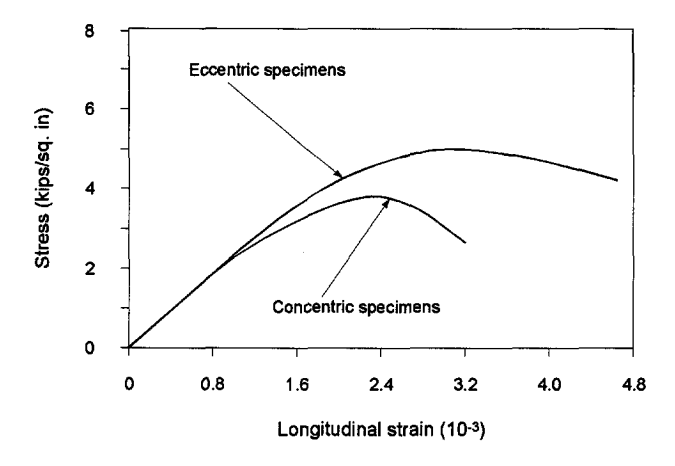


Fig. 3.13 The relationship between stress and strain [after Sturman, Shah and Winter (1965)].

In the discussion of the investigation of Sturman, Shah and Winter (1964), Barnard (1964) indicated that the peak stress and the shape of the concrete stress-strain curve has an insignificant effect on the theoretical ultimate or maximum moment of resistance of a particular cross-section. However, an increase of the strain at maximum stress will result in a considerable increase in curvature at maximum moment and a decrease in the slope of the falling branch of the moment-curvature curve. He pointed out that if the maximum stress and the corresponding strain are greater in flexure than in centric compression, the use of a stress-strain curve obtained in concentric compression would result in conservative predictions of the behaviour of structural elements in which strain gradients exist. Rich

(1964) even suggested that the ultimate stress in the widely accepted equivalent mathematical model should be increased to a value closer to the cylinder strength obtained by the concentric compressive test without sacrificing any factor of safety.

Swamy (1966) quoted the results of the investigation carried out by Slater and Lyse (1930), which concerned the effect of strain gradient on the behaviour of concrete. It was found that the maximum compressive stress developed in $200 \times 200 \times 300$ mm prisms loaded at the edge of the middle third of the cross-section was about 20 percent larger than the strength of the control cylinders from the same mix. This results seem to be further confirmed by that from Sturman, Shah and Winter (1965). Swamy pointed out that in a concentric compression test, every transverse section is under the influence of a uniform tensile field, while under eccentric loading, the strain gradient produces a nonuniform or even a tension-compression field which retards and reduces cracking. The presence of compression has an inhibiting influence on tensile crack propagation.

Clark, Gerstle and Tulin (1967) conducted a series of tests in which the effect of a strain rate and a strain gradient could be separated. The purpose of this investigation was to study the relative significance of these two effects. An experimental procedure was developed, which provided for the individual control of bending and axial loads permitting the maintenance of a constant strain gradient under uniform strain rates, making it possible to separate these two effects. In their research, the stress-strain curves were examined for three critical parameters: the maximum stress, the strain corresponding to the maximum stress and the maximum strain. It was found that if the strain gradient increased, the ultimate strain increased for all combinations of materials and strain rates. The maximum ratio of the ultimate strain under the maximum gradient to that under a zero gradient was between 1.3 to 1.5 for the mortar tests, and about 1.15 for the concrete tests. However, the maximum stress appeared to be independent of the strain gradient. This is at variance with results from Sturman, Shah and Winter (1965). To reconcile this conflict, the authors indicated that in those tests without controlling the strain gradient, a differential strain rate prevailed for different fibres of the specimen. Consequently, they concluded that it is the strain rate in stead of the strain gradient which influences the behaviour of concrete in flexure.

An experimental research program was carried out by Karsan and Jirsa (1970) in order to determine the applicability of stress-strain relationships obtained for concrete under repeated concentric loadings to concrete subjected to repeated eccentric loadings. Various strain gradients were adopted in this investigation, while the time effects were excluded, namely, the strain rate was held constant throughout. It was indicated that for steadily increasing strains to failure, the stress-strain curve for concrete under a strain gradient was essentially the same as for concentric compression for the specimens tested. The only

deviation was observed for strains in the descending part of the stress-strain curve. There was an apparent upward shift of the declining portion under a strain gradient.

In his considerable work concerning the stress-strain relationship of concrete, in addition to other important parameters, Sargin (1971) also took the strain gradient into account. He pointed out that in the evaluation of different results, two points should be kept in mind. At first, a larger ultimate strain measurement in flexure does not necessarily mean that the stress-strain relationships in flexure and centric compression are different, since the maximum resistance capacities of a section under flexure and direct compression correspond to different maximum strain values, even when the same stress-strain curve is used. In direct compression the failure takes place at maximum stress, i.e. $\varepsilon_{cu} = \varepsilon_{c0}$, while the ultimate strains in flexure are always larger than ε_{c0} and are dependent on the shapes of the stress-strain relations used. At second, in practice the strain gradient changes during loading. Therefore, in order to fully understand the different behaviour of concrete in flexure and in compression, the action of strain rates and strain gradients has to be combined.

On the basis of the stress-strain relationship proposed by Sargin (1971), Sargin and Ghosh (1971) carried out an experimental investigation in which concrete strength, specimen size, spacing and grade of lateral reinforcement, strain gradient and thickness of cover were taken into consideration. From the analysis, the authors indicated that the strain gradient has no effect on the peak stress. However, it causes 25% and 10% increases in the values of the strain related to the peak stress and E-modulus, respectively. Based on this conclusion, a more general model was developed for the stress-strain relationship of plain concrete under both concentric and eccentric compression.

In order to study more thoroughly the differences between the stress-strain curves for compression and for flexure, Morita and Adachi (1972) carried out flexural and compression tests on prismatic specimens and compression tests on control cylinders for a wide range of strengths of normal-weight and all-lightweight concrete. Through this research, the authors found that there are many factors which might influence the shape of the stress-strain curves for flexure and for compression. These factors include the strain gradient as an internal-crack retarder, the shape and dimensions of the test specimen, the gage length and location of strain measurement, etc. After careful analysis, the authors indicated that the peak of the flexural curve was at a higher stress and at a larger strain than the peak of the concentric compression curve of the prismatic specimens. The authors also implied that high strength concrete and all-lightweight concrete are likely to rupture in conventional compression tests of cylindrical specimens at a stress lower than the peak stress of the flexural curve.

Concluding Remarks

As it can be seen from the above survey, the effects of a strain gradient on the concrete behaviour are not completely known. However, qualitatively the following comment can be made concerning the stress-strain relationship of concrete under flexural compression. The stress-strain curves obtained from flexure or eccentrically loading are not identical with that from concentric compression. The peak points of the stress-strain relationships for eccentric loading are located at higher strains and also perhaps higher stresses than the peak points of the corresponding curves for concentric compression. The most arguments point at an increase of the peak stress in flexure while the point of large increase of strain under the peak stress seems to be generally agreed. Possibly the testing method also plays a very important roll. In order to reconcile the conflict from various researches, this point has to be taken into account. If all of these investigations are reorganized according to their strain control method, generally speaking, they can be divided into three groups. The investigations from Karsan and Jirsa (1970), Sargin and Ghosh (1971), Morita and Adachi (1972) belong to one group, where during the test the strain of one face of the specimen is kept at zero while simultaneously the load is increased. Theoretically the method of Rasch (1962) and Rüsch (1960) also can be incorporated into this group. In this case, if the strain rate of the extreme fibre increases constantly, the strain gradient also increases at a constant rate. In the second group, the research of Sturman, Shah and Winter (1965) has to be mentioned. In this investigation, a constant eccentricity is held during the whole loading process. Because of the transverse deflection in the eccentric compressive tests of prismatic specimens, the strain gradient introduced by the eccentricity varies irregularly. Consequently, the strain rate of various fibres also changes irregularly. In the third group, Clark, Gerstle and Tulin (1967) carried out a research programme in order to separate the effects of strain rate and strain gradient. In their test, an initial strain gradient is adopted, which is held constant during the entire test, whereas, various strain rates are used. However, if the initial effect is neglected, which is also pointed out by the authors, this method is nearly the same as the concentric situation, in which all fibres are subjected to the same strain rate. Through this careful comparison of the testing methods it can be clearly seen that the effects of strain rate and strain gradient can not be separated. They have some logical relation. In practice, such as in the case of a reinforced concrete beam, the strain gradient varies quite irregularly, causing very different strain rates in different fibres, resulting in a different stress-strain relationship.

3.3 Modelling of the influence of the strain rate and the strain gradient

In comparison to numerous models describing the stress-strain behaviour of concrete without considering the rate effect [Popovics (1970)], rare cases could be surveyed concerning modelling the behaviour of concrete under the influence of strain rate and strain gradient. Here two cases are reviewed separately.

Desayi (1968) had developed a simple model to represent the strength and deformation characteristics of concrete when subjected to a rate of strain, a rate of stress or creep or relaxation testing under centric compression. This model is simply described as follows: the specimen under test is assumed to consist of a large number of elements and f is the load that a single element can carry; at the compressive strain ε_c the number of elements carrying the load are $N(\varepsilon_c)$ so that the total load which can be carried by the specimen is

$$F = f \cdot N(\varepsilon_c) \tag{3.1}$$

Assuming that the individual elements behave elastically, the load f carried by the element can be related to the strain ε_c according to

$$f = \frac{\varepsilon_c}{k} \tag{3.2}$$

where k is a constant. Substituting Eq. (3.2) in Eq. (3.1), we have

$$F = \frac{\varepsilon_c}{k} \cdot N(\varepsilon_c) \tag{3.3}$$

As the strain ε_c increases, the number of elements available to share the total load F decreases because of the nonhomogeneity of the material. Thus $N(\varepsilon_c)$ can be assumed according to

$$N(\varepsilon_c) = \int_{t_c}^{\infty} \frac{1}{a} \cdot e^{-\frac{u}{a}} du \tag{3.4}$$

where a is a constant. Integrating Eq. (3.4) and substituting in Eq. (3.3), we have

$$F = \frac{\varepsilon_c}{k} \cdot e^{-\frac{\varepsilon_c}{a}} \tag{3.5}$$

If σ_{cmax} and ε_{c0} are the peak stress and the strain related to the peak stress, we get from Eq. (3.4):

$$\sigma_{c \max} = \frac{a}{e \cdot k}$$
 and $\varepsilon_{c0} = a$ (3.6)

and thus, Eq. (3.5) can be written as

$$\sigma_c = \sigma_{c \max} \cdot \left(\frac{\varepsilon_c}{\varepsilon_{c0}} \cdot e^{1 - \frac{\varepsilon_c}{\varepsilon_{c0}}} \right)$$
 (3.7)

where σ_c is the stress at the strain ε_c .

It was shown by Rüsch (1960) that the strength of concrete under a sustained load is about 80% of that under the standard short term test. Let f_{cm} be the strength of the concrete obtained from a standard short term test, the reduced strength can be assumed to be τ_{cm} . The limits for τ_r are zero for the standard rate and $\tau_{r\infty}$ for the creep limit. The reduction of the strength at any instant is

$$R_s = f_{cm} \cdot \left(\frac{\tau_r}{1 - \tau_{rm}} \cdot \frac{t}{t_{c0}} \right) \qquad \text{for} \qquad 0 < \frac{t}{t_{c0}} < 1 - \tau_{rm}$$
 (3.8)

$$R_s = f_{cm} \cdot \tau_r \qquad \qquad \text{for} \qquad \frac{t}{t_{c0}} \ge 1 - \tau_{r\infty} \tag{3.9}$$

where t_{c0} is the time in which the strain ε_{c0} is reached. From Eqs. (3.7), (3.8) and (3.9) the stress-strain relationship for concrete under a controlled strain rate is

$$\sigma_c = f_{cm} \cdot \left(\frac{\varepsilon_c}{\varepsilon_{c0}} \cdot e^{1 - \frac{t_c}{\varepsilon_{c0}}} \right) \cdot \left(1 - \frac{\tau_r}{1 - \tau_{roc}} \cdot \frac{t}{t_{c0}} \right) \qquad \text{for} \qquad 0 < \frac{t}{t_{c0}} < 1 - \tau_{roc}$$
 (3.10)

$$\sigma_c = f_{cm} \cdot \left(\frac{\varepsilon_c}{\varepsilon_{c0}} \cdot e^{1 - \frac{\varepsilon_c}{\varepsilon_{c0}}} \right) \cdot \left(1 - \tau_r \right) \qquad \text{for} \qquad \frac{t}{t_{c0}} \ge 1 - \tau_{r0} \tag{3.11}$$

For a computation using this equation, the variations of ε_{c0} and τ_r with the time of the test have to be known. Desayi has checked the stress-strain curves available in the Recommendations for an International Code of Practice [ACI and CCA (1963)] by using this model. The variations of strain under the peak stress and the factor of strength

reduction with time are shown in Fig. 3.14. The results of this calculation are illustrated in Fig. 3.15.

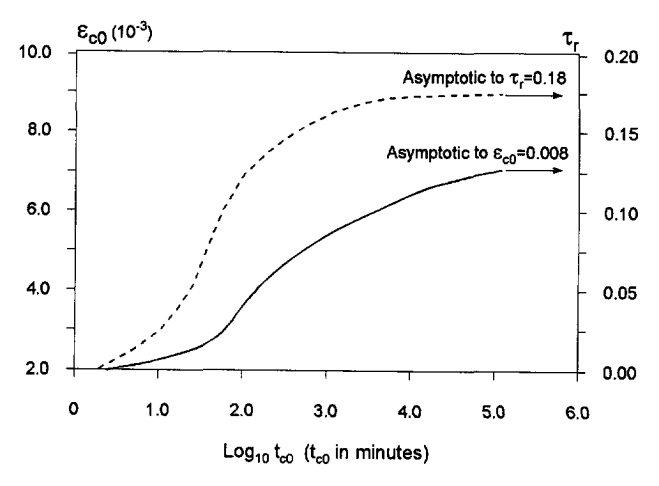


Fig. 3.14 The variation of ε_{c0} and τ_r with time t_{c0} [after Desayi (1968)].

Sturman, Shah and Winter (1965) developed an analysis for the determination of the stress-strain relationship of concrete in the existence of a strain gradient, based on using a 'least squares' method, which was later also adopted by Clark, Gerstle and Tulin (1967), Smith and Orangun (1969). This method is based on the following assumptions: 1) Equilibrium of internal and external forces and moments must be maintained; 2) Sections plane before loading remain plane under load; 3) The concrete stress is a function of the strain only, i.e., $\sigma_c = f(\varepsilon_c)$. As far as the tensile strain (or minimum compressive strain) is concerned, Smith and Orangun neglected it. They assumed that the concrete below the neutral axis is cracked and offers no contribution to the flexural strength. On the other hand, Sturman, Shah and Winter took this into account. They presumed that the stress-strain function in tension is the same as that in compression. The tensile strain at which the crack occurs was taken at a value of 0.0001. They further indicated that this value is insensitive to the final results. The notation for the analysis is shown in Fig. 3.16. According to the assumptions mentioned above, the following mathematic equations can be set up.

Equilibrium condition:

$$\sum F = 0 \qquad F = \int_0^x f(y) \cdot b \cdot dy \mp \int_0^{|d-x|} f(y) \cdot b \cdot dy \qquad (3.12)$$

$$\sum M = 0 \qquad M = \int_0^x f(y) \cdot y \cdot b \cdot dy \mp \int_0^{|d-x|} f(y) \cdot y \cdot b \cdot dy$$
 (3.13)

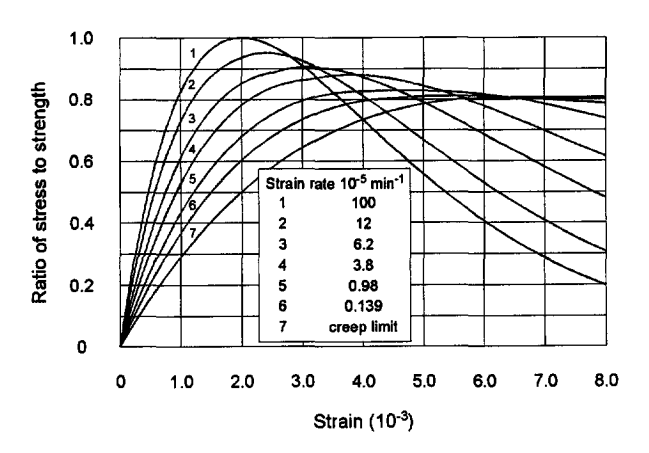


Fig. 3.15 Stress-strain relationships computed from the proposed model for testing under strain rate control [after Desayi (1968)].

Plane sections remain plane:

$$\varepsilon_c = y \cdot \frac{\varepsilon_{cc}}{x}$$
 $y = x \cdot \frac{\varepsilon_c}{\varepsilon_{cc}}$ $dy = x \cdot \frac{d\varepsilon_c}{\varepsilon_{cc}}$ $x = d \cdot \frac{\varepsilon_{cc}}{\varepsilon_{cc} - \varepsilon_{ct}}$ (3.14)

Using Eq. (3-14), the equilibrium conditions become:

$$P = \frac{b \cdot x}{\varepsilon_{cc}} \cdot \left[\int_0^{\varepsilon_{cc}} f(\varepsilon_c) \cdot d\varepsilon_c - \int_0^{|\varepsilon_{cc}|} f(\varepsilon_c) \cdot d\varepsilon_c \right]$$
 (3.15)

$$M = \frac{b \cdot x^2}{\varepsilon_c^2} \cdot \left[\int_0^{\varepsilon_c} f(\varepsilon_c) \cdot \varepsilon_c \cdot d\varepsilon_c \mp \int_0^{\varepsilon_d} f(\varepsilon_c) \cdot \varepsilon_c \cdot d\varepsilon_c \right]$$
 (3.16)

Stress-strain relationship in flexure:

$$\sigma_c = f(\varepsilon_c) = a_1 \cdot \varepsilon_c + a_2 \cdot \varepsilon_c^2 + \dots + a_n \cdot \varepsilon_c^n$$
(3.17)

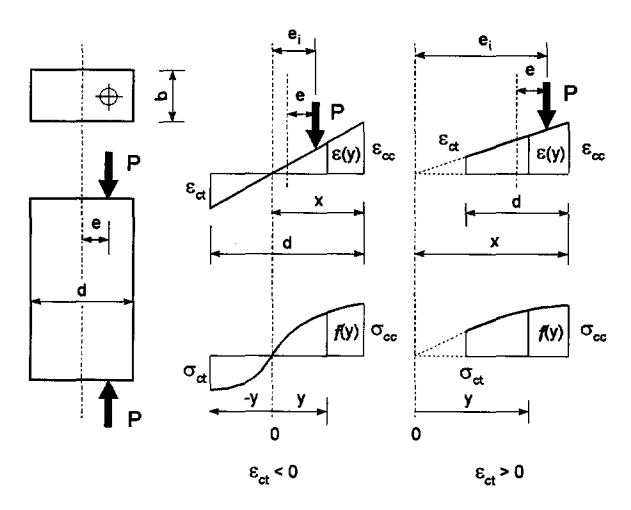


Fig. 3.16 Notation for analysis of eccentrically compressed prism [after Sturman, Shah and Winter (1965)].

If K sets of data triplets P_b ε_{ccb} ε_{cti} are obtained from tests, the differences between calculated values using Eqs. (3.15), (3.16) and (3.17) and measured value P_i and M_i can be computed as follows:

$$M_i = P_i \cdot \left(e + x - \frac{d}{2} \right) \tag{3.18}$$

$$X_i = P_{ci} - P_i$$
 $Y_i = \frac{M_{ci} - M_i}{e_i}$ (3.19)

where P_{ci} and M_{ci} come from Eqs. (3.15) and (3.16) for the *ith* set of data. The least squares criterion is to find those values of a_1 , a_2 ,..., a_n that will minimize:

$$Z^{2} = \left[f(a_{1}, a_{2}, \dots, a_{n}) \right]^{2} = \sum_{i=1}^{k} \left(X_{i}^{2} + Y_{i}^{2} \right)$$
(3.20)

This leads to n simultaneous equations for the coefficients given by:

$$\frac{\partial Z}{\partial a_1} = 0$$
, $\frac{\partial Z}{\partial a_2} = 0$, ..., $\frac{\partial Z}{\partial a_n} = 0$ (3.21)

Sturman, Shah and Winter (1965) assumed that $a_2 = ... = a_{n-1} = 0$, therefore, the stress-strain relationship becomes:

$$\sigma_c = f(\varepsilon_c) = a_1 \cdot \varepsilon_c + a_2 \cdot \varepsilon_c^n \tag{3.22}$$

The procedure is repeated for a series of values of n. Each chosen value of n will yield a different pair of values of a_1 and a_n to minimize Z^2 . The best value of n is that which gives the lowest of these values of Z^2 . The following function is obtained from calculations of 370 data points:

$$\sigma_c = f(\varepsilon_c) = 4.13 \times 10^3 \cdot \varepsilon_c - 80.4 \times 10^3 \cdot \varepsilon_c^{1.6} \tag{3.23}$$

where σ_c is the stress in ksi.

On the basis of the principle of Sargin (1971), Dilger, Koch and Kowalczyk (1984) have developed a model in which the effect of a strain rate is taken into consideration. The strength of plain concrete subjected to a strain rate *de/dt* can be expressed as:

$$f_{cr} = f_{cm} \cdot \left(1.14 + 0.03 \cdot log \frac{d\varepsilon}{dt} \right) \quad \text{for} \qquad \frac{d\varepsilon}{dt} < 1.6 \times 10^{-5}$$
 (3.24)

$$f_{cr} = f_{cm} \cdot \left(1.38 + 0.08 \cdot log \frac{d\varepsilon}{dt} \right) \text{ for } \frac{d\varepsilon}{dt} > 1.6 \times 10^{-5}$$
 (3.25)

The strain under the peak stress can be represented by the following equations:

$$\varepsilon_{c0} = \left(13 - 0.06 \cdot log \frac{d\varepsilon}{dt} + 0.07 \cdot f_{cm}\right) \times 10^{-3} \quad \text{for} \quad \frac{d\varepsilon}{dt} < 1.6 \times 10^{-5}$$
 (3.26)

$$\varepsilon_{c0} = \left(0.5 - 0.23 \cdot \log \frac{d\varepsilon}{dt} + 0.07 \cdot f_{cm}\right) \times 10^{-3} \quad \text{for} \quad \frac{d\varepsilon}{dt} > 1.6 \times 10^{-5}$$
 (3.27)

The descending branch of the stress-strain curve is defined by the following stress and strain:

$$f_{cD} = \left(0.34 \cdot \sqrt{f_{cr}}\right) \cdot f_{cr} \tag{3.28}$$

$$\varepsilon_{cD} = \left[0.7 - 125 \cdot \left(f_{cm} \right)^{-0.7} \cdot log \cdot \frac{d\varepsilon}{dt} \right] \times 10^{-3} \quad \text{for} \quad \frac{d\varepsilon}{dt} < 1.6 \times 10^{-5}$$
 (3.29)

$$\varepsilon_{cD} = 0.7 - 6 \cdot \left(f_{cm} \right)^{-0.7} \qquad \text{for} \qquad \frac{d\varepsilon}{dt} > 1.6 \times 10^{-5}$$
 (3.30)

These parameters mentioned above define the stress-strain equation of the form:

$$\sigma_c = f_{cr} \cdot \frac{A \cdot \chi + (D-1) \cdot \chi^2}{1 + (A-2) \cdot \chi + D \cdot \chi^2}$$
(3.31)

where

$$A = E_{ci} \cdot \frac{\varepsilon_{c0}}{f_{cr}};$$

$$\chi = \frac{\varepsilon_c}{\varepsilon_{c0}};$$

 f_{cm} = cylinder strength of concrete (ksi);

 E_{ci} = initial modulus of elasticity;

 f_{cr} = the modified strength by considering the strain rate;

 ε_{c0} = strain corresponding to maximum stress;

$$D = [S_D + S_D \cdot (A - 2) \cdot v - A \cdot v] + \frac{v^2}{v^2 (1 - S_D)};$$

$$v = \varepsilon_{cD} \cdot \varepsilon_{c0}$$
;

$$S_D = \frac{f_{cD}}{f_{cD}}$$
.

3.4 Influence of strain rate (or stress rate) in tension

In comparison with the research work concerning the time-dependent behaviour of concrete in compression, there are much fewer publications with respect to the tensile behaviour of concrete, in particular, concerning the time-dependent behaviour. The lack of research work on the tensile behaviour of concrete is perhaps mainly due to two reasons. Firstly, concrete is from ten to twenty times stronger in compression than in tension. Hence, in structures, the principal load-bearing function of concrete is to carry compressive stresses, whereas tensile stresses are carried by reinforcement or prestressing tendons. The tensile capacity of concrete is largely ignored by structural engineers during design work.

Secondly, the application of a truly uniaxial tension presents considerable difficulty. Specially, with regard to time-dependent tensile tests, there are additional problems: since the applied stress is relatively low, the related strains to be measured are low too. Therefore, it is difficult to obtain accurate results. Furthermore, if concrete is drying during loading, shrinkage may be concurrent, which is several times larger than creep. Consequently, a larger error may exist in the calculated time-dependent deformation.

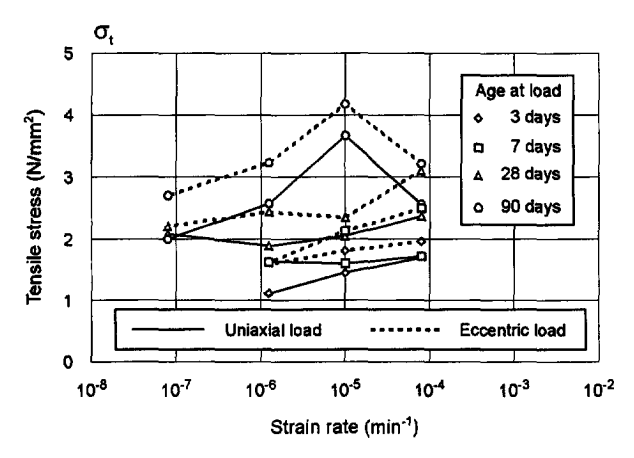


Fig. 3.17 Influence of strain rate and age at load on peak stress of a concrete with 28-day strength of 22.5 N/mm² [after Heilmann, Hilsdorf and Finsterwalder (1969)].

However, increasing emphasis on economy in design implies that the structural engineers need to understand the tensile behaviour of concrete. For example, the onset and prediction of cracking in the tensile zone of reinforced concrete members, which has direct relevance for the design of water-retaining structures or structures with specific durability requirements, are dependent on the tensile properties of concrete. Moreover, the failure in shear of reinforced concrete structures occurs by diagonal tension cracking and therefore shear strength is directly related to the tensile strength of concrete. In addition, design of many plain concrete structures, such as unreinforced concrete pipes, footings, must take the tensile behaviour of concrete into account. [Hillerborg (1991)].

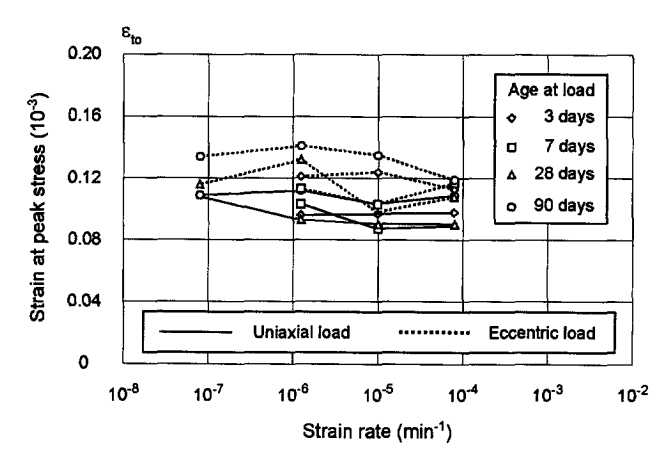


Fig. 3.18 Influence of strain rate and age at load on strain at peak stress of a concrete with 28-day strength of 22.5 N/mm² [after Heilmann, Hilsdorf and Finsterwalder (1969)].

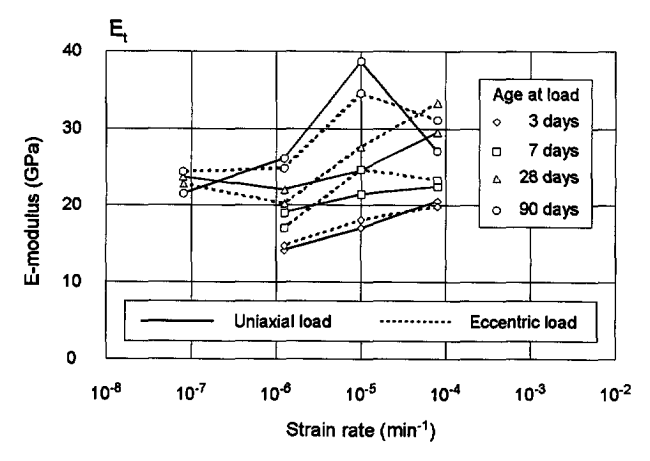


Fig. 3.19 Influence of strain rate and age at load on E-modulus of a concrete with 28-day strength of 22.5 N/mm² [after Heilmann, Hilsdorf and Finsterwalder (1969)].

A comprehensive experiment was carried out by Heilmann, Hilsdorf and Finsterwalder (1969) to investigate the influence of the age, strain rate and the compressive strength on the tensile behaviour of concrete. Four different strength classes (28-day strength of 14,

22.5, 35 and 45 N/mm²), four different ages at application of load (3, 7, 28 and 90 days) and four different strain rates (0.08, 0.01, 0.00125 and 0.00008 %/min.) were adopted in the experiment. All specimens were cured in the curing room with a temperature of 20 °C and a relative humidity of 65% till the test begins. In addition to the uniaxial tensile tests, the strain gradients were also used with the same variables (by means of eccentric tests and bending tests). The influence of strain rate and age at loading on the peak tensile stress, strain at the peak stress and E-modulus of one type of concrete are shown in Fig. 3.17, 3.18 and 3.19. The influence of strain rate and strength of concrete on the peak tensile stress is illustrated in Fig. 3.20.

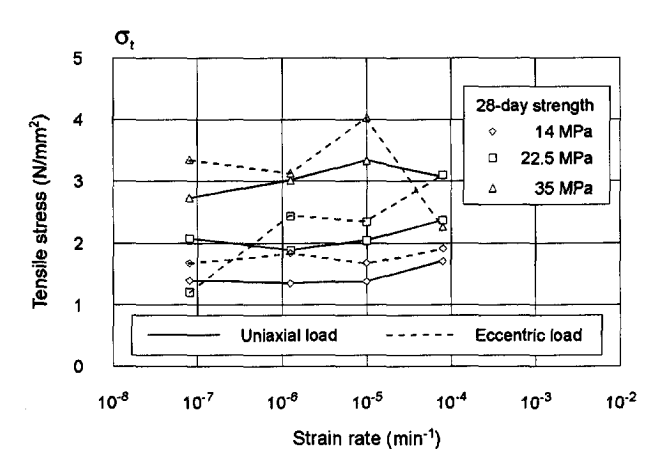


Fig. 3.20 Influence of strain rate and strength of concrete on the peak tensile stress [after Heilmann, Hilsdorf and Finsterwalder (1969)].

				· · · · · ·
type of load	uniaxial	eccentric	bending	_
at	0.55	0.66	0.86	-
age at load (days)	3	7	28	90
bt	0.68	0.79	1.00	1.27
strain rate (‰/min)	0.08	0.01	0.00125	0.00008
Ci	1.13	1	0.98	0.96

Table 3.III Parameters used in Eq. (3.32). [after Heilmann, Hilsdorf and Finsterwalder (1969)]

According to the authors, the peak stress and E-modulus of concrete are much more sensitive to the variation of strain rates than the deformation. On the basis of the

experiments, the following relation between the time-dependent tensile strength and the 28-day's compressive strength of concrete was proposed:

$$f_t(t) = a_t \cdot b_t \cdot c_t \cdot \left(f_{cm}\right)^{\frac{2}{3}} \tag{3.32}$$

where f_{cm} is 28-day compressive strength, and the parameters a_t , b_t , and c_t can be found in Table 3.III.

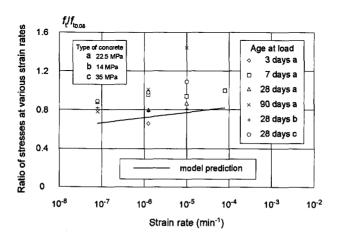


Fig. 3.21 Relationship between the tensile strength and the strain rate [after Heilmann (1976)].

Based on experimental results of Heilmann, Hilsdorf and Finsterwalder (1969), Heilmann (1976) carried out a further analysis on the influence of strain rate on the tensile behaviour of concrete. By using the strain rate of 0.08 %/min as a standard reference, all tensile properties can be derived through the least-square analysis:

$$\frac{\Theta}{\Theta_{0.08}} = A_r + B_r \cdot log \left(10^5 \cdot \frac{d\varepsilon}{dt} \right) \tag{3.33}$$

where Θ = peak stress, strain at peak stress or E-modulus at any strain rate;

 $\Theta_{0.08}$ = properties mentioned above at a strain rate of 0.08 %/min;

 A_r = peak stress 0.771, strain at peak stress 1.089, E-modulus 0.728;

 B_r = peak stress 0.054, strain at peak stress -0.025, E-modulus 0.063;

$$\frac{d\varepsilon}{dt}$$
 = strain rate used in tests (%/min).

One of the relationships is shown in Fig. 3.21. Similar to the method which Rasch (1962) used in the compressive situation, the stress distribution when a strain gradient exists is obtained on the basis of the assumption that each fibre in tensile zone is independently strained, and it only depends on the strain rate applied in that fibre. Just like in the case of compression, it is the ultimate strain that controls the behaviour of bending elements.

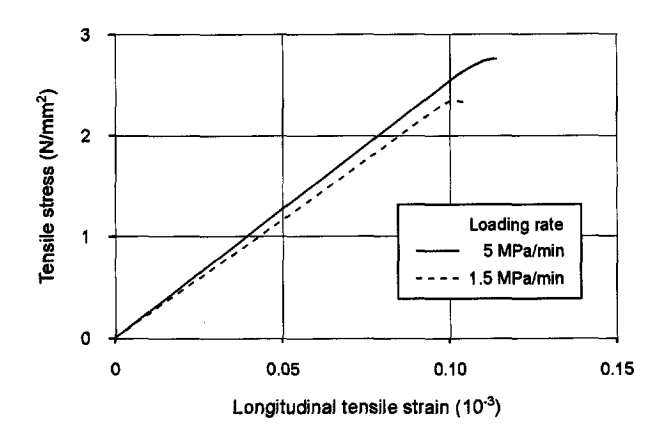


Fig. 3.22 Influence of loading rate on stress-strain relationship of concrete in uniaxial tension [after Komlos (1969)].

A research program was carried out by Komlos (1969) aiming at an investigation of the factors which influence the tensile behaviour of concrete. In his study, among other factors, the curing condition and the loading rate were considered by using three different concretes with various aggregate-cement ratio. It was found that water curing causes an increase of the strain value, whereas drying results in a decrease of the strain value. To examine the influence of the loading rate, two loading rates were used: 5 and 1.5 N/mm²/min. The tests show that a lower loading rate leads to a lower peak stress and a higher strain (see Fig. 3.22). Furthermore, the increase of the cement content causes a higher rate sensitivity of the concrete.

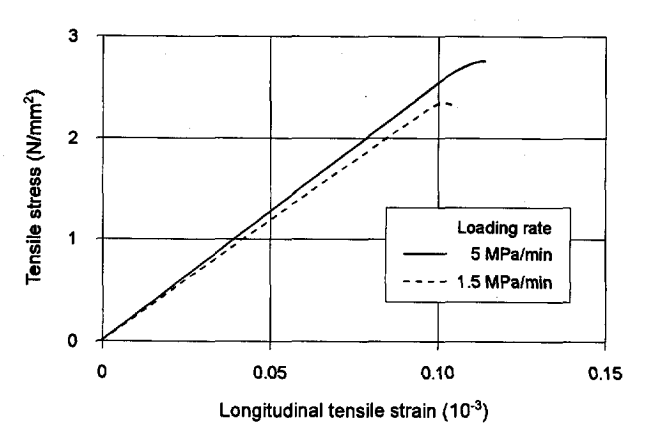


Fig. 3.23 The influence of sustained load on time to failure in tension [after Al-Kubaisy and Young (1975)].

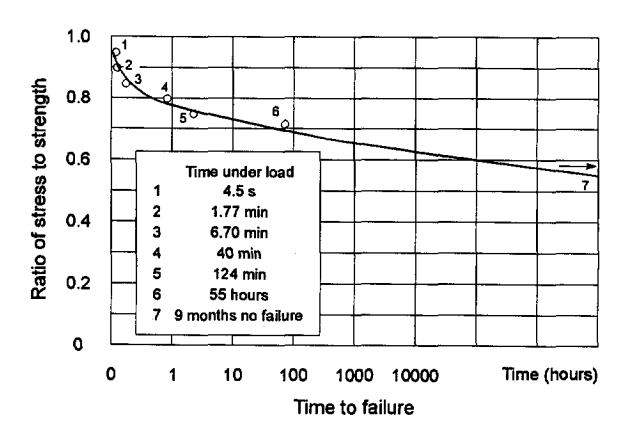


Fig. 3.24 The influence of sustained loading on the ultimate strain of concrete in tension [after Al-Kubaisy and Young (1975)].

To investigate the mechanism of cracking in concrete under sustained uniaxial tension, Al-Kubaisy and Young (1975) tested a series of concrete specimens with two loading regimes: rapid strength tests to failure (about 2.75 minutes from start of loading to failure) and sustained loading tests (loading level varying from 60% to 95% of rapid test strength).

All specimens were cured in water for 21 days, and afterwards, they were placed in a controlled environment of 65% RH and 20 °C for 7 days. A microscopic study of crack development at progressive stages of loading was also carried out. This study indicated that, even before loading, cracks can exist at the interface between the cement matrix and the aggregate. A large number of interfacial cracks begins to form at an applied stress between 20% to 30% of the rapid test strength. At higher stress levels, the interfacial cracks stabilize and do not grow up to a stress of about 70% of the rapid-test strength has been reached. Afterwards, cracks grow within the matrix and eventually link up with the interfacial cracks to produce failure. The results of the sustained loading tests demonstrated that the time to failure increases rapidly as the sustained load reduces (see Fig. 3.23). This is to say, there is a fracture limit envelope beyond which time-dependent failure will occur. The ultimate strain of concrete in tension tends to increase as the time to failure under sustained loading increases (see Fig. 3.24).

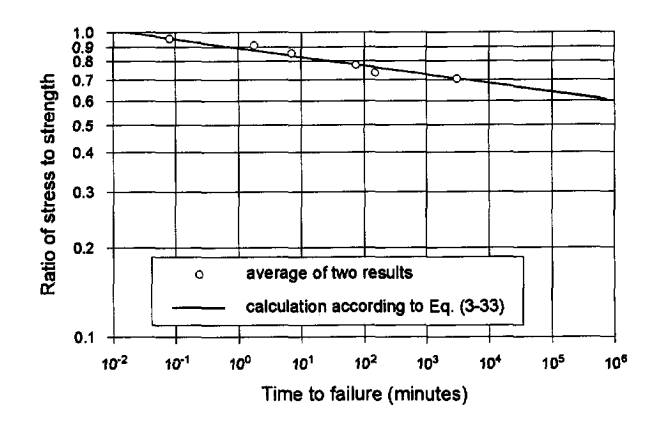


Fig. 3.25 Relationship between sustained stress and time to failure (log scales) [after Al-Kubaisy and Young (1975)].

By using Kachanov's law which models the failure with time by the growth of internal damage, Al-Kubaisy and Young (1975) derived a linear relationship between the logarithm of the time to failure t^* and the logarithm of the applied specific stress σ_i :

$$t^* = 0.016 \cdot \sigma_t^{-34.6} \tag{3.34}$$

where the time is in minutes. The high negative stress exponent in Eq. (3.34) reflects that the failure of concrete is unlike when it is stressed below 55% of the rapid test

strength. The time to failure at this stress level with the constant in Eq. (3.34) is about 30 years (see Fig. 3.25).

After a literature survey, Shkoukani and Walraven (1991) pointed out that the long-term tensile strength is not yet clearly defined. Its value strongly depends on at what rate of loading or straining the short-term tensile strength is obtained. It is also emphasized that, in many actual structures, strain gradients always exist. The time-dependent tensile behaviour under the influence of a strain gradient is not yet fully understood. Furthermore, it is also questionable if the classical sustained loading test is really representative in real situations. To answer the questions mentioned above, an experimental program was carried out. Three test categories were disdinguished in their study: uniaxial sustained loading tests; eccentric sustained loading tests and tests with combinations of loading rates and strain gradients. All concrete specimens were cured in a climate-conditioned room with a temperature of 20 °C and a relative humidity of 60%. The tests were carried out at an age of 28-40 days after casting of the concrete.

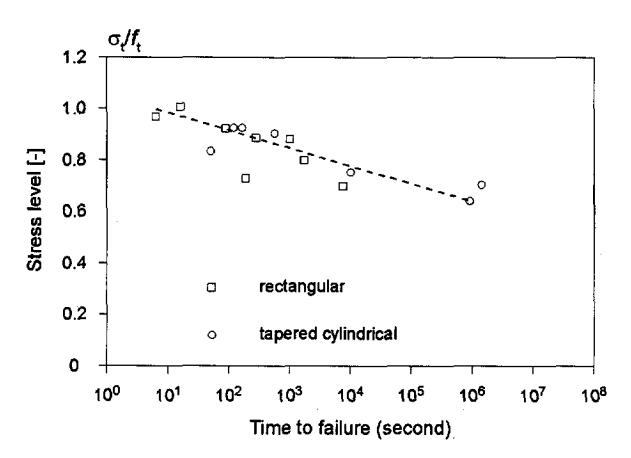


Fig. 3.26 Relationship between relative sustained stress level and time to failure for the uniaxial tensile tests [after Shkoukani and Walraven (1991)].

The results of the uniaxial sustained tensile tests are shown in Fig. 3.26. It is indicated that time to failure increases with decreasing stress level. If a specimen did not fail within the first three hours, it is claimed that no failure at all would occur. It was found that the long-term tensile strength is about 70% of the rapid test strength. The specimens which did not fail after loading during two weeks were subsequently subjected to a rapid loading to failure. Significantly higher strengths were obtained. This is attributed to the relaxation of

the cement matrix during sustained loading, which may lead to a relaxation of the stresses at the tip of the microcracks.

The results of the sustained eccentric tensile tests are illustrated in Fig. 3.27, where two eccentricities were adopted: e/d = 0.167 and 0.5. It is shown that the existence of an eccentricity can reduce the rate sensitivity. For the tests with a smaller eccentricity, the failure limit is about 80% of the short-term strength, whereas for tests with larger eccentricity, this value could reach about 90% of the short-term strength. The specimens which did not fail during sustained loading were also re-loaded to failure. An increase of the strength was also observed in this case.

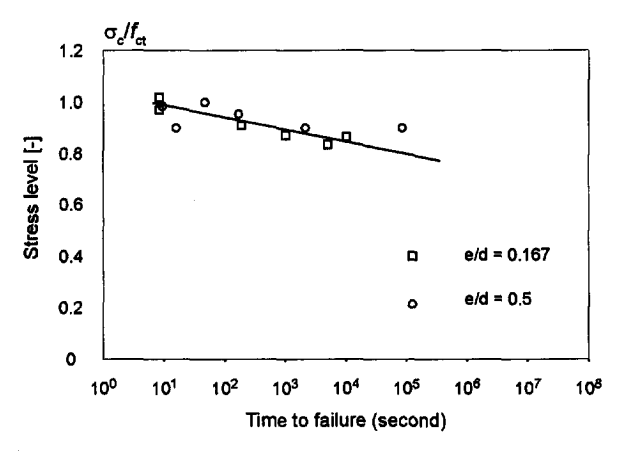


Fig. 3.27 Relation between relative stress level and time to failure by eccentric tensile loading with e/d = 0.167 and e/d = 0.5 [after Shkoukani and Walraven (1991)].

The results of eccentric tests with various loading rates are shown in Fig. 3.28. The failure occurred in about 6 seconds, 2 minutes, 20 minutes, 1 hour and 2.5 hours. It is indicated that the strength firstly decreases with a decrease of the loading rate. However, further lowering of the loading rate leads again to an increase of the strength.

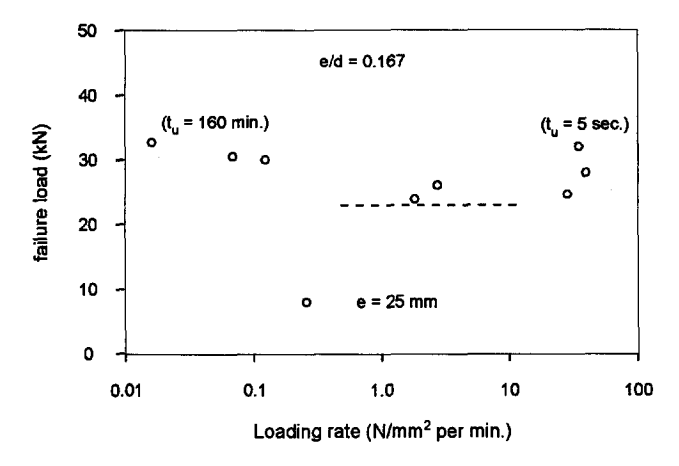


Fig. 3.28 Relationship between failure tensile load and loading rate for an eccentricity of e/d = 0.167 [after Shkoukani and Walraven (1991)].

3.5 Remarks on the basis of the literature study

On the basis of the literature survey it can be concluded that the material structure of concrete plays a dominant role as far as the rate sensitivity is concerned. The numbers and sizes of pores, flaws(voids) and microcracks inside the concrete decide upon the extent to which the loading rate or the strain rate could influence the mechanical behaviour. Clearly, all factors which have effects on the material structure of the concrete (such as the age of the concrete at testing, the curing condition, etc.) may also affect the rate sensitivity of the concrete. Up to now, one generally accepted point is that the time-dependent behaviour of concrete can be related to the presence of free water in the concrete. In practice, it is found that most concrete structures remain saturated at depth during their service life. From the literature study, it becomes evident that a good understanding of the phenomenon of rate sensitivity of concrete is of significance to structural engineers. In comparison with normal strength concrete, high strength concrete has its typical features as far as its material structure is concerned. High strength concrete has a much more dense internal structure, smaller pore sizes, a more uniform pore distribution and less microcracking before and during loading. Therefore, it is indispensable to understand the mechanical properties and the structural behaviour of high strength concrete related to the problem of rate sensitivity before this material can be safely used in practice.

Chapter 4

Creep of concrete in compression

Creep of concrete is a complex phenomenon which is not yet completely understood. Creep has a considerable impact on the performance of concrete structures, causing deflection increases as well as affecting stress distribution and prestress loss. In this chapter, a literature survey about creep behaviour of concrete in compression is presented. The factors which have an influence on creep are briefly discussed. The upto-date's knowledge on the creep mechanism and several viable predicting models are also surveyed. At a later stage of this literature study, attention is given as well to creep of young concrete. The survey is carried out for both normal and high strength concrete, whereas emphasis is placed on high strength concrete.

4.1 Introduction

It is well known that if a concrete element is subjected to a constant load, it will continuously deform for a very long period of time in addition to the initial deformation. This time-dependent deformation, which was first discovered by Hatt [Neville, Dilger and Brooks (1983)] in USA, is called creep. Unlike other structural materials, such as steel, concrete exhibits a complex time-dependent behaviour since its mechanical properties change with time and are largely influenced by temperature and relative humidity. It is found that a typical creep deformation of concrete after a year under a constant load is about two or three times the initial deformation, which already shows the practical significance of creep for the structural engineer. This complicated phenomenon causes considerable concerns for the structural designer, and therefore many research projects have been world-widely carried out since several decades. In spite of this comprehensive research, it has to be admitted that the up-to-date knowledge of the mechanism of creep is still incomplete, and empirical creep formulations derived on the basis of a huge amount of test data are used to predict structural deformation. The intention of this chapter is to

summarize the main factors that have an influence on the creep deformation of concrete, rather than to comprehensively review all aspects related to this phenomenon. There are several comprehensive reviews on this topic [Wittmann (1982), Bazant (1982), Hansen and Young (1991), Xi and Jennings (1992), Müller and Hilsdorf (1990), Smerda and Kristek (1988), Rüsch, Jungwirth and Hilsdorf (1983), Han (1994)].

For the construction industry, the knowledge of the properties of concrete at early ages becomes more and more important. This is due to technical and economic considerations. Early form work stripping, accelerating the construction process of slip form structures, shortening the production cycles in the precast industry and early prestressing of structural elements are examples. The cases mentioned before illustrate that knowledge of time-dependent deformation of concrete at early ages is indispensable. In this chapter, the main emphasis will be placed on the mechanical properties of concrete at early ages, as far as these concern the creep behaviour of concrete.

The main part of this chapter will concentrate on the time-dependent deformation of high strength concrete (or high performance concrete). High strength concrete represents a rather recent development in concrete materials technology. By virtue of the significant improvement of its material structure, high strength concrete shows a behaviour, which is superior over ordinary concrete in many respects. Among these advantages, the fast strength and stiffness development becomes more and more interesting for precasting and prestressing industries. This may improve the possibilities of early demoulding and early application of prestress. However, to fully take advantage of these properties, the knowledge of time-dependent deformation of high strength concrete is essential. In this chapter, the creep behaviour of high strength concrete at normal age will be reviewed. Afterwards, the survey will concentrate on the early age behaviour of high strength concrete. In this chapter, high strength concrete is defined as concrete with a compressive cubic strength above 60 N/mm² at an age of 28 days.

4.2 Creep of normal strength concrete in compression

4.2.1 Factors affecting creep

Concrete creep is an extremely complicated phenomenon. This is due to the change of its material structure as well as the basic mechanical properties in time. In general, there are two kinds of factors which influence creep of concrete. They are called intrinsic factors and environmental factors. Some of these factors are illustrated in Fig. 4.1. The intrinsic factors include:

- The concrete composition
- The water/cement ratio
- The stress/strength ratio
- The age at application of load
- The development of microcracks

The environmental factors include:

- Relative humidity
- Temperature

4.2.1.1 The influence of concrete composition on creep

The hydrated cement paste is the most essential concrete component governing the creep phenomenon. Different types of cements have, in contact with water, different hydrating rates, and as a result, at the same age, achieve different proportions of their final strength. It seems logical that the more has the paste hardened the lower is its creep potential at a given applied load. However, if creep of different cements is compared on the basis of specific creep, i.e. the creep under a stress of 1 N/mm², the type of cement does not influence creep [Neville {1991}].

As far as the influence of aggregates on the creep of concrete is concerned the main factors which affect creep are the quantity and the modulus of elasticity of the aggregate, both of which resist the creep of the cement paste. In general, normal-weight aggregates usually do not exhibit creep, nor do they adsorb water from the cement paste. When a concrete is subjected to a constant load, a stress redistribution takes place between the cement paste and the aggregate. The larger the difference between the mechanical properties of the cement paste and the mechanical properties of the aggregates, the more significant is the stress redistribution.

4.2.1.2 The influence of water/cement ratio on creep

It is generally noticed that the creep deformation under a certain load is nearly proportional to the square of the water/cement ratio, if other factors remain constant (see Fig. 4.1(b)). This can be attributed to the increase of the strength if the water/cement ratio decreases. The porosity of the cement paste is also influenced by the water/cement ratio, consequently, the mechanical properties of the cement paste are affected. For the same applied stress, creep decreases with a decrease in water/cement ratio. However, if the stress

is adjusted in proportion to the strength at the time of application of load, the situation may reverse. This may be explained by considering the development of strength after the load has been applied. As a proportion of the initial strength (the strength at the time t_0), the rate of development of strength is smaller for a low water/cement ratio than for a high water/cement ratio [see Fig. 4.2, at age t, $(f_2-f_1)/f_1 > (f_4-f_3)/f_3$]. Therefore, the effect of a decrease in water/cement ratio is to increase creep at a constant initial stress/strength ratio.

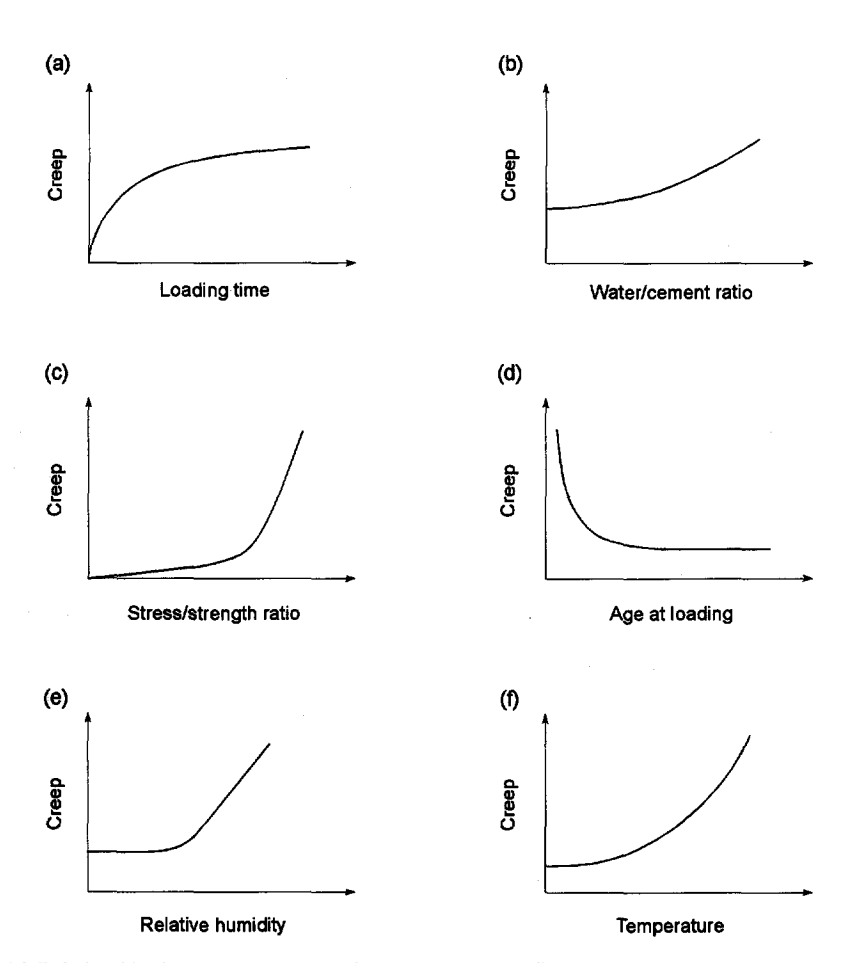


Fig. 4.1 Relationships between creep and various factors which influence creep.

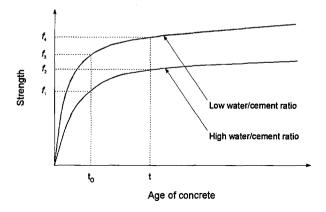


Fig. 4.2 Development of strength for concretes with different water/cement ratio.

4.2.1.3 The influence of stress/strength ratio on creep

The stress/strength ratio is a key factor in the investigation of creep. Therefore, considerable effort has been invested to make this point clear (see Fig. 4.1(c)). Up to now, it seems to be generally accepted that creep is proportional to the applied stress until a certain stress level and inversely proportional to the strength at the time of application of the load. The linear relation between creep and the applied stress has been found from a wide range of experimental results. However, it is the upper limit of this linear relation that has been often discussed. An upper limit between about 0.23 and 0.75 has been observed [Neville, Dilger and Brooks (1983)]. The significant internal microcracking, occurring in a concrete at stress/strength ratios of 0.4 to 0.6 [Hsu, Slate, Sturman and Winter (1963), Shah and Slate (1965)], may change the creep behaviour. The onset of cracking depends on the degree of heterogeneity of the concrete. A larger difference of stiffness between the cement paste and the aggregate causes a more severe stress redistribution, resulting in higher tensile stresses in the interface areas and more extended microcracking. As a result, the limit of linear proportionality may be lower. Above the limit of linear proportionality, the creep deformation increases with stress at an increasing rate. This will induce tertiary creep (see Fig. 2.5), which will lead to sustained loading failure [Rüsch, Sell, Rasch, Grasser, Hummel, Wesche and Flatten (1968), Streit (1991)]. The range of stresses for which sustained loading failure occurs is between about 0.7 and 0.9 of the short-term strength [Coutinho (1977)].

4.2.1.4 The influence of the age at application of the load on the creep deformation

The influence of the age of the concrete at the application of the load on the magnitude of creep deformation can be traced back to the degree of hardening of the cement paste in the concrete. In Fig. 4.1(d) it is shown that the creep deformation increases as the age at application of the load decreases. However, if we compare the creep of a concrete loaded at various ages but with a constant initial stress/strength ratio, we find an opposite tendency. This is due to the development of the strength of the concrete during the loading period. Since the strength development occurs at a faster rate for an earlier age, the creep deformation is relatively smaller for application of the load at an earlier age.

The effect of the age at application of the load on creep is further complicated by the possible enhancement of the strength due to a sustained stress. Average increases of strength, ranging from 2 to 30% of the short-term strength, have been reported [Coutinho (1977)], depending on the short-term strength, the duration of the load, the level of the stress and the age at application of the load. The beneficial gain in strength is explained as a result of an acceleration of the hydration process, improved healing of cracks perpendicular to the load, and an increase in the van der Waals forces on bringing the gel particles closer together, and increasing the solubility of unhydrated cement in the presence of water, leading to an increasing hydration.

4.2.1.5 The influence of development of microcracks on the creep deformation

The development of microcracks and the presence of these cracks in concrete has a significant influence on creep, especially on the linearity of creep. Microcracks in concrete can be caused by either shrinkage or the external load. From the point of view of theory of composite materials, a material composed of two linear materials behaves also in a linear way. The divergence of linearity of concrete is, in fact, due to the existence of another phase, i.e. the interface area between the cement paste and the aggregate, which is generally the weakest link in concrete, being vulnerable to microcracking. In concrete, there are two kinds of microcracks, i.e. bond cracks (in the interface area) and mortar cracks (in the cement paste) [Shah and Chandra (1970)]. For the unloaded concrete, at early ages, microcracks are mainly caused by plastic shrinkage and appear normally as bond cracks. Because of the restraint of aggregate to the shrinkage of the cement paste, microcracks may further develop in the interfacial area and in the cement paste. A more or less well developed crack pattern exists already in the concrete before an external load is applied (it was reported that about 50% of the total crack length at the peak stress is already present before loading [Stroeven (1973)]).

These pre-loading microcracks can be further developed during the application of an external load. Even after the external load is kept at a constant level, the cracks are still in progress, resulting in further creep. This phenomenon may be attributed to the shrinkage and thermal stresses during the loading period. A small increase of the stresses at a crack tip will cause a progress of the crack. Therefore, shrinkage and thermal stresses may contribute to the development of microcracks, thus, to the creep. This contribution mainly affects the drying creep.

4.2.1.6 The influence of relative humidity on the creep deformation

According to the mechanism of creep of concrete, two factors play a dominant role as far as the influence of relative humidity is concerned. The creep of concrete is affected by the amount of free water present in the cement paste at the time of application of load as well as the amount of moisture lost to the outside while under load. Under the condition of water curing (100% relative humidity), the first factor governs the creep behaviour of concrete because there is no moisture loss. The basic creep of concrete decreases with the age of application of the load due to the decrease of the amount of free (evaporable) water caused by the progress of hydration. As far as the second factor is concerned, the porosity of concrete is the main parameter. It is the porosity that determines the possibility and the capacity of free water to move through the concrete, i.e. the loss of free water to the environment. The external load is believed to compress the pores, resulting in a narrower pore entry, thus to slow down the transport of free water to the environment. The loss of free water is also influenced by the size of the concrete element because the time to reach hygral equilibrium is longer in a larger element. In general, the influence of relative humidity on creep of concrete can be distinguished on the basis of the curing condition prior to application of load or under the load. Generally, drying prior to application of load reduces the creep potential while drying under load increases the creep potential.

4.2.1.7 The influence of temperature on the creep deformation

In normal service structures, temperature seems to be less important than the relative humidity as far as its influence on creep of concrete is concerned, because the variation of operating temperatures is small. However, in recent years, the interest in the temperature effects on creep has been stimulated by the use of prestressed concrete pressure vessels in nuclear reactors. The service condition of such structures involves high temperatures (95 °C), steep temperature gradients and various combinations of temperature and pressure. Another type of structure involving the strong influence of temperature on creep is the mass structure, such as a dam, which undergoes a temperature cycle, even if the ambient temperature is constant. Generally speaking, a higher temperature results in a larger creep (see Fig. 4.1(f)). In order to identify the influence of temperature on creep, it is necessary

to distinguish between the temperature during the period of curing prior to the application of load and the temperature while the concrete is under load. In general, any change of temperature resulting in a change of the moisture content and the moisture movement will have an effect on creep. For a concrete subjected to a high temperature before an external load is applied, the evaporable water content at application of the load will be lower. When the concrete is subsequently subjected to a lower temperature under load, the creep is less. On the other hand, the age at application of the load is closely related to the moisture content inside the concrete if the other factors remain constant. Therefore, the influence of temperature on creep also depends on the age at application of the load.

4.2.2 Mechanism of creep

Although there are a huge number of research results on creep, it is still very difficult to clarify the mechanism of creep. It is generally agreed that the complex nature of concrete creep involves more than one possible mechanism because none of the mechanisms proposed up to now can account for all of the observed facts. The only non-controversial statement that can be made is that the presence of some free (evaporable) water is essential to creep. Some tests show that concrete from which all evaporable water has been removed exhibits practically no creep [Glucklich (1962)]. However, the changes in the creep behaviour of concrete at high temperature imply that at the stage the water stops playing a role, the gel itself is subjected to creep deformation. It is suggested that water movement is possibly involved only in the initial stages of creep, and that long-term creep is associated with intercrystalline slip, internal rupture of bond, microcracking and bond re-formation.

A discussion of the mechanism of creep is very important in order to understand this complicated phenomenon and to propose the most appropriate predicting model. Because of lack of solid knowledge about the physical and chemical changes inside the cement paste, the proposed mechanisms normally base on phenomenological observations. Illston (1979) has vividly described this situation: The physical and chemical happenings that are associated with creep are on a molecular scale, and there is no convincing direct evidence of what actually goes on; so the explanation of creep has, perforce, consisted of interpreting engineering level observations in terms of likely physical and chemical phenomena. Among many proposed mechanisms of creep, four representative mechanisms will be briefly reviewed, i.e. plastic flow, viscous flow, seepage and microcracking.

4.2.2.1 Plastic flow theories

It has been suggested that the creep of concrete may be largely caused by the plastic flow as crystalline slip, i.e. a slipping along planes within the crystal lattice. The plastic flow

is due to a slip in a plane of maximum shear stress. This is similar to the plastic flow of metals. The water inside the concrete acts like a lubricant and makes flow easier. However, for metals at room temperature, the plastic flow occurs only if the applied external stress exceeds the yield point. In the case of concrete, no such a yield point has been found. Additionally, a slip in a plane of maximum shear stress does not lead to a volume change, while the creep of concrete, in fact, involves a volumetric decrease. At very high stresses, the creep of concrete could be partly, if possible, explained by the plastic flow theories [Neville, Dilger and Brooks (1983)].

4.2.2.2 Viscous flow theories

In the viscous flow theories, the cement paste is considered as a fluid with a high viscosity, which increases with time as a result of chemical changes within the cement paste (ageing). When concrete is loaded, the flow of cement paste is resisted by the aggregate. Thus, the stress on the cement paste is gradually taken over by the aggregate as the cement paste continuously deforms. Since the creep of cement paste is proportional to the applied stress, the rate of creep will be progressively reduced as the load is transferred from the cement paste to the aggregate. However, the viscous flow theories are not trouble free. Like the plastic flow, viscous flow requires a constant volume, which is not the case for concrete. Furthermore, viscous flow needs a proportionality between stress and strain and between the rates of stress and strain at any stress. This is only suitable for concrete when a applied stress is in the range of 30 to 50% of the strength. It is believed that the limitation of stress-strain proportionality of concrete is due to the existence of microcracking. Nevertheless, to some extent, the viscous flow theories can be used to explain the creep behaviour of concrete.

4.2.2.3 Seepage theories

In the seepage theories, the creep of concrete is considered as seepage of gel water under pressure. The gel water in concrete is in a state of equilibrium vapour pressure. As an external load is applied to the concrete, the pressure of the gel water is changed. To obtain equilibrium again, the gel water is reorganised. This further affects the colloidal stresses and the van der Waals forces. This equilibrium is achieved by a seepage of gel water inside the cement gel. From the nature of seepage, it is easily understood that the density (porosity) of the cement paste has a strong effect on the seepage. After a removal of the external load, the pressure on gel water reduces, the original equilibrium tends to re-establish. However, creep recovery tests do not confirm this re-establishment. This is probably due to formation of new gel during the load period. The new gel is in a state of equilibrium when the external load is applied, but is not in a state of equilibrium at the time of unloading. The one basic argument about the seepage theories is that if the gel water is slowly squeezed out of the

gel pores and the capillary water evaporates, a larger weightloss should be expected during creep. Experiments do not prove this assumption to be true. While the external seepage may not involve, the internal seepage is still possible. The displacement of water may be from pores oriented in a direction perpendicular to the applied stress to the pores parallel to that direction, which would have opened out due to the Poisson effect [Neville, Dilger and Brooks (1983)]. Even for the external seepage, it is argued that the test equipment used to determine the loss of gel water is not accurate enough to measure such a small amount of water [Powers (1965)].

4.2.2.4 Contribution of microcracking to creep

It is estimated that microcracking is responsible for 10 to 25% of the total creep deformation in concrete. This part of deformation is normally irrecoverable. The extent of the development of microcracking due to creep depends on the quantity of existing microcracking prior to the application of a load. At a high stress, the role of microcracking is of considerable importance. However, the stress/strength ratio at which microcracking develops extensively is not constant. It is found that this value is higher the stronger is the concrete. There is another fact which could confirm the role of microcracking in the process of creep. The development of microcracks associated with creep has been confirmed by acoustic measurements. Elastic and viscous deformation produce no noise.

4.2.3 Models to predict creep

There are two ways in developing models to predict the creep behaviour of concrete. One way is to develop complex and accurate material models on the basis of all available knowledge on the internal structure of concrete. Since concrete is a heterogeneous material, it is advantageous to introduce three different levels to characterise its structure [Wittmann (1982)]. According to the microstructure of concrete, the materials science models are developed to represent the microlevel. Because the behaviour of the composite material can not be linked directly with the mechanisms of the microstructure, i.e. the effect of pores and inclusions also have to be considered, the materials engineering models are made on the mesolevel. By using the models of the micro- and mesolevel, materials laws for the creep behaviour of concrete can be derived on the macrolevel. The models developed on this level are termed engineering models. In general, models derived in this way are used to carry out advanced numerical analyses.

Another method is to formulate empirical creep models on the basis of the huge amount of test data. This approach is still of utmost practical significance, although it is not as comprehensive as the first method and suffers a number of basic weaknesses. An empirical predicting model is sufficiently accurate in most practical cases, particularly, it is convenient to be adopted in the practical design code. Today, our knowledge on the creep behaviour of concrete also enables us to involve more sophisticated models in our codes by introducing some identified mechanisms of the creep process. Thus, this kind of model also can be used to carry out more complicated analyses, such as FE analyses.

4.2.3.1 Models of microstructure

For the time-being, the models for the microstructure of concrete are generally classified into three kinds [Xi and Jennings (1992)]:

- adsorption of water based on thermodynamics; the Powers-Brunauer model [Powers (1968)], the Feldman-Sereda model [Feldman and Sereda (1968)], the Munich model [Wittmann (1982)];
- phase analysis with X-ray diffraction; the Taylor model [Xi and Jennings (1992)];
- analysis of hydration process and simulating the process by computer techniques; the Jennings-Johnson model.

More details of these models are discussed by Xi and Jennings (1992). The following section only briefly discusses the first kind of models.

In the Powers-Brunauer microstructural model, C-S-H consists of colloidal particles with two or three layers of thin sheets that are bonded together. Bond forces are mainly surface forces. The water within the particle or between the layers is interlayer water, and the water on the surface of particles is adsorbed water (see Fig. 4.3). The water held between the sheets is irreversibly lost only at low relative humidity. Because the size of the interlayer space and the entrances of the wedge-shaped space allow only water molecules to enter, the measurements of the specific surface areas with water and nitrogen are different.

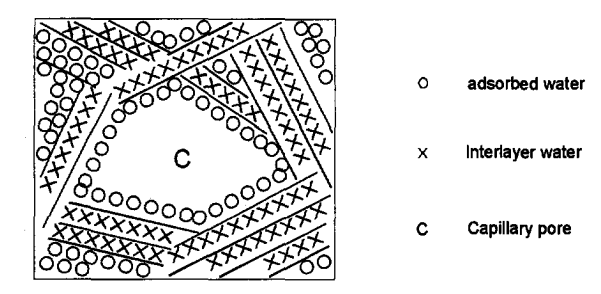


Fig. 4.3 Powers-Brunauer model for C-S-H [after Powers (1968)].

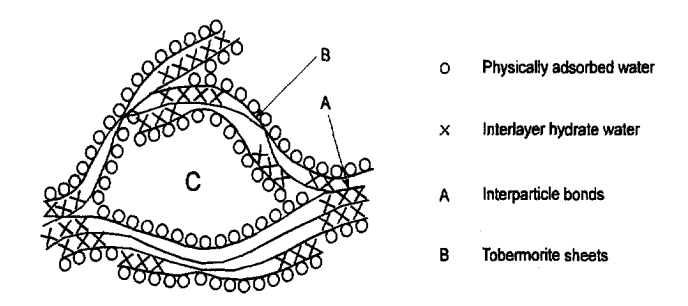


Fig. 4.4 Feldman-Sereda model for C-S-H [after Feldman and Sereda (1968)].

In the Feldman-Sereda microstructural model, C-S-H is suggested to be a completely irregular array of single layers which come together to create interlayer regions (see Fig. 4.4). Bonding between layers is considered to be through solid-solid contacts. In comparison with the Powers-Brunauer model, the interlayer regions randomly vary in thickness. The interlayer water is part of the C-S-H structure, therefore, affecting its mechanical and physical properties. The interlayer water can move reversibly in and out of the interlayer space.

In the Munich microstructural model, C-S-H is described as a three-dimensional network of microporous colloidal particles (see Fig. 4.5). The chemical bonds and the van der Waals attraction are equally important in the bonding of the gel particles. Adsorbed and desorbed water affects the surface free energy of the solid, resulting in expansion or

contraction. On rewetting in the small micropores, a disjoining pressure is created. This force increases with increasing relative humidity and competes against the van der Waals attraction. On drying, the C-S-H particles contract due to increasing particle attraction.

On the basis of the Munich model, Wittmann and others use the activation energy approach to describe creep of concrete. It is assumed that movement of solid particles is responsible of creep. The probability P_a of a given unstressed particle of gel having energy U necessary to overcome the bond, i.e. depart from the equilibrium position is expressed mathematically as follows:

$$P = C_o \cdot e^{-\frac{Q_o}{RT}} \tag{4.1}$$

where C_a is a constant, Q_a is activation energy, R is gas constant and T is absolute temperature. The application of an external stress decreases the activation energy in the direction of the applied stress by a quantity u_e (decrease in loading direction and increase in the opposite direction). Hence, Eq. (4.1) according to the two cases becomes:

$$P_{a} = C_{a} \cdot e^{\frac{Q_{a} - u_{e}}{RT}} - C_{a} \cdot e^{\frac{Q_{a} + u_{e}}{RT}} = 2 \cdot C_{a} \cdot e^{\frac{Q_{a}}{RT}} \cdot sinh\left(\frac{u_{e}}{R \cdot T}\right)$$

$$\tag{4.2}$$

The movement of concrete at the macroscale, associated with such an activation, is the cause of creep. If u_e is taken to be proportional to the applied stress σ_c , and Q_a is a function of time:

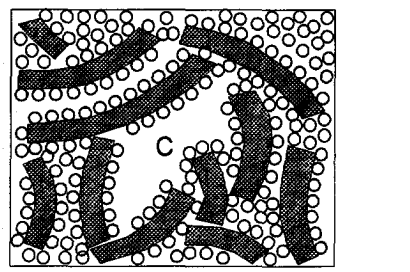
$$\frac{u_e}{R \cdot T} = A_e \cdot \sigma_c \tag{4.3}$$

$$Q_a(t) = Q_0 + m_e \cdot \ln(t) \tag{4.4}$$

where A_e , Q_0 and m_e are constants. From the above assumptions, the creep of concrete can be obtained as follows:

$$\varepsilon_{cr} = \left(\frac{A_1}{t^{m_e}}\right) \cdot \left(A_2 \cdot e^{-\frac{Q_0}{R \cdot T}}\right) \cdot \left[A_3 \cdot \sinh\left(\frac{V_a}{R \cdot T \cdot \sigma}\right)\right] \tag{4.5}$$

where A_1 , A_2 and A_3 are constants, ε_{cr} is the creep of concrete, V_a is activation volume, activation energy per unit stress. The first term in Eq. (4.5) can be determined by a creep-time test, the second by a creep-temperature test, and the third by a relaxation test or other methods.



- O Adsorbed water
- Gel particle
- C Capillary pore

Fig. 4.5 Munich model for C-S-H [after Wittmann (1982)].

4.2.3.2 Generalization of practical models for predicting creep

The most difficult points for modelling creep behaviour of concrete to be suitable for practical application can be classified into two categories:

- Non-linear behaviour is due to: a) non-uniform moisture distribution caused by drying, resulting in high internal stresses and microcracking; b) ageing induced by load stress, i.e. creep due to a stress increment applied at a time t_n depends on the load history, $t_0 \le t \le t_n$, which concrete has experienced, where t_0 is the age of concrete at application of the load; c) non-linearity caused by high stress, i.e. $\sigma_c > 0.4 f_{cm}(t_0)$, where $f_{cm}(t_0)$ is the compressive strength of concrete at a time t_0 .
- Creep of concrete depends on a large number of parameters which can only be estimated by the structural engineers at the stage of design.

Because of the difficulties mentioned above, the linear model is still the most popular approach for many cases of practical interest. In general, two types of models have been used: summation models and product models. In the following sections, the main features of these type of models will be briefly discussed.

The product model (ageing model)

This model describes the creep of concrete ε_c as a product of a function dealing with the effect of age at the application of the load and a function dealing with the development of creep with loading duration $(t-t_0)$. It is generalised as follows:

$$\varepsilon_{cr} = \beta(t_0) \cdot \Phi(t - t_0) \tag{4.6}$$

where $\beta(t_0)$ is a monotonically decreasing ageing function and $\Phi(t-t_0)$ is a monotonically increasing function standing for the time development of creep. The predicting methods given by ACI [ACI 209 (1992)], BP-model [Bazant and Panula (1978a, b, c, 1979 a, b)], British Concrete Society [Neville, Dilger and Brooks (1983)] and CEB-FIP Model Code (1990) [CEB-FIP (1991)] belong to the product models.

The summation model (rate of flow model or improved Dischinger model)

The characteristic point of this type of model is the separation of creep into delayed elasticity and flow. It can be generalised as follows:

$$\varepsilon_{cr} = \Psi(t - t_0) + \left[\Gamma(t) - \Gamma(t_0)\right] \tag{4.7}$$

where $\Psi(t-t_0)$ is a monotonically increasing function standing for delayed elasticity; the function $\Gamma(t)$ - $\Gamma(t_0)$ also increases with time and represents flow which is an irreversible part of the creep deformation. The effect of age at application of the load and the time development are expressed by one unique function. The approaches to predict the creep behaviour adopted in DIN 4227 [Müller and Hilsdorf (1990)] and in CEB-FIP Model Code 1978 [CEB-FIP (1984)] belong to this group.

4.2.3.3 CEB-FIP Model Code 1990

This model is a linear product model without separation into time dependent deformation components. In addition to the basic function, some extensions have been given in order to consider some effects on creep of concrete, such as type of cement, curing temperature, higher stress level.

Basic model

Within the range of service stresses $\sigma_c < 0.4 f_{cm}(t_0)$, for a constant stress applied at time t_0 , the creep of concrete is given by:

$$\varepsilon_{cr}(t,t_0) = \frac{\sigma_c(t_0)}{E_{ci}} \cdot \phi_{28}(t,t_0)$$
(4.8)

where $\phi_{28}(t, t_0)$ is creep coefficient, E_{ci} is modulus of elasticity at the age of 28 days, given as follows:

$$E_{ci} = \alpha_E \cdot 10^4 \cdot \left(\frac{f_{ck} + \Delta f}{f_{cmo}}\right)^{\frac{1}{3}}$$

$$\tag{4.9}$$

in which f_{ck} is the characteristic strength (MPa), Δf is taken as 8 MPa, f_{cmo} is taken as 10 MPa, α_E is taken as 2.15×10^4 MPa.

Creep coefficient

The creep coefficient $\phi_{28}(t, t_0)$ can be calculated as follows:

$$\phi_{28}(t, t_0) = \phi_0 \cdot \beta_c(t - t_0) \tag{4.10}$$

where ϕ_0 is the notional creep coefficient, β_c is coefficient to describe the development of creep with time after loading, t is the age of the concrete at the moment considered (days), t_0 is the age of the concrete at the application of the load. The notional creep coefficient can be estimated as follows:

$$\phi_0 = \phi_{RH} \cdot \beta(f_{cm}) \cdot \beta(t_0) \tag{4.11}$$

$$\phi_{RH} = 1 + \frac{1 - RH/RH_0}{0.46 \cdot (h/h_0)^{1/3}} \tag{4.12}$$

$$\beta(f_{cm}) = \frac{5.3}{\sqrt{f_{cm}/f_{cmo}}} \tag{4.13}$$

$$\beta(t_0) = \frac{1}{0.1 + (t_0/t_1)^{0.2}} \tag{4.14}$$

where $f_{cm} = f_{ck} + \Delta f$, h is the notional size of the member (mm), $h = (2A_c/u)$, A_c is the cross-section and u is the perimeter of the member in contact with the atmosphere, h_0 is 100 mm, RH is relative humidity of the ambient environment (%), RH_0 is 100%, t_1 is 1 day.

The development of creep with time is given as follows:

$$\beta_c(t-t_0) = \left[\frac{(t-t_0)/t_1}{\beta_H + (t-t_0)/t_1}\right]^{0.3}$$
(4.15)

$$\beta_H = 150 \cdot \left[1 + \left(1.2 \cdot \frac{RH}{RH_0} \right)^{18} \right] \cdot \frac{h}{h_0} + 250 \le 1500$$
 (4.16)

Effect of type of cement and curing temperature

The effect of type of cement on the creep coefficient of concrete can be considered by modifying the age at application of the load t_0 :

$$t_0 = t_{0,T} \cdot \left[\frac{9}{2 + \sqrt{(t_{0,T}/t_{1,T})}} + 1 \right]^{\alpha} \ge 0.5 \text{ days}$$
 (4.17)

where $t_{1,T}$ is 1 day, α is a parameter which depends on type of cement: -1 for slowly hardening cements; 0 for normal or rapid hardening cements; 1 for rapid hardening high strength cements. $t_{0,T}$ is the age of the concrete at application of the load adjusted by the following equation:

$$t_{0,T} = \sum_{i=1}^{n} \Delta t_i \cdot e^{-\left[\frac{4000}{273 + T(\Delta t_i)/T_0} - 13.65\right]}$$
(4.18)

where $T(\Delta t_i)$ is temperature during the time period Δt_i (°C), T_0 is 1°C, Δt_i is number of days where a temperature T prevails.

Effect of high stresses

For stress levels in the range of $0.4f_{cm}(t_0) < \sigma_c < 0.6f_{cm}(t_0)$, the non-linearity of creep may be estimated by using the following equations:

$$\phi_{0,k} = \phi_0 \cdot e^{1.5(k_\sigma - 0.4)}$$
 for $0.4 < k_\sigma \le 0.6$ (4.19)

$$\phi_{0,k} = \phi_0$$
 for $k_{\sigma} \le 0.4$ (4.20)

where $\phi_{0,k}$ non-linear notional creep coefficient, which replaces ϕ_0 in Eq. (4.10), k_{σ} is the stress/strength ratio, σ_c/f_{cm} .

4.2.3.4 American Concrete Institute (ACI 209), 1992

Creep of concrete is defined the same as in Eq. (4.8) with a creep coefficient, expressed as follows:

$$\phi_{28}(t,t_0) = \phi_{\infty}(t_0) \cdot \frac{(t-t_0)^{0.6}}{10 + (t-t_0)^{0.6}}$$
(4.21)

where $\phi_{\infty}(t_0)$ is the ultimate creep coefficient with the correction factor γ_c if concrete is exposed to situations other than 'standard conditions'. The ultimate creep coefficient can be expressed as:

$$\phi_{\infty}(t_0) = \gamma_c \cdot \phi_{\infty} \tag{4.22}$$

The constant $\phi_{\infty} = 2.35$ is recommended. The correction factors γ_c consist of the following terms:

$$\gamma_c = \gamma_{la} \cdot \gamma_{RH} \cdot \gamma_{al} \cdot \gamma_s \cdot \gamma_a \cdot \gamma_a \tag{4.23}$$

Loading age yla

For loading ages later than 7 days for moist cured concrete and later than 1-3 days for steam cured concrete, the factor of loading age is taken as:

$$\gamma_{la} = 1.25 \cdot (t_0)^{-0.118}$$
 for moist cured concrete (4.24)

$$\gamma_{la} = 1.13 \cdot (t_0)^{-0.094}$$
 for steam cured concrete (4.25)

where t_0 is the loading age in days.

Ambient relative humidity γ_{RH}

For ambient relative humidity greater than 40 percent, the factor of relative humidity γ_{RH} is:

$$\gamma_{PH} = 1.27 - 0.0067 \cdot RH$$
 for $RH > 40$ (4.26)

where RH is ambient relative humidity in percent.

Average thickness ⁷⁾	Creep γ _{at}		
(mm)	less than one year	ultimate value	
51	1.30	1.30	
76	1.17	1.17	
104	1.11	1.11	
127	1.04	1.04	
Equations	(4.27)	(4.28)	
152	1.00	1.00	
203	0.96	0.96	
254	0.91	0.93	
305	0.86	0.90	
381	0.80	0.85	

Table 4.1 Correction factors for average thickness of members, from Eqs. (4.27) and (4.28). [after ACI 209 (1992)]

Average thickness of member yat

When the average thickness or volume to surface ratio of a structural member differs from 150 mm or 38 mm, respectively, two methods are offered for estimating the factor of member size γ_{at} :

(a) Average-thickness method

For an average thickness of a member smaller than 150 mm, the factors given in Table 4.I are used. For an average thickness of a member larger than 150 mm and up to about 300 to 380 mm, the factor of average thickness is:

$$\gamma_{at} = 1.14 - 0.00092 \cdot h_a$$
 during the first year after loading (4.27)

$$\gamma_{at} = 1.10 - 0.00067 \cdot h_a$$
 for ultimate values (4.28)

where h_a is the average thickness of a member in mm.

(b) Volume-surface ratio method

$$\gamma_{at} = \frac{2}{3} \left[1 + 1.13 \cdot e^{-0.0213 \left(\frac{\gamma}{s}\right)} \right]$$
 (4.29)

where v/s is the volume to surface ratio in mm.

Factors for concrete composition γ_s , γ_ρ , and γ_α

Since the concrete mix characteristics are unknown at the design stage, and these correction factors are normally not excessive and tend to offset each other, it is suggested that they may be neglected for design purpose.

$$\gamma_s = 0.82 + 0.00264 \cdot S_t$$
 $S_t = \text{slump in mm}$ (4.30)

$$\gamma_{\rho} = 0.88 + 0.0024 \cdot \rho_{\alpha}$$
 $\rho_{\alpha} = \text{fine to total aggregate ratio}$ (4.31)

$$\gamma_{\alpha} = 0.46 + 0.09 \cdot \alpha_{\alpha}$$
 $\alpha_{\alpha} = \text{air content}$ (4.32)

4.2.4 Comparison of linear creep prediction models

According to the various relevant load histories, the differences between the product model and the summation model are shown in Fig. 4.6 [Müller and Hilsdorf (1990)].

Constant stress

For a constant stress, the product model gives a correct prediction. The effect of age at loading and the time development of creep may be relatively well estimated. In comparison with the performance of a product model, the summation model reveals some systematic error due to the presentation of flow as a unique function, coupling the effects of age at loading and duration of loading. Consequently, creep after a short duration of loading is underestimated if the prediction after a long duration of loading is correct, even if the correction term rapid initial flow is included.

The product model considers concrete at any time at which a load increment is applied as "virgin". However, in fact, concrete shows a pronounced stress dependent ageing. Thus, for an increasing stress, creep is overestimated by the product model. The summation model tends to underestimate the creep under increasing loads due to the particular formulation of flow.

Decreasing stress but increasing time dependent strain

It is indicated that both the product model and the summation model give acceptable results

Decreasing stress and decreasing time dependent strain

The product model generally overestimates the strain reduction on unloading while the summation model may give correct predictions if delayed elasticity is modelled correctly.

Land bioton	Outh-size	Accuracy of prediction		
Load history	Criterion	Product model	Summation model	
Constant stress	Loading age	good	acceptable	
	Time development	good	acceptable	
Increasing stress	G _c t	acceptable	acceptable	
Decreasing stress	σ _c	acceptable	acceptable	
		poor	acceptable	
Relaxation	very young age at loading and thick member or high relative humidity	poor	acceptable	
	other cases	acceptable	acceptable	

Fig. 4.6 Comparison of the product model and the summation model for the prediction of creep of concrete under various load histories [after Müller and Hilsdorf (1990)].

Relaxation

In most cases, the product model gives reasonably good predictions in the case of relaxation. However, for very early application of load and high relative humidity or large member sizes, no reasonable relaxation coefficient may be obtained from the product model. This will not occur as the summation model is used.

The results of this comparison show that the prediction errors of the two models mainly come from the fact that the creep of concrete actually is a non-linear process. This is particular the case for the product model, because for the summation model, the prediction errors may be reduced due to the specific formulation of the flow term. The correct prediction can be only achieved when the non-linear creep model is used.

4.2.5 A non-linear model for creep prediction

It is clearly seen from the preceding section that the weaknesses of linear creep models come from the actual non-linear creep behaviour of concrete. The best solution is to find a non-linear creep model. Up to now, there are some proposals on models for the non-linear creep behaviour of concrete. In the following section, one of these models is briefly discussed.

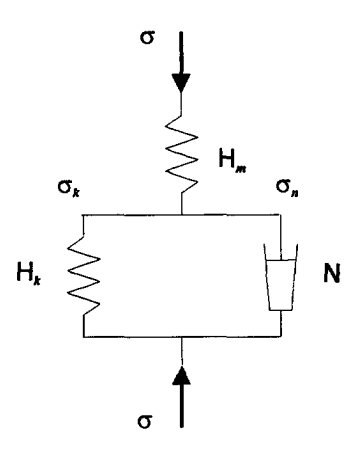


Fig. 4.7 Non-linear model for concrete consisting of two springs and one dashpot [after Shen (1993)].

On the basis of the classical rheology, an expanded non-linear creep model has recently been developed [Shen (1992), Walraven and Shen (1993)]. This non-linear model consists of two non-linear springs and a non-linear dashpot (modified Poynting-Thomson model). (see Fig. 4.7) The spring H_m describes the instantaneous strain of the concrete (short term non-linear behaviour), the spring H_k and the dashpot N describe the non-linear creep. The characteristics of the spring H_m can be written as follows:

$$\alpha_m = f_m(\theta_m) = \frac{c_m \cdot \theta_m - \theta_m^2}{1 + (c_m - 2) \cdot \theta_m} \qquad \text{for loading}$$
 (4.33)

$$\alpha_m = f_m(\theta_m) = \alpha_m^* + c_{u,m} \cdot \Delta\theta$$
 for unloading and reloading (4.34)

where:

 c_m = nonlinearity factor for concrete, with c_m =2 the usual parabolic stress-strain relation is obtained:

 $c_{u,m}$ = material factor for unloading;

 α_m = stress level, i.e. σ_m/f_m ;

 α_m^* = the highest stress level in the history;

 $f_m =$ compressive strength of spring H_m ;

 ε_m = strain of spring H_m ;

 σ_m = stress of spring H_m ;

 θ_m = strain level in spring H_m , with $\theta_m = \varepsilon_m / \varepsilon_{mui}$,

 ε_{mu} = ultimate strain of spring H_m .

The characteristics of the spring H_k are basically same as those of spring H_m . From the basic condition of equilibrium of this model, it can be written as:

$$\omega \cdot dt = \frac{1 + (c_k - 2) \cdot \theta_k}{\zeta - 2 \cdot \xi \cdot \theta_k + \mu_k \cdot \theta_k^2} \cdot d\theta_k$$
(4.35)

where ω is the creep rate factor:

$$\omega = \frac{f_{coo}}{\eta_b \cdot \varepsilon_{ba}} \tag{4.36}$$

$$\mu_k = 1 - (c_k - 2) \cdot \lambda \tag{4.37}$$

$$\xi = \frac{1}{2} \cdot \left[c_k - \left(c_k - 2 \right) \cdot \zeta + \lambda \right] \tag{4.38}$$

$$\zeta = \alpha_m(t_0) + \lambda \cdot \theta_k(t_0) \tag{4.39}$$

$$\lambda = 0$$
 for creep (4.40)

$$\lambda = c_k \cdot \frac{E_{m,del}}{E_{k,0}}$$
 for relaxation (4.41)

 $E_{m,del}$ is the modulus of elasticity for unloading, $E_{k,0}$ is the modulus of elasticity for initial loading, η_k is the modulus of viscosity of dashpot N.

The general constitutive equation can be derived according to the Eq. (4.35):

$$\int_{t_0}^{t} \omega \cdot dt = \int_{\theta_k(t_0)}^{\theta_k(t)} \frac{1 + (c_k - 2) \cdot \theta_k}{\zeta - 2 \cdot \xi \cdot \theta_k + \mu \cdot \theta_k^2} \cdot d\theta_k$$
(4.42)

The right term of Eq. (4.42) can be solved analytically. The left term contains the viscous properties of concrete, which may be a function of the actual time t, the age at application of the load t_0 , the stress level α_i and the level of creep strain θ_k , i.e.:

$$\Omega = \int_{L}^{t} \omega(t, t_0, \alpha_i, \theta_k) \cdot dt \tag{4.43}$$

An empirical function is further given for the time function [see Eq. (4.43)]:

$$\Omega = \frac{1}{m_{\nu}} \cdot \frac{1}{(1 - \alpha_{i})^{n_{\nu}}} \cdot \left[\left(\frac{t_{i+1} - t_{0}}{T_{\nu}} \right)^{m_{\nu}} - \left(\frac{t_{i} - t_{0}}{T_{\nu}} \right)^{m_{\nu}} \right]$$
(4.44)

where α_i is the average stress level in the time interval (t_{i+1}, t_i) . The parameters in Eq. (4.44) m_v , n_v and T_v can be determined through experiments.

4.3 Creep of HSC at a normal age in compression

4.3.1 New features of high strength concrete

Concrete is a kind of composite material consisting of aggregates, cement and water. The cement contributes to the properties of the concrete through the hydration process. To complete this process, a certain amount of water is required. Additionally, water has another role: to contribute to the workability of fresh concrete, consequently, to give the material satisfactory rheological properties. However, the second role of water also brings detrimental effects to concrete, i.e. the concrete has an amount of non-hydrated water, which increases the porosity of concrete and decreases the strength of the material. To satisfy both conditions, a new material called superplasticizer has been introduced into concrete. The function of a superplasticizer is to defloculate the cement grains and to reduce the friction between the particles. As a result, the desired workability is achieved with a significant decrease of the water demand. In addition, extremely fine chemically reactive materials (such as silica fume) can be used. It is believed that this kind of material has both a physical and a chemical function. The first function is to act as a filler, i.e. to fill the microvoids in the grain packing, thus, to improve the compactness of the material, and,

meanwhile, to improve the rheological properties of the fresh mix, resulting in a further reduction of the water demand. The second function is, through the pozzolanic reaction, to eliminate the C_a(OH)₂ crystals which are considered to be the weakest link inside the concrete, resulting in a more densified and homogeneous material [Regourd (1992), CEB-FIP (1990), ACI 363 (1992), Mindess (1994), Regourd (1984), Mindess (1984), Gjφrv (1992), Hjorth (1982), Sellevold and Nilsen (1987)].

The considerable improvement of the mechanical properties of high strength concrete has been achieved by modifying the microstructure of the concrete, i.e. by improving the microstructure of the cement paste and the cement-aggregate interface.

Cement paste

Hardened cement paste is a porous, inhomogeneous material. The degree of porosity and heterogeneity of the material is a decisive factor controlling its properties. It is indicated that the strength of the cement paste depends on the total porosity, pore size distribution and the nature of the solid phase of the cement paste [Mindess (1984)]. With the reduction of water in the cement paste (lower water/cement ratio) by using the superplasticizer, the degree of porosity of the cement paste is remarkably decreased. The cement paste is further densified by using silica fume, which refines the microstructure of the cement paste, and reduces the total pore volume and the average pore size [Mehta (1986), Sellevold (1987), Sellevold and Radjy (1983)]. Since the silica fume particles are two orders of magnitude smaller than the cement grains, their size and spherical geometry allow them to fill effectively the voids between the larger, angular cement grains. (see Fig. 4.8) During the cement hydration, silica fume particles are sites of nucleation for cement hydrates and then react as a pozzolanic material, resulting in a denser and more homogeneous gel structure [Mehta (1989)].

Cement paste-aggregate interface

In a normal strength concrete, the cement paste-aggregate interface is often a weak link, characterising to be better crystallised, more porous and less resistant than the bulk paste matrix. This is due to an excess of water. The addition of silica fume can drastically change the microstructure of the interface area. Silica fume improves cement paste-aggregate bond, which is associated with the formation of a less porous transition zone in concrete [Goldman and Bentur (1989), Bentur, Goldman and Cohen (1988), Darwin, Shen and Shraddhaker (1988), Cong, Gong, Darwin and McCabe (1992)]. Due to these interfacial effects, the aggregates in high strength concrete become active load-bearing components, contributing to the overall strength.

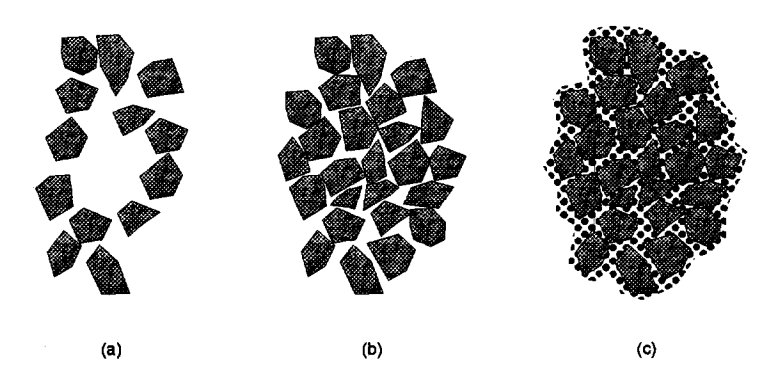


Fig. 4.8 The structure of cement paste in fresh concrete based on (a) cement, (b) cement plus superplasticizer and (c) cement plus silica fume and superplasticizer [after CEB-FIP (1990)].

The fundamental difference in microstructure between a high strength concrete and a normal strength concrete lies in the two factors mentioned above [Sarkar and Aïtcin (1987), Sarkar (1992)]. After the comparison, it is indicated that the microstructure of normal and high strength concrete shows similarities as well as dissimilarities. The similarity lies in the overall composition, which in both types is C-S-H and C-H. However, the proportion of C-H in high strength concrete is considerably lower, together with a dense microstructure composed mainly of C-S-H resulting from using very a low water content. The presence of superplasticizer makes it possible to use a much lower amount of water than is otherwise required. The cement paste-aggregate interface bond in high strength concrete is stronger and corresponds to a direct contact between C-S-H and the aggregate, while in normal strength concrete C-H is preferentially oriented at the interface, resulting in a loss of strength.

4.3.2 Creep behaviour of high strength concrete

The experimental data of creep of high strength concrete are still limited in comparison with that of normal strength concrete. In the following section, the existing experimental data on the creep behaviour of high strength concrete will be briefly reviewed.

It is perhaps Parrot (1969) who firstly reported on the creep behaviour of high strength concrete. He observed that the total strain in sealed high strength concrete under a sustained loading of 30% of the ultimate strength was the same as that of lower strength

concrete when expressed as a ratio of the short-term strain. Under drying conditions, this ratio was 25% lower for high strength concrete than that of lower strength concrete. The total long-term strains of drying and sealed high strength concrete were 15% and 65% higher, respectively, than those of a corresponding lower strength concrete at a similar relative stress level.

Ngab, Slate and Nilson (1981a) used sealed and unsealed specimens, which were subjected to a uniaxial compressive stress for load periods up to 90 days, to investigate the creep behaviour of high strength concretes ranging from 62 to 83 MPa (cylinder strength). It was found that creep was much less for high strength concrete than for normal strength concrete, especially when specimens are permitted to dry under sustained load. A sustained compressive stress up to about one-half of the short-term strength would increase the strength of concrete. However, higher sustained stresses had a detrimental effect on the strength. It was also indicated that the ratio of the sustained loading strength (long-term strength) to the short-term strength is higher in high strength concrete than in normal strength concrete.

In their following paper, Ngab Slate and Nilson (1981b) presented their experimental results on the relationship between creep and internal microcracking of high strength concrete. It was confirmed that the amount of cracking, as well as the increase of the cracking related to the initial state, was significantly less in high strength concrete. The amount of creep strain associated with internal cracking in high strength concrete is negligible, whereas such creep is significant in normal strength concrete, particularly at high stress. The differences of the ratio of the sustained loading strength to the short-term strength between high strength concrete and normal strength concrete also could be related to the differences in microcracking.

Nagataki and Yonekura (1992) carried out experiments to investigate the drying creep behaviour of high strength concrete (compressive strength up to 100 MPa). Specific attention was paid on the different curing conditions (standard, steam and autoclave). Measurements were continued till 1250 days. It was found that the drying creep is smaller for a higher strength concrete. In particular, for a 100 MPa concrete, the drying creep was found to be nearly zero. It was also reported that the specific creep of high strength concrete cured in air was about 1/3 to 1/4 of that of normal strength concrete after 1250 days. This phenomenon was also reported by other investigations [Russell and Corley (1978)]. The difference in creep strains between air-cured and water-cured specimens diminishes with an increase of the strength of concrete.

Wolsiefer (1984) reported that a high strength silica fume concrete (with a 28-days strength of 124 MPa) under a drying condition demonstrated about 30% less creep than that of normal strength concrete.

Buil and Acker (1985) conducted creep tests by using high strength concrete having a very special mix proportion (silica fume 40% of the weight of the cement, water/cement ratio exceeding 0.5). It was shown that the basic creep differed little from that of normal strength concrete. However, there was a significant reduction of drying creep for high strength concrete.

Smadi, Slate and Nilson (1985) compared the creep behaviour of three different concretes without silica fume (low-, medium- and high-strength) under higher sustained loads. It was found that the creep strain, creep coefficient and specific creep at failure are smaller for a higher strength concrete. The sustained loading strength of high strength concrete was higher than that of low- and medium-strength concrete.

Penttala (1987) conducted creep tests on high strength concrete containing various binders (cement, silica fume, slag, fly ash, etc.). The specimens were subjected to two drying conditions (60 and 80% relative humidity). The measured creep was compared with that calculated from the CEB-FIP Model Code 1978. It was found that the high strength silica fume concrete having a 28-day's compressive strength of 110 MPa presented 80% of the creep deformation that was calculated using CEB model.

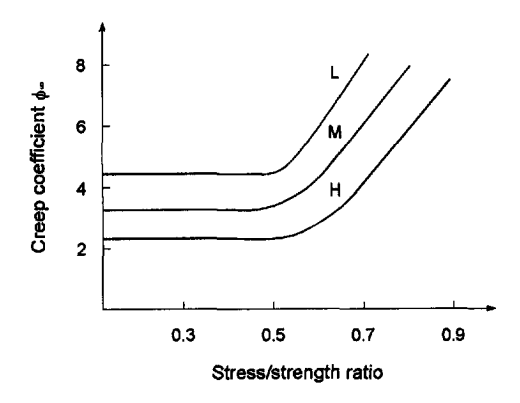


Fig. 4.9 Relationship between creep coefficient ϕ_{∞} and stress/strength ratio for low, medium and high strength concrete [after Holand (1987)].

In his report, Holand (1987) pointed out that, because of the linear relationship between stress and strain for high strength concrete, the gradual destruction of the material during loading is less pronounced for high strength concrete than for normal strength concrete. It was shown that a reduction of the creep coefficient of 25% or higher was found for high strength concrete. The creep coefficient was also constant up to a higher stress/strength ratio for high strength concrete. (See Fig. 4.9)

Smadi, Slate and Nilson (1987) carried out an investigation to study the influences of sustained compressive stress, at and in excess of the normal working stress level and under drying conditions, on the creep properties of high-, medium-, and low-strength concretes. It was found that the total strain at a given stress-strength ratio was larger for higher strength concrete, particularly at early ages after loading. Higher strength concrete had a higher creep-stress proportionality limit than lower strength concrete. The stresses in high strength concrete could increase up to 65% of the short-term strength without causing significant microcrack formation.

Collins (1989) presented experimental results on the creep behaviour of high strength concrete. The main variables in the tests were the paste content, the maximum aggregate size and the presence of a superplasticizer. The creep tests were carried out under a drying condition (50% relative humidity and room temperature). It was found that a concrete with a large maximum aggregate size and a low paste content would provide less creep. The use of a superplasticizer did not show a significant effect on creep deformation.

By using x-ray techniques, Smadi and Slate (1989) conducted an investigation to study the effects of a sustained compressive load on the microcracking and creep of high strength concrete. It was found that the amount of microcracking observed in high strength concrete was significantly smaller than that in normal strength concrete. This observation was explained to be a result of the higher bond strength in the interfacial area, relatively smaller aggregate content and smaller influence of stress corrosion in high strength concrete. Consequently, smaller inelastic deformations and higher creep-stress linearity limits were obtained.

Two series of samples, with two different kinds of high strength concrete (one with silica fume and one without), were taken from two real structures to investigate the creep behaviour [De Larrard (1990), De Larrard and Acker (1992)]. The experiments were carried out under both a wet and a dry condition. It was found that the magnitude of the creep deformations was dependent on the age at application of the load for the high strength silica fume concrete. The creep was generally much lower except for a very early-age loading of the high strength concrete. The drying creep was smaller for the non-silica fume high strength concrete, and it totally disappeared for high strength silica fume

concrete. It was found that the presence of silica fume had a remarkable influence on the drying creep.

An investigation dealing with three high strength concretes produced by low heat Portland cement with silica fume, blast furnace slag cement, and rapid hardening Portland cement were carried out by Penttala and Rautanen (1990). The variation of the porosities of concretes subjected to creep with time were studied. It was found that the initial creep rate of high and normal strength concretes is governed by the amount of evaporable water lost to the ambient environment. The creep deformations of high strength concretes were from 40 to 70% of that of a normal strength concrete. It was found that by creep deformation of high strength concrete no pore water was squeezed out of the specimen but the pore entrances were narrowed which hindered the water evaporation.

The influence of the compressive stress/strength ratio at long-term sustained loads was shown by Bjerkeli, Tomaszewicz and Jensen (1990). At loading ranges between 50 to 80% of the short-term strength, the development of the concrete strains measured during a loading time from 28 to 70 days, indicated a significantly lower creep coefficient and smaller specific creep for high strength concrete than for normal strength concrete.

Marzouk (1991) presented test results on creep behaviour of high strength concrete (70 MPa) and normal strength concrete (40 MPa) exposed to temperatures ranging from -10 °C to 20 °C and subjected to stresses of 25, 50 and 75% of their 28-day strength for one year. It was shown that creep deformations of high strength concrete are smaller than those of normal strength concrete at all adopted stress/strength ratios. The relation between creep and stress/strength ratio at room temperature was found to be linear for both kinds of concretes. It was also shown that the adopted low temperature had a minor effect on the magnitude of creep deformation for both types of concrete. It was pointed out that the diffusion of absorbed moisture was the main cause of a large change in the energy of the system. Additionally, at a low temperature, the gel deformation also contributed to the slightly large increasing creep deformation.

4.3.3 Models for predicting creep of high strength concrete

Up to now, there are several models available to predict the creep of high strength concrete. Most of the models come from the extension of the existing models for normal strength concrete.

4.3.3.1 CEB-FIP Model Code 1990

In this Model Code, the concrete is classified on the basis of its compressive strength ranging from C12 to C80, i.e. 28-day's cylindrical mean strength from 20 MPa to about 90 MPa. That means that Eqs. (4.8) to (4.20) can be directly used to predict the creep behaviour of high strength concrete [CEB-FIP (1991)].

4.3.3.2 Modifications of CEB-FIP Model Code 1990

Yue and Taerwe (1993) conducted an investigation aiming to evaluate the possibility of the use of the CEB-FIP Model Code 1990 (MC 90) expressions for creep. Based on the test data, modified parameters which are functions of the concrete strength were suggested. According to Yue and Taerwe, Eqs. (4.12) and (4.16) can be modified as follows:

$$\beta(f_{cm}) = \frac{2.6}{\sqrt{f_{cm}/10} - 1} \tag{4.45}$$

$$\beta_H = \frac{130}{f_{cm}} \cdot \left[1 + (0.012 \cdot RH)^{18} \right] \cdot h + 250 \le 1500$$
 (4.46)

4.3.3.3 Bazant-Panula model (modification)

On the basis of test data from Ngab, Slate and Nilson (1981), Bazant and Panula (1984) extended the BP model to high strength concrete. It was shown that the basic creep was predicted reasonably well by using the BP model for high strength concrete. The only modifications were made with regard to the drying creep:

$$\varphi_d' = \left(1 + \frac{t_0 - t_{s0}}{a_d \cdot \tau_{sh}}\right)^{-\frac{1}{2}} \cdot \varphi_d \tag{4.47}$$

where $a_d = 10$ for $f_{cm} \le 41$ MPa, and $a_d = 1$ for $f_{cm} \ge 69$ MPa.

$$S_d(t, t_0) = \left(1 + b_d \cdot \frac{\tau_{sh}}{t - t_0}\right)^{c_d \cdot n} \tag{4.48}$$

where $b_d = 10$ for $f_{cm} \le 41$ MPa, and $b_d = 100$ for $f_{cm} \ge 69$ MPa. Linear interpolation could be used for a_d and b_d when the strength falls in the range between 41 MPa and 69 MPa. In Eqs. (4-47) and (4-48), t_{s0} is the age at the start of drying, t_0 is the age at application of load, n is the exponent of double power law, c_d is a correction coefficient given by Bazant and Panula (1978a, b, c, 1979a, b). τ_{sh} is the shrinkage-square half-time,

proportional to the square of thickness of concrete and f_{cm} is the standard cylindrical strength at age of 28 days.

4.3.3.4 AFREM model

At LCPC (Paris), de Larrard, Acker and Roy (1994) carried out an experimental program to investigate the creep of high strength concrete. Based on the experimental data [Schaller, de Larrard, Sudret, Acker and Roy (1992)], a predicting model was proposed, which is recently adopted by AFREM (the French chapter of RILEM), as follows [Roy and de Larrard (1996)]:

$$\varepsilon_{cr}(t,t_0) = \frac{\sigma_c(t_0)}{E_{cl}} \cdot \left[\Phi_b(t,t_0) + \Phi_d(t,t_0) \right]$$
 (4.49)

where $\Phi_b(t, t_0)$ and $\Phi_d(t, t_0)$ are the basic creep coefficient and the drying creep coefficient, respectively; E_{ci} is the modulus of elasticity at an age of 28 days. The basic creep coefficient can be expressed as:

$$\Phi_b(t, t_0) = \phi_{b0} \cdot \frac{\sqrt{t - t_0}}{\sqrt{t - t_0} + \beta_{bc}}$$
(4.50)

$$\phi_{b0} = \frac{3.6}{f_{cm}(t_0)^{0.37}}$$
 for silica-fume concrete (4.51)

$$\phi_{b0} = 14$$
 for non silica-fume concrete (4.52)

$$\beta_{bc} = 0.37 \cdot e^{\frac{2.8 \cdot f_{con}(t_0)}{f_{con}}}$$
 for silica-fume concrete (4.53)

$$\beta_{bc} = 0.4 \cdot e^{\frac{3.1 \cdot f_{cm}(t_0)}{f_{cm}}}$$
 for non silica-fume concrete (4.54)

Under the assumption that the drying creep of a concrete is closely related to the drying shrinkage, the drying creep coefficient can be expressed by the following simplified equation, which makes the difference between the silica-fume concrete and the non silica-fume concrete:

$$\boldsymbol{\Phi}_{d}(t,t_{0}) = \boldsymbol{\phi}_{d0} \cdot \left[\boldsymbol{\varepsilon}_{ds}(t,t_{s0}) - \boldsymbol{\varepsilon}_{ds}(t_{0},t_{s0}) \right] \tag{4.55}$$

where $\phi_{d0} = 1000$ for a silica-fume concrete and $\phi_{d0} = 3200$ for a non silica-fume concrete. The drying shrinkage ε_{ds} comprises a kinetics item β_{ds} , which is an hyperbolic function tending towards 1, multiplied by two factors which take the influences of the relative humidity and the strength of the concrete into account:

$$\varepsilon_{ds}(t, t_{s0}) = K(f_{cm}) \cdot A(f_{cm}, h) \cdot \beta_{ds}(t, t_{s0})$$

$$\tag{4.56}$$

$$K(f_{cm}) = 18$$
 if $f_{cm} \le 57 \text{ N/mm}^2$ (4.57)

$$K(f_{cm}) = 30 - 0.21 \cdot f_{cm}$$
 if $f_{cm} \ge 57 \text{ N/mm}^2$ (4.58)

$$A(f_{cm}, h) = 72 \cdot e^{-0.046 \cdot f_{cm}} + 75 - RH \tag{4.59}$$

$$\beta_{ds}(t, t_{s0}) = \frac{t - t_{s0}}{(t - t_{s0}) + \beta_{ds0} \cdot h^2} \cdot 10^{-3}$$
(4.60)

where $\beta_{ds0} = 0.007$ for a silica-fume concrete and $\beta_{ds0} = 0.021$ for a non silica-fume concrete. The descriptions of all symbols used in AFREM are listed in Appendix G.

4.4 Creep of concrete at early ages in compression

The traditional concrete research mainly concentrated on the properties of the fresh concrete (its rheological behaviour) and the hardened concrete (its mechanical properties). The intermediate stage, when the newly cast concrete is beginning to solidify and certain mechanical properties have already developed, is relatively unknown. In practice, however, concrete is very often exposed to loads at this stage due to the behaviour of the material itself, due to mechanical influences, due to the design and due to modern construction methods. Under this condition, RILEM appointed a committee (42-CEA) to comprehensively study the up-to-date knowledge by the end of 1970's [Bergström and Byfors (1980), RILEM C42-CEA (1981)]. Since then, several larger scale research programs were carried out to investigate the early-age properties of concrete. A number of models were developed to predict the behaviour of young concrete. The appearance of high strength concrete in the practical field created a new challenge to engineers.

4.4.1 Properties of concrete at early ages

When "early age" or "young concrete" is mentioned, it is natural to raise the question: what is the exact definition of young concrete? Some authors referred to the

properties of concrete during the first 1 or 2 days after casting, while others referred to 24 hours. It is clear a definition of early age with the parameter time is definitely not suitable. Different cements, temperatures and admixtures may cause quite different rates of development of properties in a concrete. Therefore, it is probably more suitable to define early age by the degree of hydration or strength.

4.4.1.1 Degree of hydration

The degree of hydration \mathcal{G} is defined as a measure of how far the reactions between cement and water have developed. $\mathcal{G}=0$ means that no reactions have occurred and $\mathcal{G}=1$ means that complete hydration has been reached. It was found that an approximately linear relation exists between the development of compressive strength and the development of porosity of concrete and the degree of hydration [Byfors (1980)]. It was found that the factors which influence the hydration process would also affect the development of the concrete properties. For example, a rise in temperature will increase the rate of hydration, as a result, the rate of strength growth. Generally, there are six kinds of definitions of the degree of hydration:

$$\mathcal{G} = \frac{Quantity \ of \ cement \ gel \ formed}{Quantity \ of \ cement \ gel \ formed \ at \ complete \ hydration}$$
(4.61)

$$\vartheta = \frac{Quantity of hydrated cement}{Original quantity of cement}$$
(4.62)

$$\mathcal{G} = 1 - \frac{Quantity of unhydrated cement}{Original quantity of cement}$$
(4.63)

$$\mathcal{G} = \frac{\left(w_n/c\right)}{\left(w_n/c\right)_{max}} \tag{4.64}$$

$$\theta = \frac{Quantity of heat developed}{Quantity of heat developed at complete hydration}$$
(4.65)

$$\mathcal{G} = \frac{V_{sd}}{0.063 \cdot c} \tag{4.66}$$

where w_n is the quantity of bound water, c is the cement content and V_{sd} is the quantity of water adsorbed by the concrete when stored in water.

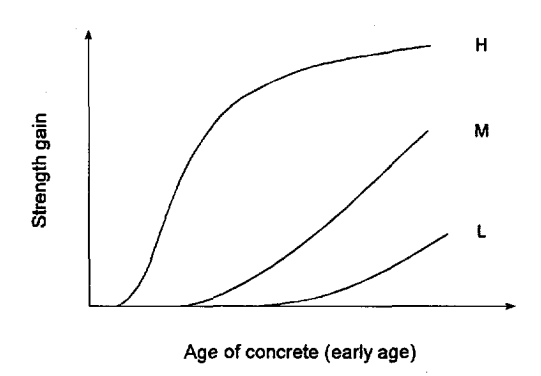


Fig. 4.10 Compressive strength gain in concrete with various curing temperatures (linear scale) [after Byfors (1980)].

It is almost impossible to make a direct determination of the quantity of cement gel formed or the quantity of hydrated cement. However, it is possible to determine the quantity of unhydrated cement with x-ray analysis. This is the reason why Eq. (4.63) was proposed. It was found that Portland cement binds about 25% by weight of water at complete hydration. On this basis, the quantity of bound water (w_n) can be used as a measure of the degree of hydration [Eq. (4.64)]. In Eq. (4.65), definition is based on the total heat created by hydration (Q). Normally, there are three methods to determine Q: a) adiabatic calorimeter; b) heat of solution and c) conduction calorimeter. The adiabatic condition creates a gradually increasing temperature field, which, in turn, influences the hydration process. The heat of solution method is found to be suitable for ages up to three days, but gives relatively unreliable results. The conduction calorimeter is preferable for determining the heat development. The specimen is kept at a constant temperature and the heat development is continuously measured.

4.4.1.2 Development of strength

The development of strength depends on various factors, such as cement, water/cement ratio, admixtures (chemical and mineral) and curing conditions (temperature, moisture situation). In Fig. 4.10 the influence of the temperature with a linear time axis is shown. If the temperature is raised, the hydration starts earlier, so does the development of the strength. The water/cement ratio seems to have no effect on the time when the development of strength begins. However, at a lower water/cement ratio, the rate of strength growth is higher. As mentioned in the previous section, the development of strength can be related to the degree of hydration. Furthermore, the degree of hydration

also has a close relation with the change of the microstructure. As the hydration process is going on, the cement gel forms a coherent structure. Further hydration entails continued structure formation (see Fig. 4.11). It can be seen that the higher water/cement ratio shows a greater distance between the cement particles. This implies that a higher degree of hydration is required for a high water/cement ratio before setting and strength gains are obtained. The degree of hydration at which setting occurs is termed as the critical degree of hydration (θ_{cr}). It is found that this degree of hydration is dependent on the water/cement ratio:

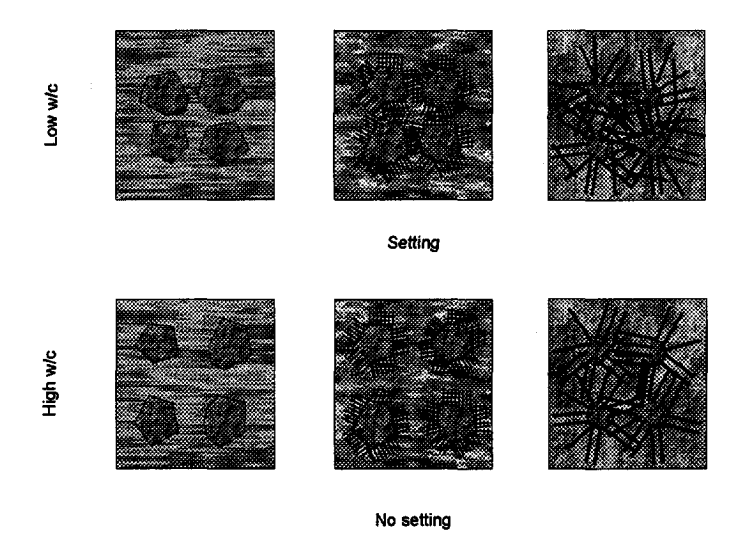


Fig. 4.11 Schematic presentation of structure formation in cement paste [after Mindess and Young (1981)].

$$\mathcal{G}_{cr} = k_h \cdot \frac{w}{c} \tag{4.67}$$

where k_h is in the range of 0.40 to 0.46. In Fig. 4.12 the relation between the critical degree of hydration and the water/cement ratio is schematically shown. However, from the results of Byfors (1980) it can be seen that the critical degree of hydration in concrete is comparatively independent of the water/cement ratio (see Fig. 4.13). The relation between the strength and the degree of hydration is linear except for the early stage, i.e. from the setting and a few hours after, at which this relation appears exponentially.

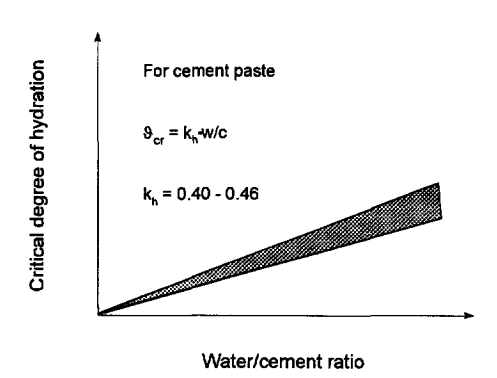


Fig. 4.12 Relation between critical degree of hydration and water/cement ratio [after Byfors (1980)].

There is another way to practically predict the development of strength by including the porosity into the expression. The porosity of concrete is closely related to the water/cement ratio and the degree of hydration. As a result, the following expression can be written:

$$P_{p} = \frac{(w/c) - 0.19 \cdot \vartheta + (A_{0}/c)}{0.32 + (w/c) + (A_{0}/c)}$$
(4.68)

$$f_{cm} = f_0 \cdot \left(1 - \frac{P_p}{P_{cm}}\right) \tag{4.69}$$

where P_p is porosity of paste, w/c is the water/cement ratio, c is cement content (kg/m³), \mathcal{G} is the degree of hydration, A_0 is the air content (l/m³), f_{cm} is the strength of concrete, f_0 is a constant, P_{cr} is the critical porosity of paste (related to \mathcal{G}_{cr}).

4.4.1.3 Practical models for predicting the strength development of concrete

In practice, the 28-day's compressive strength of concrete is the most used property. Therefore, if the relative gain of strength with time is known, the development of strength of a concrete can be determined. In the following discussions, four models will be mentioned concerning the prediction of the strength development of concrete.

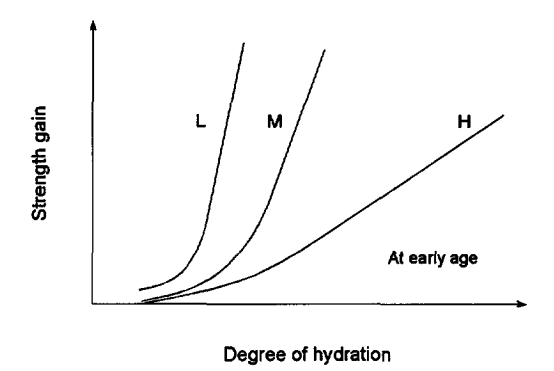


Fig. 4.13 Relation between strength gain and degree of hydration at early ages with various water/cement ratio [after Byfors (1980)].

Model after Byfors (1980)

In general, the curve of the strength development with time in a log-log scale can be regarded as a combination of two straight lines together with a transitional curve (see Fig. 4.14). On the basis of the assumptions mentioned above, the straight lines can be mathematically expressed as follows:

$$\mathfrak{R} = a_i \cdot t^{b_i} \tag{4.70}$$

where $\Re = f_{cm}(t)/f_{cm}$ is the relative strength at a time t, f_{cm} is the strength of the concrete at 28 days, a_i and b_i are constants (being dependent on the concrete composition), t is the age of the concrete in hours (being dependent on the temperature). A complete expression of the strength development can be expressed by two parts (Fig. 4.14). At very early ages, the expression corresponds to the first part (line 1) and at later ages, it will be related to the second part (line 2):

$$\Re = \frac{a_{i1} + t^{b_{i1}}}{1 + t \cdot (a_{i1}/a_{i2}) \cdot (b_{i1} - b_{i2})}$$
(4.71)

The influence of water/cement ratio on the strength development is only related to the parameter a_{i1} . This implies that the line 2 is independent of the water/cement ratio and the slope of line 1 is also independent of the water/cement ratio. Hence, the water/cement ratio affects the strength development by means of a parallel displacement of line 1. The four parameters in Eq. (4.71) can be determined by experiments.

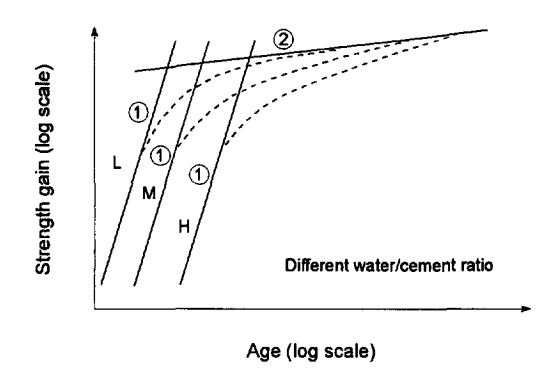


Fig. 4.14 Theoretically estimating the strength development with age of concrete in various water/cement ratios [after Byfors (1980)].

CEB-FIP Model Code 1990 [CEB-FIP (1991)]

It is shown that the compressive strength of concrete at an age t depends on the type of cement, temperature and curing conditions. For a mean temperature of 20 °C and curing under a standard condition, the relative compressive strength of concrete at various ages $f_{cm}(t)$ can be estimated as follows:

$$f_{cm}(t) = f_{cm} \cdot \beta_{cc}(t) \tag{4.72}$$

$$\beta_{cc}(t) = e^{s\left[1-\sqrt{28/(t/t_1)}\right]} \tag{4.73}$$

where f_{cm} is the concrete compressive strength at an age of 28 days, $\beta_{cc}(t)$ is a coefficient which depends on the age of the concrete t, t is the age of the concrete (days) adjusted according to Eq. (4.18), t_1 is a constant taken as 1 day, and s is a coefficient which depends on the type of cement.

In MC 90, another factor which is regarded as important as far as the strength development of concrete is concerned, is the sustained loading effect. It was found that the compressive strength of concrete under a sustained compressive stress decreased with time [Rüsch (1960)]. This strength reduction was counteracted by a strength increase due to continued hydration. The combined effect of sustained stresses and of continued hydration is given as follows:

$$f_{cm,sus}(t,t_0) = f_{cm} \cdot \beta_{cc}(t) \cdot \beta_{c,sus}(t,t_0)$$
(4.74)

$$\beta_{c,sus}(t,t_0) = 0.96 - 0.12 \cdot \sqrt{ln[72 \cdot (t-t_0)/t_1]}$$
(4.75)

where $f_{cm,sus}(t, t_0)$ is the mean compressive strength of the concrete at time t when subjected to a sustained compressive stress at an age of loading $t_0 < t$, $\beta_{cc}(t)$ is a coefficient according to Eq. (4.73), $\beta_{c,sus}(t, t_0)$ is a coefficient which depends on the time under sustained loads $(t-t_0)$ (days), t_0 is the age of concrete at application of the load, t_1 is taken as 1 day and $t-t_0$ is the time under a sustained load. One thing which is not clearly defined in MC 90, is the stress/strength ratio.

Model from American Concrete Institute

According to ACI 209 (1992), the concrete compressive strength at any time t can be predicted by the following expression:

$$f_{cm}(t) = f_{cm} \cdot \frac{t}{\alpha' + \beta' \cdot t} \tag{4.76}$$

where f_{cm} is the 28-day's strength of concrete; α' and β' are constants which are functions of the type of cement used and the curing conditions, respectively.

Model from AFREM

According to the model of AFREM [Roy and de Larrard (1996)], the concrete compressive strength at any time t can be predicted as follows:

$$f_{cm}(t) = \frac{t}{1.40 + 0.95 \cdot t} \cdot f_{cm} \tag{4.77}$$

where f_{cm} is the 28-day's strength of concrete (N/mm²), and t is the age of the concrete in days.

4.4.2 Creep of concrete at early ages

Davis [Neville, Dilger and Brooks (1983)] studied the creep properties of concrete at early loading ages. The creep of water-stored concretes subjected to the same stress, but at three different loading ages (7, 28 and 90 days) were compared. It was found that the ratio of creep deformations for concrete loaded at 7 days and 90 days was 3. It was also found that, for dry-stored concrete, the influence of the age at application of the load was considerably smaller. It was indicated that the rate of creep during the first few weeks

under loading was much larger for young concretes than for old concretes. A similar observation was reported by Wischers and Dahms (1977) and by Ruetz (1968).

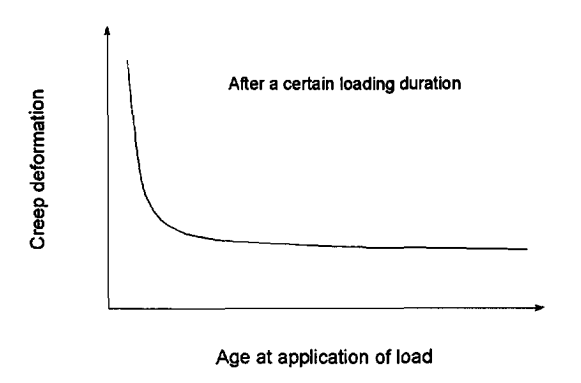


Fig. 4.15 Variation of creep of concrete with age at application of load [after Byfors (1980)].

Timusk and Ghosh (1971) carried out uniaxial creep tests at constant stress-strength ratio's on maturing cement paste. The ages of loading ranged from 0.75 to 28.75 days. It was pointed out that creep was not a linear function of the stress-strength ratio when the paste was hydrating under load, and when load is continually increased in order to maintain a constant stress-strength ratio. It was noted that, if hydration did not continue after the application of the load, the creep varied linearly with the stress-strength ratio. It was also shown that a greater increase in E-modulus occurred under a moderate stress level when loading is concurrent with hydration than without hydration [Ghosh and Timusk (1974)]. When hydration was stopped prior to loading, there was a very little gain in E-modulus under sustained load.

The general influence of the age of application of the load is shown in Fig. 4.15. The figure shows a remarkable dependency of creep on the age of loading, particularly with regard to very early ages of concrete. However, Byfors (1980) used the total absolute deformation from his tests at a stress level equal to one third of the ultimate strength as a function of a loading age, and found that creep was somewhat less at an early age of loading. The instantaneous deformation in particular is smaller at an early age. The stress is linked to the compressive strength and this grows more slowly than the E-modulus at an early age, leading to small instantaneous deformations.

Meyers and Slate (1970) showed that the increase in the rate of creep with a decrease of the age at application of the load did not apply to the application of a load at early ages

for sealed concrete, i.e. to basic creep. It was found that the influence of an increase of the age at application of the load from 7 to 26 days increases the basic creep, whereas the effect disappears in the case of total creep (unsealed concrete). Niyogi, Hsu and Meyers (1973) reported that, while basic creep increased for early ages at application of the load, total creep is unaffected (see Fig. 4.16).

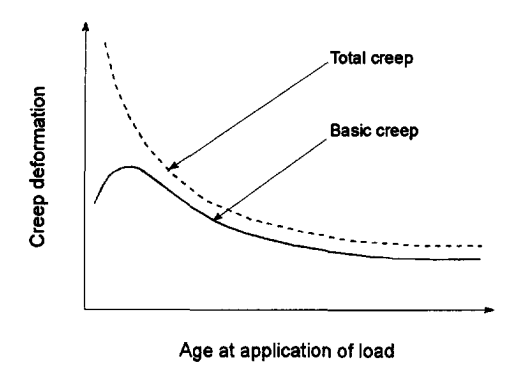


Fig. 4.16 Influence of age at application of load on the basic creep and total creep deformation [after Niyogi, Hsu and Meyers (1973)].

Sicard, Francois, Ringot, and Pons (1992) carried out tests to investigate the effect of early-age loading on the microcracking in high strength concrete. Specimens were stored and tested for 400 days in an air conditioned room (50% RH and 20 °C). The loads at three levels (20, 40 and 75% of the strengths at the time at application of load) were applied 28 hours after casting. At the mean time, the unloaded specimens were also stored in the same situation for studying the drying shrinkage. Microcracking was observed by SEM technique. It was shown that the non-uniform state of stress in young concrete subjected to both creep and shrinkage could be revealed by a surface network of microcracks. The early loading disturbed the orientation and density of surface microcracking caused by drying shrinkage.

Jensen (1992) conducted a comprehensive research program to investigate the creep and shrinkage behaviour of high strength concrete. Part of his program involved the effect of the age at application of the load. Two ages at application of the load were used, i.e. 8 and 29 days after casting. Three types of concretes (normal strength concrete, high strength concrete and very high strength concrete) were studied. In general, it was found that the specific creep decreased as the age at application of the load increased for all three types of concretes. After one year of loading, it was shown that the specific creep of the normal

strength concrete loaded at 29 days after casting was about 76% of that of the same concrete loaded at 8 days after casting. The same ratio was about 51% for high strength concrete and 59% for very high strength concrete. It was also indicated that CEB-FIP Model Code 1990 (MC 90) could predict the creep behaviour of normal strength concrete very well, while for high strength concrete, this approach showed less success.

Persson (1993) demonstrated some test results on the creep behaviour of high strength concrete at early ages when the load was applied rapidly. The concretes were loaded at 18 hours and 2 days after casting at stress levels of 30 and 60% of the strength at that moment. The moisture exchange was prevented during the tests. It was found that shortly after loading, at a load-level of 60%, the creep coefficient was about four times as high as that at a load-level of 30%. The difference between the load-levels diminished as the loading duration increased. This implied that for young high strength concrete, the creep, particularly, the rate of creep is not proportional to the applied stress.

4.4.3 Models to predict the creep of concrete at early ages

4.4.3.1 Model of Byfors (1980)

On the basis of experiments, Byfors (1980) proposed a model in which the age dependency was taken into consideration. According to Byfors (1980), the creep coefficient $\phi_{bl}(t, t_0)$ in terms of the basic creep depends on three factors:

- the composition of the concrete
- the age (degree of hydration) at application of the load
- the loading time (duration)

The influences of these factors can be considered by taking a basic value of the creep coefficient $\phi_{b/0}$, which is dependent on the concrete composition. This basic value is then multiplied by two correction factors which consider the age at application of the load $\phi_{b/0}(t_0)$ and the loading duration $\phi_{b/0}(t_0)$, i.e.:

$$\phi_{bf}(t, t_0) = \phi_{bf0} \cdot \phi_{bf}(t_0) \cdot \phi_{bf}(t - t_0)$$
 (4.78)

Since only the age dependence was taken into account, the loading duration was held constant for the different loading ages. The correction factor for the influence of the age at application of the load is expressed as:

$$\phi_{bf}(t_0) = \frac{\phi_{bf}(t - t_0)}{\phi_{bf}(t, t_0 = 28 \, days)} \tag{4.79}$$

For practice, the ageing effect can be related to the strength development of concrete, which in turn has a relation with the degree of hydration. According to Byfors, Eq. (4.79) can be further written as:

$$\phi_{bf}(t_0) = \left[\frac{a_{bf} + (f_{cm}(t_0)/f_{cm})}{1 + a_{bf}} \right]^{\frac{2}{3}}$$
(4.80)

where $f_{cm}(t_0)$ is the strength of concrete at the age of application of the load, f_{cm} is the strength of the concrete at the age of 28 days. The constant a_{bf} was suggested by Byfors as 0.17 on the basis of his tests.

4.4.3.2 CEB-FIP Model Code 1990

In MC 90 [CEB-FIP (1991)], the creep coefficient is expressed as in Eq. (4.10), where the notional creep coefficient can be calculated by Eq. (4.11). Like the model of Byfors, this notional creep coefficient also considers three factors: relative humidity, compressive strength of concrete and the age at application of the load. The effect of the age at loading is explicitly expressed by Eq. (4.14), where the age at application of the load, t_0 , also takes the curing temperature into consideration [see Eq. (4.18)].

4.4.3.3 Model of the American Concrete Institute

In the model of ACI [ACI 209 (1992)], the creep coefficient is expressed as in Eq. (4.21), where the ultimate creep coefficient can be calculated by Eq. (4.22), which considers six factors. The effect of the age at loading is specially expressed by Eqs. (4.24) and (4.25), which are applicable for loading ages later than 7 days for moist cured concrete and later than 1-3 days for steam cured concrete.

4.4.3.4 Model of AFREM

In the model of AFREM [Roy and de Larrad (1996)], the creep coefficient comprises two parts: the basic creep coefficient and the drying creep coefficient expressed as in Eqs. (4.50) and (4.55), respectively. The effect of the age at loading is considered in the basic creep coefficient [see Eqs. (4.51), (4.53) and (4.54)].

Chapter 5

Description of experimental program

The experimental program is subdivided into four series. Any of these four series involves several parameters, which are relevant to the time-dependent behaviour of high strength concrete. In this chapter, the extent of this experimental research program, as well as the materials, test set-up, measurements and test procedure are described in detail. The experimental results are generalized and arranged for further analysis, whereas the detailed test results are listed in Appendices.

5.1 Introduction

5.1.1 Aim of the experimental program

As shown in the previous two chapters, the time-dependent behaviour of concrete is one of the most complicated subjects in concrete research. A large number of factors, which are interrelated, have an influence on the behaviour. Although extended research has been carried out since the last decades, the knowledge of the time-dependent behaviour of concrete is still incomplete, and predicting models can not purely be derived on a theoretical basis. In addition, the application of high strength concrete requires even an improved understanding of the time-dependent behaviour due to the different material structure. This can only be realized through fundamental experimental research. The aim of this experimental project is to provide the necessary experimental evidence for further understanding of the time-dependent behaviour of high strength concrete, as well as to generate a basis for theoretical analysis.

5.1.2 Scope of the experimental program

The total experimental program can be subdivided into four categories:

Rate sensitivity tests

Rate sensitivity tests have been carried out on prismatic specimens $100 \times 100 \times 400$ mm. In this test series, the main variables were the strength of the concrete, the strain rate and the eccentricity of the load e/d for both compressive and tensile loading. In general, for any parameter combination, two or three tests were carried out.

Two types of concrete with 28-day's mean cube compressive strengths of about 120 N/mm^2 and 43 N/mm^2 , respectively, were used (the strength is obtained by standard tests on $150 \times 150 \times 150 \text{ mm}$ cubes).

Besides the centric tests, two eccentricities were adopted both in compression and in tension. In compression the ratio's e/d = 0, 0.075 and 0.15 applied. In tension the ratio's e/d were 0, 1/6 and 1/3.

In centric compression, six different transverse strain rates were used as feed-back signal to control the test. At the highest strain rate, the time to reach the maximum load was about two minutes, whereas at the lowest strain rate, the time to reach the maximum load was about two to three days. An additional series of tests on NSC with longitudinal strain rate control has been carried out. The range of time to reach the maximum load was kept the same as in the transverse strain rate controlled tests. Five different longitudinal strain rates were used in the tests. In centric tension, six different longitudinal strain rates were adopted as control signal. The time to reach the maximum load ranged from about five seconds to about five hours. Additionally, a number of tensile softening tests was carried out with two different longitudinal strain rates for both HSC and NSC. The time to reach the peak stress was about one minute and ten minutes, respectively.

In eccentric compression and tension, different longitudinal strain rates at the most strained fibre were used as feed back signal to control the test. The range of time to reach the peak load was about the same as in centric compression and in centric tension, respectively.

In addition, 9 cubes and 9 prisms for HSC and 5 cubes and 5 prisms for NSC, respectively, have been used for the control tests to obtain the 28-day's cube strength, 28-day's prism strength and E-modulus.

In this test series, the total number of tests carried out for HSC in both compression and tension was 88, whereas 78 tests for NSC in both compression and tension have been carried out. The distribution of the number of tests according to the parameters is shown in Table 5.I. More details about the test program are presented in Appendix A.

Table 5.1 The number of specimens used in the series of rate sensitivity tests

Series	Eccentricity (e/d)	Strength class	Number of strain rates	Number of specimens	
1.1	C0°	HSC	6	13	
1.2	C0.075#	HSC	4	8	
1.3	C0.15	HSC	9	14	
2.1	то**	HSC	6	16	
2.2	T1/6	HSC	6	12	
2.3	T1/3	HSC	6	18	
2.4	ST0 [™]	HSC	2	7	
The total number of tests for HSC is 88					
The total number of control tests for HSC is 18					
3.1	C0	NSC	6	14	
3.2	CL0"	NSC	5	8	
3.3	C0.075	NSC	6	11	
3.4	C0.15	NSC	6	10	
4.1	Т0	NSC	6	18	
4.2	T1/3	NSC	5	9	
4.3	ST0	NSC	2	8	
	The total number of tests for NSC is 78				
	The total number of control tests for NSC is 10				

^{*} C0 means centric loading in compression

High sustained loading tests

In this test series, the same type of high strength concrete specimens as used in the rate sensitivity tests were centrically loaded to values of 75%, 85% and 95% of the 28-day's prism strength of the concrete. The load was subsequently kept constant until either failure occurs or the test was deliberately stopped. The loading histories are shown in Fig. 5.1.

[#] C0.075 means compression with e/d = 0.075

^{**} T0 means centric loading in tension

^{***} ST0 means centric loading in tensile softening test

^{****} CL0 means centric loading in compression with longitudinal strain rate control

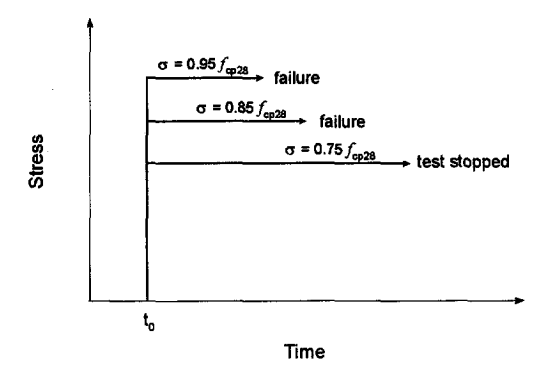


Fig. 5.1 Loading histories in high sustained loading tests.

For any of the three loading levels, three tests have been carried out. Besides, three cubes and three prisms were used for control tests in order to determine the aimed loading level. The distribution of the number of tests according to the parameters is shown in Table 5.II. More details about the test program are presented in Appendix A.

Series	Stress-strength ratio	Strength class	Number of specimens
1	0.75	HSC	3
	The number of	of control tests is 6	
2	0.85	HSC	3
	The number of	of control tests is 6	
3	0,95	HSC	3
	The number of	of control tests is 6	

Table 5.II The number of specimens used in the series of high sustained loading tests

Tests on creep at normal ages

In this series, the tests can be further subdivided into two groups. In the first group, creep tests with loading at a concrete age of 28 days were carried out for high strength concrete with a 28-day's mean cube compressive strength of about 118 N/mm² (the strength was obtained by using standard tests on $150 \times 150 \times 150$ mm cubes, i.e. the cylinder strength is about 100 N/mm²). The type of aggregate used was crushed gravel. Three stress to 28-day's prism strength ratios were adopted, i.e. 0.15, 0.35 and 0.5, which

were kept constant for about 210 days. For any loading level, six control tests (by using three cubes and three prisms) have been carried out. For any creep test, two specimens were used for measuring the creep, and another two specimens were used to measure the shrinkage. The environmental conditions were kept constant during the tests (temperature 20 °C and relative humidity 60%). A survey of the tests is given in Table 5.III.

In the second group of tests, concretes with a 28-day's mean compressive strength of about 106 N/mm^2 (the strength is obtained by using standard tests on $100 \times 100 \times 100 \text{ mm}$ cubes, i.e. the cylinder strength is about 85 N/mm^2) were tested with three loading histories. The type of aggregate used was crushed gravel. The environmental conditions were kept constant during the tests (temperature 20 °C and relative humidity 50%). The three loading histories can be described as follows (see Fig. 5.2):

- 1) A sustained load equal to 50% of the short term strength was applied during 45 days. After 45 days the specimen was unloaded [Fig. 5.2 (a)]. Creep recovery was measured for another 45 days.
- 2) Stepwise loading and unloading was applied in steps of 25% of the short term strength according to Fig. 5.2 (b).
- 3) Stepwise loading and unloading was applied in steps of 12.5% of the short term strength according to Fig. 5.2 (c).

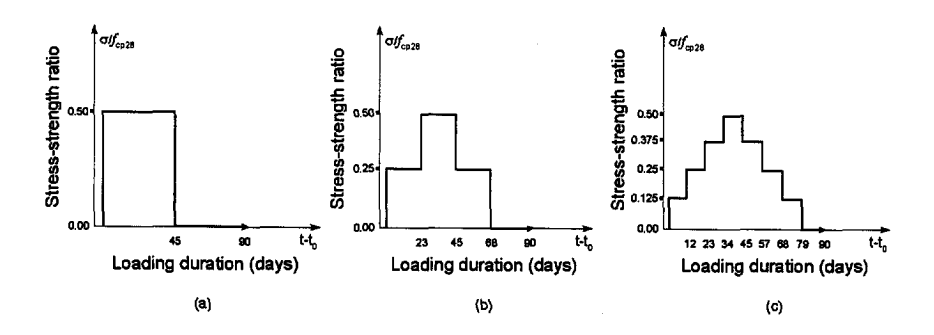


Fig. 5.2 Loading histories in creep tests at normal ages with stepwise loading.

In this group, altogether six control tests (three cubes and three prisms) have been carried out. For each loading history, two specimens were used to measure the creep, and another two specimens to measure the shrinkage.

The distributions of the number of tests on creep at a normal age are shown in Table 5.III. More details about the test program can be found in Appendix A.

Loading histories	Initial stress-strength ratio	Number of specimens
constant	0.15	2
constant	0.35	2
constant	0.50	2
•	•	
step wise	0.50	2
step wise	0.25	2
step wise	0.125	2
	constant constant constant Six sp The tota step wise step wise	constant 0.15 constant 0.35 constant 0.50 Six specimens for shrinkage tests The total number of control tests is 18 step wise 0.50 step wise 0.25

Table 5.III The number of specimens used in the series of tests on creep at normal age

Tests on creep at early ages

In this test series, the main factors to be investigated were the age of application of the load, the type of aggregate and the loading level.

HSC with three different types of aggregates (crushed gravel, granite and limestone) were used. For all types of HSC, two ages of application of the load (10 hours and 16 hours after casting of the concrete) were adopted. For any age of application of the load, three different loading levels were used. For each loading level, two specimens were used to measure the creep and the creep recovery. In addition, two specimens were used to measure the shrinkage. The loading duration was about 90 days. Afterwards, the specimens were unloaded and the creep recovery was measured for another 90 days.

Besides, for each type of HSC at each adopted age of application of the load, 36 control tests (18 cubes plus 18 prisms) at different ages have been carried out. The total number of control tests was 216. The total number of creep and shrinkage tests was 36, respectively.

The distributions of the number of specimens used in the series of tests on creep at early ages are shown in Table 5.IV. More details about the test program can be found in Appendix A.

Table 5.IV The number of specimens used in the series of tests on creep at early ages

Series	Aggregate	Age at loading	Type of test	Number of specimen
			creep	6
1.1	crushed gravel	10 hours	shrinkage	6
			control	36
			creep	6
1.2	granite	10 hours	shrinkage	6
			control	36
			creep	6
1.3	limestone	10 hours	shrinkage	6
			control	36
			creep	6
2.1	crushed gravel	16 hours	shrinkage	6
			control	36
			creep	6
2.2	granite	16 hours	shrinkage	6
			control	36
			creep	6
2.3	limestone	16 hours	shrinkage	6
			control	36

5.1.3 Identification of the tests

For the convenience of further reference, every test is identified by six symbols. In Fig. 5.3 an example is given. The specifications of all symbols are listed in the Tables 5.V to 5.X. A general overview of the research program is given in Appendix A (from Table A-1 to Table A-4).

Table 5.V Specification of the first symbol - Series number.

Symbol	Representation		
R	Rate sensitivity tests		
s	High sustained loading tests		
C _n	Creep tests at normal ages		
C _e 10	Creep tests at early ages - 10 hours		

Table 5.VI Specification of the second symbol - Type of concrete.

Symbol		Representation	
Н		High strength concrete	
N		Normal strength concrete	
	cg	Concrete with crushed gravel	
Subscript	gr	Concrete with granite	
	is	Concrete with limestone	

Table 5.VII Specification of the third symbol - Type of load.

Symbol	Representation	
С	Compression	
Т	Tension	

Fig. 5.VIII Specification of the fourth symbol - Loading method.

Symbol		Representation	
U		Centric loading	
E		Eccentric loading	
Number following	150	Eccentricity in compression (e/d=0.15)	
E 1/3		Eccentricity in tension (e/d=1/3)	

Fia	5 IY	Specification	of the fifth	symbol - Strain	rate or stress level.
FIR.	J.LA	Specification	ու աթ աա	Symbol - Sham	Tale of Stress level.

Symbol		Representation	
T25		Transverse strain rate control followed by strain rate in 10 ⁻⁶ s ⁻¹	
SRL		Longitudinal strain rate control - control test	
85		Initial stress level at 85% of short term prism strength	
SFL		Tensile softening tests - longitudinal strain rate control	
Subscript	С	Constant sustained loading (Fig. 5.1)	
for stress level	V	step-wise sustained loading (Fig. 5.2)	

Fig. 5.X Specification of the sixth symbol - Test number.

Symbol	Representation
-1	The first test
- 1.3	The first test in the third step of loading
- 2.4	The second test in the fourth step of loading

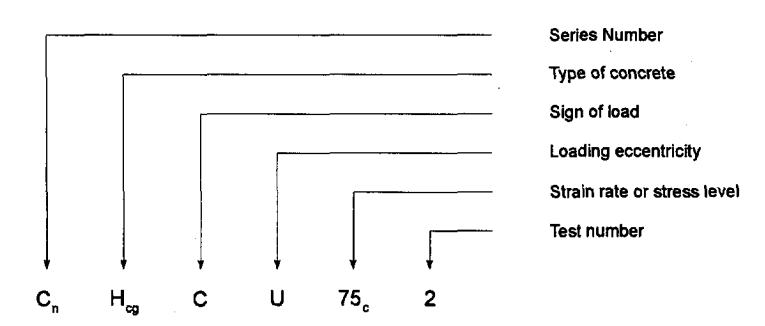


Fig. 5.3 An example of the test identification: creep test of HSC with crushed gravel, centrically loaded at a normal age in compression; the initial loading level is 75% of short term prism strength; the load is kept constant during the loading period; this is the second test.

5.2 Materials and preparation of the specimens

5.2.1 Mix proportions

5.2.1.1 Mix proportions for high strength concrete

All mixes for high strength concrete were prepared with rapid hardening Portland Cement (class C). River sand was used as fine aggregate, whereas, in the test series R, S and C_n, crushed gravel was used as coarse aggregate. In test series C_e, in addition to crushed gravel, also granite and limestone were used as coarse aggregate. The fine and coarse aggregate was totally dried in the air so that no moisture existed in the aggregates before mixing. The maximum size of the coarse aggregate particles was 16 mm. Silica fume was added in the form of dry powder. In the test series R, S and C_n, a superplasticizer consisting of lignosulfonate with a little Na-gluconate, lignosulfonate and naphthalene was used, whereas in test series C_e, a melamine-based superplasticizer (Tillman OFP4) was added. The percentage of superplasticizer was measured by the weight of cement and silica fume. The mix proportions of high strength concrete are given in Appendix B (Table B-1).

5.2.1.2 Mix proportions for normal strength concrete

All mixes for normal strength concrete were prepared with blast-furnace cement. River sand and crushed gravel were used as fine and coarse aggregate, respectively. Since there was a little amount of water in the aggregates before mixing, this amount of water was also considered when the total amount of water used in the concrete was calculated. A superplasticizer consisting of lignosulfonate with a little Na-gluconate, lignosulfonate and naphthalene was used. The percentage of superplasticizer was measured by the weight of cement and silica fume. The mix proportions of normal strength concrete are given in Appendix B (Table B-2).

5.2.2 Moulds, casting and curing

5.2.2.1 Preparation of the moulds

In test series R, all specimens were cast in the laboratory of MEBIN in Amsterdam. The moulds adopted for the prismatic specimens had a size of 100×100 mm in cross-section and 500 mm in length. For the other test series, the specimens were cast in the Stevin Laboratory, and the size of the moulds of the prismatic specimens was 100×100 mm in cross-section and 400 mm in length. The moulds for the cubic specimens had a size

 $150 \times 150 \times 150$ mm and $100 \times 100 \times 100$ mm, respectively. All the moulds were made of steel. The moulds were firstly oiled, then they were placed horizontally on the floor.

5.2.2.2 Mixing procedure

Mixing procedure for the high strength concrete

First of all, the total amount of cement and silica fume and half of the fine and coarse aggregates were dryly mixed during one minute. Then the total amount of water was added and mixed during one minute. Afterwards, a superplasticizer was added and the mixing process was continued for one more minute. Subsequently, the other half of the fine and coarse aggregates were added. The mix was then further mixed for five minutes. The slumps of all mixes were larger than 200 mm.

Mixing procedure for the normal strength concrete

At first, the total content of cement and aggregates was mixed for fifteen seconds. Then, the water was added and the mixing was continued for three further minutes. Afterwards, the total amount of superplasticizer was added and the mix was mixed for two further minutes. The slumps of all mixes were larger than 160 mm.

5.2.2.3 Curing

Curing conditions for the test series R, S and C,

All the specimens used for the test series R, S and the first part of C_n were kept in the moulds for 24 hours after casting. The casting surface of a specimen was covered with a plastic foil. The specimens with the moulds were then put into a curing room with a room temperature of 20 ± 3 °C and a relative humidity (RH) of about 60%. Then, the moulds were removed and the specimens were immediately wrapped in plastic foil to avoid moisture losses and were put back into the curing room. During the preparation of the specimens, the plastic foil was removed. After the preparation was completed, the specimens were put back into the curing room until the tests started. During testing, a normal room ambient condition was present for the test series R and S. For the test series C_n the ambient condition was kept at 20 ± 3 °C in temperature and 60% in relative humidity.

Curing conditions for the test series C_e and C_n

The specimens used for the test series C_e and the second part of C_n were kept in moulds with a temperature of 20 ± 3 °C and a relative humidity (RH) of about 50% until

one hour before the tests started (10 hours and 16 hours after casting for test series C_e , 1 day for test series C_n). During the tests, the ambient condition was kept at 20 \pm 3 °C in temperature and 50% in relative humidity.

5.2.3 Preparation of the specimens

5.2.3.1 Specimens for the test series R in compression

In the test series R, for compression tests, the prismatic specimens were shortened from 500 mm to 400 mm in length by using a sawing machine. Then the sawn surfaces were ground to get smooth and parallel flat surfaces.

5.2.3.2 Specimens for the test series R in tension

In the test series R, for tensile tests, prisms were sawn through in the middle into two parts to form two specimens with a length of 250 mm. Then, the specimens were notched on the two opposite sides at the middle. The sawn surfaces were ground and coated with a polyester resin. When this coating was sufficiently hardened, the surface was sandpapered until it looked dull. Then, the end-faces of the specimen were glued to the steel platens, which can be fixed to a frame. Afterwards, the specimens were loaded with a small compressive force in the frame for a short while.

5.2.3.3 Specimens for the test series S, C, and C,

No further preparations were needed for these specimens.

5.3 Measurements and test procedures

5.3.1 Loading and deformation measurements

5.3.1.1 Loading measurements

For the test series R in compression and S, a closed-loop servo-hydraulic machine with a loading jack, which has a maximum capacity of 2000 kN was used (see Fig. 5.4). The top block can be moved along the steel bars of the main frame. The loading cell was attached to this block. The upper hinged steel platen was also connected to this block by means of springs. The other hinged steel platen situated below the specimen was supported by a loading jack, which was on the base of the main frame. The load was applied by the upward

movement of the loading jack with its own hydraulic servomechanism and was measured by means of a load cell with a maximum capacity of 1600 kN (\pm 0.5 kN).

For the test series R in tension, a smaller testing machine with the same working principle as mentioned above was used. For the test series C_n, the load was applied by means of a flat hydraulic jack with a maximum load of 1600 KN. A load cell was used to control the actual load on the specimen. The load could be adjusted by using a handle connected to a valve, which controls the oil pressure in the jack. For the test series C_e, the load was applied by using a flat hydraulic jack with a loading capacity of 400 KN. The jack was inflated by an oil pump. The load was maintained by means of a high pressure nitrogen bulb (accumulator) and a reducing valve. The actual load was measured by a load cell, which was fixed with the loading frame. The test machines for each test series are shown in Appendix C.

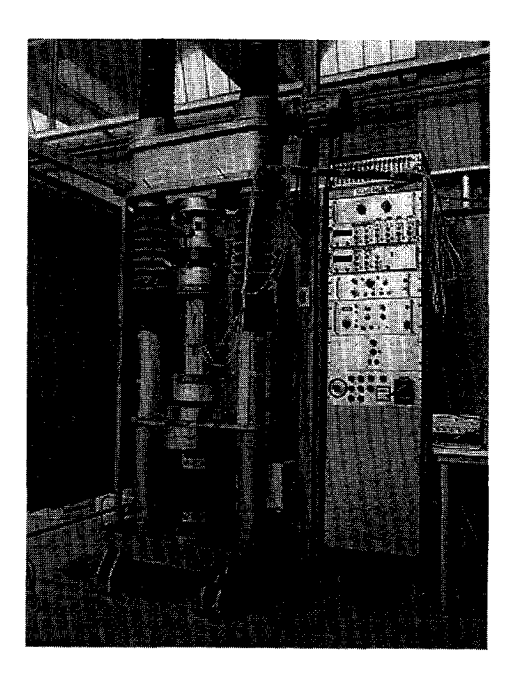


Fig. 5.4 The testing machine used in the rate sensitivity tests in compression and in the high sustained loading tests, respectively.

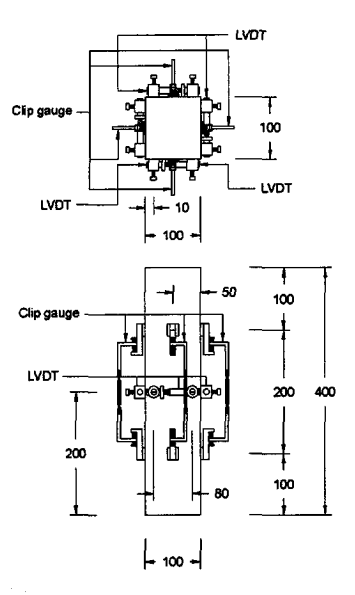


Fig. 5.5 The measurement set-up for the centric compression test in the rate sensitivity series.

5.3.1.2 Deformation measurements

Measurements in test series R in centric compression

In the test series R in centric compression (see Fig. 5.5), the transverse deformations were measured by four LVDT's with a measuring length of 80 mm (Sangamo A65, range of \pm 5 mm with an accuracy of \pm 0.0015 mm), which were attached to the four sides of a prismatic specimen. Four clip gauges with a measuring length of 200 mm were used to measure the longitudinal deformation. However, there was one test series, in which the LVDT was used to control and measure the longitudinal deformation, whereas a clip gauge was used to measure the transverse deformation. All deformation data were recorded automatically by a computer controlled datalogger. More details about the test set-up are shown in Appendix C.

Measurements for the remaining tests in the series R and S in compression

For the other tests in the series R and S in compression, four LVDT's were used to control and measure the longitudinal deformations, whereas four clip gauges were used to measure the transverse deformations. All deformation data were recorded automatically by

a computer controlled datalogger. More details about the test set-up can be found in Appendix C.

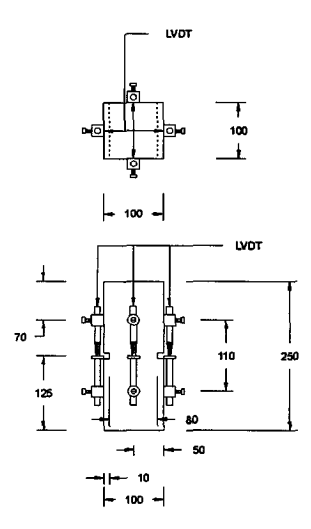


Fig. 5.6 The measurement set-up for the centric tension test in the rate sensitivity series.

Measurements in test series R in centric tension

In the test series R in centric tension (see Fig. 5.6), the longitudinal deformations were measured by four LVDT's with a measuring length of 110 mm (Sangamo A65, range of \pm 5 mm with an accuracy of \pm 0.0015 mm), which were attached to the four sides of the prismatic specimen. All deformation data were recorded automatically by a computer controlled datalogger. More details about the test set-up are shown in Appendix C.

Measurements in test series R in eccentric tension

In the test series R in eccentric tension, the longitudinal deformations at both the most strained fibre and the least strained fibre were measured by two LVDT's on each side with a measuring length of 110 mm (Sangamo A65, range of \pm 5 mm with an accuracy of \pm 0.0015 mm). All deformation data were recorded automatically by a computer-controlled datalogger. More details about the test set-up are shown in Appendix C.

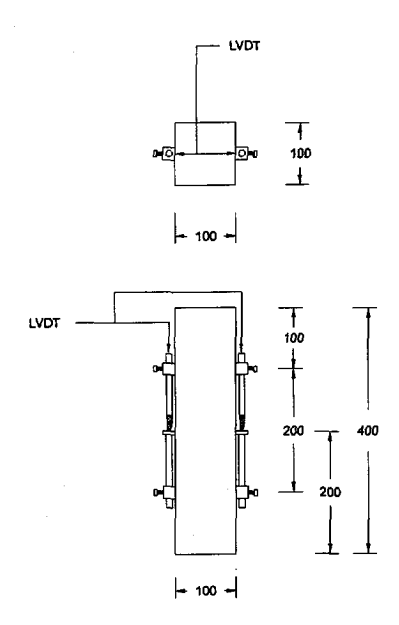


Fig. 5.7 The measurement set-up for the creep and shrinkage tests in the creep at normal ages series.

Measurements in test series C_n

In this series of tests, two LVDT's with a measuring length of 200 mm were used on the opposite side for each specimen to measure the longitudinal deformations (see Fig. 5.7). No transverse deformation was measured. All the deformation data were recorded automatically by a computer controlled datalogger.

Measurements in test series C.

In this series of tests, two strain clocks with a measuring length of 200 mm were attached on the opposite sides for any specimen to measure the longitudinal deformations. The data were manually recorded (see Fig. 5.8).

Measurements in control tests

For all the control tests, a clip gauge with a measuring length of 135 mm was attached on each of the four sides of a specimen to control and to measure the longitudinal deformation. Besides, a clip gauge with a measuring length of 60 mm was attached on any of the four sides of a specimen to measure the transverse deformation (see Fig. 5.9).

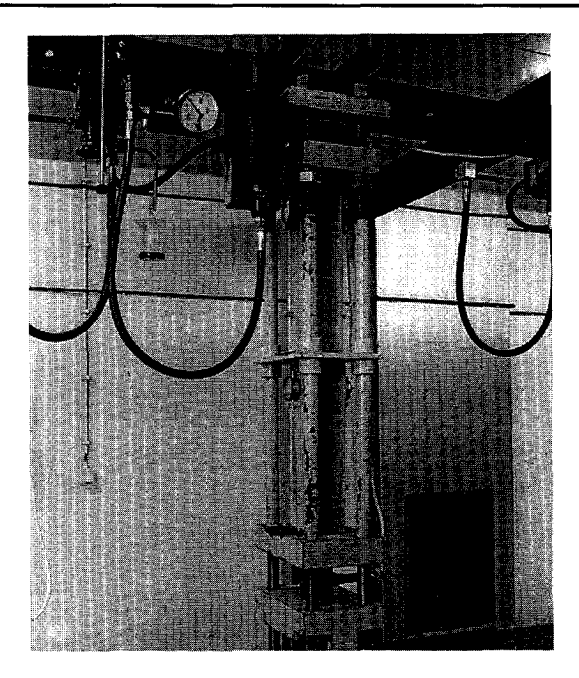


Fig. 5.8 The test set-up for the creep and shrinkage tests in the creep at early ages series.

5.3.2 Test procedures

5.3.2.1 Test procedure in the series R

Since the failure of high strength concrete can be much more sudden and explosive, a normal longitudinal deformation control system, as generally used in the case of normal strength concrete, is not suitable. Therefore, in the centric compressive tests for high strength concrete, the measurements of the transverse deformation by means of LVDT's were used as feed-back signals. In the centric compressive tests for normal strength concrete, the transverse deformation control system was also adopted for the sake of easy comparison. However, a series of tests for normal strength concrete was also carried out in which the longitudinal deformation control system was used. For the remaining tests in the series R, the longitudinal deformation control system was used for feed-back signals. A preprogrammable function equipment (PFE) was used to realise the expected deformation rates. As a specified strain rate (or deformation rate) is defined, the feed-back signal at every moment is compared with this specified parameter. During a loading period, the average value of the controlling LVDT's is calculated by a high speed processor and transferred to the PFE as a feedback signal. If the difference between the specified value and the feed-back signal exceeds the allowed limit,

the machine will automatically readjust the loading jack at a very high speed to guarantee the expected strain rate.

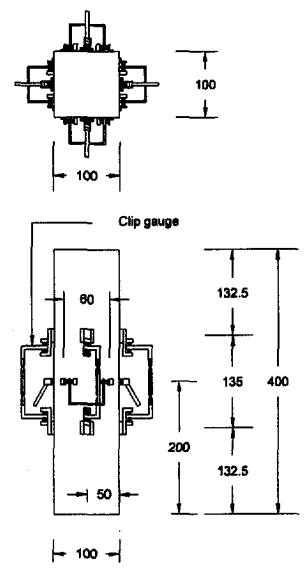


Fig. 5.9 The measurement set-up for the control test.

5.3.2.2 Test procedure in the series S

In this series of tests, during the loading period, the longitudinal deformation control system was used. After the defined loading level had been reached, the control system was switched to the loading control system, and this control method was kept for the sustained loading period. All procedures were automatically controlled by a computer.

5.3.2.3 Test procedure in the series C_n

In this series of tests, the load was manually applied at a reasonably fast speed to the defined loading level. At the mean time, the deformation was measured through LVDT's by computer. The loading level was manually maintained in order to guarantee that the deviation from the defined loading level was not larger than 5%.

5.3.2.4 Test procedure in the series C.

In this series of tests, the load was manually applied at a reasonably fast speed to the defined loading level. At the mean time, the deformation was manually recorded by reading the strain clock

5.4 Test results

5.4.1 General

The key parameters in all standard reference tests are given in Appendix D. The test results from all the test series are listed in Appendix E. Results of experimental analysis of all test series are given in Appendix F to form a basis for discussion carried out in *Chapter* 6 and 7

The key terms used to define the test results in Appendix E and F are defined as follows:

stress σ = applied load (N) divided by the cross section of a specimen;

strain ε = measured deformation (mm) divided by the initial measuring length (mm);

E-modulus E = slope of the linear regression curve obtained by using stress data up to the one third of the maximum applied stress and the corresponding strain data;

All terms used in Appendix E are the average values for each tested specimen (depending on the number of measurements per term for each specimen).

5.4.2 Control tests

In Appendix D, results of the statistical analysis are given for the control tests. Normally, a set of control test has been carried out with three cubes (to obtain the cube strength) and three prisms (to obtain the prism strength and the E-modulus). The cube strength was determined at a constant loading rate of 13.5 KN/s, whereas the prism strength was determined at a constant longitudinal strain rate of 7.3×10^{-6} s⁻¹. The strain ε_0 is the average strain from four measurements when the maximum stress had been reached.

5.4.3 Test results in series R

5.4.3.1 Centric compression

Test data are arranged in Appendix E from Table E-1 to E-6 to show the following aspects:

- the age of the concrete at application of the load to (days);
- the measured transverse strain rate $(d\varepsilon)/dt$ (s⁻¹);
- the peak stress σ_{cmax} (N/mm²);
- the ratio between the peak stress to the 28-day's cube strength obtained from the standard test σ_{cmax}/f_{cc28} ;
- the longitudinal and transverse strain at the peak stress ε_{cl0} and ε_{ctr0} ;
- the calculated longitudinal strain rate $(d\varepsilon)/dt$ (s⁻¹) (calculated by using linear regression analysis from the data of measured longitudinal strain and time up to the moment when the stress reaches one-third of the strength);
- the initial E-modulus E_{ci} (GPa) (the slope of the linear regression line calculated by using the stress data up to the one third of the maximum applied stress and the corresponding strain data);
- the initial Poisson's ratio μ (the slope of the linear regression line determined by using the transverse strain data and the corresponding longitudinal strain data up to the moment when the stress reaches one third of the strength):

The statistical analysis of the results with the average value and the standard deviation for the same terms mentioned above is given in Appendix F from Table F-1 to F-4.

5.4.3.2 Centric tension (including softening)

The test data are arranged in Appendix E from Table E-7 to E-8 to show the following aspects:

- the age of the concrete at application of the load t_0 (days);
- the longitudinal strain rate (dε)/dt (s⁻¹);

- the peak stress σ_{tmax} (N/mm²);
- the initial E-modulus E_t (GPa) (the slope of the linear regression line determined by using the stress data up to the one third of the maximum applied stress and the corresponding strain data);
- the longitudinal strain at the peak stress ε_0 . (measuring length 110 mm)

5.4.3.3 Eccentric compression and tension

The test data are arranged in Appendix E from Table E-9 to E-12 for compression and from Table E-13 to E-15 for tension to show the following aspects:

- the age of the concrete at application of the load t_0 (days);
- the longitudinal strain rate (dε)/dt (s⁻¹);
- the peak load P_{max} (KN);
- the strains at the near or far side from the loading position at the peak load ε_{cc0} and ε_{cc0} ;
- the measured ultimate strain at the near or far side from the loading position ε_{ccu} and ε_{ctu} .

The statistical analysis of the results with the average value and the standard deviation for the eccentric compressive tests are given in Appendix F from Table F-5 to F-8. The following aspects are considered:

- the longitudinal strain rate (dε)/dt (s⁻¹);
- the peak load P_{max} (KN);
- the strain at the near side from the loading position at the peak load ε_{cc0} ;
- the strain gradient at the peak load φ_0 (rad/mm);
- the rate of change of the strain gradient with time $d\varphi_0/dt$.

The statistical analysis of the results with the average value and the standard deviation for the eccentric tensile tests are given in Appendix F from Table F-9 to F-11. The following aspects are considered:

Chapter 5 Description of experimental program

- the peak load P_{tmax} (KN);
- the strain at the near or far side from the loading position at the peak load ε_{t0} and ε_{tc0} (measuring length 110 mm);
- the calculated position of the neutral axis x (mm);
- the calculated peak stress σ_{tm} under the assumption of a linear stress distribution (N/mm²) according to x.
- the calculated peak stress σ_{ttc} under the assumption of a linear stress distribution (N/mm²) according to the adopted eccentricity e.

5.4.4 Test results in series S

The test data are arranged in Appendix E from Table E-17 to E-18 to show the following items:

- the age of the concrete at application of the load to (days);
- the stress/strength (28-day prism strength) ratio σ/f_{cp28} ;
- the loading duration t-t0 (hours) until failure (f) or end of test (e);
- the initial longitudinal and transverse strain ε_{cli} and ε_{ctri} ,
- the ultimate longitudinal and transverse strain ε_{clu} and ε_{ctru} ,
- the 28-day's prism strength f_{cp28} (N/mm²);
- the initial longitudinal strain rate $[(d\varepsilon)_i/dt]_i$ (s⁻¹);
- the initial stress σ_{ci} (N/mm²);
- the initial E-modulus E_{ci} (GPa) (the slope of the linear regression by using stress data up to one third of the maximum applied stress and the corresponding strain data).

5.4.5 Test results in the series Cn and Ce

5.4.5.1 Creep under a constant sustained or stepwise increased stress

The test data are arranged in Appendix E from Table E-19 to E-20 and from Table E-22 to E-27 to show the following aspects:

- the age of the concrete at application of the load t_0 (days);
- the stress/strength ratio $\sigma_c(t_0)/f_{cp}(t_0)$ at the time t_0 ;
- the loading duration t-t₀ (days);
- the 28-day's prism strength f_{cp28} (N/mm²);
- the prism strength $f_{cp}(t_0)$ at the time t_0 (N/mm²);
- the totally measured strain (shrinkage plus initial elastic strain plus creep) $\varepsilon_c(t, t_0)$;
- the shrinkage $\varepsilon_{sh}(t, t_0)$;
- the initial elastic strain $\varepsilon_{ie}(t_0)$.

The statistical analysis of the results with the average value and the standard deviation for the constant sustained loading or the increasing loading tests are given in Appendix F from Table F-12 to F-13 and from Table F-15 to F-20. In addition to the items mentioned above, extra terms are also included:

- the creep $\varepsilon_{cr}(t, t_0) \left[\varepsilon_{cc}(t, t_0) = \varepsilon_c(t, t_0) \varepsilon_{ie}(t_0) \varepsilon_{sh}(t, t_{s0}) \right]$
- the creep coefficient referring to t_0 , $\phi_{t0} = \varepsilon_{cr}(t, t_0) / \varepsilon_{ie}(t_0)$;
- the creep coefficient referring to 28 days, $\phi_{28} = \varepsilon_{cr}(t, t_0) / \varepsilon_{ie}(28)$;
- the specific creep $C(t, t_0) = \varepsilon_{cr}(t, t_0)/\sigma_c(t_0)$ (MPa⁻¹).

5.4.5.2 Creep under a decreasing stress (recovery)

Test data are arranged in Appendix E in Table E-21 and from Table E-26 to E-31 to show the following aspects:

the age of the concrete at unloading t₀ (days);

Chapter 5 Description of experimental program

- the creep recovery duration t-t₀ (days);
- the shrinkage $\varepsilon_{sh}(t)$;
- the total measured strain $\varepsilon_c(t, t_0)$ after recovery;
- the initial total strain before unloading $\varepsilon_c(t_0)$;
- the initial recovery strain $\varepsilon_{irec}(t_0)$.

The statistical analysis of the results with the average value and the standard deviation for the decreasing loading test are given in Appendix F in Table F-14 and from Table F-21 to F-26. In addition to the aspects mentioned before, extra terms are also included:

- the creep recovery $\varepsilon_{rec}(t, t_0) \left[\varepsilon_{rec}(t, t_0) = \varepsilon_c(t_0) \varepsilon_c(t, t_0) \varepsilon_{irec}(t_0) + \varepsilon_{sh}(t) \varepsilon_{sh}(t_0) \right]$
- the ratio between creep recovery and creep $\varepsilon_{rec}(t, t_0)/\varepsilon_{cr}(t, t_0)$;
- the specific creep recovery $C_{rec} = \varepsilon_{rec}(t, t_0)/\sigma_c(t_0)$ (MPa⁻¹).

Chapter 6

Experimental research and analysis - strain rate sensitivity

On the basis of the test data, a comprehensive experimental analysis has been carried out, which has mainly focused on the influence of the strain rate as well as the strain gradient on the fundamental mechanical properties of high strength concrete and normal strength concrete (for comparison) in compression as well as in tension. The phenomena observed in the experiments are interpreted by referring to a proposed mechanism of rate sensitivity of concrete, whereas the differences between the internal material structure of high strength concrete and normal strength concrete are emphasised.

6.1 Introduction

On the basis of the experimental data from the series R and S mentioned in the previous chapter, a comprehensive experimental analysis is conducted in this chapter, whereas the experimental analysis of the test series C_n and C_e is shown in the following chapter. According to the different loading methods, the experimental analysis is generally classified into two parts. In the first part, the analysis is totally related to the compressive behaviour of concrete. The influences of various strain rates on the mechanical properties of both high strength concrete and normal strength concrete are analyzed and compared. In addition, the influences of strain gradients in combination with strain rates on the key mechanical properties of concrete are also studied. In the second part, the same procedures as that in the first part are applied to study the time-dependent behaviour of concrete in tension. Furthermore, the phenomena observed in the experiments are interpreted by referring to a possible mechanism of rate sensitivity of concrete, whereas the differences of the internal material structure between high strength concrete and normal strength concrete are emphasised.

6.2 An explanation for the strain rate sensitivity

In order to fully understand the strain rate sensitivity of concrete, a mechanism aiming at qualitatively explaining the strain rate sensitivity of concrete is proposed. The key considerations in this rate-sensitivity model concern the material structure, where emphasis is put on the pore structure and the moisture content of the concrete.

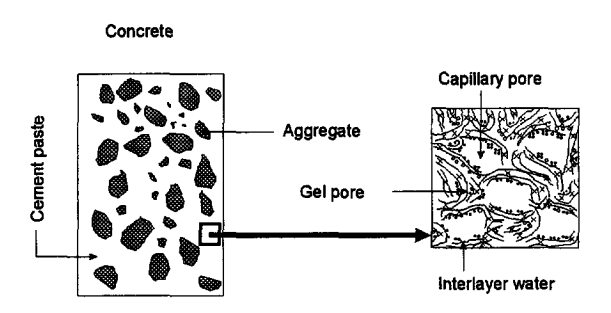


Fig. 6.1 Pore structure inside the concrete.

6.2.1 Material structure of concrete and classification of water

The material structure of concrete is very complicated. In general, concrete can be considered as a multi-phase material composed of at least seven components: coarse aggregate, sand, unhydrated cement particles, cement gel, gel pores, capillary pores and entrapped air voids along with various states of water [Neville (1991), Mindess (1984)]. Water in concrete can be classified into three categories according to the degree of firmness held by the solid phase. At one extreme, there is capillary water or free water inside the air voids or the microcracks. This kind of water is beyond the surface forces of the solid phase. At the other extreme, there is chemically bounded water or water of hydration, forming a definite part of the hydrated compounds. Between these two categories there is gel water which consists of adsorbed water, i.e. water held by the surface forces of the gel particles (van der Waals forces), and interlayer water which is held between the surfaces of hydrated calcium silicate. (see Fig. 6.1)

In addition, microcracks existing in the interface area between matrix and aggregate before and during loading can be regarded as macropores, which are several orders larger

than the gel pores and capillary pores. Microcracks existing already before loading are caused by segregation and by tensile stresses resulting from early volume changes that are largely associated with hydration and shrinkage of the cement paste. During loading, these microcracks tend to develop further to form even larger cracks.

6.2.2 Assumed mechanism of rate sensitivity of concrete

When concrete is subjected to external loading, the water in various voids and pores behaves in different ways. Here two different loading situations are considered: compression and tension, which are the general loading cases in practice. Because of their random orientation in the concrete (especially gel pores), voids and pores are generalized, for reasons of simplicity, in two directions: perpendicular and parallel to the direction of loading (see Fig. 6.2).

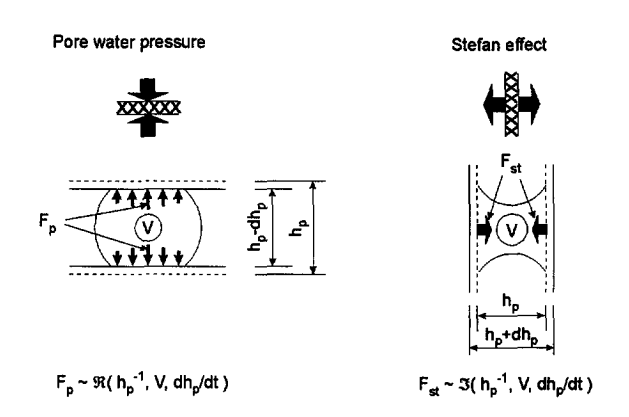


Fig. 6.2 The proposed mechanism of strain rate sensitivity

When a compressive force is applied on a concrete element, the pores perpendicular to the loading direction tend to close, resulting in a movement of the water in the pores. Because of the viscosity of the liquid, the movement of water will go together with a pressure gradient. This hydrostatic pressure (pore water pressure) F_p depends on the size of the pore h_p , the amount of pore water V, and the closing speed of two opposite pore walls dh_p/dt (see Fig. 6.2 left). The increase of this pore water pressure can help the solid phase in the concrete to resist the external force (by adding further resistance to the longitudinal deformation). The contributions of the pores parallel to the loading direction can be

explained on the basis of the Stefan Effect, well known to physicists, which is described as follows: the presence of a thin viscous film V (for example, water or other liquid phase) between two perfectly plane and parallel plates, separated by a certain distance h_p , creates an opposing force if an attempt is made to separate the two plates at a velocity dh_p/dt [Rossi (1991)]. The plates separated by the water can be considered as an analogy to the walls of pores in concrete. If a load is applied, the walls parallel to the loading direction tend to separate from one another, creating an opposing force F_{st} which will counteract this separation (see Fig. 6.2 right). This will further reduce the development of microcracks and restrict the transverse deformation, resulting in a higher compressive strength. If the loading speed or strain rate decreases, the created pore pressure and the Stefan Effect also tend to decrease. At an extreme, the rate sensitivity disappears, and the concrete only has its strength from the solid phase.

When a tensile force is applied, it is clear that only the Stefan Effect plays an important role. In this case, the Stefan Effect will directly restrict the longitudinal deformation and counteract the development of cracking perpendicular to the loading direction.

From the above discussion, it can be seen that both the pore water pressure F_p (in the case of pore-compression) and the opposing force by the Stefan Effect F_{st} (in the case of pore-tension) are functions of the following parameters: a) size of the pores; i.e. the distance between the opposite walls of a pore; the smaller is the distance, the higher is the pore pressure or the opposing force; b) the volume of the water; the larger is the volume of the water, the higher is the pore pressure or the opposing force; c) the velocity of the relative displacement of the pore walls (strain rate); the higher is the velocity, the higher is the pore pressure or the opposing force.

6.3 Influence of the strain rate on the behaviour in centric compression

In this section, only the effect of the strain rate on the behaviour of concrete in centric compression is considered. Various mechanical properties such as failure mode, stress-strain relation, strength, deformation, E-modulus, Poisson's ratio, critical stress at various strain rates are analyzed. In Appendix E, the mechanical properties of high strength concrete and normal strength concrete at various strain rates under either transverse strain rate control or longitudinal strain rate control obtained from the tests are given in Table E-1 to Table E-6. On the basis of a statistical analysis, the same properties are presented in Table F-1 to Table F-4 in Appendix F. The mechanical properties of the standard centric compressive tests are summarized in Table D-1 and Table D-2 in Appendix D. In the following section, the differences of the mechanical properties between high strength

concrete and normal strength concrete are compared and discussed. Some qualitative conclusions are drawn

6.3.1 The failure mode of concrete in compression

In comparison with normal strength concrete, all specimens with high strength concrete fail more violently in the centric compressive tests at the adopted strain rates. That is also the reason while the transverse strain rate control was used for high strength concrete [Han (1992c)]. Even with this control method, at a higher strain rate, specimens in high strength concrete still fail abruptly and violently. A larger number of fragments are produced at higher strain rates than at lower strain rates for high strength concrete. Mostly, the cracks go through the aggregates, forming a relatively smooth crack surface.

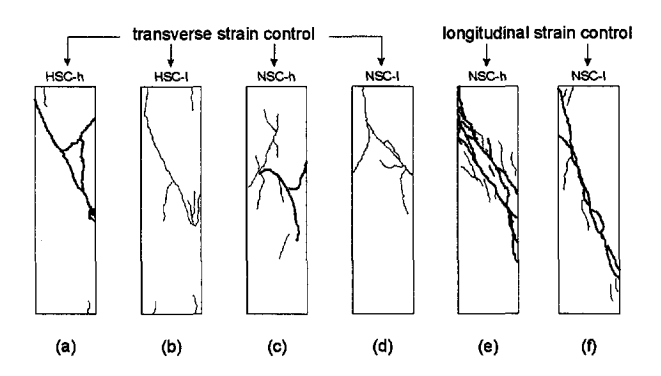


Fig. 6.3 The failure modes for HSC and NSC. (a) HSC at a higher strain rate, TSC; (b) HSC at a lower strain rate, TSC; (c) NSC at a higher strain rate, TSC; (d) NSC at a lower strain rate, TSC; (e) NSC at a higher strain rate, LSC; (f) NSC at a lower strain rate, LSC (TSC and LSC mean transverse strain control and longitudinal strain control respectively).

In high strength concrete, the matrix-aggregate transition zone becomes very compact and its microstructure is as dense as that of the paste matrix. In addition, the strength of this interface area is at least as strong as that of matrix and aggregate [Goldman and Bentur (1989)]. In this case, the crack goes through the aggregate. The behaviour of high strength concrete has similarities with that of a homogeneous material. Due to the relative homogeneity of high strength concrete, once the failure plane is formed, it develops in a sudden way and causes a violent failure. Very few surface cracks can be observed except for the main cracks [see Fig. 6.3(a)]. At lower strain rates (i.e. the transverse strain rate is

smaller than 1.9×10^{-7} s⁻¹), although the failure mode is about same, the specimens fail with relatively less violence [see Fig. 6.3(b)].

For normal strength concrete, the violence of failure is much less than for high strength concrete. In normal strength concrete, the cracks generally originate at the interface between matrix and aggregate and propagate through the matrix. The crack surface is rough, because the aggregate particles do not fracture. Due to the larger difference in strength between the aggregate and the matrix than in HSC, the aggregate particles act as crack arrestors causing the formation of several potential failure planes [see Fig. 6.3(c)]. By means of longitudinal strain rate control, the failure of a specimen occurs in a quite violent way, especially at higher strain rates. For both normal and high strength concrete, as the strain rate decreases, the number of cracks observed also decreases. The shear failure mode is observed in both high and normal strength concrete, although for high strength concrete, it is very difficult to observe the definite failure mode at higher strain rates due to the explosive failure. The general failure modes of high strength concrete and normal strength concrete under the two strain rate control methods (longitudinal and transverse) are shown in Fig. 6.3. The failure modes observed in the experiments are nearly identical to that reported by Carrasquillo, Slate and Nilson (1981b).

6.3.2 Stress-strain relationships

Typical stress-strain curves for high strength concrete and normal strength concrete for different strain control methods at various strain rates are shown in Fig. 6.4, Fig. 6.5 and Fig. 6.6. The ordinate represents the stress, whereas the abscissa represents the longitudinal strain and the transverse strain. In Fig. 6.4, the stress-strain relations for high strength concrete obtained in the centric compressive tests are shown, whereas in Fig. 6.5, the stress-strain relations for normal strength concrete obtained in the centric compressive tests are displayed. In both cases, the transverse deformation is controlled during the test. In Fig. 6.6, the stress-strain curves from centric compressive tests with normal strength concrete are shown, where longitudinal strain rate control is adopted.

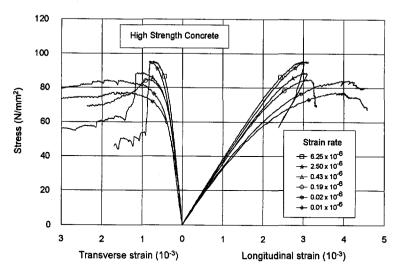


Fig. 6.4 Stress-strain relations for HSC in centric compression at various transverse strain rates.

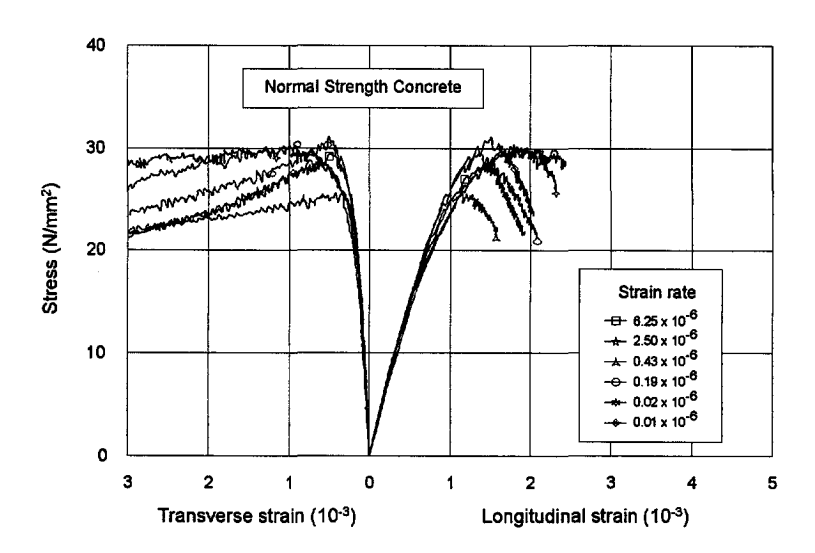


Fig. 6.5 Stress-strain relations for NSC in centric compression at various transverse strain rates.

For high strength concrete (Fig. 6.4), the shape of the stress-strain curve up to the peak stress is much more linear and steeper, especially at higher strain rates, than for

normal strength concrete. As the strain rate decreases, some significant changes in the stress-strain curve take place. First of all, the slope of the stress-strain curve decreases, and the non-linearity becomes more and more distinct. The strain under the peak stress also increases as the strain rate decreases. The peak stress is significantly influenced by the strain rate. The post-peak stress behaviour is also observed.

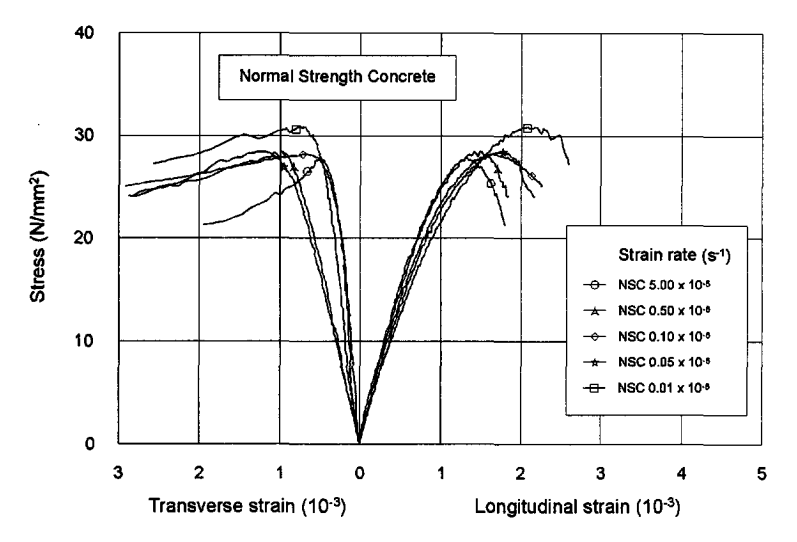


Fig. 6.6 Stress-strain relations for NSC in centric compression at various longitudinal strain rates.

Since a lot of factors can influence the softening behaviour of concrete in compression, such as the strain rate or the loading rate, the equipment adopted to measure the deformation, the measuring length, the size of the specimen, the boundary conditions of the specimen during testing, the stiffness of the testing machine, and so on [Carrasquillo, Nilson and Slate (1981a), Schickert (1980), Kotsovos (1983), Van Mier (1984), Vonk (1992)], uncertainties in the post-peak behaviour of concrete are unavoidable. However, From Fig. 6.4, it can be seen that, both for the longitudinal and the transverse strain, the post-peak parts of the stress-strain curves become less steep as the strain rates decreases. This observation indicates that the strain rate plays a very important role as far as the softening behaviour of concrete in compression is concerned. The snap back in the stress-longitudinal strain relations may imply two things. Firstly, the measurement devices could have been situated outside the range of the fracturing zone, causing partly elastic unloading within the measuring area after the peak stress has been reached. Secondly, behind the peak stress, high strength concrete behaves as a less redundant material due to the smooth crack surfaces. Therefore, failure occurs mostly very sudden and in an explosive way, without a

large deformation. In spite of this, the post-peak parts of the stress-longitudinal strain curves gradually rise to a certain extent as the strain rate decreases.

In comparison with high strength concrete, the stress-strain relations for normal strength concrete at various strain rates under transverse strain rate control show less regularity (see Fig. 6.5). Contrary to high strength concrete, the influence of the strain rate on the peak stress is not significant. With decreasing strain rate, the slope of the ascending part of the stress-strain curves show a smaller decrease than in the case of high strength concrete.

Comparing Fig. 6.5 and Fig. 6.6 it can be concluded that for NSC the way in which the test is controlled makes hardly any difference. The diagram obtained with transverse strain rate control (Fig. 6.5) gives about the same results as the diagram obtained with longitudinal strain rate control (Fig. 6.6). This is different to HSC, for which a stable test is only obtained with transverse strain rate control.

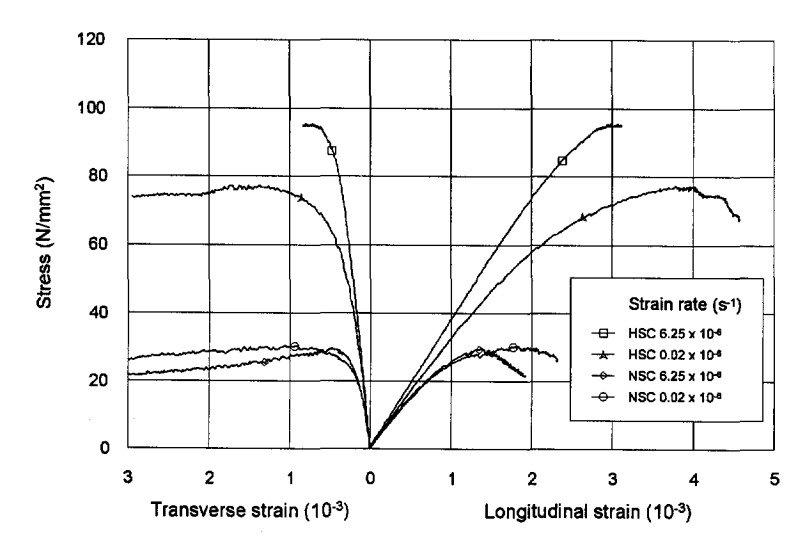


Fig. 6.7 Comparison of stress-strain relations for HSC and NSC at two strain rates.

The differences between the stress-strain relations of high strength concrete and normal strength concrete at various strain rates can be explained by the differences of their material structure. The material structure of high strength concrete has been explored on either micro- or meso-levels, by Carrasquillo, Slate and Nilson (1981b), Bentur, Goldman and Cohen (1987), Sarkar and Aïtcin (1987), Goldman and Bentur (1989), Mehta and Aïtcin (1990). It is assumed that the higher strength mainly follows from the reduced water

content, resulting in a refinement of the pore sizes and the use of silica fume leading to an improved bond between aggregate and matrix. Additionally, silica fume can act as a filler, which leads to a reduction of the volume of the water filled spaces, that may form around the aggregates. These improvements of the material structure will certainly result in modified mechanical characteristics. In Fig. 6.7, the differences between the stress-strain relations of high strength concrete and normal strength concrete at two different strain rates under transverse strain rate control, respectively, can be clearly recognized.

As the strain rate decreases, the slope of the stress-strain curve for both high and normal strength concrete decreases. For high strength concrete this influence is more obvious. The point at which the stress-strain curve starts to be non-linear is lower in this case. The strain at the same stress level increases significantly for high strength concrete, but only a little for normal strength concrete.

6.3.3 The strength (peak stress) in compression

In Fig. 6.4 and 6.5 it can be seen that the strain rate does have an influence on the strength (peak stress). The associated tests are documented in Table F-1 and Table F-3 in Appendix F. However, the extent to which the strain rate influences the peak stress for high strength concrete and normal strength concrete is quite different. The effect of strain rate on the peak stress seems to increase significantly as the strength of the concrete increases.

In Fig. 6.8 the peak stresses obtained for high strength concrete and normal strength concrete are shown as a function of the transverse strain rate. It is evident, that high strength concrete is more sensitive to a variation in the strain rate than normal strength concrete. The decrease of the peak stress for high strength concrete, as the transverse strain rate decreases from $6.25 \times 10^{-6} \text{ s}^{-1}$ to $2.0 \times 10^{-8} \text{ s}^{-1}$, is about 20%. For normal strength concrete the effect of strain rate on the strength, - at least for the range of strain rates considered - is not significant. This observation corresponds with findings of Rasch (1962) who carried out tests on normal strength concrete. It is seen that also in Rasch's tests on normal strength concrete, no significant influence of the strain rate is found.

As mentioned before, the rate sensitivity of concrete is assumed to be a function of the amount of water in the pores, the size of the pores (also including the size of the flaws), and the changing rate of the dimension of the pores (loading rate and strain rate). Hence, any parameter which influences the physical structure of the solid phase of the concrete, will also influence the rate sensitivity. The matrix of high strength concrete has a high compactness, whereas in normal strength concrete, the matrix is much more open. In addition, studies of the pore size distribution indicate that much finer pores exist in high strength concrete.

Additionally, Goldman and Bentur (1989) indicate that in high strength concrete, the aggregatematrix transition zone, which is usually porous and weak due to bleeding, shrinkage and temperature differences during the hardening process of the concrete, is very compact and its microstructure is as dense as that of the matrix

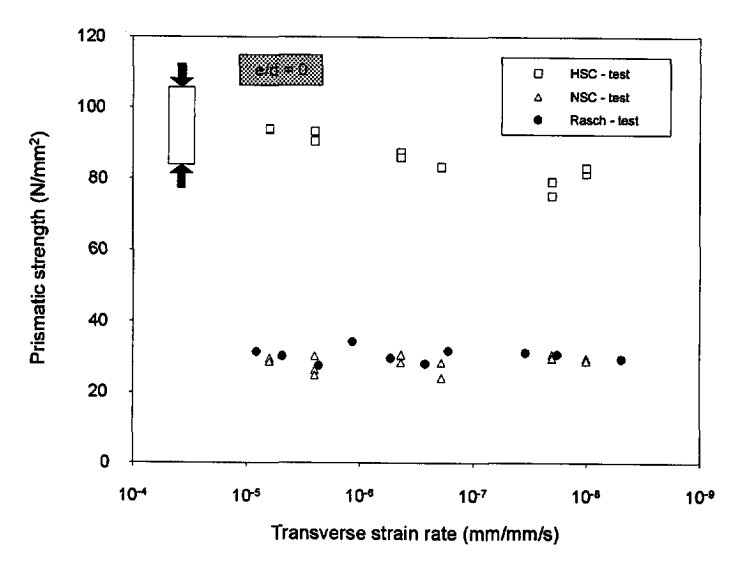


Fig. 6.8 The peak stress versus transverse strain rate in centric compression.

The experimental observations might possibly be explained on the basis of the previously assumed mechanism (Fig. 6.2): for HSC in compression, at a higher strain rate, higher pore-water pressure is built up due to the smaller pore size, which mainly contributes to the restraint of the longitudinal deformation, while the Stefan Effect explains the delayed development of the transverse deformation; moreover, because of the difficulty of the movement of free water through the concrete, less free water could evaporate during the periods of curing, thus, more free water is available in creating pore-water pressure, and the Stefan Effect is enhanced at loading; at a lower strain rate, the stressed water in the pores will get enough time to flow through the channels (microcracks and flaws) to the unstressed regions, causing a relaxation of the pore-water pressure; additionally, the opposite force produced by the Stefan effect also decreases due to a lower strain rate; hence, the concrete tends to show the strength values of the solid phase.

In NSC, even before the load is applied to the concrete, about 50% of the total crack length at the peak stress is already present [Stroeven (1973)]. Smadi and Slate (1989) also found that for NSC (28-day's compressive strength of 102×203 mm cylinder of 23 N/mm²),

cured in water for 28 days, the totally measured crack length is about three times as large as for HSC (with a 28-day's compressive cylinder strength of 64 N/mm²). If the concrete is cured in air for 30 days, the totally measured crack length due to shrinkage in NSC is about nine times as long as that in HSC. In addition, relatively larger pore sizes and more flaws (air voids) are another characteristic of NSC. Hence, it is very difficult to build up porewater pressure in compression (except if a very high strain rate is applied) during loading because the free water can easily flow through these channels to the less stressed areas. Furthermore, less free water (or even gel pore water) is available in NSC to create a significant pore-water pressure and to activate the Stefan effect due to its open internal structure, resulting in no significant difference in peak stress if the strain rate varies. The results of the experiments show that the strain rate within the adopted range has only little influence on the peak stress of NSC.

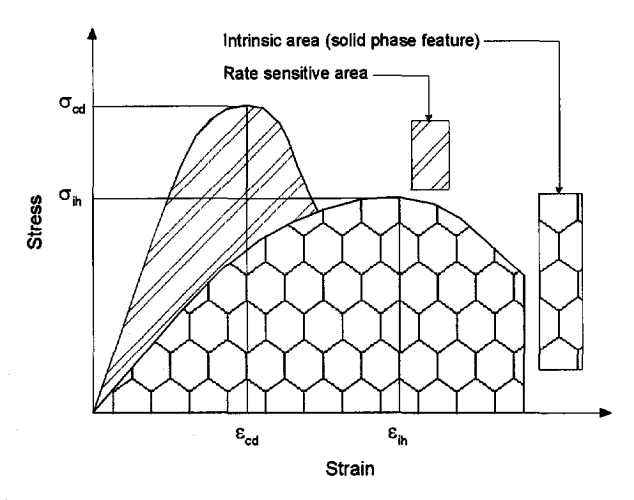


Fig. 6.9 The rate sensitive area in a stress-strain relationship of concrete.

It is clear that the strength, which is generally regarded as a basic material property, is in fact rate sensitive. Along with the strain rate, any change related to the pore structure and the pore-water condition may result in a difference in strength. At an extreme, if there is little or no free water in the concrete, there will be no change of strength at all: in that case, concrete shows the strength of the solid phase. This strength can be defined as the intrinsic strength of concrete. Normally, the strengths obtained from standard tests fall into the range which is beyond that of the intrinsic strength. This area can be called the rate-sensitive area (see Fig. 6.9).

6.3.4 Initial modulus of elasticity

The initial modulus of elasticity E_{ci} is calculated by taking the slope of the best fit line from the stress-longitudinal strain curve between 5% and 30% of the peak stress. The reasons to select this method to get the initial modulus of elasticity are: a) to avoid initial setting errors; b) to take the range wide enough in order to limit the scatter; c) to keep the upper point at a value till where the response is approximately linear. All of the calculated data of the initial modulus of elasticity for high strength concrete and normal strength concrete are given in Table E-2, Table E-4, and Table E-6 (see Appendix E).

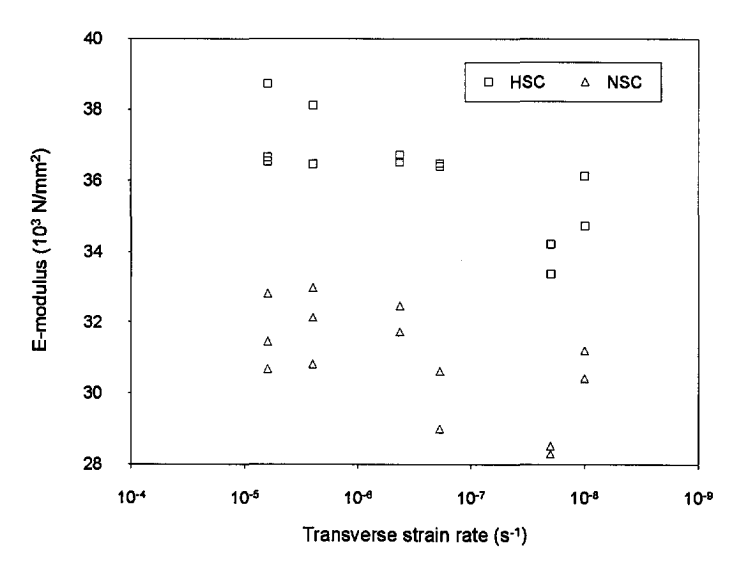


Fig. 6.10 Relationship between E-modulus and transverse strain rate for both HSC and NSC.

With respect to the E-modulus (see Fig. 6.10), it is clearly seen that the strain rate does have some effect on the E-modulus for both high strength concrete and normal strength concrete.

6.3.5 Initial Poisson's ratio

In Table E-2 and E-4 (see Appendix E) it can be seen that Poisson's ratio of high strength concrete at any strain rate used in the tests is smaller than that of normal strength concrete at the corresponding strain rate. This phenomenon can be related to the smaller number of microcracks developed during loading in high strength concrete. As far as the effect of the strain rate is concerned, a slight tendency of increase of Poisson's ratio could

be found for both high strength concrete and normal strength concrete as the strain rate decreases (see Fig. 6.11). The initial Poisson's ratio seems not to depend significantly on the strain rate.

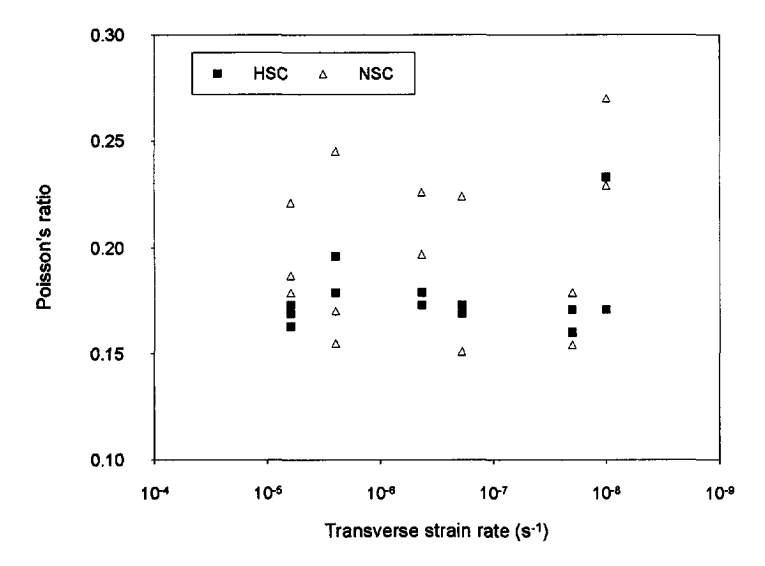


Fig. 6.11 Initial Poisson's ratio versus transverse strain rate for both HSC and NSC in centric compression.

6.3.6 Sustained loading and the long-term strength

The capacity-reduction factors, which are used in building codes for long-term or sustained loading, are based on experiments carried out by Rüsch (1960). In these tests, however, the load was not supplied according to a certain strain rate, but in another way: the load was applied in a very short time and was then kept constant for a long period. Failure occurred, if the loading level was sufficiently high, after a certain time. This way of loading is more or less "academic", but is considered to be more detrimental in comparison with the loading procedure according to constant strain rate (see Fig. 3.10). The explanation is that at a constantly high load level the microcracks will develop faster. Shah and Chandra (1970) also pointed out that because of two opposing effects appear as a load is applied to the concrete, i.e. consolidation (strengthening) and cracking (weakening), the relative magnitudes of these effects depend on the level of load (sustained load) and the way to apply the load (at a constant strain rate or sustained load). At a higher load, crack propagation may predominate over any strengthening effect of stress, while at a constant

strain rate (if the strain rate is not very high), these two effects could take place at the same time; which one will dominate depends on the strain rate adopted.

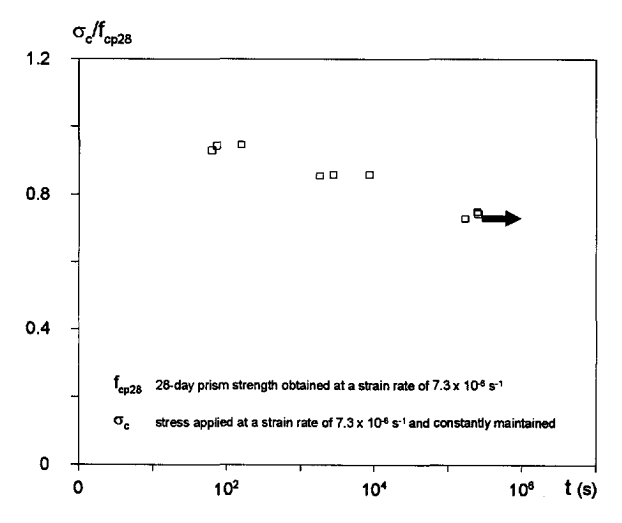


Fig. 6.12 Relationship between stress-prismatic strength ratio and time in high sustained loading tests.

It was therefore decided to carry out the test series S (high sustained loading tests), in which Rüsch's loading principle was followed. This series of tests was limited to high strength concrete. The test results are shown in Fig. 6.12 and in Table E-17 and E-18 in Appendix E, respectively. The load was supplied centrically to values of 0.95 f_{cp28} , 0.85 f_{cp28} and 0.75 f_{cp28} and was subsequently kept constant. Here f_{cp28} is the 28-day prismstrength, determined with a longitudinal strain rate of 7.3×10^{-6} s⁻¹. This strain rate is usual for a standard-prism test and results in a failure in 5-7 minutes for the concrete considered.

In the tests with a loading value of $0.95 f_{cp28}$ failure occurred after about 1.5 to 2.5 minutes. In the case of $0.85 f_{cp28}$ failure occurred after about 0.5 to 2.5 hours. With a loading value of $0.75 f_{cp28}$ failure did not occur during a loading period of about 3 days. Then the specimens were loaded to failure. In comparison with the results of strength tests by using the unloaded virgin specimens, the average gain in strength for the specimens under the sustained load was about 5%.

In combination with the results of tests in series R, it can be concluded that the long-term strength of HSC is about or below 80% of its short-term strength.

6.3.7 Concluding remarks

From the comprehensive discussion about the rate sensitivity of both high strength concrete and normal strength concrete, the following concluding remarks can be made:

- The general failure modes of high strength concrete and normal strength concrete at various strain rates show some differences. For high strength concrete, less cracks on the surface of the specimen are observed as failure occurs. Failure mostly occurs in a single crack surface. The crack surface is generally smooth. More sudden and violent fracture occurs than for NSC. For normal strength concrete, more potential failure surfaces are observed. The crack surface is rough and the failure happens in a less violent way. For both concretes, as the strain rate slows down, relatively more cracks are observed and failure takes place in less violent way.
- For both concretes, the stress-strain relations change as the strain rate decreases, however, in a different scale. For high strength concrete, the ascending part of the stress-strain curve deviates from the linear characteristics at a more early stage as the strain rate decreases, resulting in an increase of both longitudinal and transverse strain at the same stress level. This increase is larger for high strength concrete than for normal strength concrete. The influence of the strain rate on the post-peak behaviour of the stress-strain relation of high strength concrete and normal strength concrete seems to be consistent, i.e. as the strain rate decreases, the descending part of the stress-strain curve tends to fall in a less sudden way, resulting in a more ductile behaviour as far as the softening behaviour of concrete is concerned.
- Under compressive loading at various strain rates, high strength concrete suffers a more severe reduction of the peak stress than normal strength concrete does, as the strain rate decreases, resulting in a more unfavourable behaviour as far as the time-dependent behaviour is concerned.
- The initial modulus of elasticity of both high strength concrete and normal strength concrete decreases as the strain rate decreases, but in a less significant way than in the case of the peak stress.
- In comparison with the initial modulus of elasticity, the initial Poisson's ratio seems to be less effected by the strain rate. This could be explained by the similar influence of the strain rate on both longitudinal and transverse strain, as a result, keeping the initial Poisson's ratio unaffected.

• In combination with the results from the rate sensitivity tests and the high sustained loading tests, it can be concluded that, for high strength concrete, the long-term strength is about or below 80% of its short-term strength.

6.4 Influences of strain gradients on the behaviour in eccentric compression

Most load-bearing elements (such as beam, columns, slab, and so on) experience strain gradients. It is also pointed out by several researchers [Rüsch (1960), Rasch (1962), Sturman, Shah and Winter (1965), Shah and Slate (1965), Clark, Gerstle and Tulin (1967), Markeset (1993)] that the mechanical properties of concrete obtained from the centric compressive tests are not directly applicable to the situation where strain gradients dominate. In recent years, as fracture mechanics of concrete in tension has largely developed, several researchers have also tried to introduce the principle of fracture mechanics to the study of compressive behaviour of concrete as well [Van Mier (1984), Hillerborg (1988), Hillerborg (1989), Vonk (1992) and Markeset (1993)]. It is demonstrated that in compression localization of deformations occurs as the failure stage is approached. Therefore, the stress-strain curve obtained from a centric loading test can not realistically represent the behaviour of concrete subjected to strain gradients, especially for the post-peak behaviour. Since compression failure is always accompanied by transverse strains, which may cause a complicated three-dimensional state of stress [Kotsovos (1982)], depending on the confinements due to a longitudinal strain gradient, transverse strain gradient, reinforcement and so on, it is clear that the properties in this situation are not any more the material properties.

In order to better understand the behaviour of high strength concrete subjected to a strain gradient and a strain rate, an experimental analysis has been carried out. The load-strain relations at various strain rates and strain gradients for both high strength concrete and normal strength concrete are compared. In order to be able to simulate the time-dependent behaviour of high strength concrete under an eccentric loading, a model based on the idea of the compressive damage zone (CDZ) from Markeset (1993) is developed. On the basis of the knowledge of the time-dependent behaviour of HSC in centric tests, several parameters have been used in this model to simulate the influences of strain rates and strain gradients on the stress distributions in the compression zone. The calculated load-strain curves are compared with those from the eccentric compressive tests. Finally, a case study is carried out by using two recently adopted Dutch and German codes for HSC. Based on the previous analysis, some conclusions will be drawn.

6.4.1 General experimental observations

In Table E-9, Table E-10, Table E-11 and Table E-12 (see Appendix E), the maximum load P_{max} and the strains of the extreme fibres ε_{cc0} and ε_{cn0} at the maximum load are given. In addition, in Table F-5, Table F-6, Table F-7 and Table F-8 (see Appendix F), the strain gradient at the maximum load φ_0 and the calculated strain gradient rate $d\varphi/dt$ are given for both high strength concrete and normal strength concrete for the two eccentricities tested.

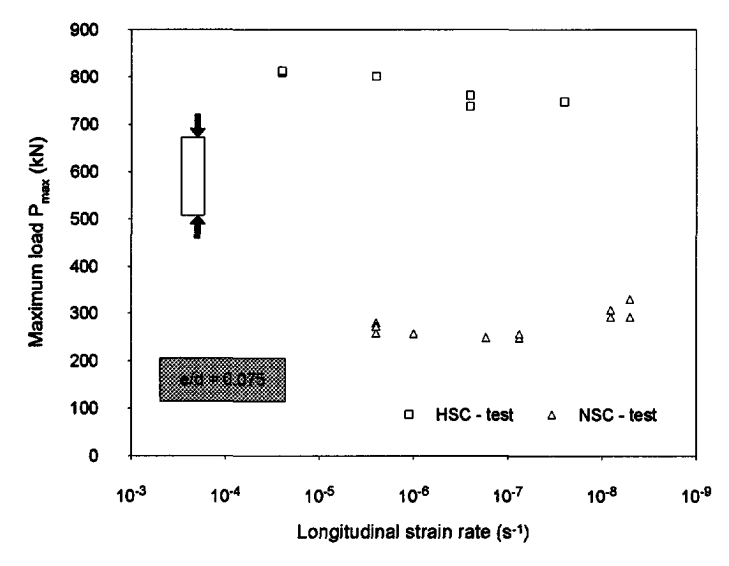


Fig. 6.13 Maximum load versus the longitudinal strain rate for both HSC and NSC at an eccentricity of e/d = 0.075.

From the results, it can be found that at a smaller strain gradient (e/d=0.075), the rate sensitivity of high strength concrete and normal strength concrete is higher than that at a larger strain gradient (e/d=0.15), as far as the load-carrying capacity is concerned (see Fig. 6.13 and Fig. 6.14). Obviously the strain rate sensitivity decreases with increasing e/d (compare also Fig. 6.8). Normal strength concrete shows, remarkably, even a slight increase of the strength with decreasing strain rate, both for e/d = 0.075 and e/d = 0.15. The number of specimens is, however, too small to draw definite conclusions.

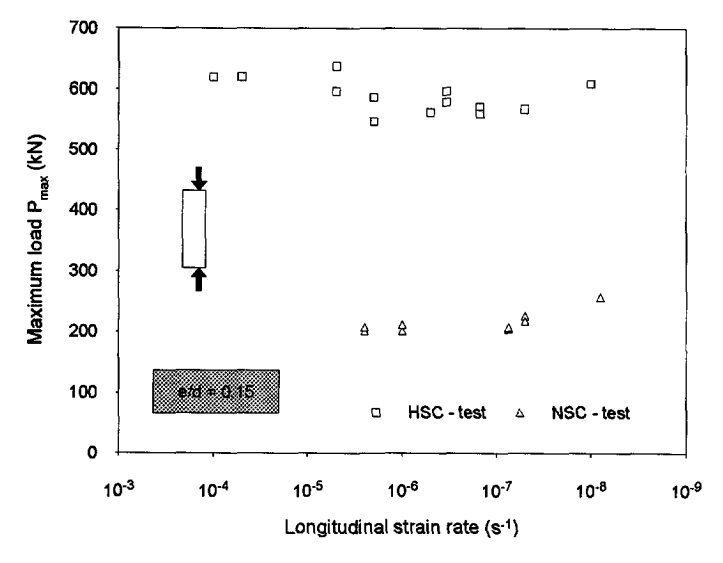


Fig. 6.14 The maximum load versus the longitudinal strain rate for both HSC and NSC at an eccentricity of e/d = 0.15.

6.4.2 Description of the compressive damage zone model

The basic idea of this compressive damage zone model (CDZ), developed by Markeset (1993), focuses on the descending branch of the stress-deformation diagram of concrete. The descending part is described by means of two curves related to the longitudinal cracks and the localized shear bands, respectively. A very important parameter, tensile fracture energy G_F , is introduced into the CDZ model, taking account of the interdependence between compressive failure and lateral deformation.

6.4.2.1 Failure hypothesis

It is believed that the microcracks are the main contributors to the non-linearity of the compressive stress-strain curve. Microcracks normally initiate at the interface area between the mortar and the aggregate. Once the inclined bond cracks begin to slip, transverse compressive support is provided from the surrounding material, resulting in compressive stresses in the interface and tensile stresses in the mortar matrix. These tensile stresses cause the growth of the longitudinal cracks and the transverse deformations.

In the post-peak region two different fracture processes may develop. A sliding mode of failure occurs when the inclined microcracks come together to form inclined localized shear bands. A tensile mode of failure (axial splitting) occurs when a critical lateral deformation is exceeded.

For a concrete specimen loaded in compression the fundamental failure mode is a combination of both axial splitting and sliding. However, the influence of each failure mode may depend on concrete material factors such as concrete composition, type of aggregate and maximum size.

6.4.2.2 Model description

Fig. 6.15 illustrates the CDZ model on a specimen loaded in centric compression. When no frictional restraint prevails in the end zones the longitudinal strain is regarded as uniformly distributed along the whole length of the specimen prior to peak load. After peak load, longitudinal tensile cracks and transverse deformations occur within a limited part of the specimen (see Fig. 6.15). This zone is named 'damage zone' with a length L^d . Along with this tensile fracture process inclined microcracks may come together to form a localized shear band, where the adjoining parts tend to slide relatively to each other.

Based on these ideas the CDZ model consists of three curves shown in Fig. 6.15. Outside the damage zone, the behaviour of the material is described by a conventional ascending branch and an unloading branch from the peak stress (upper curve). Inside the damage zone the deformations caused by the tensile fracture process is assumed to be uniformly distributed and the properties can then be given by a stress-strain relation (middle curve). The behaviour in the shear-band is given by a stress-displacement relation (bottom curve).

The composition of the complete stress-strain curve is illustrated in Fig. 6.16. The average compressive strain ε_m for a specimen with a length $L > L^d$ can be expressed as:

$$\varepsilon_m = \varepsilon + \varepsilon_d \frac{L^d}{L} + \frac{w}{L} \tag{6.1}$$

where ε is the strain outside the damage zone, ε_d is the additional compressive strain after peak stress caused by the splitting cracks, w is the additional deformation in the fracture zone.

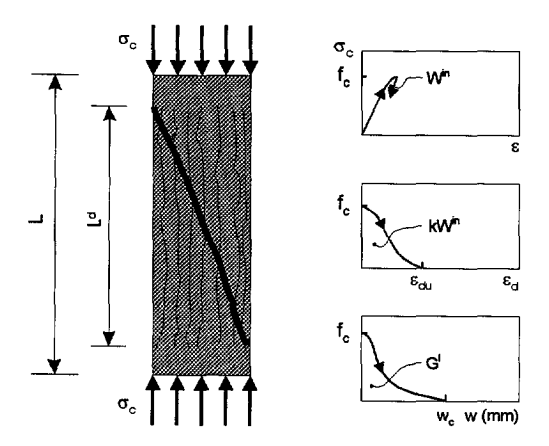


Fig. 6.15 Illustration of the CDZ model on a specimen loaded in centric compression.

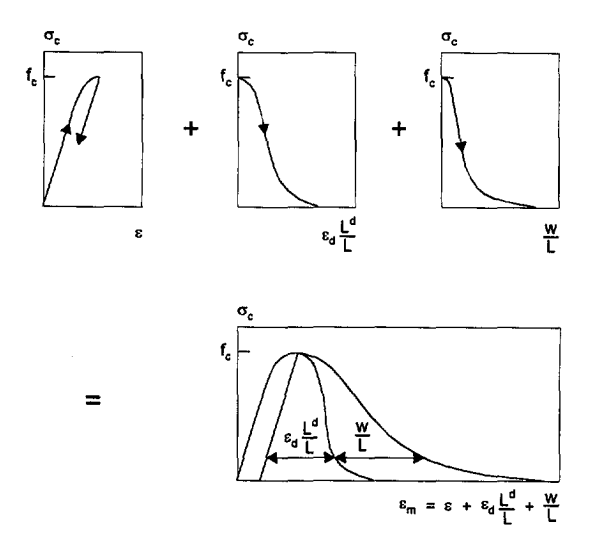


Fig. 6.16 Composition of the complete stress-strain curve.

The total energy absorbed in the specimen is given as the summation of the energy absorbed in the inclined shear band and in the longitudinal tensile cracks inside and outside

the damage zone. In general, the area beneath the complete compressive stress-strain curve can be described as the compressive fracture energy per unit volume:

$$W^{c} = W^{in} + W^{s} \frac{L^{d}}{L} + G^{l} \frac{1}{L}$$
 (6.2)

where W^c is the compressive fracture energy per unit volume, W^m is the energy per unit volume absorbed in the longitudinal cracks up to peak stress, W^s is the energy per unit volume absorbed in the longitudinal cracks after peak stress, G^l is the energy per unit area perpendicular to the σ_c consumed in the shear band, L^d is the length of the damage zone, L is the specimen length.

The energy per unit area G' consumed in the localized inclined crack can be given as:

$$G^{l} = \beta \cdot f_{c} \cdot w_{c} \tag{6.3}$$

where f_c is the compressive strength, w_c is the vertical component of the sliding deformation along the shear band at failure, βf_c is the average stress during the deformation. The value of βw_c reflects the frictional restraint in the shear band.

The energy dissipated in the longitudinal tensile cracks is assumed to be proportional to the tensile fracture energy G_F (per unit area). However, at the peak stress, the longitudinal cracks are only partly opened and thus only a part of the fracture energy G_F is consumed. The area W^s corresponds to the remaining part of G_F . Suppose that W^s is proportional to W^{in} :

$$W^s = k \cdot W^{in} \tag{6.4}$$

the following relationship is suggested for the total energy per unit volume consumed in the longitudinal tensile cracks W^d :

$$W^{d} = W^{in} + W^{s} = (1+k) \cdot W^{in} = \frac{G_{F}}{r}$$
(6.5)

where k and r are material properties. The parameter r has the dimension of a length. Probably, r is proportional to the average distance between successive longitudinal cracks, as more cracks per unit volume will give a higher energy absorption per unit volume.

Win can be obtained from Eq. (6.5) as:

$$W^{in} = \frac{G_F}{r \cdot (1+k)} \tag{6.6}$$

Inserting Eqs. (6.3), (6.5) and (6.6) into Eq. (6.2), the compressive energy per volume W^c is obtained:

$$W^{c} = W^{in} + kW^{in}\frac{L^{d}}{L} + \beta f_{c}\frac{w_{c}}{L} = \frac{G_{F}}{r(1+k)} \left(1 + k\frac{L^{d}}{L}\right) + \beta f_{c}\frac{w_{c}}{L}$$
(6.7)

Ensuring that no friction restraint prevails in the end-zones, Eq. (6.7) can be applied for specimens shorter than L^d by inserting $L^d = L$. Consequently, the energy per unit volume consumed in a specimen of length L equal to or less than L^d is:

$$W^{c} = \frac{G_{F}}{r} + \beta f_{c} \frac{w_{c}}{L} \qquad \text{for } L \le L^{d}$$
 (6.8)

6.4.2.3 Material parameters

The parameter k

To obtain the parameter k, the nonlinearity of the stress-strain relation in the pre-peak region has to be experimentally studied. The relations between the elastic energy as well as the inelastic energy and several mechanical properties can be established. as illustrated in Fig. 6.17, the elastic energy at peak stress is given as:

$$W^{el} = \frac{f_c^2}{2E_c} \tag{6.9}$$

where E_c is the modulus of elasticity in compression and f_c the compressive strength.

By using Eqs. (6.6) and (6.9) the ratio between inelastic and elastic energy at peak stress may be written as:

$$W^{in} / W^{el} = \frac{2}{r(1+k)} \frac{G_F E_c}{f_c^2}$$
 (6.10)

The inelastic and elastic energy may also be written in another form:

$$W^{in} = \alpha \varepsilon^{in} f_c$$
 where α is a shape factor (6.11)

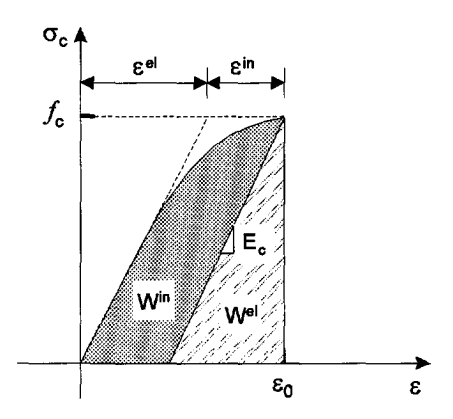


Fig. 6.17 Definition of the inelastic and elastic energy.

$$W^{el} = \frac{\varepsilon^{el} f_c}{2} \tag{6.12}$$

Inserting Eqs. (6.11) and (6.12) into Eq. (6.10) yields:

$$W^{in} / W^{el} = \frac{2\alpha f_c \varepsilon^{in}}{f_c \varepsilon^{el}} = 2\alpha \frac{\varepsilon^{in}}{\varepsilon^{el}} = \frac{2}{r(1+k)} \frac{G_F E_c}{f_c^2}$$
(6.13)

Solving Eq. (6.13) with respect to the ratio between inelastic and elastic strain yields:

$$\frac{\varepsilon^{in}}{\varepsilon^{el}} = \frac{1}{\alpha r(1+k)} \frac{G_F E_c}{f_c^2} = \gamma \frac{G_F E_c}{f_c^2}$$
(6.14)

where
$$\gamma = \frac{1}{\alpha r(1+k)}$$
 (6.15)

Inserting Eq. (6.15) into Eq. (6.6) yields:

$$W^{in} = \alpha \gamma G_F \tag{6.16}$$

According to the experimental results, the relationship between $\varepsilon^{in}/\varepsilon^{el}$ and G_rE_c/f_c^2 can be obtained. Hence, the parameter γ is figured out. On the basis of the analysis by Markeset (1993), the following values are found for γ .

for normal density concrete
$$\gamma = 0.25 \text{ mm}^{-1}$$
 (6.17)

for light-weight concrete
$$\gamma = 0.50 \text{ mm}^{-1}$$
 (6.18)

The strain at peak stress $(\varepsilon_0 = \varepsilon^{el} + \varepsilon^{in})$ can be expressed as:

$$\varepsilon_0 = \frac{f_c}{E_c} + \gamma \left(\frac{G_F}{f_c}\right) \tag{6.19}$$

According to Markeset (1993), the remnant tensile strength at ultimate compressive strength is about 65%. At the tensile stress level of 0.65 f_i , approximately 25 and 50% of the fracture energy G_F , is consumed for the normal density and the light-weight aggregate concrete, respectively. Therefore, the ratio between the energy consumed in the longitudinal tensile cracks at the peak stress W^{in} , and at failure W^{i} , is:

for normal density concrete
$$\frac{W^{in}}{W^d} = \frac{1}{1+k} = 0.25$$
 (6.20)

for light-weight concrete
$$\frac{W^{in}}{W^d} = \frac{1}{1+k} = 0.50$$
 (6.21)

Solving Eqs. (6.20) and (6.21) with respect to k yields:

for normal density concrete
$$k = 3.0$$
 (6.22)

for light weight concrete
$$k = 1.0$$
 (6.23)

The parameter r

Solving Eq. (6.15) with respect to r yields:

$$r = \frac{1}{\alpha \gamma (1+k)} \tag{mm}$$

Inserting the value of k and γ into Eq. (6.24) yields:

$$r = \frac{1}{\alpha} \tag{6.25}$$

Assuming the shape factor α to be 0.8, r becomes then 1.25 mm. As a material parameter, r is proportional to the distance between successive longitudinal cracks.

6.4.3 Compressive strain gradients

6.4.3.1 Extra assumptions

In Chapter 3, a comprehensive survey about the influence of the strain gradient on the strength and ductility of concrete was carried out. In general, when a strain gradient exists, different fibres across a section experience different strains. The transverse deformation of the mostly stressed fibre is restrained by the less stressed fibres. This leads to confining compressive stresses in the mostly stressed fibre, and a corresponding increase in ultimate stress. The longitudinal strain of the most stressed fibre can not develop freely, but is governed by the rather uniform deformation of the underlying less stressed fibres. As soon as localization starts to develop at one point the stress decreases at that point and the forces are partly taken over by the underlying fibres. The decrease in stress in the mostly stressed fibre spreads along a distance L^d in the stress direction. If the material is homogeneous and the gradient is constant along the specimen, another localization appears at a constant distance L^l (see Fig. 6. 18).

It is assumed that the damage zones are close together so that the distance L^I becomes approximately equal to the length of each damage zone L^d . Inserting this assumption into Eq. (6.1) the average strain in the mostly stressed fibre can be written as:

$$\varepsilon_m = \varepsilon + \varepsilon_d + \frac{w}{L^1} \tag{6.26}$$

It is also assumed that the length of the damage zone L^d is proportional to the depth of the damage zone, d. According to Fig. 6.18, the depth of the damage zone can be calculated as:

$$d^{l} = \frac{\varepsilon_{m} - \varepsilon_{o}}{\varepsilon_{m}} \cdot x \tag{6.27}$$

where x is the depth of the compression zone. According to Markeset (1993), in centric compression, the length of the damage zone L^d is about 2.5d, whereas in bending, the length of the damage zone L^d is found to be about 5 times the depth d.

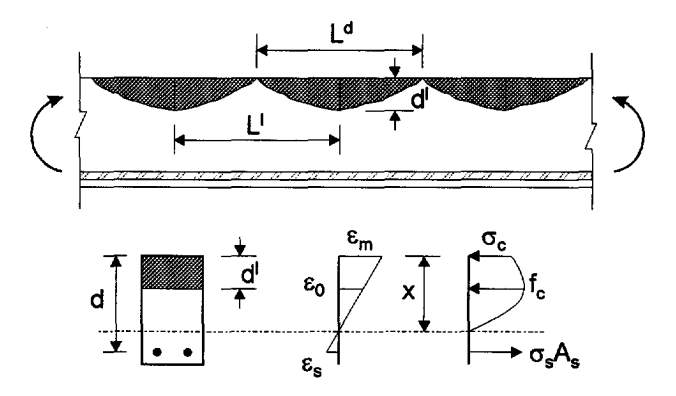


Fig. 6.18 Damage localization in a bent beam.

As indicated in *Chapter 3*, when a strain gradient exists, the fibres in the compression zone experience different strains, and thus, there is no general stress-strain relation for a compression zone. As an approximation it is assumed that any fibre in the compression zone has the same stress-strain relation.

In the case of the existence of a strain gradient, a stress-strain relation obtained in centric compression with a descending branch may be used. According to Eqs. (6.26) and (6.27), this relationship is size dependent or more precisely strain gradient dependent. When the ultimate moment is reached, a final localization is growing at one point. Then, the moment will decrease whereas the deformation will further increase. Therefore, beyond the peak moment, Eq. (6.26) is only valid for the material within the final damage zone. Outside the final damage zone, the material is unloaded. This phenomenon can be seen in Fig. 6.19.

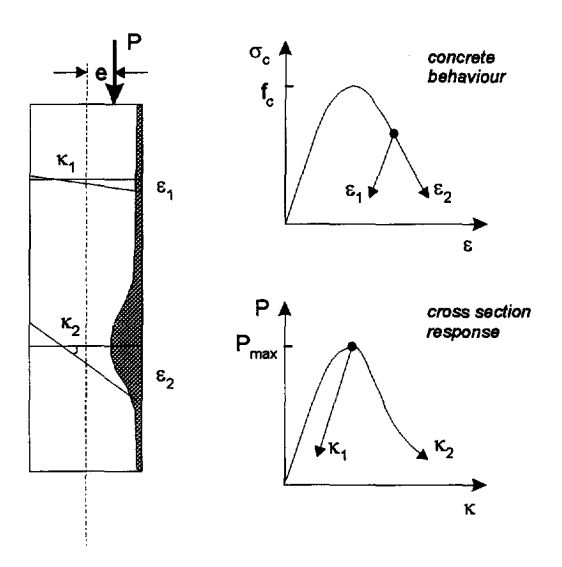


Fig. 6.19 Material behaviour and structural response of an eccentrically loaded prism.

6.4.3.2 CDZ model for eccentric load

On the basis of all assumptions described in the last two sections, a concrete material model (CDZ model) is developed for the numerical simulation of a specimen under an eccentric load. This model is illustrated in Fig. 6.20. Contrary to Markeset's assumption of a bilinear ascending branch, the ascending part is simulated by using a parabolic curve according to CEB-FIP Model Code 1990. The slope of the unloading curve is assumed to be equal to the modulus of elasticity E_c :

$$\sigma_{c} = \frac{\frac{E_{c}}{E_{c0}} \cdot \frac{\varepsilon_{c}}{\varepsilon_{c0}} - \left(\frac{\varepsilon_{c}}{\varepsilon_{c0}}\right)^{2}}{1 + \left(\frac{E_{c}}{E_{c0}} - 2\right) \cdot \frac{\varepsilon_{c}}{\varepsilon_{c0}}} \cdot f_{c}$$
(6.28)

where E_c is the tangent modulus; σ_c is the compression stress; ε_c is the compression strain; ε_{c0} is the compression strain related to the peak compressive stress f_c ; $E_{c0} = f_c/\varepsilon_{c0}$ is the secant modulus from the origin to the peak compressive stress f_c .

The softening curves, that is σ_c - ε_d and σ_c - w, are assumed to be straight lines. A further simplification is made in that the stress-strain relation in tension is assumed to be a straight line with a slope equal to the E-modulus in compression.

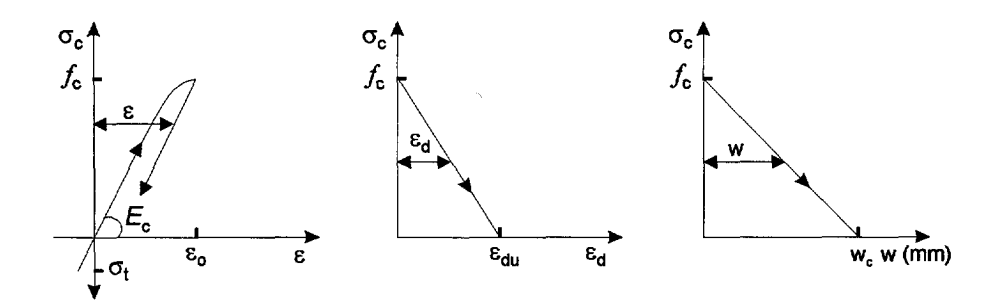


Fig. 6.20 Simplified stress-strain and stress-deformation curve.

This simplified softening branch in Markeset's model can be written as:

$$\varepsilon_{m} = \varepsilon_{o} - \left(\frac{f_{c} - \sigma_{c}}{E_{c}}\right) + \varepsilon_{du} \left(1 - \frac{\sigma_{c}}{f_{c}}\right) + \frac{w_{c}}{k^{l} d^{l}} \left(1 - \frac{\sigma_{c}}{f_{c}}\right)$$
(6.29)

Solving Eq. (6.29) with respect to σ_c yields:

$$\frac{\sigma_c}{f_c} = 1 + \frac{\varepsilon_m - \varepsilon_o}{\frac{f_c}{E_c} - \varepsilon_{du} - \frac{w_c}{k^l d^l}}$$
(6.30)

On the basis of the assumption of a linear strain distribution the depth d can be calculated as (see Fig. 6.21):

$$d^{1} = \left(\frac{\varepsilon_{a} - \varepsilon_{o}}{\varepsilon_{a} - \varepsilon_{b}}\right) \cdot h \tag{6.31}$$

where ε_a corresponds to ε_m in Eq. (6.30).

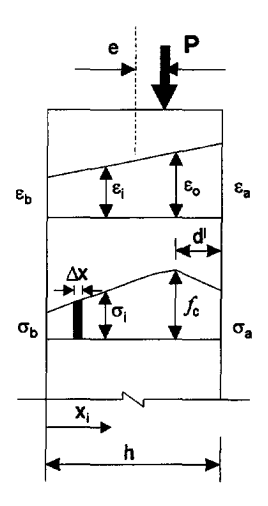


Fig. 6.21 Numerical model, stress and strain [Markeset (1993)].

6.4.3.3 Effect of the strain rate

From the discussion in §6.3 it can be concluded that the conventional material parameters, such as the strength of concrete, the E-modulus of concrete, the strain under the peak stress and the strain at failure are strain rate sensitive. On the basis of the experimental observations, these time-dependent properties might be linearly related to the strain rate, which can be introduced into the CDZ model. Basically, the material properties obtained by using the standard strain rate (short-term test) are taken as a reference. As the strain rate decreases, the strength and the E-modulus of HSC linearly decrease, whereas the strain under the peak stress and the strain at failure linearly increase. Beyond a certain strain rate [defined as $(de/dt)_{\infty}$], no further decrease or increase of these parameters occur. For high strength concrete, it is assumed that the maximum reduction of the strength and the Emodulus are about 20% and 10%, respectively; the maximum increase of the strain under the peak stress is about 50% and the maximum increase of the strain at failure is about 25%, as the strain rate decreases from the value taken by the standard test value to a certain low value, $(d\varepsilon/dt)_{\infty}$. The time-dependent linear relations of these material parameters with the strain rate are illustrated in Fig. 6. 22. In this figure, the parameter with the index r refers to that obtained from the standard strain rate test.

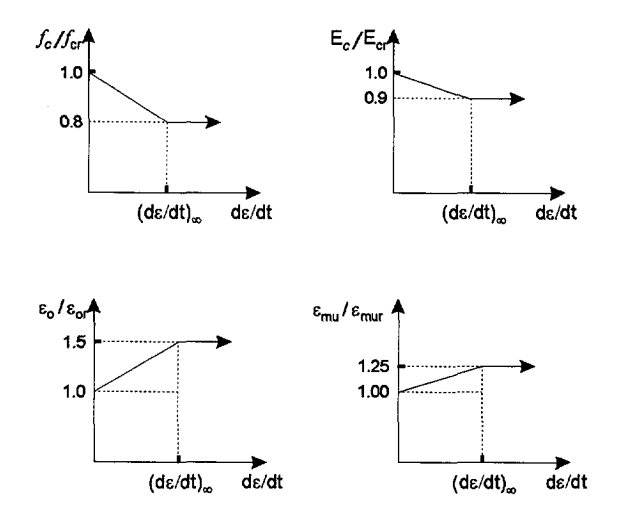


Fig. 6.22 Simplified models for the strain rate sensitivities of mechanical properties of HSC.

The fracture energy G_F and the parameter γ , which is discussed in the section 6.4.2.3 are assumed to be not sensitive to the variation of the strain rate (see also 6.5). According to Markeset (1993), for normal density concrete, γ is taken as 0.25 mm⁻¹. For a given f_{cr} , E_{cr} and G_F obtained from the standard test, the strain under the peak stress, ε_0 can be calculated by means of Eq. (6.19).

In Markeset's original model, the softening parameters ε_{du} and w_c [see Eq. (6.29)] are described by using the following two assumptions: 1) the area beneath the σ - ε_d curve is equal to 0.75 G_F/r ; 2) by introducing the mean compressive strain at failure, ε_{mu} , the value of the localized deformation w_c can be estimated with the basic material properties.

According to the first assumption, the value of ε_{du} can be expressed as:

$$\varepsilon_{du} = \left(\frac{2k}{1+k}\right) \cdot \frac{G_F/r}{f_c} \tag{6.32}$$

where k is 3.0 and r is 1.25 mm (see section 6.4.2.3). It is shown in Eq. (6.32) that the value of ε_{du} is strain rate sensitive, because f_c is rate dependent (see Fig. 6.22). As the strain rate decreases, ε_{du} increases.

According to the second assumption, the value of the mean compressive strain at failure, ε_{mu} , can be expressed based on Eq. (6.1):

$$\varepsilon_{mu} = \varepsilon^{in} + \varepsilon_{du} \frac{L^d}{L} + \frac{w_c}{L} \tag{6.33}$$

Solving Eq. (6.33) with respect to we yields:

$$w_c = \left(\varepsilon_{mu} - \varepsilon^{in}\right)L - \varepsilon_{du}L^d \tag{6.34}$$

Inserting Eq. (6.19), Eq. (6.32) and $L^d = 2.5D$ into Eq. (6.34) yields:

$$w_c = \left(\varepsilon_{mu} - \gamma \frac{G_F}{f_c}\right) L - \frac{5k}{1+k} \left(\frac{G_F/r}{f_c}\right) D \tag{6.35}$$

According to Markeset (1993), using a linear softening curve, the material parameter ε_{mu} is estimated to be about 0.00375 for a standard test.

6.4.4 Numerical study of the eccentrically loaded prisms

6.4.4.1 Numerical model

According to the proposed material model in 6.4.3 the stress distribution is determined. The internal force P, and the moment M, are then calculated by numerical integration of the stresses by means of the two following equations:

$$P = b \cdot \Delta x \sum_{i} \sigma_{i} \tag{6.36}$$

$$M = P \cdot e = b \cdot \Delta x \sum_{i} \sigma_{i} x_{i}$$
 (6.37)

where Δx , σ_i and x_i are shown in Fig. 6.21, b is the width of the prism.

For a given eccentricity, the correct strain distribution is found by an iteration procedure. These calculations are carried out by using a set of increasing ε_a values to obtain a load-strain curve.

6.4.4.2 Numerical simulations

For numerical simulations a high strength concrete with prism strength of 100 N/mm² is chosen. The basic concrete parameters which are used in this simulation are listed in Table 6.I and 6.II. On the basis of the assumptions in §6.4.2 and §6.4.3, the parameters can

be subdivided into two categories: rate-dependent and rate-independent. The rate-independent parameters are listed in Table 6.I, whereas the rate-dependent parameters are listed in Table II. In addition to the strain rate sensitivity the influence of the strain gradient on some parameters is also taken into account. This is shown in Table 6.II.

Based on the basic parameters listed in Table 6.I and Table 6.II the ultimate deformation described in Fig. 6.20, ε_0 , ε_{du} and w_c can be calculated according to Eqs. (6.19), (6.32) and (6.35), respectively.

Table 6.1 Strain rate independent concrete parameters used in numerical simulation

	r (mm)	γ (mm ⁻¹)	k ^l	G _F (N/mm)	L (mm)	D(mm)
HSC	1.25	0.25	5	0.18	400	100

Table 6.II Strain rate dependent concrete parameters used in numerical simulation

Strain		e/d = 0		e/d =	0.075	0.15	
rate	f _{cp}	E₀	ε _{mu}	f _c	€c0	fc	€c0
(10 ⁻⁵)	N/mm²	N/mm ²	10 ⁻³	N/mm²	10 ⁻³	N/mm²	10 ⁻³
1.0-10	100	45000	3.75	105	1.1 εο	100	1.1 ε ₀
0.1-1.0	95	43875	4.00	99.75	1.2 ε ₀	95	1.2 ε ₀
0.01-0.1	90	42750	4.25	94.5	1.3 ε ₀	90	1.3 ε ₀
0.001-0.01	85	41625	4.50	89.25	1.4 ε ₀	85	1.4 εο
0.0001-0.001	80	40500	4.75	84	1.5 ε ₀	80	1.5 ε ₀

With all basic parameters the procedure of numerical simulation described in §6.4.4.1 is followed. With a set of ε_a values, the internal force P and the moment M are calculated by numerical integration of the stresses σ_i by means of Eqs. (6.36) and (6.37). The stress σ_i can be calculated by using Eqs. (6.28) and (6.30).

The numerical study reveals that the basic shape of the load-strain curve can be correctly simulated by using the modified CDZ model in dependence of strain gradient and strain rate. As the strain rate decreases, the peak load decreases and the strain at the extreme fibre, corresponding to the peak load, increases (see Fig. 6.23 and 6.24). An increasing of the strain gradient reduces the peak load and increases the strain at the extreme fibre at a constant strain rate.

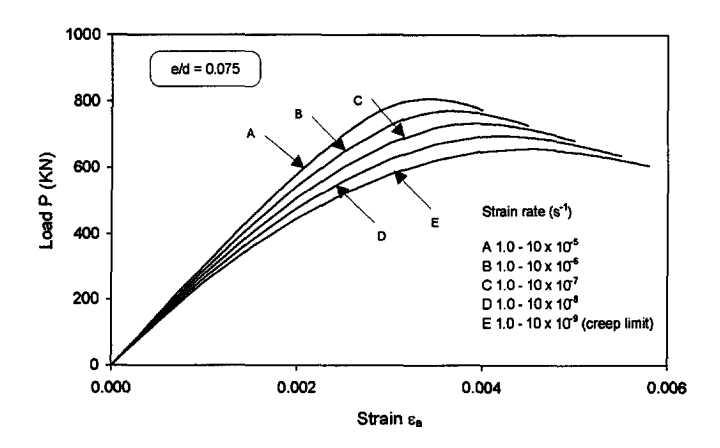


Fig. 6.23 Calculated load-strain relations for an eccentrically loaded HSC prism with e/d = 0.075 at various strain rates.

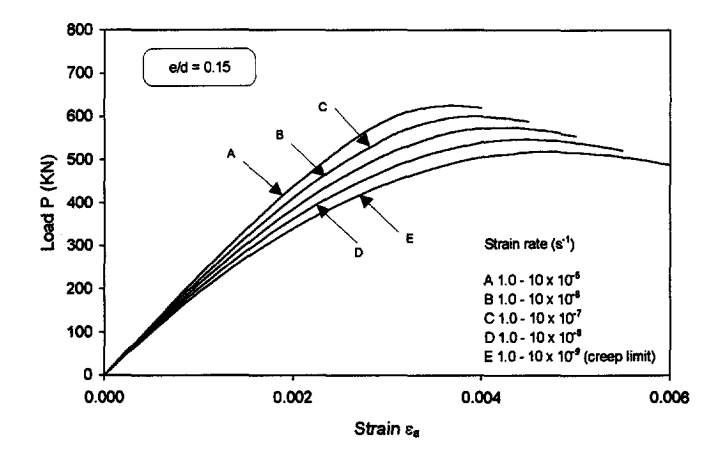


Fig. 6.24 Calculated load-strain relations for an eccentrically loaded HSC prism with e/d = 0.15 at various strain rates.

In Table 6.III and 6.IV the calculated maximum load P_{max} and the corresponding strain ε_{max} in the mostly stressed fibre for two eccentricities are respectively compared with those obtained from the tests. It can be seen that, by introducing several key parameters, the

modified CDZ model can reasonably well predict the behaviour of a concrete prism loaded eccentrically with different strain rates in combination with different strain gradients.

Numerical simulation			Experi	mental results (€ _{max}		
Strain rate 10 ⁻⁵ s ⁻¹	P _{max} kN	ε _{max} 10 ⁻³	Strain rate	P _{max} kN	ε _{max} 10 ⁻³		
1.0-10	807.1	3.400	2.5	811.6	3.294		
0.1-1.0	771.8	3.700	0.25	801.6	3.397		
0.01-0.1	735.0	3.900	0.025	749.6	4.010		
0.001-0.01	697.2	4.200	0.0025	715.6	4.787		
0.0001-0.001	658.4	4.500	****	****	****		

Table 6.IV Comparison between theoretical and experimental results with e/d = 0.15

Numerical simulation			Experi	mental results (mean)
Strain rate 10 ⁻⁵ s ⁻¹	P _{max} kN	ε _{max} 10 ⁻³	Strain rate	P _{max} kN	ε _{max} 10 ⁻³
1.0-10	625.2	3.700	5.0-10	620.0	3.645
0.1-1.0	600.8	3.900	0.2-0.5	592.4	3.728
0.01-0.1	574.9	4.200	0.015-0.05	573.9	4.132
0.001-0.01	547.5	4.500	0.001-0.005	588.8	5.743
0.0001-0.001	519.3	4.700	****	****	****

The calculated load-strain relationships for two eccentricities are compared with some of the experimental results in Fig. 6.25 and 6.26, respectively. As it can be seen, the modified CDZ model under the current assumptions gives a good prediction of the load-strain curve. The bottom line, defined as "creep limit", can be regarded as the border line between the rate-sensitive area and the intrinsic area described in Fig. 6.9.

From the preliminary numerical study by means of the CDZ model, it can be clearly concluded that the parameters which are used by this model can strongly influence the final results. Basically, the strain rate sensitivity of the conventional material parameters, such as f_c , E_c and ε_0 , are relatively well understood. The strain rate sensitivity of additional parameters, such as G_F , ε_{mu} , ε_{du} , w_c and k', need to be further studied. Besides, the existence of the strain gradient further complicates the strain rate sensitivity of all parameters mentioned above, which has to be considered during modelling.

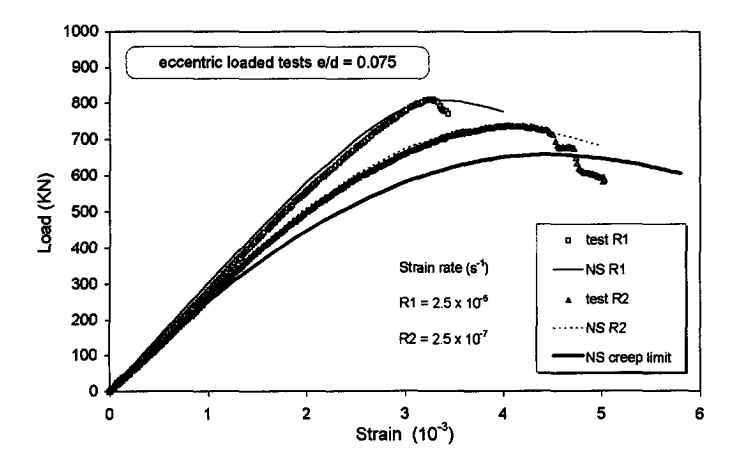


Fig. 6.25 Calculated and experimental load-strain relations for an eccentrically loaded prism with e/d = 0.075 at two different strain rates.

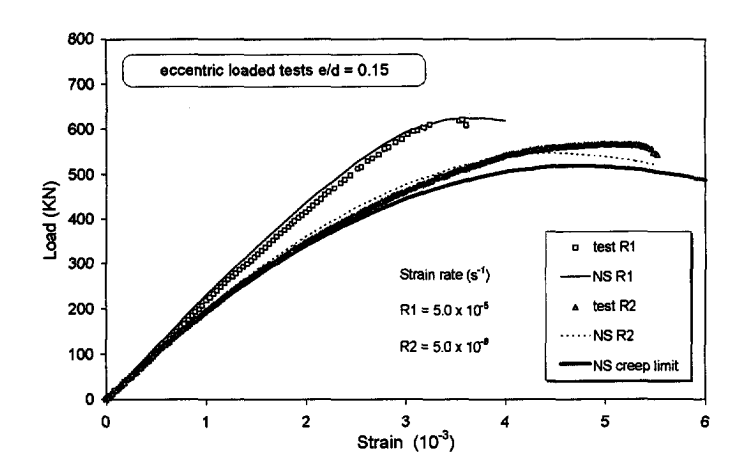


Fig. 6.26 Calculated and experimental load-strain relations for an eccentrically loaded prism with e/d = 0.15 at two different strain rates.

6.4.5 Evaluations of the stress-strain relations in two extended codes for HSC

As an example, two stress-strain relations, as recently adopted by the Dutch and the German extended code for HSC, are used to calculate the maximum load capacity of the test specimens. The calculated results are compared with those obtained from the tests, and the differences between these two formulations are discussed.

For the same class of concrete (for example, B105, with a 28-day's characteristic cube strength $f_{ck} = 105 \text{ N/mm}^2$), the expression of the design strength of concrete f_{cd} in the German Code (Draft July, 1993) is:

$$f_{cd} = 0.85 \cdot 0.85 \cdot \left[0.95 \cdot \left(1 - \frac{f_{ck}}{600} \right) \right] \cdot f_{ck}$$
 (6.38)

where the first two factors 0.85×0.85 consider the conversion from the cube strength to the prism strength and the long-term loading effect, respectively. The factor $0.95 \times (1-f_{ck}/600)$ considers the difference of the strength in a real structure and that measured in the laboratory.

The corresponding expression in the Dutch code is:

$$f_{cd} = 0.85 \cdot 0.85 \cdot \frac{1}{1.27} \cdot f_{ck} \tag{6.39}$$

where the first factor 0.85 considers the conversion from the cube strength to the prism strength, whereas the second factor 0.85 takes the long-term loading effect into account. The factor (1/1.27) is the material safety factor.

The stress-strain relations according to the two codes for a concrete B105 are shown in Fig. 6.27. On the basis of Eq. (6.38), the stress-strain relation in the German formulation is:

$$\sigma = f_{cd} \cdot \left[1 - \left(1 - \frac{\varepsilon}{\varepsilon_0} \right)^n \right] \qquad 0 \le \varepsilon \le \varepsilon_0$$
 (6.40)

$$\sigma = f_{cd} \qquad \qquad \varepsilon_0 \le \varepsilon \le \varepsilon_u \tag{6.41}$$

where ε_0 (taken as 0.00217 for B105) is the strain corresponding to the peak stress, ε_u (taken as 0.0023 for B105) is the ultimate strain of the concrete, and n is a parameter which considers the influence of f_{cd} , ε_0 and E_c (E-modulus of concrete), according to:

$$n = E_c \cdot \frac{\varepsilon_0}{f_{cd}} \qquad \text{(for B105, } n = 1.48\text{)}$$

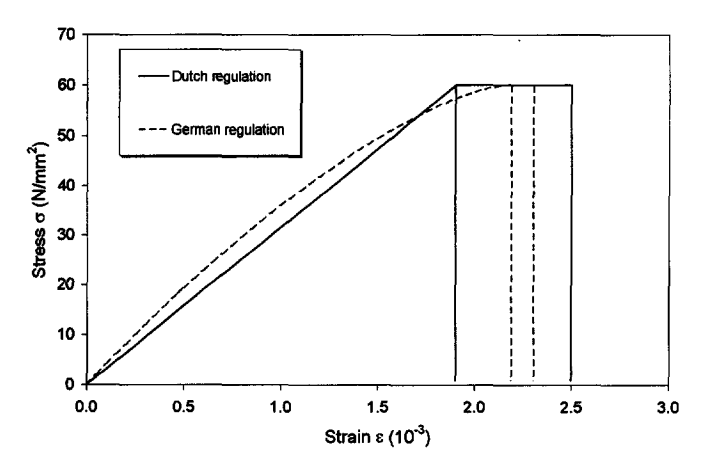


Fig. 6.27 Calculating stress-strain relations in Dutch and German Codes for a concrete B105.

On the basis of Eq. (6.39), the stress-strain relation in the Dutch Code is:

$$\sigma = f_{cd} \cdot \left(\frac{\varepsilon}{\varepsilon_0}\right) \qquad 0 \le \varepsilon \le \varepsilon_0 \tag{6.43}$$

$$\sigma = f_{cd} \qquad \qquad \varepsilon_0 \le \varepsilon \le \varepsilon_u \tag{6.44}$$

where ε_0 (taken as 0.0019 for B105) is the strain corresponding to the peak stress, and ε_u (taken as 0.0025 for B105) is the ultimate strain of the concrete.

In Fig. 6.28 the test results for e/d = 0, 0.075 and 0.15 respectively and the lowest strain rate as used in the tests are compared with the values calculated according to the Dutch and the German codes. For the sake of a clear comparison with the test results, in the German expression (Eq. 6.38) the third factor and the coefficient of safety γ_c have been ignored. In the Dutch expression (Eq. 6.39), the third factor has been ignored.

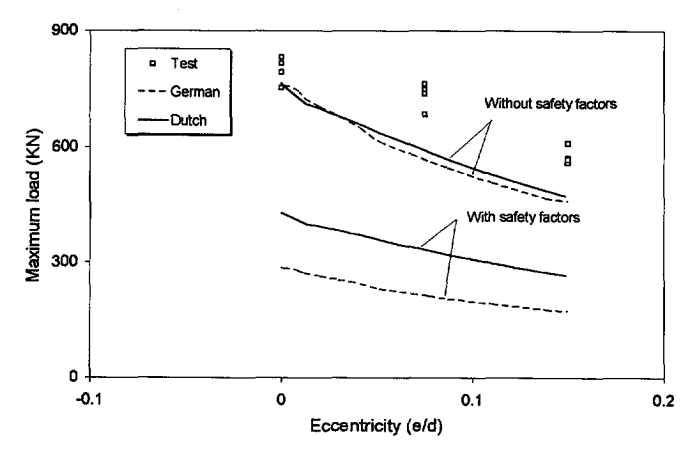


Fig. 6.28 Comparison of load-bearing capacity of HSC obtained from tests with that calculated according to the German and Dutch Regulations.

From the comparison, it can be seen that the calculated values, without consideration of the safety factors, for both the German and the Dutch Recommendations are nearly the same, forming a lower limit for the test results. However, the load-bearing capacity according to these two codes allowed in reality is significantly different. In the Dutch Code, for a concrete B105, the material safety factor is 1.27 and the safety factor on the load is between 1.35 (only self-weight) and 1.5 (only variable load). If the loading safety factor is taken as 1.4, the total safety factor is $\gamma_{ts} = 1.27 \times 1.4 = 1.78$. In the German Regulation, for the same concrete, in the case of failure without pre-warning, the combined safety factor is 2.1. In combination with the consideration of a difference between the laboratory and a real structure, the total safety factor obtained is $\gamma_{ts} = 2.1/0.784 = 2.678$. The German Code obviously takes a much larger safety margin for HSC into account than the Dutch Code.

6.4.6 Concluding remarks

- The existence of a strain gradient influences the rate sensitivity of high strength concrete. As the strain gradient increases, the rate sensitivity of HSC decreases. This effect is more pronounced for HSC than for NSC. In normal strength concrete subjected to strain gradients no significant strain rate influence is observed.
- By introducing an extension in order to regard the strain rate sensitivity, the CDZ
 model can be used to simulate load-strain relationships for eccentrically loaded prisms
 when, various strain rates and strain gradients apply.

- The comparison between results of the numerical calculation and the experimental
 results show, that for a good prediction of the ultimate load a strain rate and e/d
 dependent stress-strain relation is necessary. If a single stress-strain relation, based on
 centric loading tests, independent from the strain rate, is used like in many codes the
 results will never be very accurate.
- The strain rate sensitivity of conventional material parameters, such as the strength, E-modulus and the strain at the peak stress, as well as the additional parameters, such as the fracture energy, the ultimate strain, etc. need to be further studied in order to take advantage of the modified CDZ model.
- With respect to the safety margin in the case of compression for HSC, The Dutch and the German Recommendations significantly differ from each other.

6.5 The influence of strain rate and strain gradient on the behaviour in centric and eccentric tension

In this section, the influence of strain rate and strain gradient on the behaviour of concrete in tension is discussed. The key properties which are considered in the experimental analysis are: the peak tensile strength, the tensile strain at the peak stress, the softening behaviour and the maximum load-bearing capacity when a strain gradient exists. The basic test data including the maximum tensile stress, the initial E-modulus and the tensile strain at peak stress from the centric tensile tests for both HSC and NSC are given in Table E-7 and Table E-8 in Appendix E. The basic data including the maximum load, the tensile strain at the maximum load for the eccentric tensile tests for both HSC and NSC are given in Table E-13, Table E-14 and Table E-15. The basic data from the centric tensile softening tests for both HSC and NSC are given in Table E-16. The results of the experimental analysis for the eccentric tensile tests are arranged in Table F-9, Table F-10 and Table F-11 in Appendix F. Some fracture properties from the tensile softening tests are given in Table F-27.

6.5.1 Influence of the strain rate on the tensile peak stress

The stress-deformation relationships for both HSC and NSC in tension are illustrated in Fig. 6.29. The strain rates mentioned in this figure concern the longitudinal direction. It can be seen that for both HSC and NSC, if the strain rate decreases, the slope of the ascending part of the stress-deformation curves slightly decreases. The deformation at peak stress increases only very slightly as the strain rate decreases. There is no systematic strain

rate influence in the post peak part for NSC. For HSC, a slight upward shift of the stress deformation curve was observed as the strain rate decreased.

The peak stresses for both HSC and NSC in the centric tensile tests are shown in Fig. 6.30 as a function of the longitudinal strain rate. It can be seen that for HSC, the peak stress firstly increases, than decreases as the strain rate decreases within the adopted strain rate range. The same phenomenon was also observed by Heilmann, Hilsdorf and Finsterwalder (1969). Their observations are shown in Fig. 3.17 and Fig. 3.20.

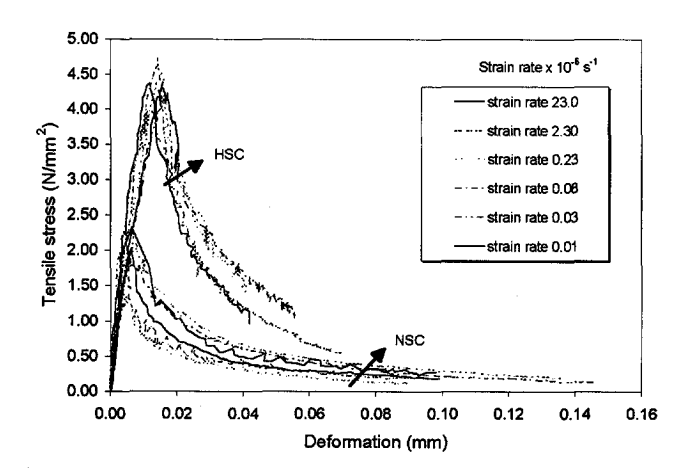


Fig. 6.29 Stress-deformation curves for HSC and NSC in centric tensile tests at various longitudinal strain rates.

The experiments show that between the strain rates 2.3×10^{-6} and 1.0×10^{-8} s⁻¹, the reduction of the peak stress is small both for HSC and NSC. From the basic mechanism for the rate sensitivity (see section 6.2), it is understood that only the Stefan Effect plays a role as far as the strain rate sensitivity in tension is concerned. For different loading conditions (compression and tension), the Stefan Effect works out in a different way. In compression, the Stefan Effect reduces the transverse deformation, whereas further a reduction of the longitudinal deformation is obtained due to pore water pressure, resulting in an increase of the compressive strength at a higher strain rate. In tension, only the Stefan Effect works, which is directly related to the reduction of the longitudinal deformation. Form this point of view, it is obvious that the influence of the strain rate in compression is higher than in tension.

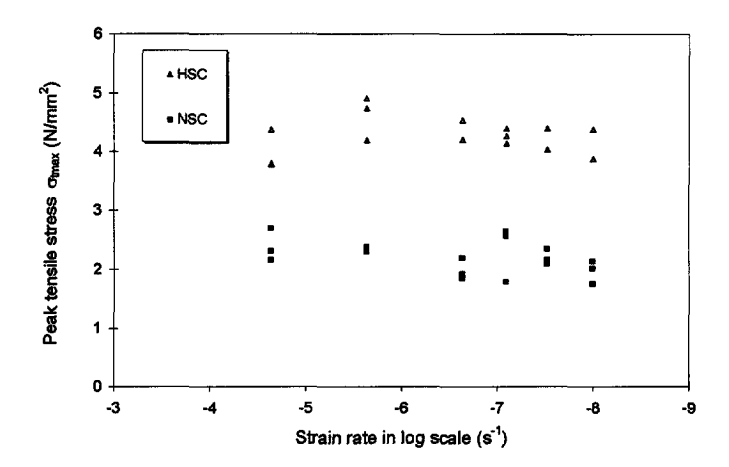


Fig. 6.30 Peak stresses versus longitudinal strain rates for HSC and NSC in centric tensile tests.

6.5.2 Influence of the strain rate on the tensile deformation

The longitudinal strain at peak stress for both HSC and NSC in centric tension are shown as a function of the longitudinal strain rate in Fig. 6.31. No significant differences are found between HSC and NSC with regard to the strain rate sensitivity for the deformation. As observed by Heilmann, Hilsdorf and Finsterwalder (1969), the longitudinal strain very slightly increases when the strain rate decreases (see also Fig. 3.18). However, from the test results, it can be seen that the increase of the longitudinal strain at peak stress for HSC is more consistent than that for NSC.

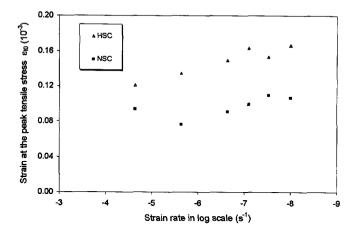


Fig. 6.31 Strain at the peak stress versus the longitudinal strain rate for HSC and NSC in centric tensile tests.

6.5.3 Influence of the strain rate and the strain gradient on the tensile behaviour

In Table E-13, Table E-14 and Table E-15 (see Appendix E), the maximum load P_{tmax} , and the strain in the extreme fibres ε_{tt0} and ε_{tc0} at the maximum load are given. Additionally, under the assumption that plane sections remain plane, the position of the neutral axis x is calculated according to the measured deformation.

The load-carrying capacities of HSC and NSC versus the longitudinal strain rates for e/d = 1/6 and e/d = 1/3 are shown in Fig. 6.32 and Fig. 6.33. All registered points are the average of two or three test values. From the results, it can be seen that for HSC in tension, to a certain extent, the existence of the strain gradient can reduce the rate sensitivity of the load-carrying capacity. For NSC, the load-carrying capacity seems to be not sensitive to the variation of the strain rate.

The observation in the centric tensile tests that, when the strain rate decreases, the peak stress firstly increases, then decreases (see Fig. 6.30) does appear again for the eccentricities (e/d = 1/6 and 1/3) for HSC (see Fig. 6.32 and Fig. 6.33).

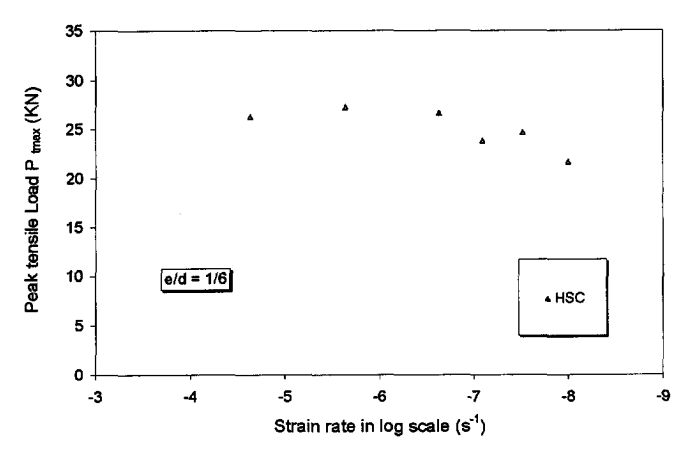


Fig. 6.32 Relation between the measured maximum tensile load and the strain rate for HSC at an eccentricity of e/d = 1/6.

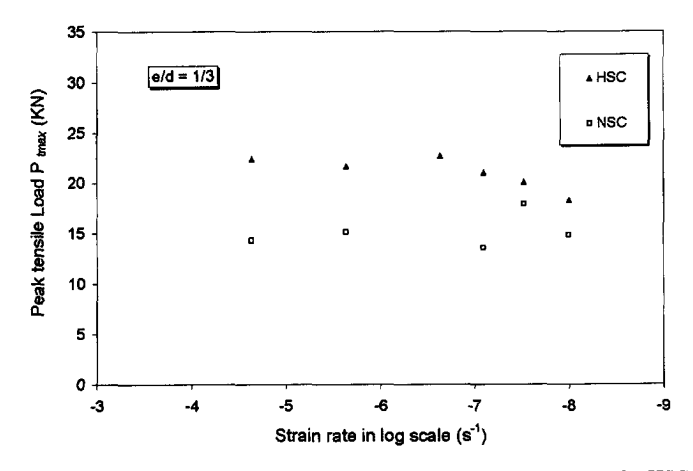


Fig. 6.33 Relation between the measured maximum tensile load and the strain rate for HSC and NSC at an eccentricity of e/d = 1/3.

6.5.4 The influence of the strain rate on the fracture energy

In Fig. 6.29 the descending branch showed some scatter: this was due to the loading equipment, which was not specially designed for strain softening tests. Therefore some additional tests have been carried out in a more appropriate testing equipment, specially for

softening tests. The influence of the strain rate on the tensile softening behaviour of HSC and NSC was also studied. Two strain rates were applied in the tests. In Table E-16 (see Appendix E) the measured maximum tensile stress σ_{lmax} , the E-modulus E_t which is calculated by using linear regression up to a stress of 60% of the peak stress, the strains at the peak stress measured by using both a short measuring length (35 mm) ε_{lsh0} and a long measuring length (110 mm) ε_{il0} are given. The statistical analysis of the softening properties is given in Table F-27 (see Appendix F). The fracture energy G_F is obtained by calculating the area under the tensile stress - crack width curve. The tensile stress - crack width relationship is obtained subtracting the elastic deformation from the total deformation in Fig. 6.34. The characteristic length l_{ch} which is normally used to reflect the toughness of concrete, is calculated according to the expressions:

$$l_{ch} = \frac{E_t \cdot G_F}{\sigma_{tmax}^2} \tag{6.45}$$

where E_t is the E-modulus in tension, G_F is the fracture energy and σ_{tmax} is the peak tensile stress.

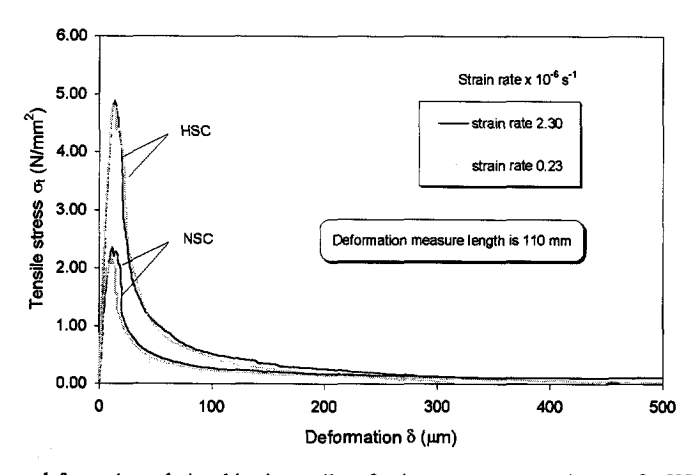


Fig. 6.34 Stress-deformation relationships in tensile softening tests at two strain rates for HSC and NSC.

In Fig. 6.34 the typical tensile stress - longitudinal displacement relationships for both HSC and NSC are shown. These curves are obtained with a measuring length of 110 mm at strain rates which differed by a factor of 10. It can be seen that, for a factor of 10, the influence of the strain rate is very small, either on the ascending part of the stress - deformation relationship or on the softening part for both HSC and NSC.

From Table 6-5, it is found that the fracture energy G_F for HSC and NSC with the used two strain rates is nearly constant, i.e. the fracture energy seems to be independent of the strain rate. However, slight differences are found for both HSC and NSC as far as the characteristic length is concerned. In general, the characteristic length increases as the strain rate decreases.

ID	d∉dt	O _{tmax}	G _F	E _t	lch				
item	10 ⁻⁶ s ⁻¹	(N/mm²)	N/m	10 ³ N/mm ²	mm				
	RH _{op} TUSFL25 (3)								
average	2.30	4.77	188	48.00	397				
SD		0.09	20.1	2.117					
	RH _{cg} TUSFL2.5 (4)								
average	0.23	4.52	173	47.57	403				
SD		0.33	20.8	1.043					
		RN _{cg} TUS	SFL25 (4)						
average	2.30	2.18	107	29.09	665				
SD		0.12	12.1	1.157					
	RN₀gTUSFL2.5 (4)								
average	0.23	2.12	102	31.15	707				
l sp		0.31	15.0	2.821					

Table 6-5 Results for HSC and NSC in centric tensile tests (softening)

An important observation is that the characteristic length of HSC is much lower than that of NSC. This implies that HSC is much more brittle than NSC.

6.5.5 Concluding remarks

The experimental observations show that, in comparison with compression, the
reduction of the peak tensile stress in tension does not differ very much between HSC
and NSC as the strain rate decreases. The rate sensitivity of the peak stress in tension is
also less obvious than in compression.

^{*} The fracture energy is calculated by considering the area under the stress-deformation curve. Depending on the sensitivity of the test machine, this area may vary significantly. As a result, the calculated fracture energy G_F can be very different.

- On the basis of the mechanism of rate sensitivity, the function of the Stefan Effect in compression differs from that in tension. In tension the effect of moisture stress is smaller than in compression.
- When a strain gradient exists, the strain rate sensitivity of the load-carrying capacity in tension is reduced. However, the strain gradient has a less significant effect on the strain rate sensitivity in tension than in compression.
- The fracture energy in tension is virtually independent of the strain rates used. The fracture energy of HSC is higher than that of NSC, but the characteristic length is significantly lower for HSC.

Chapter 7

Experimental research and analysis - creep and shrinkage of HSC

On the basis of the test data, a comprehensive experimental analysis has been carried out, which has mainly focused on the influences of the age at application of the load, the stress level and the type of aggregate on creep, as well as on creep recovery of high strength concrete in compression. The development of strength and E-modulus and the autogeneous shrinkage, which are believed to be significant as far as the time-dependent behaviour of HSC at early ages is concerned, are fully discussed. The experimental results are compared with predictions according to several well-known existing formulations.

7.1 Introduction

A comprehensive experimental analysis was conducted on shrinkage and creep of concrete loaded at normal and early ages (series C_n and C_e, see *Chapter* 5), which is described in this chapter. With regard to the various parameters, the experimental analysis is subdivided into four parts. In the first part, the development of strength and E-modulus which are important for the time-dependent behaviour of concrete loaded at early ages is discussed. Because of the close relation between creep and shrinkage, the shrinkage observed in the experiments is presented in the second part. The influence of the type of aggregate and the age at which the concrete is exposed to drying on shrinkage is investigated. In the third part, creep of the concrete loaded both at early ages and at a normal age is analyzed. The influences of the stress level and the type of aggregate on creep are discussed. In the last part, creep recovery is considered. In all four parts, the test data are compared with the predictions calculated by using several existing formulations. The comparisons form a basis for the further development of appropriate predicting

formulations for shrinkage and creep of high strength concrete loaded at normal and early ages.

7.2 Development of strength and E-modulus of HSC

Concrete is an ageing material, which implies that its properties change with time. In fact, a lot of influencing factors are involved in this process. Among others, the type of cement used and the curing conditions, including the relative humidity and the temperature, play a role. Basically, the strength and the E-modulus develop very fast in the first period after casting (about several hours to several days). From then on, the rate of development decreases

Fig. 7.1 and 7.2 show the development of strength and E-modulus versus time obtained from the tests for a period of about 180 days. Fig. 7.3 and 7.4 show this development in detail for the first 7 days after casting. The last figures indicate that at an early age, the E-modulus develops faster than the strength.

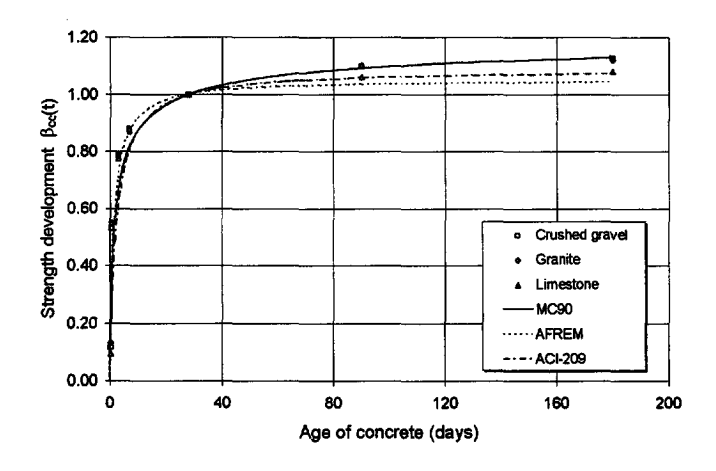


Fig. 7.1 Strength development of HSC with different types of aggregates.

It has to be emphasized that the test data concerning the development of strength and E-modulus are based on measurements on reference specimens which are free of external load. Actually, all the specimens in the creep tests, to some extent, are subjected to pressure. Consequently, two contradictory tendencies appear: at a low loading level, the

external pressure may result in a beneficial effect to the strength as well as the E-modulus, whereas a high initial stress may lead to a detrimental effect, as far as the later development of mechanical properties of the concrete is concerned. This last aspect is also considered in the CEB-FIP Model Code (MC90) in the strength development under high sustained loads [see Eqs. (4.74) and (4.75) in *Chapter 4* of this thesis].

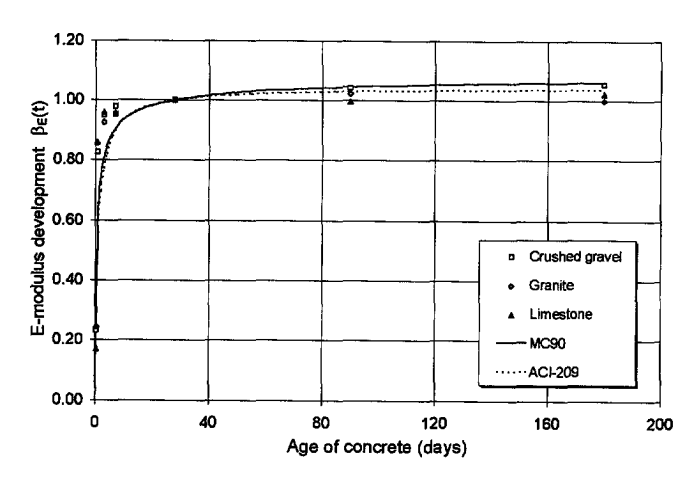


Fig. 7.2 E-modulus development of HSC with different types of aggregates.

In Fig. 7.1, 7.2, 7.3 and 7.4 the developments of the strength and the E-modulus versus time, obtained from the reference tests, are compared with the predictions from MC90, ACI-209 and AFREM [the new French Code, Le Roy, de Larrard and Pons (1996)]. AFREM only gives an expression for the strength development. The compressive strength of the concrete at a time t is estimated in MC90 by using Eq. (4.72) and (4.73) from *Chapter 4* in this thesis. The E-modulus at an age t is described in MC90 by:

$$E_{ci}(t) = E_{ci} \cdot \sqrt{e^{s \left[1 - \left(\frac{28}{t/t_1}\right)^{0.5}\right]}}$$
(7.1)

where E_{ci} is the modulus of elasticity at 28 days. Other parameters correspond with those in Eqs. (4.72) and (4.73). The compressive strength of the concrete at a time t is estimated in ACI-209 by using Eq. (4.76). The E-modulus at an age t is estimated in ACI-209 by:

$$E_{ci}(t) = g_{ci} \cdot \sqrt{w^3 \cdot f_{cm}(t)}$$
 (7.2)

where $g_{ct} = 0.043$; w is the unit weight of the concrete (in kg/m³); $f_{cm}(t)$ is obtained from Eq. (4.76) (in N/mm²). The compressive strength of the concrete at a time t is estimated in AFREM by using Eq. (4.77).

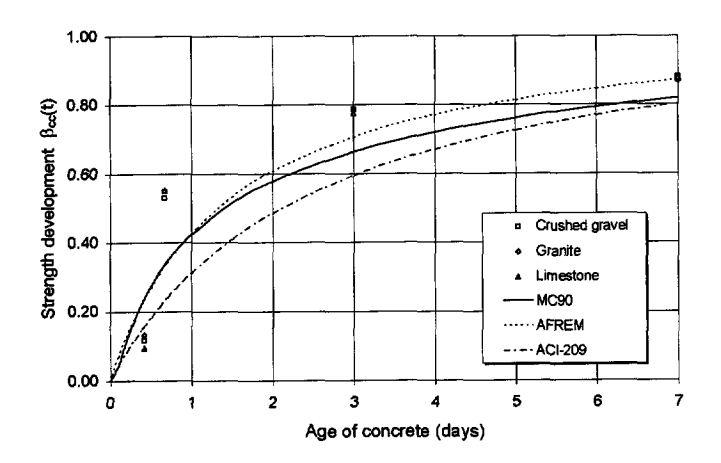


Fig. 7.3 Strength development of HSC with different types of aggregates at early ages.

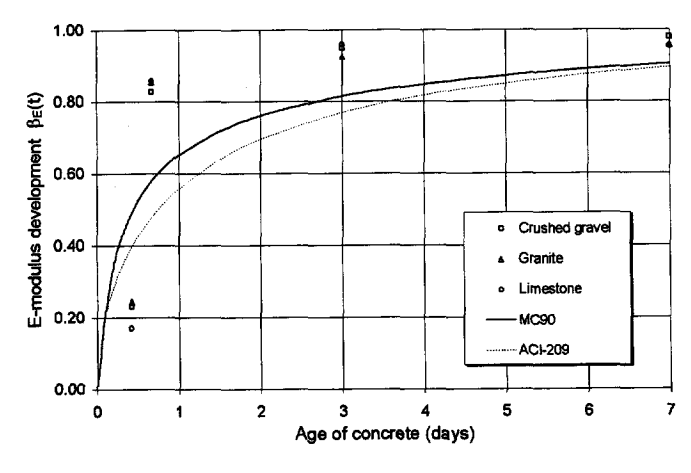


Fig. 7.4 E-modulus development of HSC with different types of aggregates at early ages.

From the comparison, it can be seen that, for an age of the concrete higher than about 28 days, MC90 and ACI-209 simulate the development of both strength and E-modulus well, whereas the formulation of AFREM slightly underestimates the strength development

of HSC (see Fig. 7.1 and Fig. 7.2). For an age of the concrete between 7 days and 28 days, AFREM gives a better prediction than the other two formulations. It has to be mentioned that all three formulations do not explicitly consider the contribution of silica fume to the strength development.

The formulations of MC90, ACI-209 and AFREM lose accuracy for concrete at early ages, specially at an age lower than one day (see Fig. 7.3 and 7.4). They can not catch up with the rate of development from the setting time to a certain hydration level.

As far as the influence of the type of aggregate on the development of strength and E-modulus of high strength concrete is concerned, no significant difference was found between the various aggregates used, especially at later ages.

7.3 Shrinkage of HSC

In Fig. 7.5 and Fig. 7.6 the shrinkage of HSC with different aggregates exposed to a constant climate of 50% relative humidity and 20 ± 3 °C in temperature are presented. The concrete is exposed to drying at ages of 8 hours and 14 hours after casting, respectively. The shrinkage measuring started at ages of 10 hours and 16 hours, respectively. The measuring lasted about 180 days. In Fig. 7.7 the shrinkage of HSC with crushed gravel exposed to drying at an age of 28 days is displayed. The shrinkage measuring started at an age of 28 days. The measuring lasted about 200 days. During the shrinkage process the concrete was exposed to a constant climate of 60% relative humidity and 20 ± 3 °C in temperature. When comparing these predictions with the experimental results it is noted that only the AFREM curves show a good agreement. This is not completely surprising because those curves have been specially derived for HSC. The ACI-209 and MC90 curves have been derived for concretes with a considerably lower strength, so that their accuracy is considerably less, which clearly appears from the figures The 28-day's strength of the concrete for the shrinkage calculations was 90 N/mm² (Fig. 7.5), 97 N/mm² (Fig. 7.6) and 100 N/mm² (Fig. 7.7).

Normally, when shrinkage is considered, drying shrinkage, which is caused by a loss of water from the concrete, dominates. Autogeneous shrinkage (self-desiccation) is generally related to the hydration process, which is regarded as a secondary factor if the water/cement ratio is higher than about 0.40 and if the concrete is exposed to drying at a relatively high age. It is found that if the concrete is exposed to drying at an age of 14 hours after casting and the shrinkage is measured from an age of 16 hours, the total shrinkage value is about twice as large as in the case of drying from an age of 28 days and a drying time of 2000 hours (compare Fig. 7.6 and 7.7) [Han and Walraven (1995b), Han

(1995)]. This also implies that, at an early age, a significant contribution of the autogeneous shrinkage to the total time-dependent deformation is found. For HSC, autogeneous shrinkage plays a dominant role at an early age due to the low water-cement ratio (lower than 0.40) and the use of silica fume, which results in a much finer pore-structure of the concrete [de Larrard, Acker and le Roy (1994)].

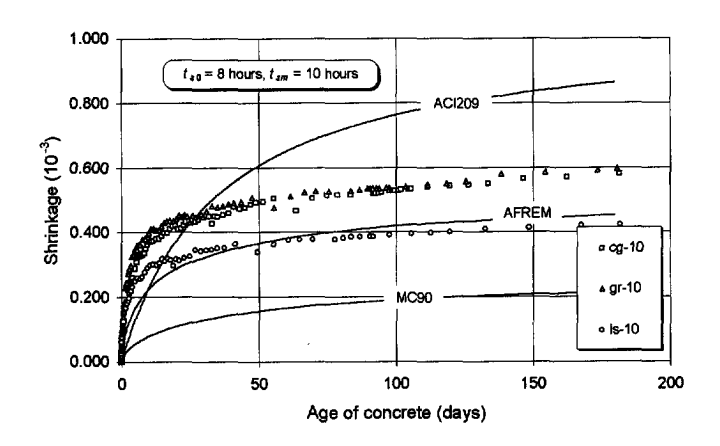


Fig. 7.5 Shrinkage of HSC; drying started at an age of 8 hours, measuring started at an age of 10 hours.

As far as the influence of the type of aggregate on shrinkage is concerned, HSC with limestone shows a smaller shrinkage than the two other types of aggregates used(see Fig. 7.5 and Fig. 7.6). The rate of shrinkage of limestone concrete is also smaller than that of the other concretes. This is believed to be due to the lower E-modulus of the aggregate limestone in comparison with the other aggregates. When the matrix around the aggregate shrinks, the restraining action of the limestone is less, so that less microcracks occur. As a consequence the evaporation of water is smaller which reduces the shrinkage.

The factors considered in the expression for predicting the shrinkage of concrete exposed to drying by MC90 are, among others, the compressive strength of the concrete, the type of cement, the relative humidity, the size and the shape of the specimen, and the period of drying. However, it has to be pointed out that this expression does not consider the use of silica fume. From Fig. 7.5, 7.6 and 7.7, it can be seen that MC90 quite considerably underestimates the shrinkage of the HSC. This is possibly due to not considering the autogeneous shrinkage, which gives the main contribution to the total shrinkage of HSC. Moreover, MC90 does not consider the ageing effect on the total shrinkage value, i.e. at what age concrete is exposed to drying.

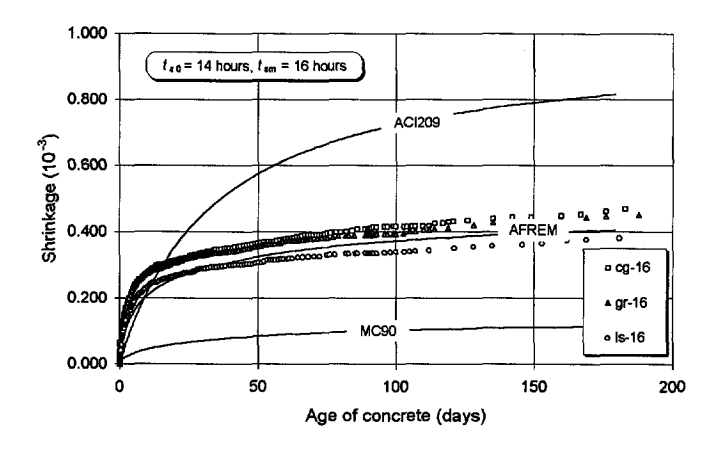


Fig. 7.6 Shrinkage of HSC: drying started at an age of 14 hours, measuring started at an age of 16 hours.

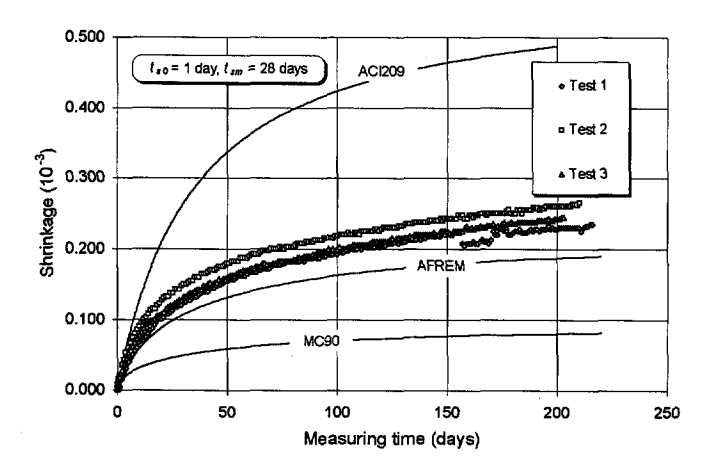


Fig. 7.7 Shrinkage of HSC: drying started at an age of 1 day, measuring started at an age of 28 days.

In addition to the factors considered in the formulations of MC90, the expressions in ACI-209 also take the composition of the concrete into account. It is found that, for a concrete exposed to drying at early ages (earlier than 28 days), ACI-209 firstly underestimates the shrinkage of HSC. From a certain age of the concrete, it significantly overestimates the shrinkage of HSC (see Fig. 7.5 and 7.6). For a concrete exposed to drying at an age of 28 days, ACI-209 totally overestimates the shrinkage of HSC (see Fig.

7.7). It is also found that the rate of shrinkage calculated by using the formulation of ACI-209 is smaller in the early period of shrinkage, but larger in a later period of shrinkage.

In comparison with MC90 and ACI-209, the formulation of AFREM, where the compressive strength, the relative humidity, the size and the shape of the specimen and the period of drying are considered, shows a better agreement, although it slightly underestimates the shrinkage of the crushed gravel and granite specimens exposed at an age of 10 hours (see Fig. 7.5). For the concrete exposed at an age of 28 days, AFREM also shows a slight underestimation of the shrinkage (see Fig. 7.7). In addition to the drying shrinkage, this model also explicitly considers the autogeneous shrinkage.

7.4 Creep of HSC

7.4.1 Creep of HSC under a constant sustained load applied at an age of 28 days

7.4.1.1 Load-related strain, creep strain and creep coefficient

In this series (C_n) the influence of the initial stress level on the creep behaviour was investigated. Only high strength concrete with crushed gravel was considered. Two creep tests were carried out at any of the loading levels, 15%, 35% and 50% of the short term prism strength. The load was applied at a concrete age of 28 days with stress values of 15.1 N/mm², 35.9 N/mm² and 48.8 N/mm², respectively. The measured initial elastic strains for the three stress levels were 0.291×10^{-3} , 0.763×10^{-3} and 1.005×10^{-3} , respectively. A complete set of data is given in Table E-19 in Appendix E, where apart from the age at application of the load and the initial relative stress level, the duration of the test, the short term prism strength, the total shrinkage, the total strain and the initial elastic strain are given. Fig. 7.8 shows the relation between the load-related strain (initial elastic strain plus creep) and the time.

The creep strain of concrete is generally described by the following expression:

$$\varepsilon_{c\sigma}(t,t_0) = \varepsilon_c(t,t_0) - \varepsilon_{sh}(t) = \varepsilon_{ie}(t_0) + \varepsilon_{cr}(t,t_0) = \varepsilon_{ie}(t_0) [1 + \phi_{28}(t,t_0)]$$
 (7.3)

where $\varepsilon_{c\sigma}(t, t_0)$ is the load-related strain, $\varepsilon_c(t, t_0)$ is the total measured strain, $\varepsilon_{sh}(t)$ is the shrinkage strain, $\varepsilon_{le}(t_0)$ is the initial elastic strain, $\varepsilon_{cr}(t, t_0)$ is the creep strain [see Eq. (4.8)], $\phi_{28}(t, t_0)$ is the creep coefficient, t_0 is the time at which the load is applied and t is any time after the load has been applied, i.e. t_0 is the duration of loading.

The creep coefficient $\phi_{28}(t, t_0)$ needs to be further clearly defined [see Eq.(4.8)]:

$$\phi_{28}(t,t_0) = \frac{\varepsilon_{cr}(t,t_0)}{\varepsilon_{io}(t_0)} = \frac{E_{ci}}{\sigma_c(t_0)} \varepsilon_{cr}(t,t_0)$$
(7.4)

where $\sigma_c(t_0)$ is the stress applied at the time t_0 and E_{ci} is the E-modulus of the concrete at an age of 28 days.

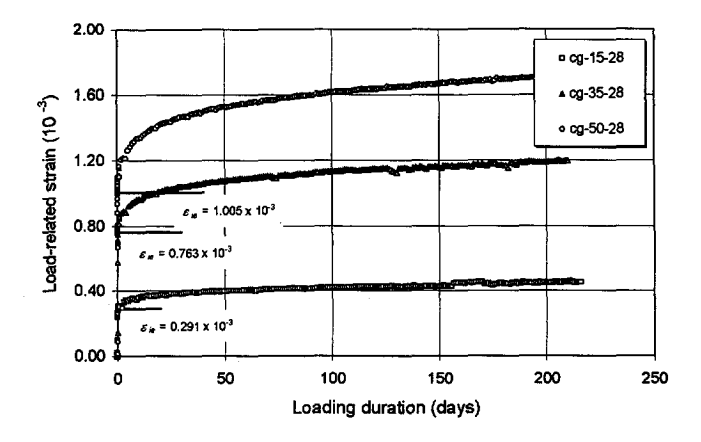


Fig. 7.8 Relation between load-related strain and time for HSC with crushed gravel $[f_{cp}(28) = 100 \text{ N/mm}^2]$ loaded at an age of 28 days under the stress levels $\sigma_c(28) = 0.15 f_{cp}(28)$, 0.35 $f_{cp}(28)$ and 0.5 $f_{cp}(28)$.

According to the definitions in Eqs. (7.3) and (7.4), the creep and creep coefficient in this series of tests can be calculated. Fig. 7.9 shows the relation between the creep strain and the loading duration, whereas Fig. 7.10 shows the relation between the creep coefficient and the loading time with different initial stress levels.

Regarding the test results, a first impression is that the creep strain and the creep coefficient of HSC are quite small. As indicated in *Chapter* 4, with respect to the physical origin of creep, no consensus has yet been reached. However, it is generally agreed that the volume of hydration products and the free water content play a dominant role. As mentioned before, the microstructure of HSC is quite different from that of normal strength concrete. The lower water/cement ratio in HSC results in a smaller volume of hydration products and a smaller water content. Furthermore, as indicated in *Chapter* 3, the time-dependent deformation of concrete is largely due to the movement of water in capillary and gel pores. This movement depends on the relative volume of pores and spaces in the cement gel, as well as the amount of water in these pores at the time of loading. As a result,

HSC is a material which shows a smaller creep strain than NSC, if the applied stress is the same.

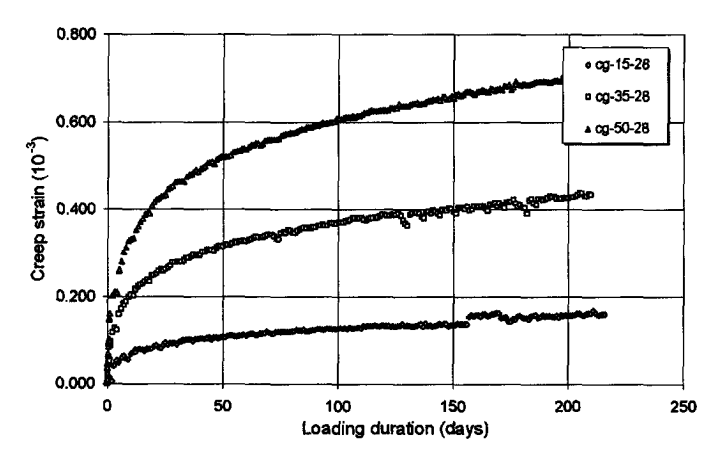


Fig. 7.9 Relation between creep strain and loading duration of HSC loaded at an age of 28 days, calculated based on the data in Fig. 7.8 and Eq. (7.3).

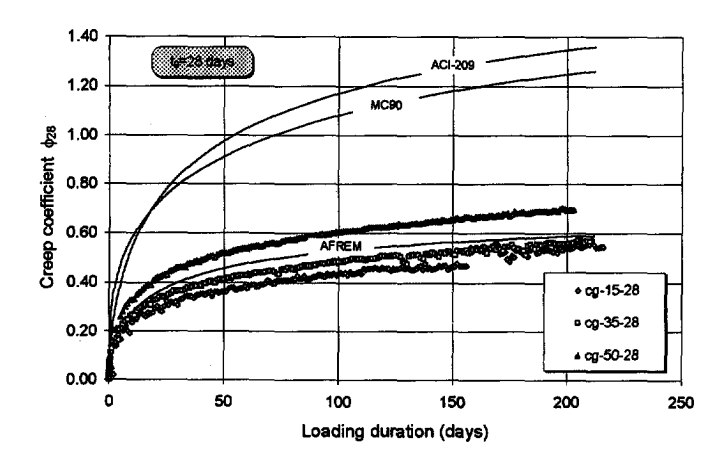


Fig. 7.10 Relation between creep coefficient and time of HSC loaded at an age of 28 days, derived on the basis of the data in Fig. 7.8 and Eq. 7.4.

However, the total strain is the sum of the initial strain, the shrinkage strain and the creep strain. At any stress-strength ratio, the initial strain is always larger the higher is the strength. Consequently, HSC will generally have a larger total strain than NSC shortly after

loading at any stress-strength ratio. Depending on the stress level, the long-term total strain of HSC might be larger than that of NSC.

7.4.1.2 Comparisons of test results with three creep prediction approaches

In order to verify their appropriateness for HSC, three existing creep predicting formulations are compared with the experimental results. The factors considered in these models are, among others, the compressive strength of the concrete (28-day's cylinder strength in N/mm²), the type of cement used, the relative humidity, the size and the shape of the specimen, the loading period and the age at application of the load. In addition, the formulations in ACI-209 take the composition of the concrete into account, but they do not consider concrete's with a strength higher than 40 N/mm². The strength limitation of MC90 (CEB-FIP Model Code 1990) is 80 N/mm². The expressions in AFREM (French chapter of RILEM) also consider the use of silica fume. The strength limitation in this model is 80 N/mm². The upper limit for linear creep in ACI-209 is taken as 50% of the strength of the concrete, whereas this limit in MC90 is taken as 40% of the strength of the concrete. AFREM does not give a clear indication of the upper limit for linear creep.

In Fig. 7.10 it can be clearly seen that the creep coefficient of HSC loaded at an age of 28 days is generally much smaller than predicted by the formulations of MC90 and ACI-209. The estimation of the expression of AFREM shows a good agreement with the test results. However, the formulations of AFREM do not explicitly consider the non-linear creep.

7.4.2 Creep of HSC under variable stresses applied at various ages starting from an age of 28 days

7.4.2.1 Load-related strain

In this series (C_n) the influence of the load history on the creep behaviour of HSC was also investigated. Again, only high strength concrete with crushed gravel was used. Two tests were carried out for any of the load histories, i.e. one step, two and four steps of loading to reach the stress level of 50% of the short term prism strength at an age of 28 days. The time intervals between each step were equally divided. The short term prism strength at an age of 28 days was 75.9 N/mm². For the one step stressing test, the stress of 37.95 N/mm² was applied at an age of 28 days, and then kept constant during 45 days. For the two step stressing test, the initial stress of 18.98 N/mm² was applied at an age of 28 days, and then kept constant during 22.5 days. At an age of 50.5 days, the stress was increased to a value 37.95 N/mm², and then kept constant during another 22.5 days. For the four step stressing test, the initial stress was 9.49 N/mm². The step interval was 11.25

days. The stress increment at the beginning of each step was 9.49. The detail of the loading histories for this series are also given in Fig. 5.2 in *Chapter* 5. A complete set of data for this series is given in Table E-20 in Appendix E, including the age at loading, the initial relative stress level at each step, the duration of the load, the 28-day's prism strength, the shrinkage strain, the total strain and the initial elastic strain.

Stressing method	age at loading (days)	$\sigma_c(t_0) \text{ N/mm}^2$	$\varepsilon_{ie}(t_0) \times 10^{-3}$	
one step	28	37.95	0.843	
two	28	18.98	0.428	
steps	51	37.95	0.344	
	28	9.49	0.199	
four	40	18.98	0.209	
steps	51	28.46	0.198	
	62	37.95	0.196	

Table 7.1 Basic data measured from the step-wise stressing tests

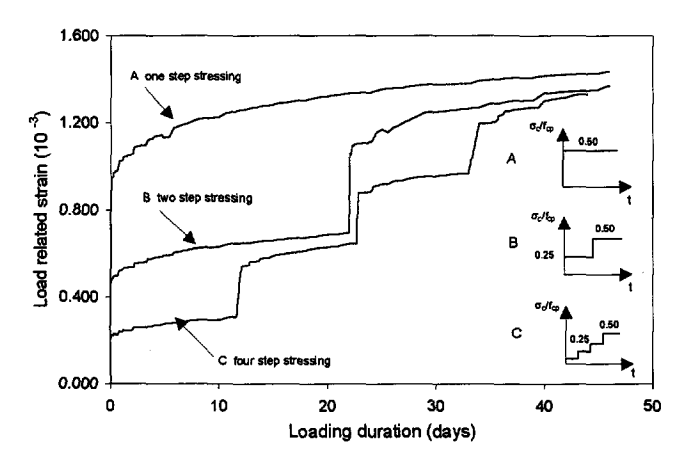


Fig. 7.11 Load-related strain of HSC ($f_{cp} = 75.9 \text{ N/mm}^2$) versus time loaded at various stress levels with different stress histories.

In Fig. 7.11 load-related strains versus time are shown for HSC loaded at different ages starting from 28 days with step-wise increased stress. The basic data including the age at loading, the stress value at each step and the initial elastic strain at each step are given in Table 7.I. The aim of this series of tests is to check the validity of the principle of superposition to the creep of HSC under variable stresses. From Fig. 7.11 it can be seen

that a stress immediately applied to a certain level generates a larger creep than a stress which is step-wise applied to the same level. This shows the well-known effect of ageing.

7.4.2.2 Comparison of test results with three existing formulations on the basis of the assumption of the principle of superposition

According to Eqs. (7.3) and (7.4), the load-related strain $\varepsilon_{co}(t, t_0)$ can be rewritten as:

$$\varepsilon_{c\sigma}(t,t_0) = \sigma_c(t_0) \left[\frac{1}{E_c(t_0)} + \frac{\phi_{28}(t,t_0)}{E_{ci}} \right] = \sigma_c(t_0) \left[\frac{1}{E_c(t_0)} + C(t,t_0) \right] = \sigma_c(t_0) J(t,t_0)$$
 (7.5)

where $E_c(t_0)$ is the E-modulus at the time of loading t_0 , $C(t, t_0)$ is the specific creep, defined as the creep per unit stress, $J(t, t_0)$ is the creep function or creep compliance, defined as the total load-related strain per unit stress.

For a constant stress, Eq. (7.5) can be used to calculate creep or load-related strain. However, for a variable stress, the principle of superposition has to be used in order to calculate the creep or load-related strain at any time t. The principle of superposition can be mathematically expressed by:

$$\varepsilon_{c\sigma}(t,t_0) = \sigma_c(t_0)J(t,t_0) + \int_{t_0}^{t} J(t,\tau) \frac{\partial \sigma_c(\tau)}{\partial \tau} d\tau$$
 (7.6)

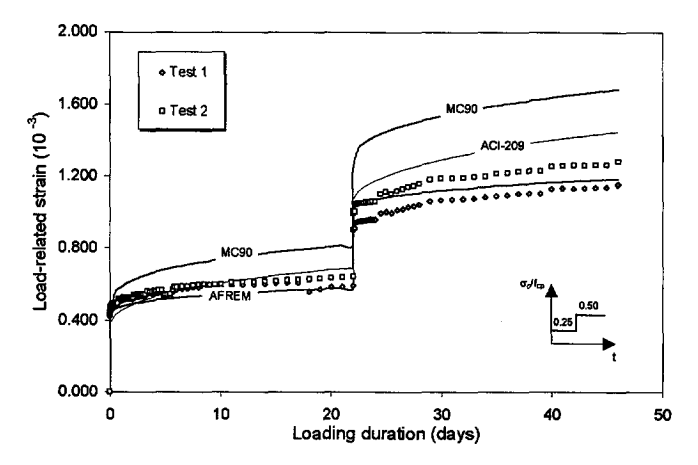


Fig. 7.12 Comparison of the load-related strain obtained in two step stressing tests with those calculated by means of formulations from three existing codes.

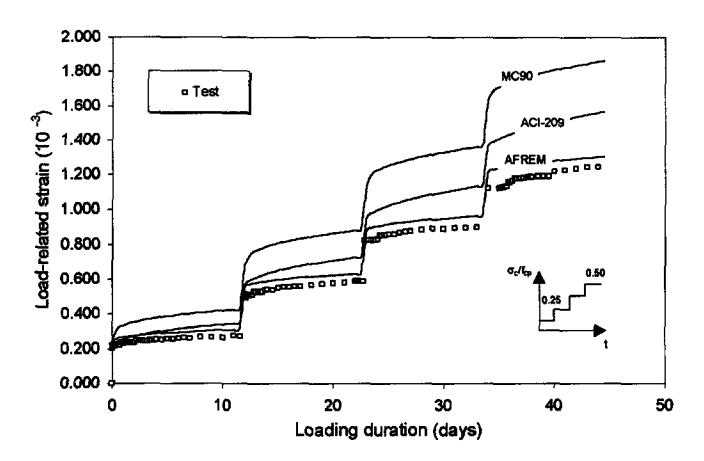


Fig. 7.13 Comparison of the load-related strain obtained in four step stressing tests with those calculated by means of formulations from three existing codes.

On the basis of the principle of superposition, the load-related strain under two stress histories were calculated according to three existing prediction formulations. The 28-day's cylinder strength used in the calculation was 85 N/mm². The calculated results together with the test results are shown in Fig. 7.12 (two step stressing) and in Fig. 13 (four step stressing), respectively.

Comparisons of the load-related strains of HSC at two different stress histories with predictions by using three existing formulations (MC90, AFREM and ACI-209) generally indicate that MC90 and ACI-209 overestimate the creep strain, whereas AFREM again predicts the creep quite well.

7.4.3 Creep of HSC under a constant sustained load applied at early ages

7.4.3.1 Load related strain, creep strain and creep coefficient

The key variables in the series C_e are the age of the concrete at the application of the load, the stress level and the type of aggregate. The load was applied at two early ages, namely, 10 hours and 16 hours after casting. Three stress levels were used, i.e. 30%, 50% and 70% of the mean prism strength obtained from the reference tests at the time of loading. Three types of aggregate (crushed gravel - cg, granite - gr and limestone - ls) were tested.

Table 7.II Basic data concerning the creep tests loaded at an age of 10 hours

Type of	to	Indicative	Mean f _{cp} (t ₀)	σ _c (t _o)	ε _{ie} (t ₀)
aggregate	hours	$\sigma_c(t_0)/f_{cp}(t_0)$	N/mm ²	N/mm ²	10 ⁻³
	10	0.30	8.46	2.54	0.152
crushed gravel	10	0.50	8.46	4.23	0.457
	10	0.70	8.46	5.92	0.560
	10	0.30	9.42	2.83	0.155
granite	10	0.50	9.42	4.71	0.320
	10	0.70	9.42	6.59	0.415
	10	0.30	5.80	1.74	0.120
limestone	10	0.50	5.80	2.90	0.182
	10	0.70	5.80	4.06	0.292

Table 7.III Basic data concerning the creep tests loaded at an age of 16 hours

Type of aggregate	t _o hours	Indicative $\sigma_c(t_0)/f_{cp}(t_0)$	Mean f _{cp} (t ₀) N/mm ²	σ₀(t₀) N/mm²	ε _{ie} (t ₀) 10 ⁻³
	16	0.30	46.4	13.9	0.492
crushed gravel	16	0.50	46.4	23.2	0.845
	16	0.70	46.4	32.5	1.297
	16	0.30	46.0	13.8	0.485
granite	16	0.50	46.0	23.0	0.810
	16	0.70	46.0	32.2	1.225
	16	0.30	43.7	13.1	0.355
limestone	16	0.50	43.7	21.9	0.610
_	16	0.70	43.7	30.6	0.932

In general, the prism strength was determined by testing three reference specimens of the same age as the test specimens. In the case of loading after 16 hours it was well possible to accurately apply the stresses $0.3 f_{cp}$, $0.5 f_{cp}$ and $0.7 f_{cp}$. In the case of loading after 10 hours, however, the hydration process performed just at a very high speed, so that it was not possible very accurately to establish the mean actual strength of the concrete on the basis of three reference tests, since these had to be carried out in series and showed increasing strength values. Therefore, in this case the relative stress levels 0.3, 0.5 and 0.7 have to be regarded as indicative. For the theoretical analysis, only the absolute stress values, which are known, are necessary. In addition, the measured initial elastic strain plays an important role for interpreting the creep and deriving the creep coefficient. Therefore,

these basic data are given in Table 7.II and 7.III. A complete set of data is given in Table E-22 to E-27 in Appendix E.

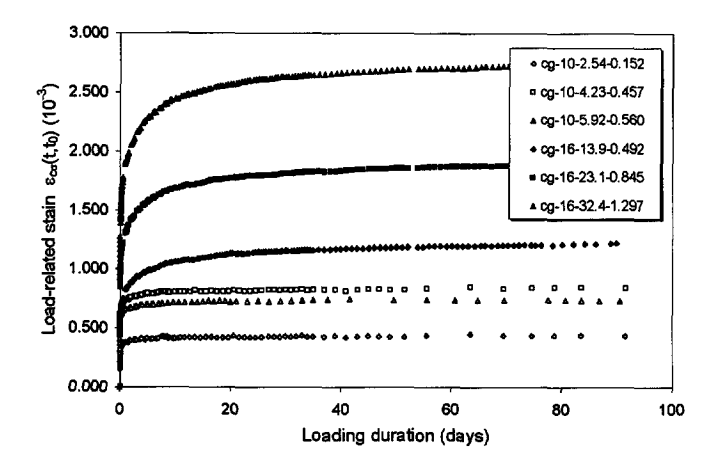


Fig. 7.14 Load-related strain $\varepsilon_{co}(t, t_0)$ of HSC with crushed gravel $[f_{cp}(t_0=10 \text{ hours}) = 8.46 \text{ N/mm}^2]$ and $f_{cp}(t_0=16 \text{ hours}) = 46.4 \text{ N/mm}^2]$, loaded at ages of 10 hours and 16 hours [cg-10-2.54-0.152 means HSC with crushed gravel, loaded at an age of $t_0=10$ hours with a initial stress $\sigma_c(t_0)=2.54 \text{ N/mm}^2$, measured initial elastic strain $\varepsilon_{ie}(t_0)=0.152 \times 10^{-3}$].

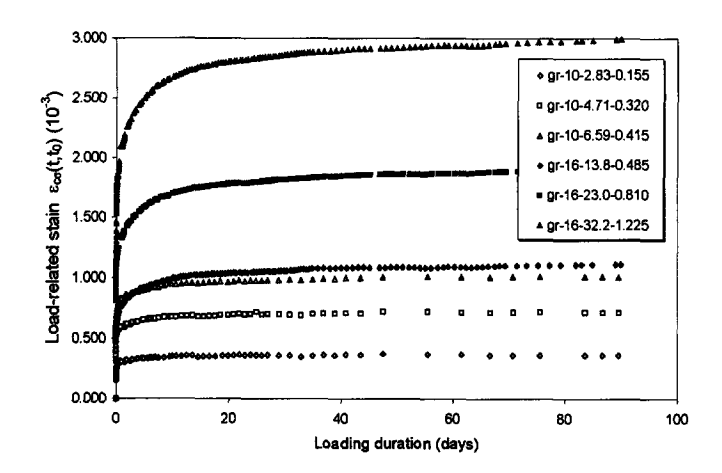


Fig. 7.15 Load-related strain $\varepsilon_{co}(t, t_0)$ of HSC with granite $[f_{cp}(t_0=10 \text{ hours}) = 9.42 \text{ N/mm}^2 \text{ and } f_{cp}(t_0=16 \text{ hours}) = 46.0 \text{ N/mm}^2]$, loaded at ages of 10 hours and 16 hours [gr-10-2.83-0.155 means HSC with granite, loaded at an age of $t_0=10$ hours with a initial stress $\sigma_c(t_0)=2.83 \text{ N/mm}^2$, measured initial elastic strain $\varepsilon_{ie}(t_0)=0.155 \times 10^{-3}$].

Fig. 7.14, 7.15 and 7.16 show the relation between the load-related strain (initial elastic strain plus creep strain) and the time for HSC with crushed gravel, granite and limestone loaded at an age of 10 hours and 16 hours, respectively.

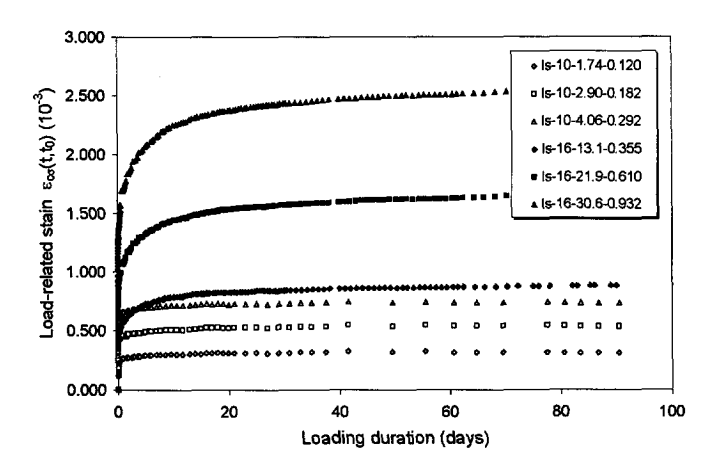


Fig. 7.16 Load-related strain $\varepsilon_{co}(t, t_0)$ of HSC with limestone [$f_{cp}(t_0=10 \text{ hours}) = 5.80 \text{ N/mm}^2$ and $f_{cp}(t_0=16 \text{ hours}) = 43.7 \text{ N/mm}^2$], loaded at ages of 10 hours and 16 hours [1s-10-1.74-0.120 means HSC with limestone, loaded at an age of $t_0=10$ hours with a initial stress $\sigma_c(t_0)=1.74 \text{ N/mm}^2$, measured initial elastic strain $\varepsilon_{to}(t_0)=0.120 \times 10^{-3}$].

Eq. (7.3) can be rewritten in a more general form to calculate the creep strain or creep coefficient:

$$\varepsilon_{c\sigma}(t,t_0) = \varepsilon_c(t,t_0) - \varepsilon_{sh}(t) = \varepsilon_{ie}(t_0) + \varepsilon_{cr}(t,t_0) = \varepsilon_{ie}(t_0) [1 + \phi(t,t_0)]$$
 (7.7)

According to the definition of the creep coefficient, the relation between $\phi(t, t_0)$ and $\phi_{28}(t, t_0)$ can be expressed by:

$$\phi(t,t_0) = \frac{E_c(t_0)}{E_{ci}}\phi_{28}(t,t_0)$$
 (7.8)

where $E_c(t_0)$ is the E-modulus obtained at the time of loading t_0 . For the concrete loaded at an age of 28 days, $\phi(t, t_0)$ is equal to $\phi_{28}(t, t_0)$.

On the basis of Eqs. (7.7) and (7.8), the creep, the creep coefficient and the specific creep (the creep strain per unit stress) in this series have been calculated by using the load-related strain in combination with the basic data in Table 7.II and 7.III. The complete results of the calculation are listed in Table F-15 to F-20 in Appendix F.

In Fig. 7.17 and 7.18, the creep strain $\varepsilon_{cr}(90, t_0)$ of HSC with three different types of aggregate loaded at an age of $t_0 = 10$ hours and $t_0 = 16$ hours are compared, respectively. In Fig. 7.19 and 7.20 the creep coefficient $\phi_{28}(90, t_0)$ of HSC with three different types of the aggregate loaded at an age of $t_0 = 10$ hours and $t_0 = 16$ hours are illustrated, respectively. In Fig. 7.21 and 7.22 the specific creep (the creep per unit stress) $C(90, t_0)$ of HSC with three different types of the aggregate loaded at an age of $t_0 = 10$ hours and $t_0 = 16$ hours are shown, respectively.

Regarding the test results, a first impression is that the creep strain of young HSC generally occurs very fast, i.e. the rate of creep of HSC is very high (see Fig. 7.14 - 7.16). The largest part of the creep strains occurs during the first 10 to 20 days and the increase thereafter is rather small. This is also confirmed by other researchers [Pentalla and Rautanen (1990)]. In the case of loading at 10 hours, the development of the creep strain is even faster than in the case of loading at 16 hours. This is due to the effect of ongoing hydration: in the case of loading at 10 hours the hydration process is in full development so that the relative level of loading, expressed as a stress-strength ratio, decreases very quickly.

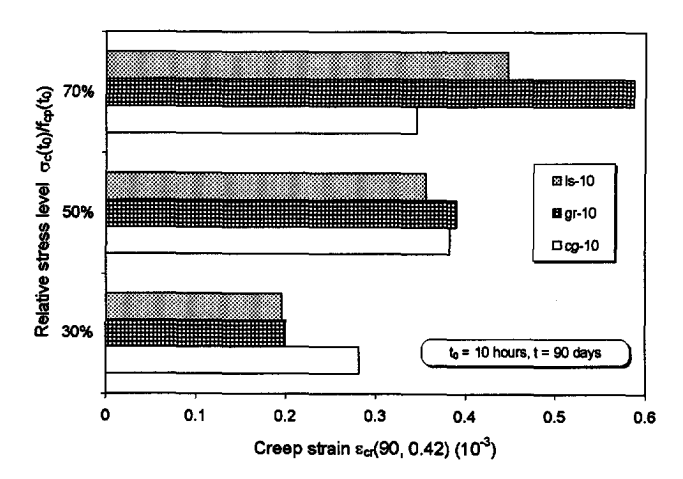


Fig. 7.17 Comparisons of the creep strain $\varepsilon_{cr}(t, t_0)$ of HSC with three types of aggregate, at the time t = 90 days, loaded at an age of $t_0 = 10$ hours with three nominal relative stress levels [the calculations base on the Eqs. (7.7) and (7.8) in combination with Table 7.II and 7.III].

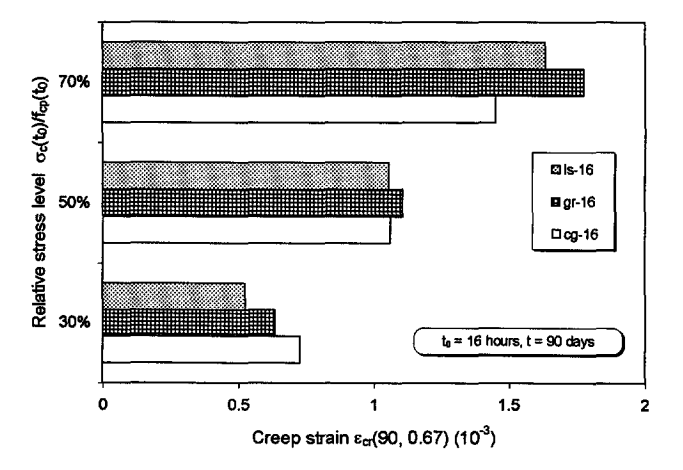


Fig. 7.18 Comparisons of the creep strain $\varepsilon_{cr}(t, t_0)$ of HSC with three types of aggregate, at the time t = 90 days, loaded at an age of $t_0 = 16$ hours with three nominal relative stress levels. [the calculations base on the Eqs. (7.7) and (7.8) in combination with Table 7.II and 7.III]

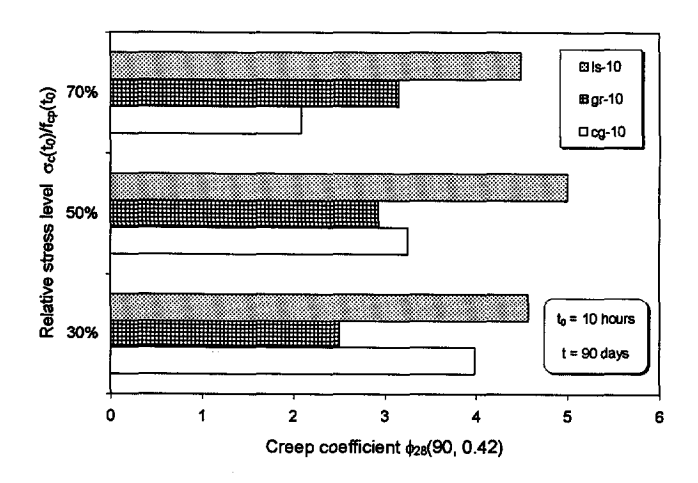


Fig. 7.19 Comparisons of the creep coefficient $\phi_{28}(t, t_0)$ of HSC with three types of aggregate, at the time t = 90 days, loaded at an age of $t_0 = 10$ hours with three nominal relative stress levels [the calculations base on the Eqs. (7.7) and (7.8) in combination with Table 7.II and 7.III].

The creep strain in Fig. 7.17 and 7.18 can not be directly compared, because the corresponding stresses differ. The creep coefficients $\phi_{28}(t, t_0)$, determined with $E_c(28)$ after 90 days show that loading in a very early stage (10 hours) leads to rather high creep coefficients (see Fig. 7.19), with considerable scatter $[\phi_{28}(t, t_0) = 2-5]$. Loading after 16

hours shows a more uniform picture (see Fig. 7.20), with lower values for the creep coefficient $[\phi_{28}(t, t_0) = 1.5-2]$. About similar observations apply to the specific creep, which is defined as $\phi_{28}(t, t_0)/E_c(28)$, where the differences in $E_c(28)$ are small (see Fig. 7.21 and 7.22).

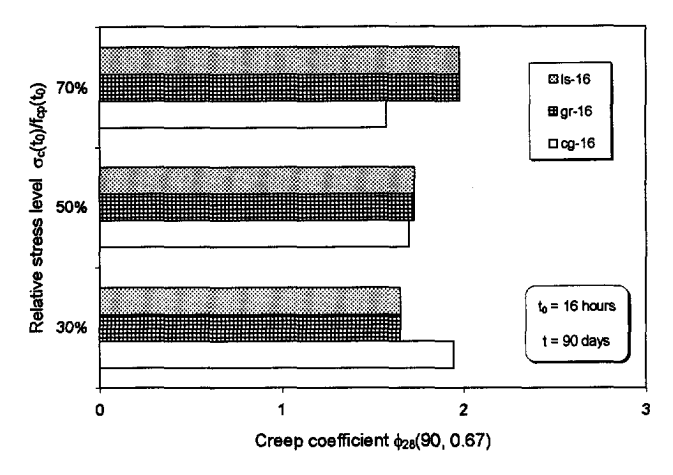


Fig. 7.20 Comparisons of the creep coefficient $\phi_{28}(t, t_0)$ of HSC with three types of aggregate, at the time t = 90 days, loaded at an age of $t_0 = 16$ hours with three nominal relative stress levels [the calculations base on the Eqs. (7.7) and (7.8) in combination with Table 7.II and 7.III].

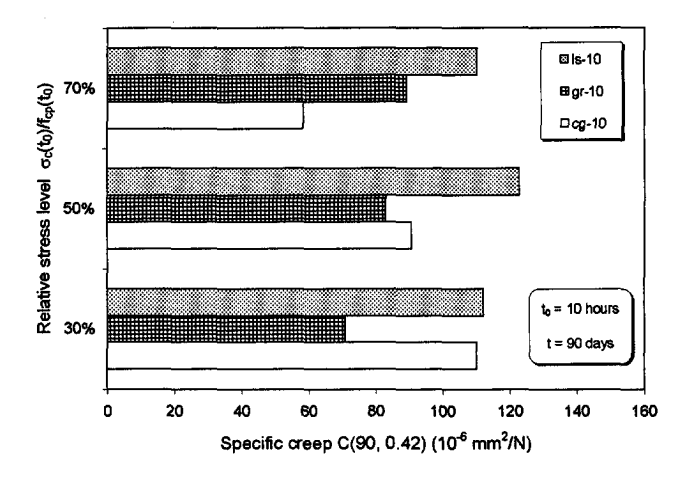


Fig. 7.21 Comparisons of the specific creep $C(t, t_0)$ of HSC with three types of aggregate, at the time t = 90 days, loaded at an age of $t_0 = 10$ hours with three nominal relative stress levels [the calculations base on the Eqs. (7.7) and (7.8) in combination with Table 7.II and 7.III].

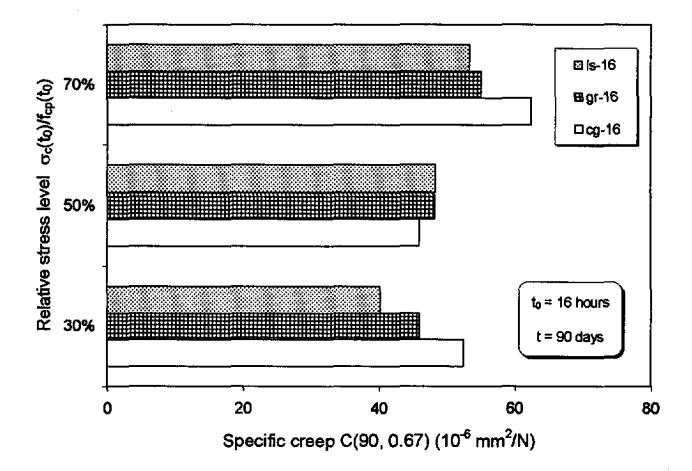


Fig. 7.22 Comparisons of the specific creep $C(t, t_0)$ of HSC with three types of aggregate, at the time t = 90 days, loaded at an age of $t_0 = 16$ hours with three nominal relative stress levels [the calculations base on the Eqs. (7.7) and (7.8) in combination with Table 7.III and 7.III].

7.4.3.2 Comparisons of test results with three creep prediction approaches

While MC90 and ACI-209 generally overestimate the creep coefficient of HSC loaded at an age of 28 days (see section 7.4.1), they do as well not match the creep coefficient of HSC loaded at very early ages. They overall underestimate the creep coefficient of HSC loaded at an age of 10 hours (see Fig. 7.23 and Fig. 7.24). As the age of application of the load increases, both MC90 and ACI-209 firstly underestimate the creep coefficient of HSC, then, after a certain period of loading, they begin to overestimate the creep of HSC (see as an example, Fig. 7.25).

The shapes of creep coefficient curves after MC90 and ACI-209 do also not agree very well with the test results. The reason for this is probably the overestimation of the development of strength and E-modulus in this period (see also Fig. 7.3 and 7.4). The shape of the creep curve according to the AFREM formulation is generally correct, but the predicted values are too low. It should be noted, however, that those curves have not been derived for loading within one day and that it is therefore not astonishing that they do not fit. In *Chapter* 8 improvements will be proposed.

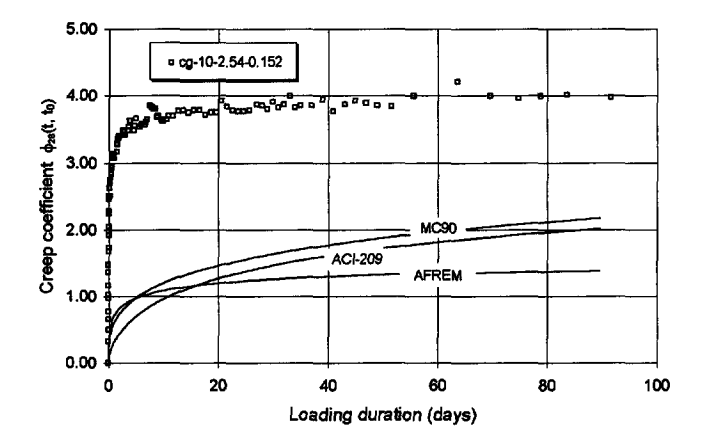


Fig. 7.23 Comparison of the creep coefficient $\phi_{28}(t, t_0)$ of HSC with crushed gravel loaded at an age of 10 hours with the predictions after MC90, ACI-209 and AFREM.

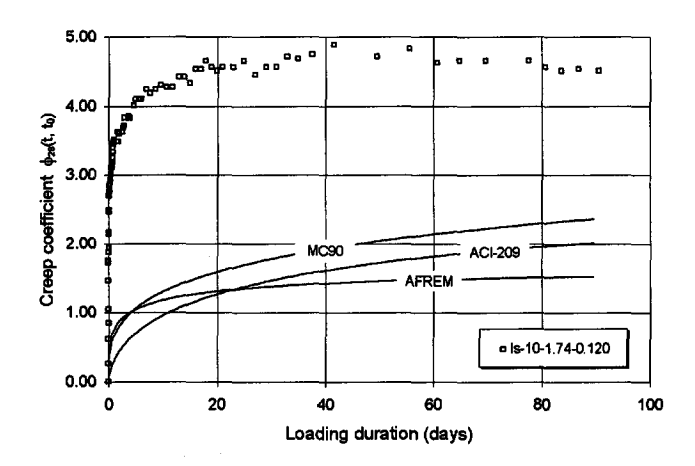


Fig. 7.24 Comparison of the creep coefficient $\phi_{28}(t, t_0)$ of HSC with limestone loaded at an age of 10 hours with the predictions after MC90, ACI-209 and AFREM.

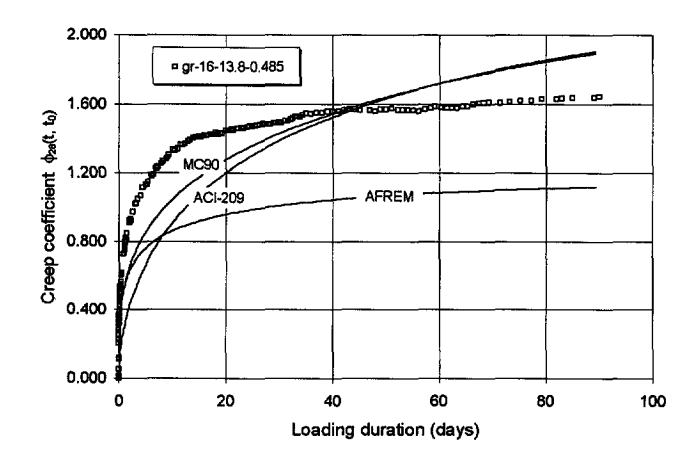


Fig. 7.25 Comparison of the creep coefficient $\phi_{28}(t, t_0)$ of HSC with granite loaded at an age of 16 hours with the predictions after MC90, ACI-209 and AFREM.

7.5 Creep recovery of HSC

7.5.1 Creep recovery of HSC totally unloaded in one step

The creep tests described in §7.4.3.1 were continued. After a loading period of 90 days, the specimens were unloaded. The creep recovery was measured for another 90 days. The initially measured basic data are listed in Table 7.IV and 7.V. A complete set of test data is given in Table E-29 to E-33 in Appendix E.

The load-related strain of HSC with three different types of the aggregate during the loading period as well as during the unloading period are shown in Fig. 7.26, 7.27 and 7.28. The test results indicate that the creep recovery is smaller than the creep deformation and the shape of the recovery curve differs from that of the creep curve. It is found that the rate of creep recovery is higher than the rate of creep, in particular, during the first few days after removal of the load. The figures 7.29 - 7.34 show further data on the absolute, the relative and the specific creep recovery.

Table 7.IV Data concerning the creep recovery for unloading at an age of 90 days (loaded at 10 hours)

Type of	to	Initial loading	Mean f _{cp} (0.42)	Unloading	Initial recovery
aggregate	days	σ _c (t ₀)/f _{cp} (t ₀)	N/mm²	σ _c (t ₀) N/mm ²	ε _{irec} (t ₀) 10 ⁻³
crushed gravel	90	0.30	8.46	-2.54	-0.053
	90	0.50	8.46	-4.23	-0.110
	90	0.70	8.46	-5.92	-0.160
granite	90	0.30	9.42	-2.83	-0.070
	90	0.50	9.42	-4.71	-0.130
	90	0.70	9.42	-6.59	-0.188
limestone	90	0.30	5.80	-1.74	-0.030
	90	0.50	5.80	-2.90	-0.058
	90	0.70	5.80	-4.06	-0.085

As far as the influence of the aggregate on the creep recovery is concerned, it is shown that HSC with limestone generally has a larger specific creep recovery C_{rec} (the creep recovery per unit stress) than the other two aggregates used, in particular as the age at application of the load is low (see Fig. 7.33 and 7.34). This is in agreement with the results of Counto (1964), who concluded that the magnitude of the creep recovery increases with a decrease in the modulus of elasticity of the aggregate.

Table 7.V Data concerning the creep recovery for unloading at an age of 90 days (loaded at 16 hours)

Type of	to	Initial loading	Mean f _{cp} (0.67)	Unloading	Initial recovery
aggregate	days	$\sigma_c(t_0)/f_{cp}(t_0)$	N/mm²	σ _c (t ₀) N/mm ²	ε _{ie} (t ₀) 10 ⁻³
crushed gravel	90	0.30	46.4	-13.9	-0.413
	90	0.50	46.4	-23.2	-0.533
	90	0.70	46.4	-32.5	-0.753
granite	90	0.30	46.0	-13.8	-0.353
	90	0.50	46.0	-23.0	-0.528
	90	0.70	46.0	-32.2	-0.815
limestone	90	0.30	43.7	-13.1	-0.233
	90	0.50	43.7	-21.9	-0.488
	90	0.70	43.7	-30.6	-0.683

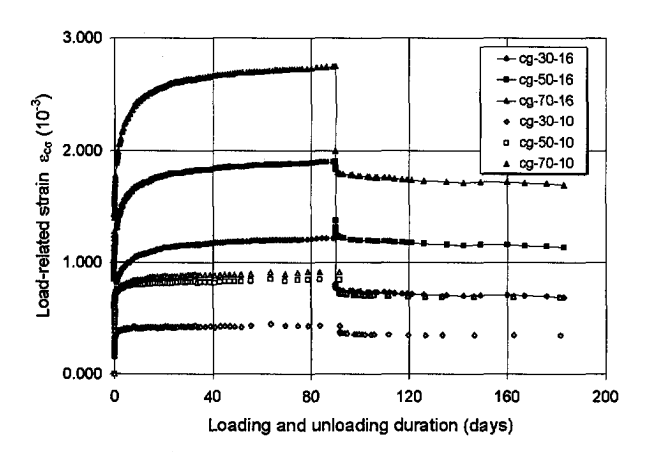


Fig. 7.26 Load-related strain $\varepsilon_{c\sigma}$ of HSC with crushed gravel loaded at ages of 10 hours and 16 hours at three different loading levels and totally unloaded at an age of 90 days.

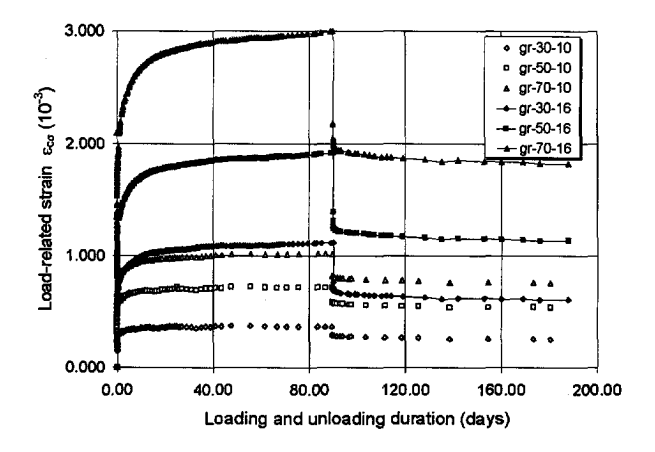


Fig. 7.27 Load-related strain $\varepsilon_{c\sigma}$ of HSC with granite loaded at ages of 10 hours and 16 hours at three different loading levels and totally unloaded at an age of 90 days.

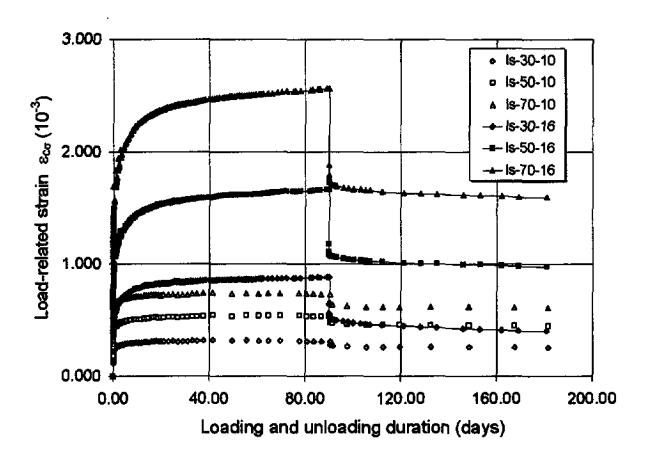


Fig. 7.28 Load-related strain $\varepsilon_{c\sigma}$ of HSC with limestone loaded at ages of 10 hours and 16 hours at three different loading levels and totally unloaded at an age of 90 days.

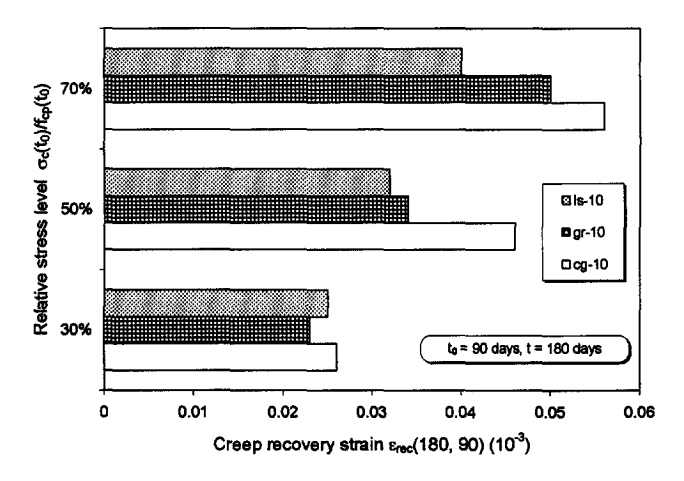


Fig. 7.29 Comparisons of the creep recovery $\varepsilon_{rec}(t, t_0)$ of HSC with three types of the aggregate at an age of the concrete of t = 180 days, loaded at an age of 10 hours under three different stress levels, totally unloaded at an age of $t_0 = 90$ days.

The test results also demonstrated that the creep recovery strongly depends on the age of the concrete at the application of load. The creep recovery is higher the higher is the age at application of the load (compare Fig. 7.29 with Fig. 7.30). In addition, the creep recovery/creep ratios are higher at all adopted stress levels for HSC loaded at an age of 16

hours than those for HSC loaded at an age of 10 hours (see Fig. 7.31 and 7.32). This also confirms the observations by other researchers [Neville, Dilger and Brooks (1983)], who concluded that the creep recovery/creep ratio is higher the higher is the age at application of the load.

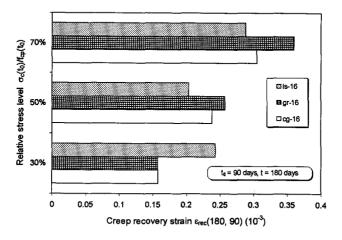


Fig. 7.30 Comparisons of the creep recovery $\varepsilon_{rec}(t, t_0)$ of HSC with three types of the aggregate at an age of the concrete of t = 180 days, loaded at an age of 16 hours under three different stress levels, totally unloaded at an age of $t_0 = 90$ days.

It is also found that the stress level at loading has a certain influence on the creep recovery/creep ratio. The creep recovery/creep ratio decreases as the stress level increases (see Fig. 7.31 and 7.32). This may be due to the non-linear behaviour at a higher stress which results in a higher irrecoverable creep, leading to a reduction of the creep recovery/creep ratio.

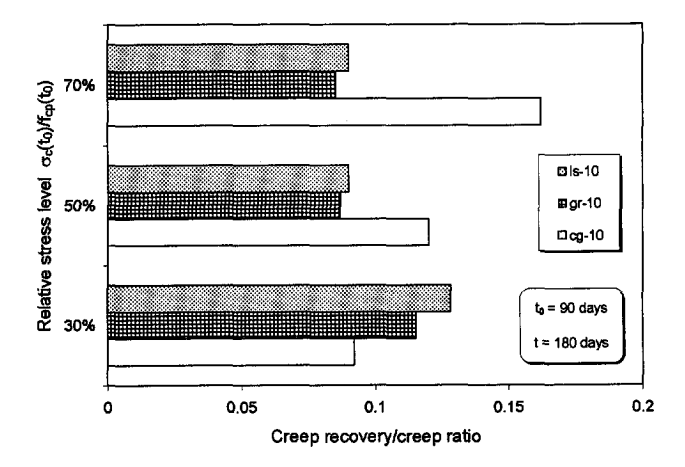


Fig. 7.31 Comparisons of the creep recovery/creep ratio $\varepsilon_{rec}(180, 90)/\varepsilon_{cr}(90, 0.42)$ of HSC with three types of aggregate at an age of the concrete of t = 180 days, loaded at an age of 10 hours under three different stress levels, totally unloaded at an age of $t_0 = 90$ days.

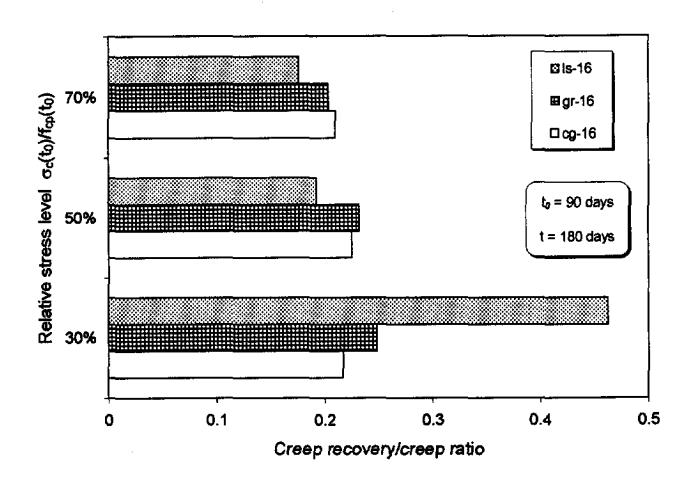


Fig. 7.32 Comparisons of the creep recovery/creep ratio $\varepsilon_{rec}(180, 90)/\varepsilon_{cr}(90, 0.67)$ of HSC with three types of aggregate at an age of the concrete of t = 180 days, loaded at an age of 16 hours under three different stress levels, totally unloaded at an age of $t_0 = 90$ days.

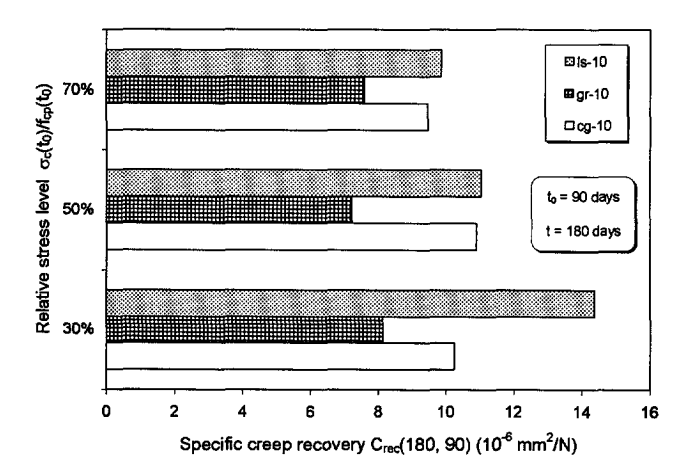


Fig. 7.33 Comparisons of the specific creep recovery $C_{rec}(t, t_0)$ of HSC with three types of aggregate at an age of the concrete of t = 180 days, loaded at an age of 10 hours under three different stress levels, totally unloaded at an age of $t_0 = 90$ days.

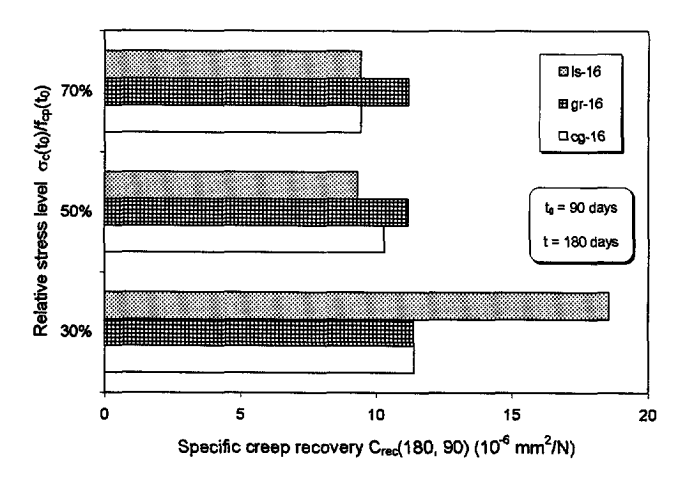


Fig. 7.34 Comparisons of the specific creep recovery $C_{rec}(t, t_0)$ of HSC with three types of aggregate at an age of the concrete of t = 180 days, loaded at an age of 10 hours under three different stress levels, totally unloaded at an age of $t_0 = 90$ days.

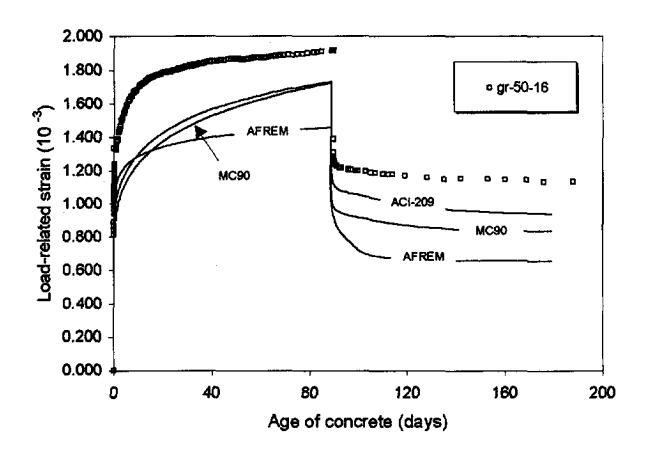


Fig. 7.35 Comparisons of the load-related strain (including creep recovery) of HSC (granite) with the predictions after MC90, ACI-209 and AFREM. The concrete is loaded at an age of 16 hours under a nominal stress/strength ratio 0.50 and totally unloaded at an age of 90 days.

The results of creep recovery tests are also compared with the predictions of three existing code formulations (MC90, ACI-209 and AFREM) on the basis of the principle of superposition. In Fig. 7.35, the load-related strain (including creep recovery) of HSC with granite loaded at an age of 16 hours under a nominal stress/strength ratio 0.50 and totally unloaded at an age of 90 days is compared with the predictions after MC90, ACI-209 and AFREM.

In Fig. 7.35 it is shown that neither MC90 nor AC-I209 can simulate the load-related strain during the loaded period as well as during the unloading period very well. Both of them overestimate the rate of creep recovery. Comparatively, AFREM can describe the tendency of creep recovery, although it still does not accurately simulate the load-related strain.

7.5.2 Creep recovery of HSC unloaded in a step-wise way

Instead of unloading in one step, in the creep tests described in §7.4.2.1, unloading was carried out in a step wise way. After a loading period of 45 days, the unloading procedure was followed for another 45 days in a one-step, two-step and four-step approach. Table 7.VI gives the basic data measured in the unloading tests. A complete set of test data is given in Table E-21 in Appendix E.

Fig. 7.36 shows the load-related strains versus time for HSC loaded at different ages starting from 28 days with the step-wise increasing stress, unloaded at different ages starting from 73 days with the step-wise decreasing approaches. The 28-day's prism strength of this concrete is 75.9 N/mm². The initial loading stress and the initial unloading stress are 37.9 N/mm² (for one step), 18.98 N/mm² (for two steps) and 9.49 N/mm² (for four steps), respectively. In Fig. 7.36 it can be seen that an immediately applied stress to a certain level generates a larger load-related strain as well as a larger recovery of the load-related strain than a step-wisely applied stress to the same level does.

unloading method	age at unloading to (days)	$\sigma_c(t_0) \text{ N/mm}^2$	$\varepsilon_{irec}(t_0) \times 10^{-3}$
one step	73	-37.95	-0.856
two	73	-18.98	-0.324
steps	96	-18.98	-0.387
-	73	-9.49	-0.146
four	84	-9.49	-0.181
steps	96	-9.49	-0.207
	107	-9.49	-0.261

Table 7.VI Basic data measured from the step-wise stressing tests

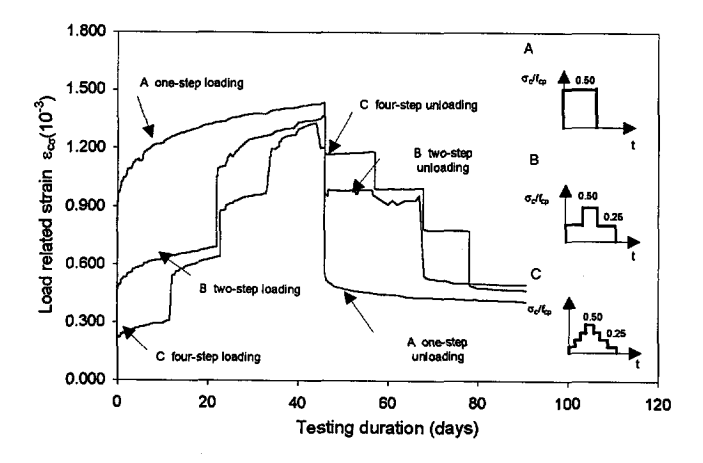


Fig. 7.36 Load-related strains versus time for HSC loaded at different ages starting from 28 days with a step-wise increasing stress, unloaded at different ages starting from 73 days with various step-wise unloading approaches.

The unfavourable effect of the one-step loading can be further demonstrated in Fig. 7.37 concerning the total initial elastic recovery and the total creep recovery. It is found that initial recovery and the creep recovery created by one-step stressing are always larger than that created by step-wise stressing.

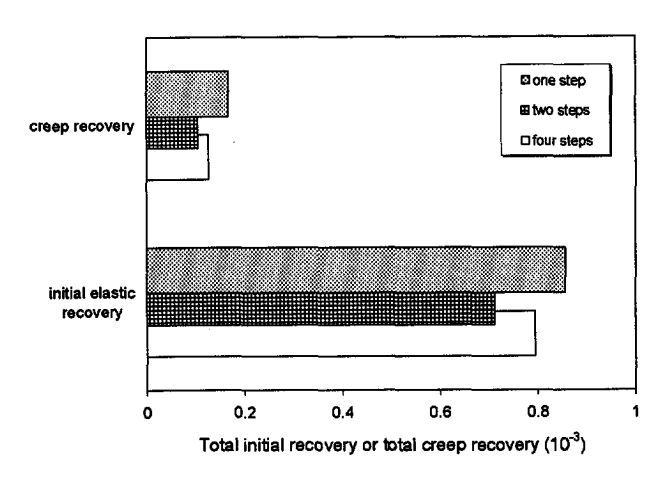


Fig. 7.37 Comparisons of the initial elastic recovery and the creep recovery of HSC unloaded with stepwise methods.

On the basis of the principle of superposition described in Eq. (7.6), the load-related strain development under four-step unloading was calculated by means of the three existing formulations (MC90, ACI-209 and AFREM). The 28-day cylinder strength used in the calculation was 85 N/mm². The calculated results together with the test results are shown in Fig. 7.38.

The comparison of the theoretical calculation with the experimental results indicates that AFREM predicts the tendency of creep recovery very well, although the absolute values do not match those from the tests. It is clear that the E-modulus plays a very important role. From Fig. 7.38 it is found that AFREM underestimates the E-modulus during the unloading period, resulting in an overestimation of the initial elastic recovery. While the overestimation of the E-modulus is also a problem for MC90 and ACI-209, the tendency of creep recovery can not be very well simulated by those two formulations.

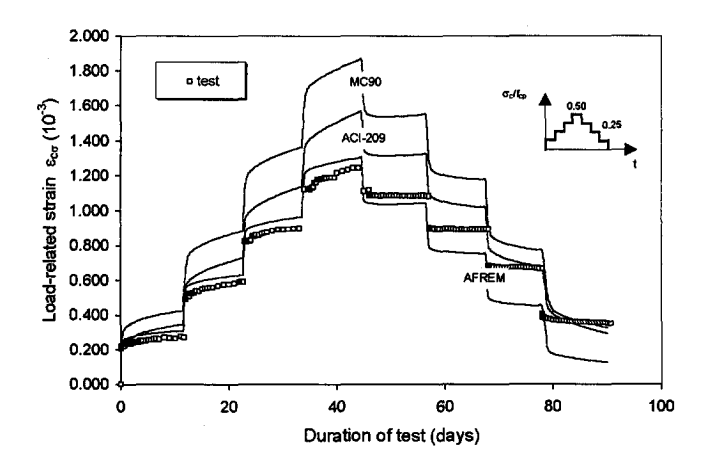


Fig. 7.38 Comparison of the results obtained in a creep recovery test with unloading in four steps with the calculations after MC90, ACI-209 and AFREM.

7.6 Concluding remarks

- The development of strength and E-modulus of HSC at early ages is faster than predicted by using the MC90, ACI-209 and AFREM formulations. At an age higher than 28 days, both MC90 and ACI-209 simulate the development of strength and E-modulus reasonably well, whereas AFREM slightly underestimates the development of strength of HSC. The influences of the type of aggregate used on the development of strength and E-modulus are rather small.
- Besides the relatively smaller creep of HSC, another time-dependent component, autogeneous shrinkage, shows a significant influence on the time-dependent behaviour of HSC. This is particularly pronounced in the case of the time-dependent behaviour at early ages. Due to lack of consideration of the aspect of autogeneous shrinkage in the formulations of MC90 and ACI-209, those expressions considerably underestimate the total shrinkage of HSC exposed to drying at early ages. AFREM shows a better prediction. However, it does not simulate the influence of the type of aggregate on shrinkage.
- The creep deformations of HSC loaded at an age of 28 days are generally much smaller than that predicted by the formulations of MC90 and ACI-209. The estimation of the expression of AFREM shows a good agreement with the test results. As far as the

influence of the age at application of the load is concerned, it is found that at any given stress-strength ratio, the specific creep is greater the lower is the strength of the concrete at the time of loading. The creep of young HSC generally occurs very fast. The largest part of the creep strains occurs during the first 10 to 20 days and the increase thereafter is rather small. No significant influence of the type of aggregate on the creep deformation was observed. MC90 and ACI-209 generally do not match the creep of HSC loaded at very early ages. The shapes of the creep coefficient curves after MC90 and ACI-209 do also not agree very well with the test results. In comparison, the shape of the creep curve according to the AFREM formulation is generally correct, but the predicted values are somewhat too low.

- Creep of HSC created by an immediately applied stress to a certain level is larger than that created by a step-wise applied stress to the same level. The same tendency was also found in the creep recovery tests with step-wisely unloading. On the basis of the principle of superposition, MC90 and ACI-209 generally overestimate the creep strain of HSC under a variable increasing stress, whereas the predictions of AFREM have a relative good agreement with the test results. Concerning the unloading situation, MC90 and ACI-209 underestimate the creep recovery, whereas AFREM can simulate the tendency of the creep recovery very well. All three formulations generally overestimate the E-modulus during the unloading period, resulting in an overestimation of the initial elastic recovery.
- For HSC, the creep recovery is smaller than the creep deformation and the shape of the recovery curve differs from that of the creep curve. The rate of creep recovery is also higher than the rate of creep, in particular, during the first few days after removal of the load. The magnitude of the creep recovery increases with a decrease in the modulus of elasticity of the aggregate. The creep recovery/creep ratios are higher at a higher age of application of load.). The creep recovery/creep ratio decreases as the stress level increases. Although AFREM gives a good simulation of the tendency of the creep recovery, the predictions of the creep recovery by using the three formulations did not have a satisfactory agreement with test results.
- The formulations of MC90 and ACI-209, which are basically derived for normal strength concrete, give rather inaccurate results if used for high strength concrete. The AFREM formulations, which are specially developed for high strength concrete, generally give good results.
- None of the formulations mentioned before is valid for loading at early ages. Here
 modifications are necessary. In Chapter 8 proposes will be developed.

Chapter 8

A modified shrinkage and creep model

A modified shrinkage and creep model on the basis of the well-known MC90 model is derived. Formulations have been derived in order to predict the development of strength and E-modulus of high strength concrete with time. Expressions are given to calculate shrinkage and creep, either at early ages or at normal ages. Under the assumption of creep linearity, the principle of superposition can be applied in order to calculate the creep deformation under variable stresses, as well as the creep recovery. Non-linearity of creep is explicitly taken into account. Finally, evaluations are carried out on the basis of the experimental results.

8.1 Introduction

As indicated in Chapter 4, although comprehensive research has been carried out during several decades, our knowledge on the physical mechanisms of the creep process is still too limited to be able to derive an overall fundamental model. However, a large number of experimental data supply a basis on which empirical creep formulations on an engineering level can be derived. For the time being, this method is still of utmost practical significance, and has been generally adopted by code writers. From the experimental analysis carried out in Chapter 7, it is found that among the three codes used for the comparison, the formulation of AFREM (the new French Code) [Le Roy, De Larrard and Pons (1996)] gives the best predictions as far as the creep of HSC loaded at an age of 28 days is concerned. The code formulations after MC90 and ACI-209 overestimate the creep deformations. However, for the creep of younger HSC, all three formulations lose accuracy. The expressions for shrinkage and creep in MC90 (CEB-FIP Model Code 1990) are well-founded and internationally accepted, as far as normal strength concrete is concerned. Therefore, it seems reasonable and practical that, on the basis of this model,

modifications and extensions are made in order to extend this model to enable a prediction of shrinkage and creep of HSC, either at early or at normal ages.

Most recently, a proposal was made to extend the formulations of MC90 to predict the creep and shrinkage of HSC [Müller and Küttner (1996)]. The aim of this extension was to propose a unified approach to cover both creep of normal strength concrete and creep of high strength concrete. It was reported that this new extended MC90 formulation can predict the creep of HSC with 28-day's cylinder strengths up to 110 N/mm². However, up to now, this new extended MC90 did not yet consider: a) the influence of the type of aggregate on either shrinkage or creep; b) the influence of various loading histories on the creep and the creep recovery (principle of superposition); c) the shrinkage and the creep at the early ages of the concrete.

In order to extent the current MC90 formulations to be able to consider the aspects mentioned above, a modified MC90 model for predicting the shrinkage and creep of high strength concrete in compression is proposed. This model is valid for concrete with 28-day's cylinder strengths up to 100 MPa. The applied stress level may be up to 40% of the strength at the time of loading (linear creep) and up to 70% of the strength at the time of loading (non-linear creep). The other limitations are the same as that defined in MC90.

In §8.2, the proposed modified formulations for the development of strength and E-modulus, and the development of shrinkage and creep will be given. The proposed modifications are based on the experimental analysis described in *Chapter* 7. The verification will be given in §8.3.

8.2 The shrinkage and creep of concrete

8.2.1 Development of strength and E-modulus with time

Concrete is an ageing material, which implies that its properties change with time. In fact, a lot of influencing factors are involved in this process. Among others, the type of cement used, the curing conditions including the relative humidity and temperature play a role. Basically, the strength and the E-modulus develop very fast in the first period after casting (about several hours to several days). From then on, the rate of development decreases.

The basic assumption for deriving an improved formulation is that the turning point where the rate of the strength or E-modulus development changes from increasing to decreasing is $f_{cm}(t)/f_{cm} = 0.55$. This time point is called the critical time t_{cr} . For different

types of cement, the critical time is determined according to experiments. In the case that no experimental data are available, the following values can be taken as t_{cr} (days): for rapid hardening high strength cement (RS) 0.67; for normal cement (NR) 2.44; for slowly hardening cement (SL) 7.22 [these values are derived from Eq. (8-7) by taking $\beta_{cc}[t_c(t)] = 0.55$].

Since the type of cement strongly influences the characteristics of the hydration process, a time t_c is defined for the calculation of strength and E-modulus, which depends on the real time and the type of cement. The basic formulation of $t_c(t)$ comes from the original expression in MC90, with modifications by introducing two key parameters: 1) the critical time t_{cr} , 2) t_{ad} ajustable time according to the type of cement used: for rapidly hardening high strength cement (RS), $t_{ad} = 0.4$, for normally hardening cement (NR), $t_{ad} = 0$, for slowly hardening cement (SL), $t_{ad} = 0$. The proposed expression of $t_c(t)$ is:

$$t_c(t) = (t) \cdot \left[\frac{9}{2 + \left(\frac{t}{t_{1:T}} \right)^{1.2}} + 1 \right]^{\alpha}$$
 for $t \le t_{cr}$ (8.1)

and

$$t_{c}(t) = (t - t_{ad}) \cdot \left[\frac{9}{2 + \left((t - t_{ad}) / t_{1.T} \right)^{1.2}} + 1 \right]^{\alpha} \quad \text{for } t \ge t_{cr}$$
 (8.2)

where all the following parameters are the same as MC90: $t_{1.T}$ is 1 day; α are the following values: for rapidly hardening high strength cement (RS), $\alpha = 1$; for normally hardening cement (NR), $\alpha = 0$; for slowly hardening cement (SL), $\alpha = -1$.

The basic formulations of the development of strength and E-modulus are the same as in MC90:

$$f_{cm}(t) = \beta_{cc} [t_c(t)] \cdot f_{cm}$$
(8.3)

$$E_{ci}(t) = \beta_E[t_c(t)] \cdot E_{ci}$$
(8.4)

However, the parameter $\beta_{cc}[t_c(t)]$ and $\beta_E[t_c(t)]$ are modified. According to the real time t, the expressions are divided into two sets. As $t \le t_{cr}$, the idea of Byfors (1980) is introduced to describe the development of strength and E-modulus of concrete at early ages [see also Eq. (4.70) in *Chapter* 4]:

for $t \le t_{cr}$:

$$\beta_{cc}[t_c(t)] = a_{st} \cdot [t_c(t)]^4 \tag{8.5}$$

$$\beta_{E}[t_{c}(t)] = a_{E} \cdot [t_{c}(t)]^{4}$$
(8.6)

As $t \ge t_{cr}$, the original expression for the strength development in MC90 is taken. The original expression for the E-modulus development in MC90 is modified to consider the fast development of the E-modulus at a very early age:

for $t \ge t_{cr}$:

$$\beta_{cc}[t_c(t)] = e^{s\left(1-\sqrt{\frac{28}{t_c(t)/t_1}}\right)}$$
(8.7)

$$\beta_{E}[t_{c}(t)] = \left\{\beta_{cc}[t_{c}(t)]\right\}^{\frac{1}{3}}$$
(8.8)

where

 $f_{cm}(t)$ is the mean concrete compressive strength (cylinder) at an age of t days;

 f_{cm} is the mean compressive strength (cylinder) after 28 days (in MPa);

 $t_c(t)$ is the adjusted time according to Eqs. (8.1) and (8.2) in days;

 t_1 is 1 day;

s is a coefficient (according to MC90) which depends on the type of cement: s = 0.2 for rapidly hardening high strength cements RS, 0.25 for normally and rapidly hardening cements N and R, and 0.38 for slowly hardening cements SL;

 $E_{cl}(t)$ is the modulus of elasticity at an age of t days (in GPa);

 E_{ci} is the modulus of elasticity at an age of 28 days (in GPa);

 β_{cc} is a coefficient according to Eqs. (8.5) and (8.7);

 β_E is a coefficient according to Eqs. (8.6) and (8.8);

 a_{st} and a_{E} are proposed to be determined through experiments as described in Chapter 7 (see §7.2). In the case that no experimental data are available, the

following values can be taken for a_{st} and a_{E} , respectively: for rapidly hardening high strength cement (RS) 0.0069 and 0.011; for normally hardening cement (NR) 0.0155 and 0.024; for slowly hardening cement (SL) 0.0017 and 0.0027.

8.2.2 Shrinkage

In the shrinkage formulation of the modified MC90, two components are taken into account: autogeneous shrinkage and drying shrinkage (in MC90 only drying shrinkage is considered). The additional expression for the autogeneous shrinkage is chosen on the basis of the formulation of AFREM with a small modification, in that the shape of the shrinkage curve is adjusted according to the experimental data. With respect to the drying shrinkage component, two modifications are introduced into the MC90 formulation. The first one is to consider the time at which the drying process starts. The second one is to change the basic shape of the shrinkage curve based on the age at the start of drying.

The total shrinkage between time t (the age of concrete) and t_{ms} (the age at starting shrinkage measurement) can be predicted as follows:

$$\varepsilon_{cs}(t, t_{ms}) = \varepsilon_{as}(t) + \varepsilon_{ds}(t, t_{s0}) - \varepsilon_{as}(t_{ms}) - \varepsilon_{ds}(t_{ms}, t_{s0})$$
(8.9)

where t_{s0} is the age at starting of drying; ε_{as} is the autogeneous shrinkage and ε_{ds} is the drying shrinkage.

The autogeneous shrinkage is calculated according to the following expressions:

$$\varepsilon_{as}(t) = (f_{cm} - 20) \cdot \{2.2 \cdot \beta_{cc}[t_c(t)] - 0.2\} \cdot 10^{-6} \text{ for } t \le 28 \text{ days}$$
 (8.10)

$$\varepsilon_{as}(t) = (f_{cm} - 20) \cdot \left[2.8 - 11 \cdot e^{-\frac{t_c(t)}{96}} \right] \cdot 10^{-6}$$
 for $t \ge 28$ days (8.11)

where f_{cm} follows from Eq. (8.3); $t_c(t)$ and $\beta_{cc}[t_c(t)]$ are calculated according to Eqs. (8.1), (8.2), (8.5) and (8.7), respectively.

The drying shrinkage component is formulated by introducing t_{s0} into the MC90 formulation:

$$\varepsilon_{ds}(t, t_{s0}) = \varepsilon_{cso} \cdot \beta_s(t - t_{s0}) \tag{8.12}$$

where

 ε_{cso} is the notional shrinkage coefficient;

 β_s is the coefficient to describe the development of shrinkage with time;

t is the age of concrete (in days);

 t_{s0} is the age of concrete (days) at the start of exposition to drying.

The notional shrinkage coefficient can be obtained from

$$\varepsilon_{cso} = \varepsilon_s (f_{cm}, t_{s0}) \cdot \beta_{RH} \tag{8.13}$$

with the modified $\varepsilon_s(f_{cm}, t_{s0})$:

$$\varepsilon_s(f_{cm}, t_{s0}) = \eta \cdot \left[160 + 10 \cdot \beta_{sc} \cdot \left(9 - \frac{f_{cm}}{f_{cm0}} \right) \right] \cdot 10^{-6}$$
(8.14)

where

 f_{cm} follows from Eq. (8.3);

 f_{cmo} is taken as 10 MPa;

 β_{sc} is a coefficient (according to MC90) which depends on the type of cement: $\beta_{sc} = 4$ for slowly hardening cement SL; $\beta_{sc} = 5$ for normally or rapidly hardening cements N and R; and $\beta_{sc} = 8$ for rapidly hardening high strength cement RS.

The newly proposed parameter η can be calculated as follows:

$$\eta = \frac{2.4 \cdot \sqrt{\beta_{ss} \left[t_c\left(t_{s0}\right)\right]}}{\gamma^4} \tag{8.15}$$

with

$$\beta_{ss}[t_c(t_{s0})] = \frac{1}{\gamma_a \cdot \beta_{cc}[t_c(t_{s0})]}$$
(8.16)

where γ_a is a proposed parameter which is obtained according to the ratio of 28-day E-modulus of concrete with the aggregate considered to that of concrete with crushed gravel; $\beta_{cc}[t_c(t_{s0})]$ is calculated according to Eqs. (8.5) and (8.7).

The original MC90 formulations are used to consider the influence of the relative humidity on shrinkage:

$$\beta_{RH} = -1.55 \cdot \beta_{RH}$$
 for $40\% \le RH < 99\%$ (8.17)

$$\beta_{RH} = +0.25$$
 for $RH \ge 99\%$ (8.18)

$$\beta_{sRH} = 1 - \left(\frac{RH}{RH_0}\right)^3 \tag{8.19}$$

where RH is the relative humidity of the ambient atmosphere (%); RH_0 is 100%; The positive sign in Eq. (8.18) means swelling, whereas the negative sign in Eq. (8.17) means shrinkage.

The development of shrinkage with time is modified by introducing a parameter θ_s :

$$\beta_s(t - t_{s0}) = \left[\frac{(t - t_{s0})/t_1}{350(h/h_0)^2 + (t - t_{s0})/t_1} \right]^{\theta_s}$$
(8.20)

with

$$0.06 \le \theta_s = 0.5^{\beta_B \left[\ell_c(t_{r0}) \right]} \le 0.5 \tag{8.21}$$

and

$$h = 2\frac{A_c}{u} \tag{8.22}$$

where h is the notional size of the member (mm); A_c is the cross-section and u is the perimeter of the member in contact with the atmosphere; h_0 is 100 mm; t_1 is 1 day; $\beta_{ss}[t_c(t_{s0})]$ is calculated according to Eq. (8.16).

8.2.3 Linear creep

The creep is assumed to be linearly related to the applied stress up to $0.4 f_{cm}(t_0)$. If the stress level falls into the range between 0.4 and 0.7 $f_{cm}(t_0)$, non-linearity of creep has to be taken into account.

For a constant stress applied at time t_0 (days), the creep can be obtained as follows:

$$\varepsilon_{cc}(t, t_0) = \frac{\sigma_c(t_0)}{E_c} \cdot \phi_{28}(t, t_0)$$
(8.23)

where $\phi_{28}(t, t_0)$ is the creep coefficient with respect to the 28-day's initial elastic strain; E_{ci} is the E-modulus at the age of 28 days (in GPa).

The creep coefficient may be calculated according to MC90 from

$$\phi_{28}(t, t_0) = \phi_0 \cdot \beta_c(t - t_0) \tag{8.24}$$

where ϕ_0 is the notional creep coefficient; $\beta_c(t-t_0)$ is the coefficient to describe the development of creep with time after loading.

The notional creep coefficient and the coefficient to describe the development of creep with time are empirically derived on the basis of experiments. The main parameters considered in these coefficients are known to the designer, such as compressive strength, dimensions of the member, relative humidity, type of cement, age at loading, duration of loading, etc.. According to the analysis in *Chapter 4*, the influences of the relative humidity, the strength of concrete at the age at loading and at the age of 28 days, the age at application of load, the type of cement and aggregate, as well as the strength development on creep are taken into account in the calculation of the notional creep coefficient:

$$\phi_0 = \phi_{RH} \cdot \beta(f_{cm}) \cdot \beta(t_0, \gamma_a) \tag{8.25}$$

The same formulation as the new extended MC90 proposed by Müller and Küttner (1996) is used:

$$\phi_{RH} = \alpha_2 \cdot \left\{ 1 + \alpha_1 \cdot \left[\frac{1 - RH/RH_0}{0.46 \cdot (h/h_0)^{\frac{1}{2}}} \right] \right\}$$
 (8.26)

with modifications of the parameters α_1 and α_2 by taking the strength at the time of loading instead of the 28-day's strength into account:

$$\alpha_1 = \left[\frac{35}{f_{cm} [t_c(t_0)]} \right]^{0.7} \le 1 \tag{8.27}$$

$$\alpha_2 = \left[\frac{35}{f_{cm} \left[t_c(t_0) \right]} \right]^{0.2} \le 1$$
 (8.28)

The original formulation in MC 90 concerning the influence of the strength is modified:

$$\beta(f_{cm}) = \frac{2.6}{\sqrt{f_{cm}/f_{cmo}} - 1}$$
 (8.29)

The original formulation in MC90 concerning the effect of the time at loading on the creep coefficient is modified by introducing an additional parameter γ_a , which considers the influence of the type of aggregate:

$$\beta(t_0, \gamma_a) = \gamma_a^{0.4} \cdot \frac{1}{0.1 + \left[t_o(t_0)\right]^{0.2}}$$
(8.30)

The definitions of all symbols are:

 t_0 is the age at the application of the load;

h is the notional size of the member (mm), which can be calculated according to Eq. (8.22) and h_0 is 100 mm;

RH is the relative humidity of the ambient environment (%) and RH₀ is 100%;

 $t_c(t_0)$ can be calculated according to Eqs. (8-1) and (8-2);

 $f_{cm}[t_c(t_0)]$ can be obtained from Eq. (8-3);

 f_{cm} is the mean compressive strength of concrete at the age of 28 days (MPa) and f_{cmo} is 10 MPa;

 γ_a is a parameter which is obtained according to the ratio of 28-day E-modulus of concrete with the aggregate considered to that of concrete with crushed gravel.

The development of creep with time is modified by introducing a parameter θ_c :

$$\beta_c(t - t_0) = \left[\frac{(t - t_0)/t_1}{\beta_H + (t - t_0)/t_1} \right]^{\theta_c}$$
(8.31)

with

$$\beta_H = 150 \cdot \left[1 + \left(12 \cdot \frac{RH}{RH_0} \right)^{18} \right] \cdot \frac{h}{h_0} + 250 \le 1500$$
 (8.32)

$$0.09 \le \theta_c = 0.3^{\beta_{ca}[t_c(t_0)]} \le 0.3 \tag{8.33}$$

with

$$\beta_{cs}[t_c(t_0)] = \frac{1}{\gamma_a \cdot \beta_{cc}[t_c(t_0)]}$$
(8.34)

where $\beta_{cc}[t_c(t_0)]$ is calculated according to Eqs. (8.5) and (8.7).

8.2.4 Stress dependent strain and the principle of superposition

The stress dependent strain can be expressed as follows:

$$\varepsilon_{c\sigma}(t,t_0) = \sigma_c(t_0) \cdot \left[\frac{1}{E_{ci}(t_0)} + \frac{\phi_{28}(t,t_0)}{E_{ci}} \right] = \sigma_c(t_0) \cdot J(t,t_0)$$
(8.35)

where $J(t, t_0)$ is the creep function or creep compliance, representing the total stress dependent strain per unit stress; $E_{ci}(t_0)$ is the E-modulus at the time of loading t_0 according to Eq. (8.4); $\sigma_c(t_0)$ is the stress applied at the time of t_0 (MPa).

For variable stresses, on the basis of the assumption of the principle of superposition, the stress dependent strain at any time t can be written as

$$\varepsilon_{c\sigma}(t,t_0) = \sigma_c(t_0) \cdot J(t,t_0) + \int_{t_0}^t J(t,\tau) \cdot \frac{\partial \sigma_c(\tau)}{\partial \tau} \cdot d\tau$$
 (8.36)

where τ is the time point at which the stress diverts from $\sigma_c(t_0)$.

8.2.5 Non-linear creep

For stress levels in the range of $0.4 f_{cm}(t_0) < \sigma_c(t_0) < 0.7 f_{cm}(t_0)$, the same formulations as in MC90 concerning non-linearity of creep are used [replacing ϕ_0 in Eq. (8.24)]:

$$\phi_{0,k} = \phi_0 \cdot e^{\alpha_{\sigma} \cdot (k_{\sigma} - 0.4)}$$
 for $0.4 < k_{\sigma} \le 0.7$ (8.37)

$$\phi_{0,k} = \phi_0$$
 for $k_{\sigma} \le 0.4$ (8.38)

where

 $\phi_{0,k}$ is the non-linear notional creep coefficient; k_{σ} is the stress-strength ratio, $\sigma_c(t_0)/f_{cm}(t_0)$; α_{σ} is taken as 1.5.

8.3 Verification of the modified shrinkage and creep formulations

8.3.1 The development of strength and E-modulus

The development of strength and E-modulus with time obtained from the experiments up to an age of 180 days, which are shown in Fig. 7.1 and 7.2 in *Chapter* 7, are displayed again in Fig. 8.1 and 8.2, together with the predictions by using the modified formulations Eqs. (8.5), (8.6), (8.7) and (8.8). The parameters used in the calculations are $a_{st} = 0.0069$, $a_E = 0.011$ and s = 0.2. In Fig. 8.3 and Fig. 8.4 the same comparisons at early ages are shown

From Fig. 8.1 it can be seen that the modified formulation is generally able to accurately predict the strength development of HSC, in spite of the slight overestimation of the strength development after the age of 28 days for HSC with limestone. At early ages, the modified formulation also simulates the strength development very well, although it slightly overestimates the strength at an age of about 3 days (see Fig. 8.3).

The development of E-modulus of HSC can be simulate very well by using the modified model at either early ages or late ages (see Fig. 8.2 and Fig. 8.4).

It has to be mentioned that this modified model does not consider the effects of silica fume and the type of aggregate used on the development of strength and E-modulus of HSC. It also does not explicitly take the influence of the environmental curing conditions (such as relative humidity and temperature) on the development of strength and E-modulus into account.

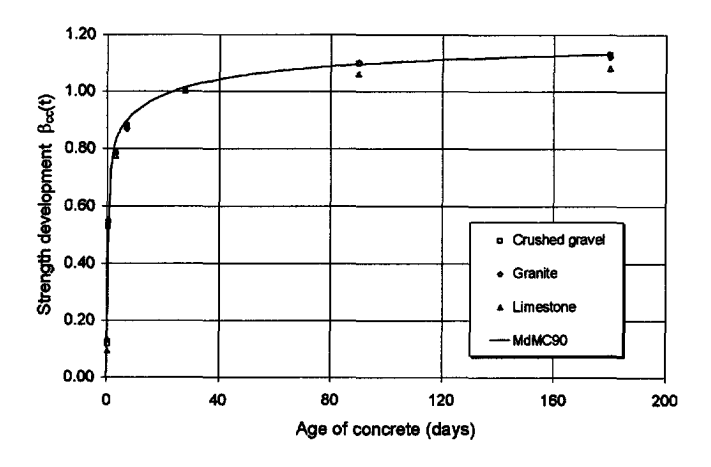


Fig. 8.1 Comparisons of the development of the strength of HSC $\beta_{cc}(t)$ in tests with the prediction by Eqs. (8.5) and (8.7).

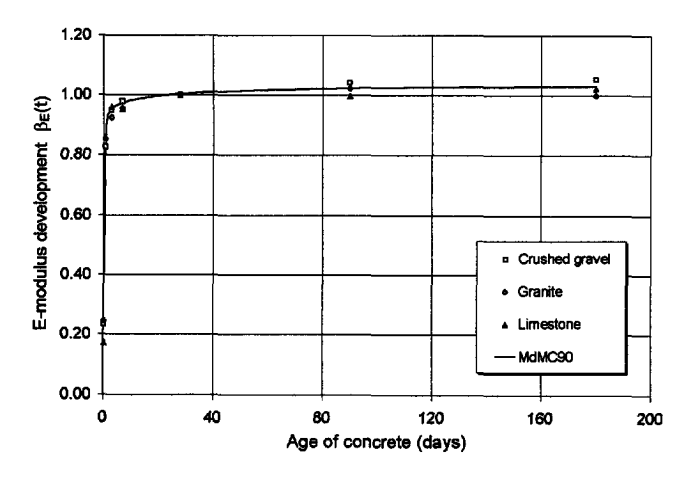


Fig. 8.2 Comparisons of the development of E-modulus of HSC $\beta_E(t)$ in tests with the prediction by Eqs. (8.6) and (8.8).

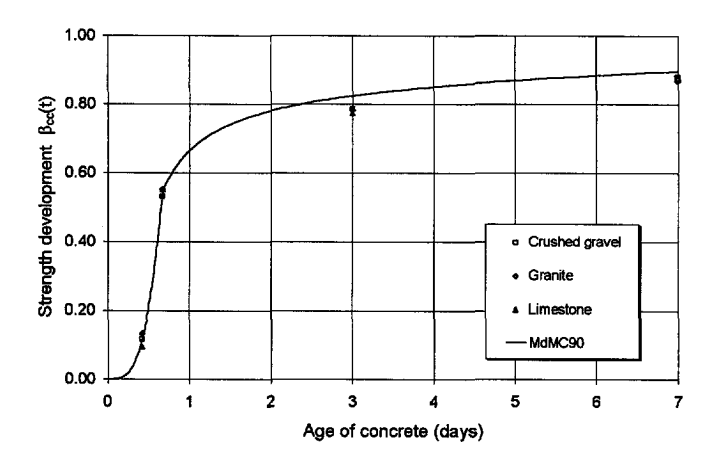


Fig. 8.3 Comparisons of the development of the strength of HSC $\beta_{cc}(t)$ in tests at early ages with the prediction according to Eqs. (8.5) and (8.7).

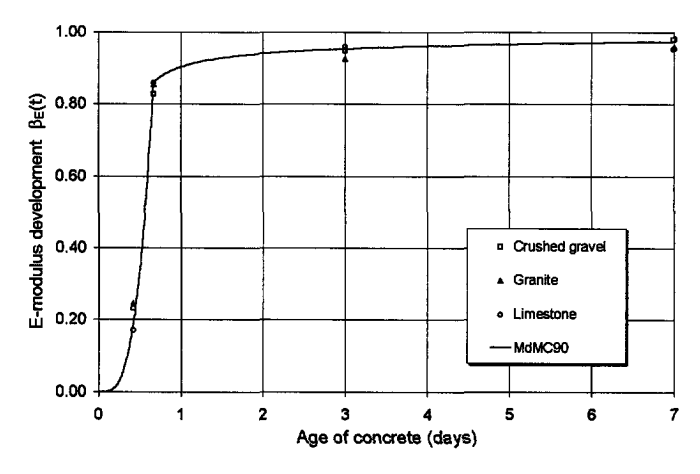


Fig. 8.4 Comparisons of the development of E-modulus of HSC $\beta_E(t)$ in tests at early ages with the prediction according to Eqs. (8.6) and (8.8).

8.3.2 Shrinkage of HSC

In Fig. 8.5 test results concerning the shrinkage of HSC with crushed gravel exposed to a constant climate of 60% RH and 20 °C in temperature at an age of 28 days ($t_{s0} = 28$ days), which are already shown in Fig. 7.7 in *Chapter* 7, are compared with the predictions

by using the modified shrinkage formulations [see Eqs. (8.9)-(8.22)]. It can be clearly seen that the Modified MC90 formulation (MdMC90) simulates the shrinkage of HSC at normal ages very well.

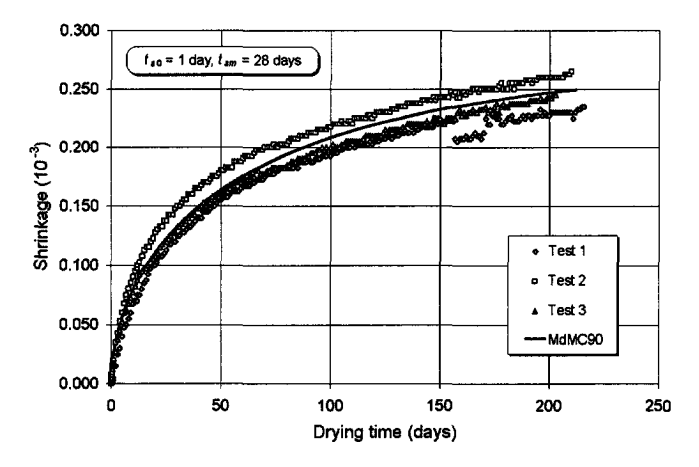


Fig. 8.5 Comparison of the shrinkage of HSC with crushed gravel exposed to drying at an age of 28 days with predictions of MdMC90 ($f_{cm} = 100 \text{ N/mm}^2$) [see Eqs. (8.9)-(8.22)].

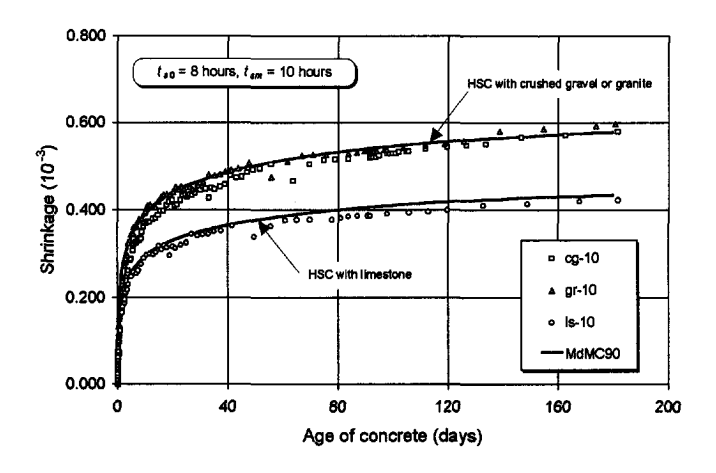


Fig. 8.6 Comparison of the shrinkage of HSC with different aggregates exposed to drying at an age of 8 hours with predictions of MdMC90 [by using Eqs. (8.9)-(8.22)] ($f_{cm} = 85 \text{ N/mm}^2$ for HSC with crushed gravel and granite, $f_{cm} = 72 \text{ N/mm}^2$ for HSC with limestone).

In Fig. 8.6 and Fig. 8.7 the shrinkage of HSC with three different aggregates exposed to a constant climate of 50% RH and 20 °C in temperature at an age of 8 hours ($t_{s0} = 8$ hours) and 14 hours ($t_{s0} = 14$ hours), respectively, which are also displayed in Fig. 7.5 and 7.6 in *Chapter* 7, are illustrated, together with predictions by using the modified shrinkage model [see .Eqs. (8.9)-(8.22)].

From the comparisons it is found that for HSC with crushed gravel or with granite, the shrinkage at early ages can be accurately simulated by MdMC90. The modified shrinkage model can also take the type of aggregate used into account. It is shown that for HSC with limestone exposed to drying at an age of 8 hours, the shrinkage is very well predicted by using MdMC90 (see Fig. 8.6). For HSC with limestone exposed to drying at an age of 14 hours, in spite of slight underestimation of the shrinkage at the early drying period, MdMC90 generally still predicts the shrinkage at the late drying period very well. (see Fig. 8.7).

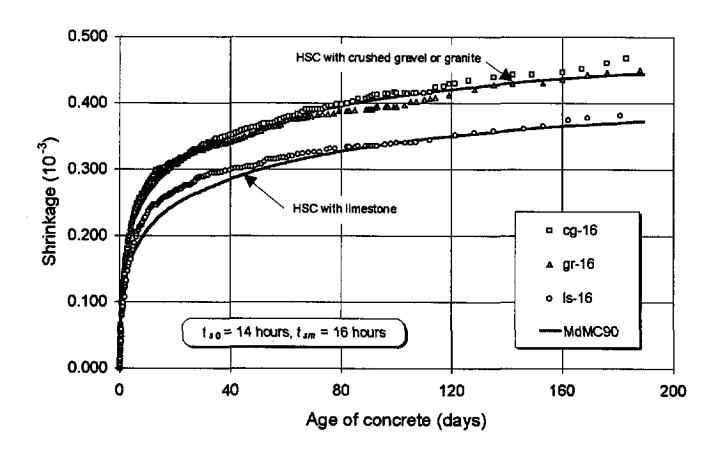


Fig. 8.7 Comparison of the shrinkage of HSC with different aggregates exposed to drying at an age of 14 hours with predictions of MdMC90 [by using Eqs. (8.9)-(8.22)] ($f_{cm} = 97 \text{ N/mm}^2$ for HSC with crushed gravel and granite, $f_{cm} = 90 \text{ N/mm}^2$ for HSC with limestone).

8.3.3 Load-related strain and total strain

8.3.3.1 Load-related strain and total strain under a constant sustained stress

The load-related strains of HSC with crushed gravel loaded at an age of 28 days at three different stress levels illustrated in Fig. 7.8 in *Chapter* 7 are compared with the calculating results by the using modified MC90 creep model in Fig. 8.8. From the

comparison it can be seen that the MdMC90 formulation very well simulates the creep behaviour of HSC loaded at an age of 28 days with a constant stress level $(0.15 f_{cm}, 0.35 f_{cm}$ and $0.5 f_{cm}$, respectively). The model also predicts the non-linear creep (at a stress level of $0.5 f_{cm}$) with good accuracy.

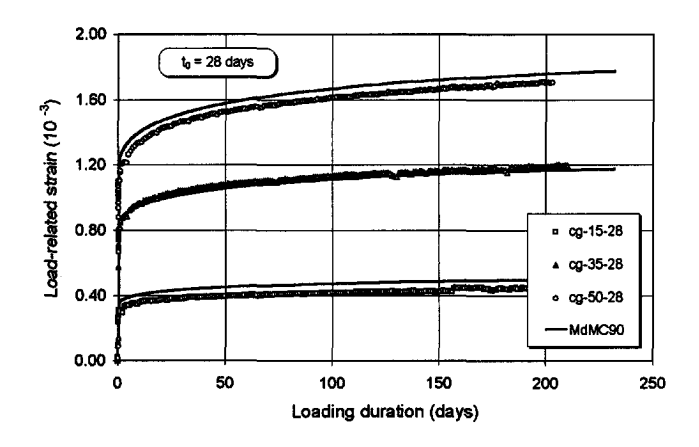


Fig. 8.8 Comparison of the load-related strains of HSC loaded at an age of 28 days at three different stress levels with predictions of MdMC90 ($f_{cm} = 100 \text{ N/mm}^2$).

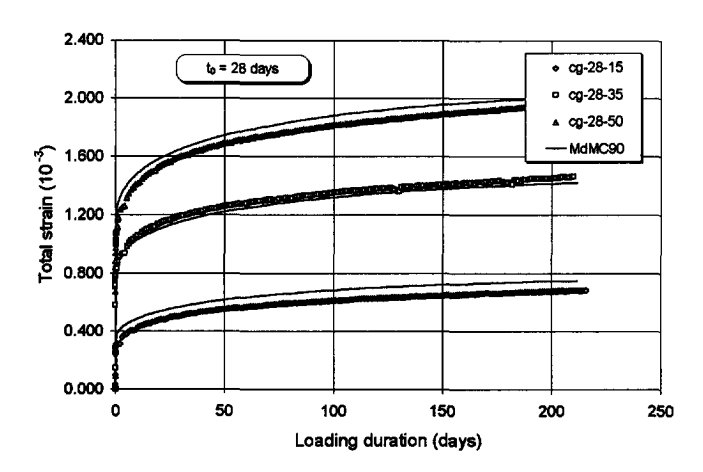


Fig. 8.9 Comparisons of the total measured strains of HSC with crushed gravel loaded at an age of 28 days with the predictions of MdMC90.

Similar facts are also demonstrated in Fig. 8.9, where the total measured strains (initial elastic strain + creep strain + shrinkage) of the same type of HSC loaded at an age of 28 days are compared with the predictions of MdMC90.

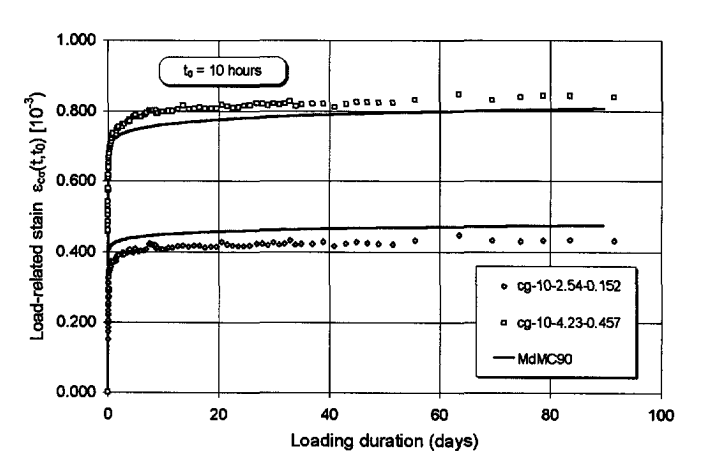


Fig. 8.10 Comparison of the load-related strains of HSC with crushed gravel loaded at an age of 10 hours at two different stress levels with predictions of MdMC90 [$f_{cm} = 90 \text{ N/mm}^2$, $f_{cp}(t_0) = 8.5 \text{ N/mm}^2$, cg-10-2.54-0.152 means HSC with crushed gravel loaded at an age of 10 hours, the initial stress is 2.54 N/mm² and the measured initial elastic strain is 0.152 × 10⁻³).

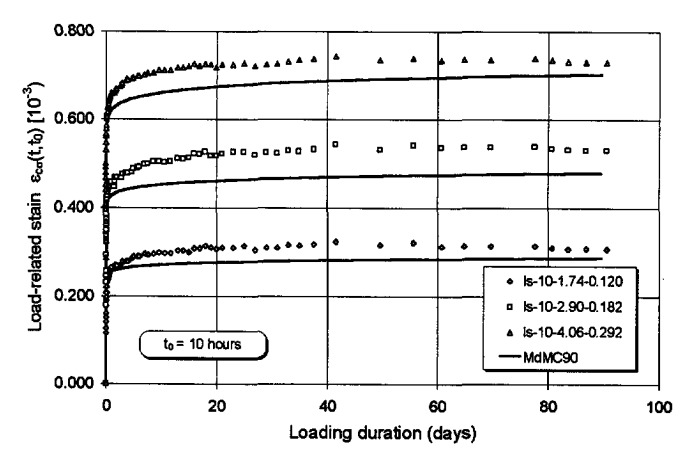


Fig. 8.11 Comparison of the load-related strains of HSC with limestone loaded at an age of 10 hours at three different stress levels with predictions of MdMC90 ($f_{cm} = 72 \text{ N/mm}^2$, $f_{cp}(t_0) = 5.8 \text{ N/mm}^2$, Is-10-1.74-0.120 means HSC with limestone loaded at an age of 10 hours, the initial stress is 1.74 N/mm² and the measured initial elastic strain is 0.120×10^{-3}).

In Fig. 8.10, 8.11, 8.12 and 8.13, the test results concerning the load-related strains of HSC with three different types of the aggregate loaded at early ages, which are already shown in Fig. 7.14, 7.15 and 7.16, are compared with predictions by using the MdMC90 formulation. In Fig. 8.10, the test data for HSC loaded at the highest stress level was eliminated due to load eccentricity occurring during the test.

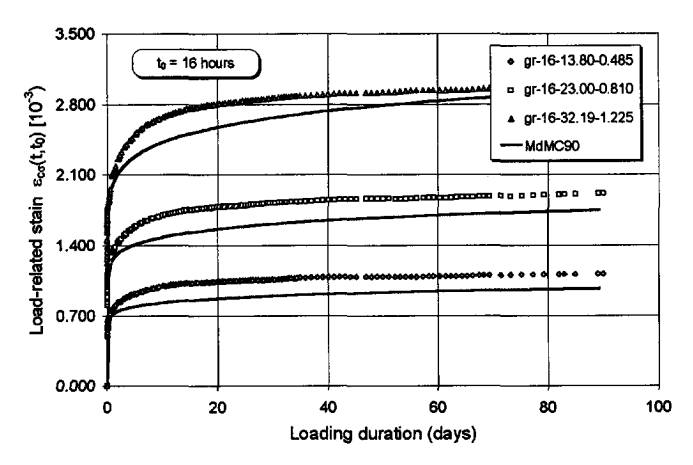


Fig. 8.12 Comparison of the load-related strains of HSC with granite loaded at an age of 16 hours at three different stress levels with predictions of MdMC90 ($f_{cm} = 97 \text{ N/mm}^2$, $f_{cp}(t_0) = 46.0 \text{ N/mm}^2$, gr-16-13.8-0.485 means HSC with granite loaded at an age of 16 hours, the initial stress is 13.8 N/mm² and the measured initial elastic strain is 0.485×10^{-3}).

For HSC with limestone, both linear creep and non-linear creep can be followed very well by MdMC90, whereas for HSC with crushed gravel and granite, the predicting accuracy is only slightly smaller.

The reason of the decreasing degree of accuracy for predicting the load-related strain of HSC with crushed gravel and granite is perhaps the lack of consideration of the influence of the type of aggregate on the development of strength and E-modulus in the modified MC90 model: at early ages, small differences in strength and E-modulus could result in the larger differences in the calculated load-related strain as well as the creep strain. For example, for HSC with granite loaded at an age of 10 hours, its strength at the time of loading is higher than that of HSC with crushed gravel. However, the 28-day's strength of HSC with granite is smaller than that of HSC with crushed gravel. This implies that the rate of the development of strength for HSC with granite is higher than that of HSC with crushed gravel. According to the experimental data, the absolute stress value for HSC with granite is higher than that for HSC with crushed gravel, but the load-related strains for both HSC are about same.

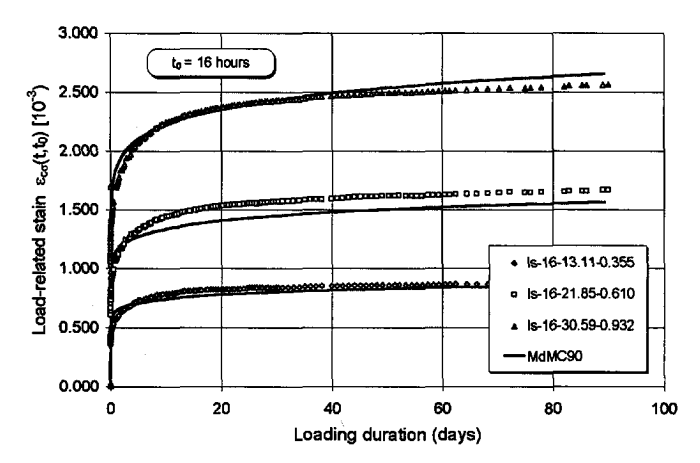


Fig. 8.13 Comparison of the load-related strains of HSC with limestone loaded at an age of 16 hours at three different stress levels with predictions of MdMC90 ($f_{cm} = 90 \text{ N/mm}^2$, $f_{cp}(t_0) = 43.7 \text{ N/mm}^2$, 1s-16-13.1-0.355 means HSC with limestone loaded at an age of 16 hours, the initial stress is 13.1 N/mm² and the measured initial elastic strain is 0.355×10^{-3}).

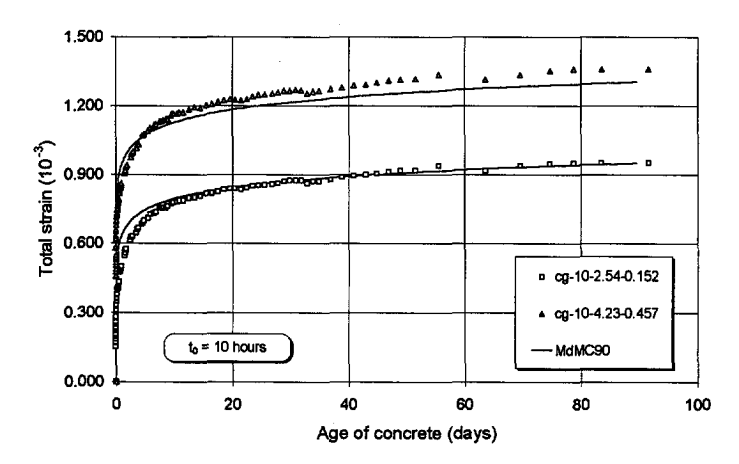


Fig. 8.14 Comparisons of the total measured strains of HSC with crushed gravel exposed to drying at an age of 8 hours and loaded at an age of 10 hours at two different stress levels with the predictions of MdMC90 (the test data for HSC loaded at the highest stress level was eliminated due to load eccentricity occurring during the test).

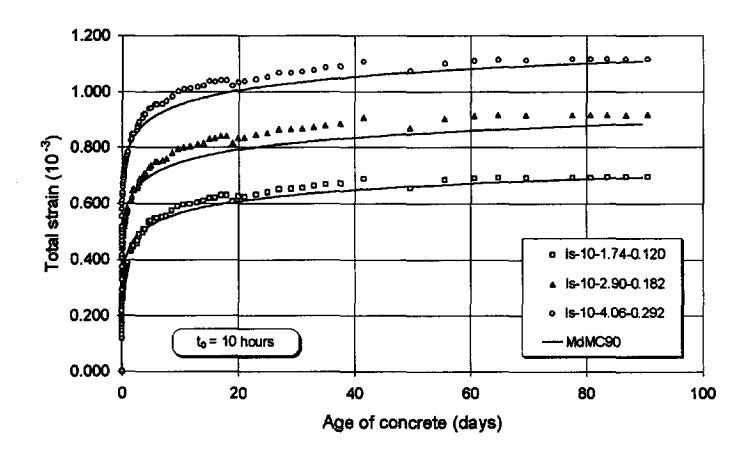


Fig. 8.15 Comparisons of the total measured strains of HSC with limestone exposed to drying at an age of 8 hours and loaded at an age of 10 hours at three different stress levels with the predictions of MdMC90.

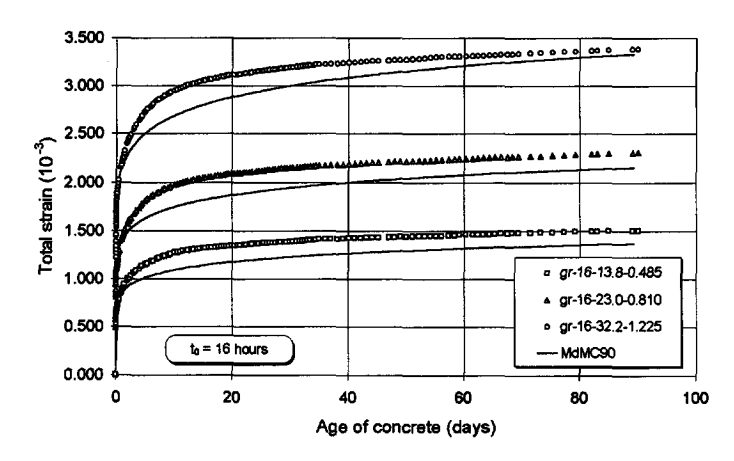


Fig. 8.16 Comparisons of the total measured strains of HSC with granite exposed to drying at an age of 14 hours and loaded at an age of 16 hours at three different stress levels with the predictions of MdMC90.

In combining the shrinkage strain and the load-related strain predicted by the modified shrinkage and creep model, the total strains are compared with the total measured strains from the experiments for HSC with three different types of aggregates exposed to drying at an age of 8 hours and 14 hours, loaded at an age of 10 hours and 16 hours, respectively, in Fig. 8.14, 8.15, 8.16 and 8.17. From the results of the evaluation, it can be concluded that the modified MC90 shrinkage and creep model can be used to predict the shrinkage and

creep of HSC exposed to drying or loaded under a constant stress level (up to about 70% of the strength at the time of loading) at early ages as well as normal ages.

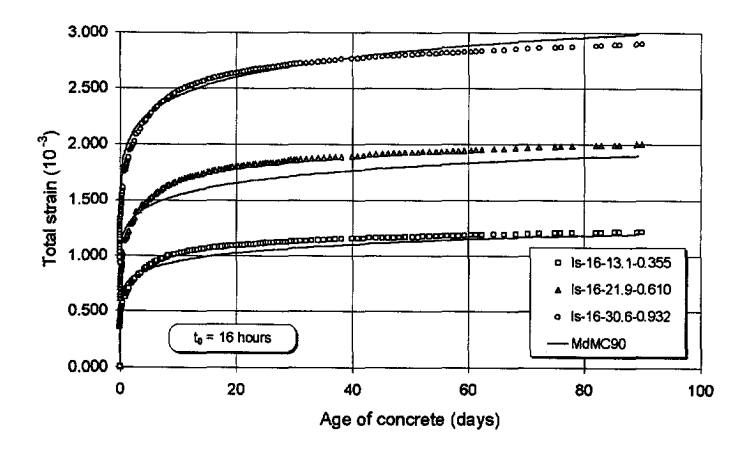


Fig. 8.17 Comparisons of the total measured strains of HSC with limestone exposed to drying at an age of 14 hours and loaded at an age of 16 hours at three different stress levels with the predictions of MdMC90.

8.3.3.2 Load-related strain under variable stresses

On the basis of the principle of superposition, MdMC90 is used to predict creep deformation under variable stresses. In Fig. 8.18 and Fig. 8.19, the load-related strains of HSC are simulated by using MdMC90, and the calculating results are compared with the load-related strain obtained from tests (see Fig. 7.11 in *Chapter 7*). The concrete is loaded from an age of 28 days under four-step stressing with an increment of 9.5 N/mm² (Fig. 8.18) and under two-step stressing with an increment of 19 N/mm² (Fig. 8.19), respectively. From the comparison, it can be seen that MdMC90 is capable to simulate the creep behaviour of HSC under the assumption of linearity.

It has to be noted, however, that non-linear creep does show, to some extent, significance. As shown in Fig. 8.18, the prediction of MdMC90 slightly diverges from the test results in the last two steps of stress increment. At the maximum load reached after four steps, the relative loading level is $\sigma/f_{cm} = 0.5$, so higher than the assumed limit for linearity 0.4.

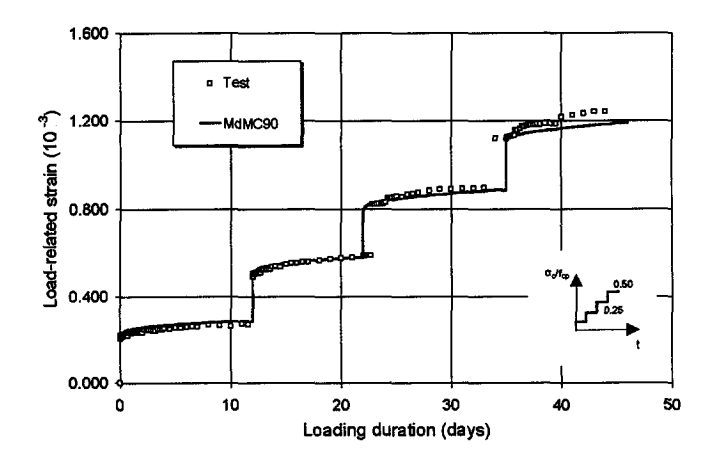


Fig. 8.18 Comparisons of load-related strains of HSC with crushed gravel ($f_{cm} = 85 \text{ N/mm}^2$) with the predictions of MdMC90 (the concrete is loaded at an age of 28 days under four-step stressing with a stress increment of 9.5 N/mm²).

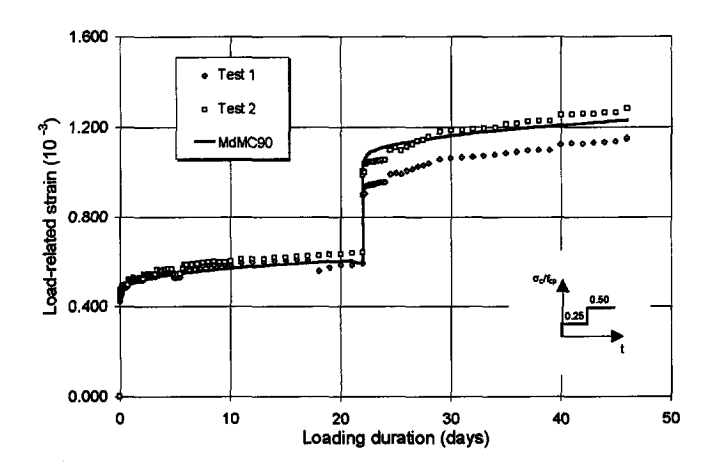


Fig. 8.19 Comparisons of load-related strains of HSC with crushed gravel ($f_{cm} = 85 \text{ N/mm}^2$) with the predictions of MdMC90 (the concrete is loaded at an age of 28 days under two-step stressing with a stress increment of 19 N/mm²).

8.3.4 Creep recovery

8.3.4.1 Creep recovery of HSC totally unloaded in one step

Fig. 8.20, Fig. 8.21, and Fig. 8.22 show the calculated results of the initial elastic recovery strain plus the creep recovery according to MdMC90. The predictions are also compared with the test results subtracted from Fig. 7.26, 7.27 and 7.28 in *Chapter* 7 on the basis of the assumption that the initial load-related strain is the same. It is clearly demonstrated that MdMC90 can simulate the creep recovery very accurately, although for HSC with crushed gravel and granite a slight overestimation is found at a relatively high stress level.

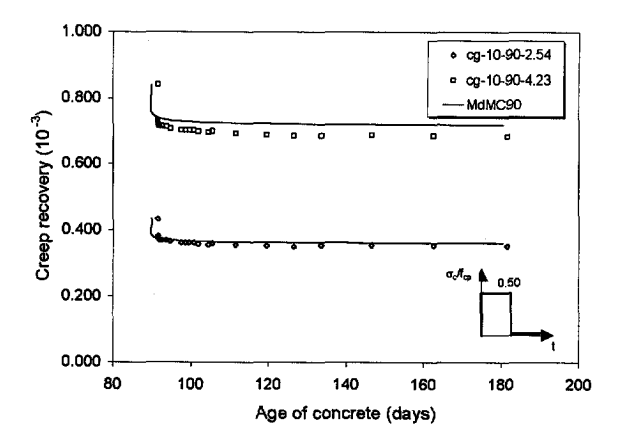


Fig. 8.20 Comparisons of the initial elastic recovery plus creep recovery of HSC with crushed gravel ($f_{cm} = 90 \text{ N/mm}^2$) with the predictions of MdMC90 (loaded at an age of 10 hours with stresses of 2.54 N/mm² and 4.23 N/mm², respectively, after a loading duration of about 90 days, totally unloaded).

The simulation of the total load-related strain at unloading by using MdMC90 may be less accurate than at loading. The reason for this is that the accumulation of predicting errors in the loading period has a strong influence on the accuracy of prediction of the total strain in the period of unloading. This is shown in Fig. 8.23 and 8.24.

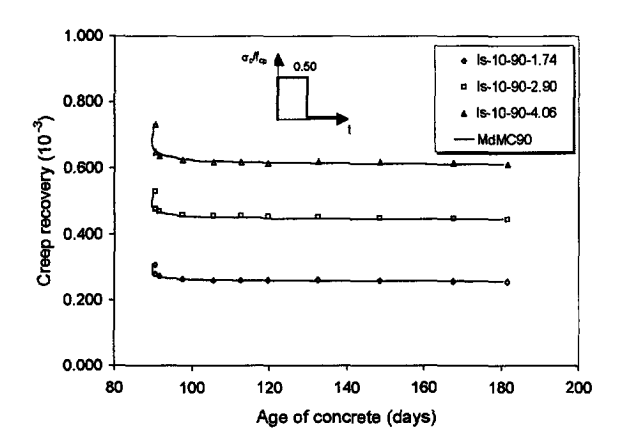


Fig. 8.21 Comparisons of the initial elastic recovery plus creep recovery of HSC with limestone ($f_{cm} = 72 \text{ N/mm}^2$) with the predictions of MdMC90 (loaded at an age of 10 hours with initial stresses of 1.74 N/mm², 2.90 N/mm² and 4.06 N/mm², respectively, after a loading duration of about 90 days, totally unloaded).

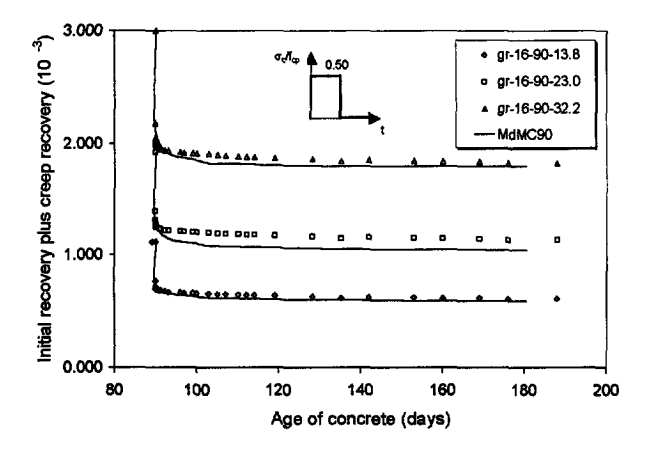


Fig. 8.22 Comparisons of the initial elastic recovery plus creep recovery of HSC with granite ($f_{cm} = 97 \text{ N/mm}^2$) with the predictions of MdMC90 (loaded at an age of 16 hours with initial stresses of 13.8 N/mm², 23.0 N/mm² and 32.2 N/mm², after a loading duration of about 90 days, totally unloaded).

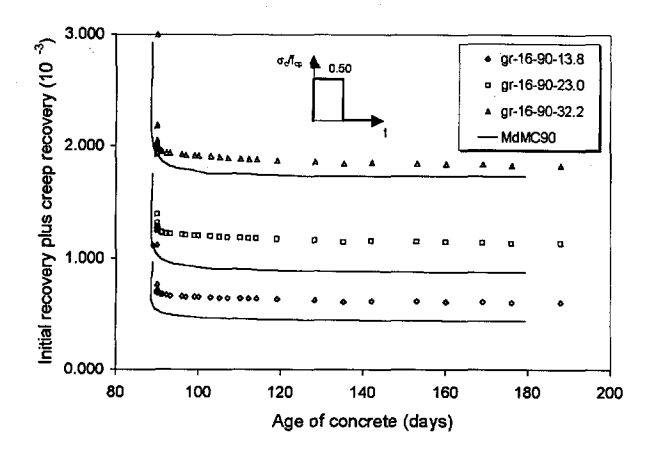


Fig. 8.23 Comparisons of the initial elastic recovery plus creep recovery of HSC with granite ($f_{cm} = 97 \text{ N/mm}^2$) with the predictions of MdMC90 based on the previous predictions (loaded at an age of 16 hours with initial stresses of 13.8 N/mm², 23.0 N/mm² and 32.2 N/mm², after a loading duration of about 90 days, totally unloaded).

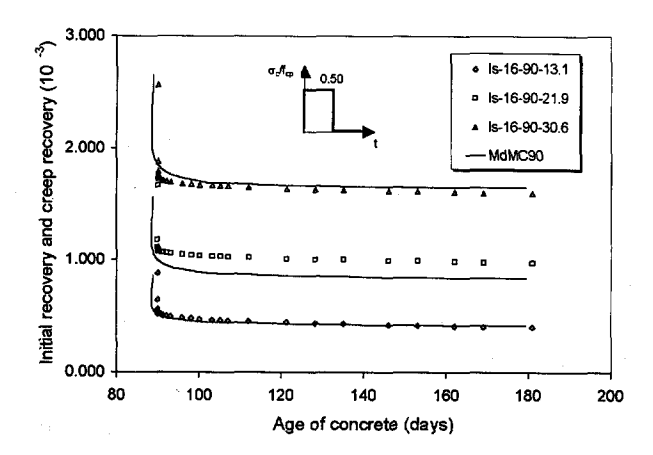


Fig. 8.24 Comparisons of the initial elastic recovery plus creep recovery of HSC with limestone ($f_{cm} = 90 \text{ N/mm}^2$) with the predictions of MdMC90 based on the previous predictions (loaded at an age of 16 hours with initial stresses of 13.1 N/mm², 21.9 N/mm² and 30.6 N/mm², after a loading duration of about 90 days, totally unloaded).

8.3.4.2 Creep recovery of HSC unloaded in a step-wise method

The calculated results of the load-related strain of HSC loaded and unloaded in a stepwise method after MdMC90 are shown in Fig. 8.25 and 8.26.. The test data already shown in Fig. 7.36 in *Chapter 7* are again displayed for the comparison. From the comparison it can be seen that MdMC90 can not follow the recovery process very well. It generally overestimate the totally recovered load-related strain.

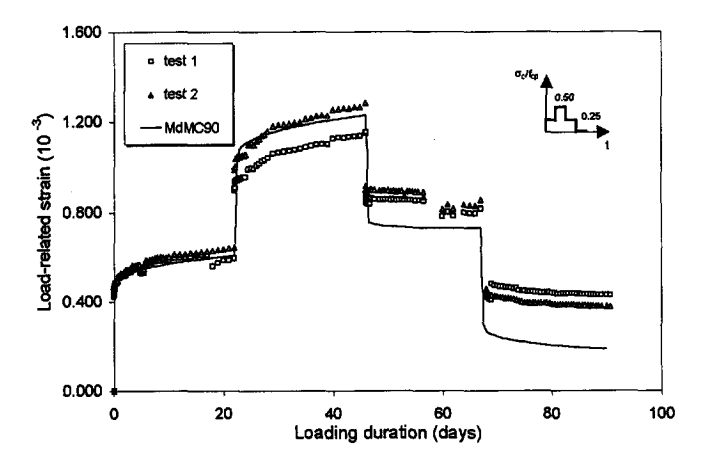


Fig. 8.25 Comparisons of the load-related strain of HSC with crushed gravel ($f_{cm} = 85 \text{ N/mm}^2$) with predictions of MdMC90 (the concrete is loaded at an age of 28 days under two-step loading with a stepwise stress increment of 19.0 N/mm², and unloaded an age of 73 days under two-step unloading with a step-wise decreasing stress of 19.0 N/mm²).

However, if the value of initial elastic strain obtained from tests are taken into the calculation, MdMC90 can simulate the creep recovery very accurately (see Fig. 8.27 and 8.28). Thus, it can be concluded that MdMC90 is able to accurately predict the creep recovery. MdMC90 generally overestimates the initial elastic recovery, i.e. perhaps it underestimates the E-modulus at the time of unloading. It might be very interesting to further investigate the development of E-modulus under compression.

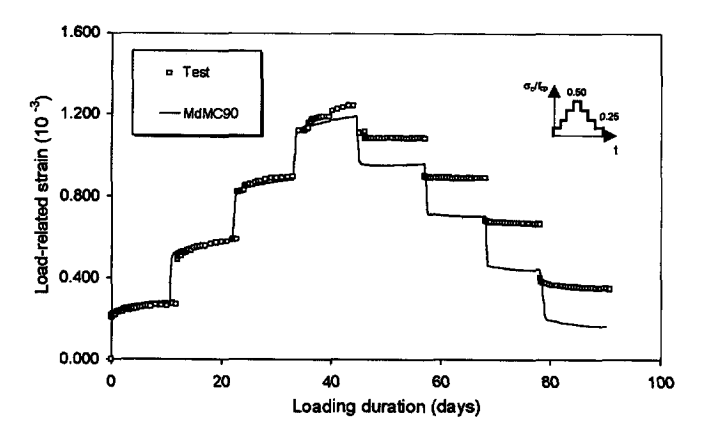


Fig. 8.26 Comparisons of the load-related strain of HSC with crushed gravel ($f_{cm} = 85 \text{ N/mm}^2$) with predictions of MdMC90 (the concrete is loaded at an age of 28 days under four-step loading with a stepwise stress increment of 9.5 N/mm², and unloaded an age of 73 days under two-step unloading with a stepwise decreasing stress of 9.5 N/mm²).

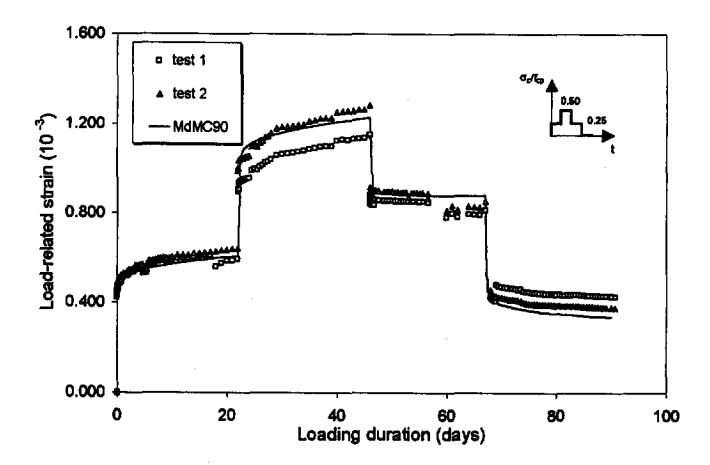


Fig.~8.27 With adjustment of the initial elastic recovery, the load-related strain in Fig. 8.25 is recalculated and compared with those obtained from tests.

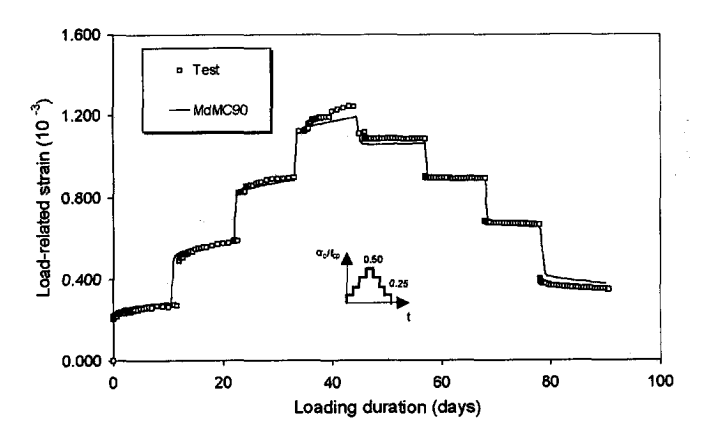


Fig. 8.28 With adjustment of the initial elastic recovery, the load-related strain in Fig. 8.26 is recalculated and compared with those obtained from tests.

8.4 Concluding remarks

On the basis of the comprehensive verifications of the proposed modified MC90 formulations (MdMC90), some important concluding remarks are summarized as follows:

- With an extension of the original formulation of CEB-FIP Model Code 1990, taking into account expressions for creep after Müller and Küttner (1996), one uniform formulation for predicting the time-dependent behaviour of HSC is obtained. All characteristics of the original model remain, i.e. the modified MC90 model can still be used to predict the time-dependent deformation for NSC with the same accuracy. Additionally, it can be used to predict shrinkage and creep of NSC and HSC at either early ages or normal ages.
- It is the development of strength and E-modulus which governs the predictions of the time-dependent behaviour, in particular, at early ages. An improved formulation has been added to MC90 in order to simulate the development of strength and E-modulus more accurately, especially at early ages. The most significant improvement is that the formulation includes the behaviour in the earliest stage. Furthermore it takes the influence of the type of aggregate into account.
- In spite of the insignificance for NSC, autogeneous shrinkage gives an important contribution to the total shrinkage of HSC. Therefore, this component is considered in

the modified MC90 model on the basis of the AFREM formulation. Moreover, the original MC90 model for shrinkage does not consider the influence of ageing on the shrinkage, i.e. at what age concrete is exposed to drying. This factor is added in the modified MC90 model.

- The basic time-shape function for both shrinkage and creep are adjusted according to
 the age at which the concrete is exposed to drying or loaded. More specifically, the
 development of strength and E-modulus are directly used to consider the influence of
 the age.
- Non-linear creep can be considered by simply using a factor which depends on the stress-strength ratio at the time of loading. For a constant sustained load, non-linear creep can be reasonably well predicted by using MdMC90.
- On the basis of the principle of superposition, the modified MC90 model can be used to simulate the creep of concrete under a variable stress. However, as the stress increases to a higher level (about more than 50% of the strength at the time of loading), the linear creep model loses its accuracy. This has to be considered when a more accurate prediction is required.
- The linear creep model can also be used to simulate the creep recovery of HSC. A very
 good agreement has been reached between the predictions and the test results. The
 further investigation is needed to model the development of E-modulus under
 compression.
- An important point of this verification of MdMC90 is that the newly proposed extension of MC90 by Müller and Küttner (1996) is about the same as MdMC90 as far as the creep of HSC loaded at an age of 28 days is concerned. From this point of view, the verification of MdMC90 for the creep of HSC under various loading histories is also valid for the newly proposed extension of MC90. However, the most important aspects of MdMC90 concern on its ability to predict the shrinkage and the creep of HSC at early ages. This also means that MdMC90, as developed here, may be regarded as a further extension of the modified MC90 formulation proposed by Müller and Küttner (1996).

Chapter 9 Summary

The last chapter of this thesis gives a summary concerning the significance of this research project to the engineering practice, the aim and the scope of the research and the main conclusions.

Time-dependent behaviour of concrete is influenced both by internal and external forces. Concrete is a kind of ageing material, i.e. its properties develop with time due to the continuous chemical reaction of cement and water (hydration), which is influenced by temperature and relative humidity. In comparison with other important structural materials, such as steel, and plastics, concrete shows a strong ageing effect.

The time-dependent properties of concrete can significantly affect the structural behaviour. In some respects, these effects are unfavourable, whereas in others, they are beneficial. On the one hand, time-dependent deformation causes losses of prestress and increase of deformations and deflections which may impair the serviceability of a structure. The reduction of strength may further decrease the load-bearing capacity of a structure. On the other hand, time dependent deformations can generate a favourable initial stress distribution which may be introduced intentionally by an imposed deformation (for example preflexed girders). Time-dependent deformation can also reduce undesirable stresses in the concrete caused by unintentionally imposed deformations such as support settlements, shrinkage and thermal gradients.

Not only the development and application of high strength concrete (HSC) has significantly increased during the last years, also in research, more and more attention is paid toward differences in fundamental properties between HSC and normal strength concrete (NSC). HSC is characterized by superior properties such as a high compressive strength, an increased modulus of elasticity, and a high density (improved durability).

The material structure of HSC remarkably differs from that of NSC. HSC has a more discontinuous and closed pore structure, smaller pore sizes, and a more uniform pore distribution. This is, among others, a result of the addition of silica fume. The pozzolanic reaction of this material leads to a better bond between aggregate and cement matrix, whereas the microparticles have a filler function as well. The interface area between the matrix and the aggregate, which usually contains larger pores and more microcracks, becomes very compact by virtue of silica fume. Less flaws and pre-loading microcracks are found in HSC, possibly due to the difficulty of moisture exchange between the inside and the outside of the concrete, resulting in a smaller drying shrinkage. Furthermore, the stronger bond within the interface area also contributes to the reduction of number and size of microcracks.

The main aim of this research program was to generally improve the knowledge of the time-dependent behaviour of HSC. On the basis of an experimental analysis, more information about several aspects of time-dependent properties of HSC was gained. The results was used to develop improved formulations for the time-dependent behaviour of HSC.

Following the introductory chapter in this thesis, the general classification of the time-dependent behaviour of concrete is given in *Chapter* 2. Three important aspects concerning the time-dependent behaviour of concrete are classified in this chapter: the external actions, the deformations of concrete and the ageing effects. With respect to the external actions, static and creep loads are considered. The total deformations under the external actions are divided into time-independent (elastic) strain, creep and load-independent strain (shrinkage). Since concrete is an ageing material, the contributions of the ageing effect to the development of the properties of concrete, in particular to strength and E-modulus, have to be taken into consideration as the time-dependent behaviour of concrete is treated.

The study of the time-dependent behaviour of HSC presented in this thesis comprises four inter-related phases:

- Literature survey
- Experimental research program
- Theoretical modelling
- Evaluation

A literature survey of the behaviour of concrete subjected to various strain rates and strain gradients in both compression and tension is presented in *Chapter 3*. The strain rate

range is mostly limited to the region between the so called static and creep loading. Various mechanical properties (such as strength, deformation, E-modulus, Poisson ratio, critical stress, long-term strength) under the influence of strain rate are discussed in detail. Additionally, the influence of the strain gradient on the behaviour of concrete is also reviewed, where the key points are the stress distribution, the peak stress and the ultimate strain of the extreme fibre. The basic mechanism which causes the rate sensitivity is explored. Several mathematical models are presented, which have been developed to evaluate the stress-strain relationship in flexure. However, most of the papers reviewed here concern normal strength concrete, while those about high strength concrete rarely appear on the list of literature. Since the material structure of high strength concrete is different from that of normal strength concrete, some remarks are also made as far as the strain rate sensitivity of high strength concrete is concerned.

On the basis of the literature survey in Chapter 3 it can be concluded that the material structure of concrete plays a dominant role as far as the rate sensitivity is concerned. The numbers and sizes of pores, flaws(voids) and microcracks inside the concrete decide upon the extent to which the loading rate or the strain rate could influence the mechanical behaviour. Clearly, all factors which have effects on the material structure of the concrete (such as the age of the concrete at testing, the curing condition, etc.) may also affect the rate sensitivity of the concrete. Up to now, one generally accepted point is that the timedependent behaviour of concrete can be related to the presence of free water in the concrete. In practice, it is found that most concrete structures remain saturated at depth during their service life. From the literature study, it becomes evident that a good understanding of the phenomenon of rate sensitivity of concrete is of significance to structural engineers. In comparison with normal strength concrete, high strength concrete has its typical features as far as its material structure is concerned. High strength concrete has a much more dense internal structure, smaller pore sizes, a more uniform pore distribution and less microcracking before and during loading. Therefore, it is indispensable to understand the mechanical properties and the structural behaviour of high strength concrete related to the problem of rate sensitivity before this material can be safely used in practice.

Creep is one of the most important aspect as far as the time-dependent behaviour of concrete is concerned. Creep of concrete is a complex phenomenon which is not yet completely understood. Creep has a considerable impact on the performance of concrete structures, causing deflection increases as well as affecting stress distribution and prestress losses. In *Chapter 4*, a literature survey about creep behaviour of concrete in compression is presented. The factors which have an influence on creep are briefly discussed. The up-to-date's knowledge on the creep mechanism and several viable predicting models are also surveyed. At a later stage of this literature study, attention is given as well to creep of

young concrete. The survey is carried out for both normal and high strength concrete, whereas emphasis is placed on high strength concrete.

The experimental program is subdivided into four series. Any of these four series involves several parameters, which are relevant to the time-dependent behaviour of high strength concrete. In *Chapter* 5, the extent of this experimental research program, as well as the materials, test set-up, measurements and test procedure are described in detail. The experimental results are generalized and arranged for further analysis.

The time-dependent behaviour of both HSC and NSC are firstly studied by loading concrete with various strain rates and strain gradients. The strain rates adopted in these experiments range from loading to failure in a few minutes to loading to failure in a number of days. Both compression and tension tests are carried out. Not only centric loading, but also eccentric loading is carried out in combination with various strain rates.

The time-dependent behaviour of HSC was furthermore investigated by subjecting concrete to a constant sustained stress. In these tests, the main parameters were the stress level and the age at application of the load; the load was applied at an age of 28 days, as well as at earlier ages. Additionally, various types of aggregate were used in the mixtures to study their influence on the time-dependent behaviour. Shrinkage and creep recovery were also included.

On the basis of the test data, a comprehensive experimental analysis concerning the strain rate sensitivity of HSC is carried out in *Chapter* 6. The analysis focuses on the influence of the strain rate and the strain gradient on the fundamental mechanical properties of high strength concrete and normal strength concrete (for comparison) in compression as well as in tension. From the experimental analysis it is concluded that HSC shows a higher rate sensitivity than NSC. Under compressive loading at various strain rates, high strength concrete suffers a more severe reduction of the peak stress than normal strength concrete does, as the strain rate decreases. Other mechanical properties of HSC also show, to various extents, rate sensitivity. It is also found that the existence of a strain gradient could moderate the rate sensitivity of concrete, both in compression and in tension. The experimental analysis indicates that the rate sensitivity of HSC in tension is less obvious than in compression.

In Chapter 7 a comprehensive experimental analysis was further conducted on shrinkage and creep of concrete loaded at normal and early ages. With regard to the various parameters, the experimental analysis is subdivided into four parts. In the first part, the development of strength and E-modulus which are important for the time-dependent behaviour of concrete loaded at early ages is discussed. Because of the close relation

between creep and shrinkage, the shrinkage observed in the experiments is presented in the second part. The influence of the type of aggregate and the age at which the concrete is exposed to drying on shrinkage is investigated. In the third part, creep of the concrete loaded both at early ages and at a normal age is analyzed. The influences of the stress level and the type of aggregate on creep are discussed. In the last part, creep recovery is considered. In all four parts, the test data are compared with the predictions calculated by using several existing formulations. The comparisons form a basis for the further development of appropriate predicting formulations for shrinkage and creep of high strength concrete loaded at normal and early ages.

In the modelling phase, one qualitative model and two mathematical models are proposed. In *Chapter* 6, the mechanism of the rate sensitivity of concrete is modelled based on the Stefan Effect (well-known in physics). The phenomena observed in the experiments are qualitatively interpreted by means of this proposed model.

In order to be able to simulate the time-dependent behaviour of high strength concrete under an eccentric loading, a mathematical model based on the idea of the compressive damage zone (CDZ) from Markeset (1993) is developed in *Chapter* 6. On the basis of the knowledge of the time-dependent behaviour of HSC in centric tests, several parameters have been used in this model to simulate the influences of strain rates and strain gradients on the stress distributions in the compression zone.

A modified shrinkage and creep model on the basis of the well-known MC90 model is derived in *Chapter* 8. Formulations have been derived in order to predict the development of strength and E-modulus of high strength concrete with time. Expressions are given to calculate shrinkage and creep, either at early ages or at normal ages. Under the assumption of creep linearity, the principle of superposition can be applied in order to calculate the creep deformation under variable stresses, as well as the creep recovery. Non-linearity of creep is explicitly taken into account.

Finally, evaluations of all three proposed models were carried out. In *Chapter* 6, the experimental observations are explained on the basis of the qualitative model concerning the mechanism of the strain rate sensitivity of concrete: for HSC in compression, at a higher strain rate, higher pore-water pressure is built up due to the smaller pore size, which mainly contributes to the restraint of the longitudinal deformation, while the Stefan Effect explains the delayed development of the transverse deformation; moreover, because of the difficulty of the movement of free water through the concrete, less free water could evaporate during the periods of curing, thus, more free water is available in creating pore-water pressure, and the Stefan Effect is enhanced at loading; at a lower strain rate, the stressed water in the pores will get enough time to flow through the channels (microcracks and flaws) to the

unstressed regions, causing a relaxation of the pore-water pressure; additionally, the opposite force produced by the Stefan effect also decreases due to a lower strain rate; hence, the concrete tends to show the strength values of the solid phase. It is also noted that the function of the Stefan Effect in compression differs from that in tension. In tension the effect of moisture stress is smaller than in compression.

With respect to the verification of the modified CDZ model, after evaluations, it is concluded that, by introducing an extension in order to regard the strain rate sensitivity, the CDZ model can be used to simulate load-strain relationships for eccentrically loaded prisms when various strain rates and strain gradients apply. The comparison between results of the numerical calculation and the experimental results show, that for a good prediction of the ultimate load a strain rate and e/d dependent stress-strain relation is necessary. If a single stress-strain relation, based on centric loading tests, independent from the strain rate, is used - like in many codes - the results will never be very accurate.

The evaluations of MdMC90 carried out in *Chapter* 8 show that, with an extension of the original formulation of CEB-FIP Model Code 1990, taking into account expressions for creep after Müller and Küttner (1996), one uniform formulation for predicting the time-dependent behaviour of HSC is obtained. All characteristics of the original model remain, i.e. the modified MC90 model can still be used to predict the time-dependent deformation for NSC with the same accuracy. Additionally, it can be used to predict shrinkage and creep of NSC and HSC at either early ages or normal ages.

An important point of this verification of MdMC90 is that the newly proposed extension of MC90 by Müller and Küttner (1996) is about the same as MdMC90 as far as the creep of HSC loaded at an age of 28 days is concerned. From this point of view, the verification of MdMC90 for the creep of HSC under various loading histories is also valid for the newly proposed extension of MC90. However, the most important aspects of MdMC90 concern its ability to predict the shrinkage and the creep of HSC at early ages. This also means that MdMC90, as developed here, may be regarded as a further extension of the modified MC90 formulation proposed by Müller and Küttner (1996).

References

ABRAMS, D. A. (1917), Effect of rate of application of load on the compressive strength of concrete, *Proceedings of the American Society for Testing Materials*, Vol. 17, Part II, pp. 364-365.

ACI and CCA (1963), Recommendations for an international code of practice, *American Concrete Institute and Cement Concrete Association*, CR 1-221, 36 pp.

ACI COMMITTEE 209 (1992), Prediction of creep, shrinkage and temperature effects in concrete structures, *Report No. ACI 209R-92*.

AL-KUBAISY, M. A. and YOUNG, A. G. (1975), Failure of concrete under sustained tension, *Magazine of Concrete Research*, Vol. 27, No. 92, September, pp. 171-178.

BARNARD, P. R. (1964), Discussion of the paper of STURMAN, SHAH and WINTER, Microcracking and inelastic behaviour of concrete, <u>Flexural Mechanics of Reinforced Concrete</u>, <u>Proceedings of the International Symposium</u>, Miami, Florida, November 10-12, ASCE-1965-50, ACI SP-12, pp. 493-494.

BAZANT, Z. P. and Panula, L. (1978a, b, c, 1979a, b), Practical prediction of time-dependent deformations of concrete, *Materials and Constructions*, Vol. 11, No. 65, 1978, pp. 301-316, pp. 317-328, Vol. 11, No. 66, 1978, pp. 415-424, Vol. 12, No. 69, 1979, pp. 169-174, pp. 175-183.

BAZANT, Z. P. (1982), Mathematical models for creep and shrinkage of concrete, <u>Creep and Shrinkage in Concrete Structures</u>, edited by BAZANT, Z. P. and WITTMANN, F. H., *John Wiley & Sons Ltd.*, pp. 163-256.

BAZANT, Z. P. and PANULA, L. (1984), Practical prediction of creep and shrinkage of high strength concrete, *Materials and Structures*, Vol. 17, No. 101, pp. 375-378.

BENTUR, A., GOLDMAN, A. and COHEN, M. D. (1988), The contribution of the transition zone to the strength of high quality silica fume concretes, <u>Bonding in Cementitious Composites</u>, *Proceedings*, *Symposium of Materials Research Society*, edited by MINDESS, S. and SHAH, S. P., Vol. 114, pp. 97-104.

BERGSTRÖM, S. G. and BYFORS, J. (1980), Properties of concrete at early ages, *Materials and Structures*, Vol. 13, No. 75, pp. 265-274.

BJERKELI, L., TOMASZEWICZ, A. and JENSEN, J. J. (1990), Deformation properties and ductility of high strength concrete, <u>Utilization of High Strength Concrete</u>, <u>Proceedings of the Second International Conference</u>, California, USA.

BROOKS, J. J. and NEVILLE, A. M. (1977), A comparison of creep, elasticity and strength of concrete in tension and in compression, *Magazine of Concrete Research*, Vol. 29, No. 100, September, pp. 131-141.

BUIL, M. and ACKER, P. (1985), Creep of a silica fume concrete, Cement and Concrete Research, Vol. 15, pp. 463-466.

BYFORS, J. (1980), Plain concrete at early age, *Thesis*, Swedish Cement and Concrete Research Institute, 345 pp.

CARRASQUILLO, R. L., SLATE, F. O. and NILSON, A. H. (1981), Microcracking and behaviour of high strength concrete subject to short-term loading, *ACI Journal*, <u>Proceedings</u>, Vol. 78, No. 3, May-June, pp. 179-186.

CEB-FIP (1984), Structural effects of time-dependent behaviour of concrete, CEB Bulletin D'Information, No. 142.

CEB-FIP (1990), High Strength Concrete - State of the Art Report, CEB Bulletin D'Information, No. 197, 61 pp.

CEB-FIP (1991), CEB-FIP Model Code 1990, Final Draft, CEB Bulletin D'Information, No. 203.

CLARK, L. E., GERSTLE, K. H. and TULIN, L. G. (1967), Effect of strain gradient on the stress-strain curve of mortar and concrete, *ACI Journal*, <u>Proceedings</u>, Vol. 64, No. 9, September pp. 580-586.

COLLINS, M. T.(1989), Proportioning high strength concrete to control creep and shrinkage, *ACI Materials Journal*, Vol. 86, No. 6, November-December, pp. 576-580.

CONG, X. F., GONG, S. L., DARWIN, D. and McCABE, S. L. (1992), Role of silica fume in compressive strength of cement paste, mortar, and concrete, *ACI Materials Journal*, Vol. 89, No. 4, July-August, pp. 375-387.

COUTINHO, A. S. (1977), A contribution to the mechanism of concrete creep, *Materials and Constructions*, Vol. 10, No. 55, pp. 3-16.

DARWIN, D., SHEN, Z. and SHRADDHAKER, H. (1988), Silica fume, bond strength, and the compressive strength of mortar, <u>Bonding in Cementitious Composites</u>, *Proceedings*, *Symposium of Materials Research Society*, edited by MINDESS, S. and SHAH, S. P., Vol. 114, 1988, pp. 105-110.

DE LARRARD, F. (1990), Creep and shrinkage of high strength field concretes, <u>Utilization</u> of <u>High Strength Concrete</u>, <u>Proceedings of the Second International Conference</u>, California, USA.

DE LARRARD, F. and ACKER, P. (1992), Creep in high and very high performance concrete, <u>High Performance Concrete - from material to structure</u>, edited by MALIER, Y., *E&FN SPON*, pp. 115-126.

DE LARRARD, F, ACKER, P. and LE ROY, R. (1994), Shrinkage, creep and thermal properties, <u>High Performance Concretes and Applications</u>, edited by SHAH, S. P. and AHMAD, S. H., *Edward Arnold*, pp. 65-114.

DE LARRARD, F. and LE ROY, R. (1992), The influence of mix-proportion on the mechanical properties of silica-fume high-performance concrete, Fourth International ACI-CANMET Conference on Fly Ash, Silica Fume, Slag and Natural Pozzolans in Concrete, Istanbul.

DESAYI, P. (1968), A model to simulate the strength and deformation of concrete in compression, *Materials and Structures, Research and Testing* (Paris), Vol. 1, No. 1, January-February, pp. 49-56.

DHIR, R. K. and SANGHA, C. M. (1972), A study of the relationships between time, strength, deformation and fracture of plain concrete, *Magazine of Concrete Research*, Vol. 24, No. 81, December, pp. 197-207.

DILGER, W. H., KOCH, R. and KOWALCZYK, R. (1984), Ductility of plain and confined concrete under different strain rates, *ACI Journal*, <u>Proceedings</u>, Vol. 81, No. 1, January-February pp. 73-81.

DOMONE, P. L. (1974), Uniaxial tensile creep and failure of concrete, *Magazine of Concrete Research*, Vol. 26, No. 88, September, pp. 144-152.

FELDMAN, R. F. and SEREDA, P. J. (1968), A model for hydrated portland cement paste as deduced from sorption-length change and mechanical properties, *Materials and Constructions*, Vol. 1, pp. 509-520.

GHOSH, R. S. and TIMUSK, J. (1974), Effect of sustained loading at early ages on the modulus of elasticity of cement paste, *Materials and Structures*, Vol. 7, No. 41, pp. 335-340.

GJΦRV, O. E. (1992), High strength concrete, <u>Advances in Concrete Technology</u>, edited by MALHOTRA, V. M., *Energy, Mines and Resources*, Canada, pp. 21-78.

GLUCKLICH, J. (1962), Creep mechanism in cement mortar, *ACI Journal*, <u>Proceedings</u>, Vol. 59, No. 7, July, pp. 923-938.

GOLDMAN, A and BENTUR, A. (1989), Bond effects in high-strength silica-fume concretes, ACI Materials Journal, Vol. 86, No. 5, September-October, pp. 440-447.

HAN, N. (1992a), Time-dependent behaviour of high strength concrete - part I literature survey, *Stevin Laboratory Report*, No. 25.5-92-14, June, Delft University of Technology, 35 pp.

HAN, N. (1992b), Time-dependent behaviour of high strength concrete - part II experimental descriptions and results, *Stevin Laboratory Report*, No. 25.5-92-15, August, Delft University of Technology, 230 pp.

HAN, N. (1992c), Time-dependent behaviour of high strength concrete - part III experimental analysis, *Stevin Laboratory Report*, No. 25.5-92-16, August, Delft University of Technology, 76 pp.

HAN, N. (1993), High strength concrete - state of the art report, Stevin Laboratory Report, No. 25.5-93.3, January, Delft University of Technology, 82 pp.

HAN, N. (1994a), The behaviour of high-strength concrete under sustained and slow increasing load, 29. Forschungskolloquium von Deutscher Ausschuss für Stahlbeton, am 24. und 25 März an der Technischen Universität Delft, pp. 13-20 (in German).

HAN, N. (1994b), Creep of high strength concrete at early ages - state of the art report, *Stevin Laboratory Report*, Delft University of Technology, September, 56 pp.

HAN, N. (1995), Creep of high strength concrete loaded at early ages, , *Progress in Concrete Research*, Vol. 4, Delft University of Technology, pp. 107-119.

HAN, N. and WALRAVEN, J. C. (1991), The effect of strain rate on the compressive properties of high strength concrete, *Progress in Concrete Research*, Vol. 2, Delft University of Technology, pp. 31-43.

HAN, N. and WALRAVEN, J. C. (1993), Sustained loading effects in high strength concrete, <u>Utilization of High Strength Concrete</u>, <u>Proceedings of the Third International Conference</u>, Lillehammer, Norway, Vol. 2, pp. 1076-1083.

HAN, N. and WALRAVEN, J. C. (1994), Properties of high strength concrete subjected to uniaxial loading, *Proceedings of ACI International Conference on High Performance Concrete*, Singapore, <u>ACI Special Publication</u>, SP-149, pp. 269-288.

HAN, N. and WALRAVEN, J. C. (1995a), Strain rate sensitivities of strength and deformation of high-strength silica-fume concrete, *Proceedings of the Fifth CANMET/ACI International Conference on Fly Ash, Silica Fume, Slag and Natural Pozzolans in Concrete*, Milwaukee, Wisconsin, USA, <u>ACI Special Publication</u>, SP-153, pp. 687-702.

HAN, N. and WALRAVEN, J. C. (1995b), Creep and shrinkage of high-strength concrete at early and normal ages, *Proceedings of the Second CANMET/ACI International Symposium on Advances in Concrete Technology*, Las Vegas, Nevada, USA, <u>ACI Special Publication</u>, SP-154, pp. 73-94.

HAN, N. and WALRAVEN, J. C. (1996), Creep and shrinkage of young high-strength concrete, *Proceedings of the Fourth International Symposium on Utilization of High-Strength/High-Performance Concrete*, Paris, France, Vol. 2, pp. 339-348.

HANSEN, W. and YOUNG, J. F. (1991), Creep mechanism in concrete, <u>Materials Science of Concrete II</u>, edited by SKALNY, J. and MINDESS, S., *The American Ceramic Society, Inc.*, pp. 185-200.

HARSH, S., SHEN, Z. and DARWIN, D. (1990), Strain-rate sensitive behaviour of cement paste and mortar in compression, *ACI Materials Journal*, Vol. 87, No. 5, September-October, pp. 508-516.

HEILMANN, H. G. (1976), Zugspannung und Dehnung in unbewehrten Betonquerschnitten bei exzentrischer Belastung, *Deutscher Ausschuss für Stahlbeton*, Heft 269, Berlin.

HEILMANN, H. G., HILSDORF, H. and FINSTERWALDER, K. (1969), Festigkeit und Verformung von Beton unter Zugspannungen, *Deutscher Ausschuss für Stahlbeton*, Heft 203, Berlin.

HILLERBORG, A. (1991), Reliance upon concrete tensile strength, <u>Structural Concrete</u>, *Proceedings of IABSE Colloquium*, Stuttgart, Germany, pp. 589-604.

HJORTH, L. (1982), Microsilica in concrete, *Nordic Concrete Research*, Publication No. 1, pp. 1-18.

HOGNESTAD, E., HANSON, N. W. and NCHENRY, D. (1955), Concrete stress distribution in ultimate strength design, *ACI Journal*, *Proceedings*, Vol. 52, No. 4, December, pp. 455-479.

HOLAND, I. (1987), High strength concrete - a major research programme, <u>Utilization of High Strength Concrete</u>, *Proceedings of International Conference*, Stavanger, Norway, pp. 135-146.

HSU, T. C., SLATE, F. O., STURMAN, G. M. and WINTER, G. (1963), Microcracking of plain concrete and the shape of the stress-strain curve, *ACI Journal*, <u>Proceedings</u>, V. 60, No. 2, February, pp. 209-224.

HUGHES, B. P. and ASH, J. E. (1970), Some factors influencing the long term strength of concrete, *Materials and Constructions*, Vol 3, No. 14, pp. 81-84.

ILLSTON, J. M. (1965), The creep of concrete under uniaxial tension, *Magazine of Concrete Research*, Vol. 17, No. 51, June, pp. 77-84.

ILLSTON, J. M., DINWOODIE, J. M. and SMITH, A. A. (1979), Concrete, Timber and Metals, *Van Nostrand Rheinhold*, 239 pp.

JENSEN, H. E. (1992), Creep and Shrinkage of High-Strength Concrete - An analysis, *Thesis*, Denmark University of Technology, Series R, No. 294.

JONES, P. G. and RICHART, F. E. (1936), The effect of testing speed on strength and elastic properties of concrete, *Proceedings of the American Society for Testing Materials*, Vol. 36, Part II, pp. 380-391.

KAPLAN, S. A. (1980), Factors affecting the relationship between rate of loading and measured compressive strength of concrete, *Magazine of Concrete Research*, Vol. 32, No. 111, June, pp. 79-88.

KARSAN, I. D. and JIRSA, J. O. (1970), Behaviour of concrete under varying strain gradients, *Journal of the Structural Division*, ASCE, Vol. 96, No. ST8, August, pp. 1675-1696.

KOMLOS, K. (1969), Factors affecting the stress-strain relation of concrete in uniaxial tension, *ACI Journal*, <u>Proceedings</u>, Vol. 66, No. 2, February, pp. 111-114.

LE ROY, R., DE LARRARD, F. and PONS, G. The AFREM code type model for creep and shrinkage of high performance concrete, *Proceedings of the Fourth International Symposium*

on Utilization of High-Strength/High-Performance Concrete, Paris, France, Vol. 2, pp. 387-396.

MARZOUK, H. (1991), Creep of high-strength concrete and normal-strength concrete, *Magazine of Concrete Research*, Vol. 43, No. 155, June, pp. 121-126.

MEHTA, P. K. (1986), Condensed Silica Fume, <u>Cement Replacement Materials</u>, edited by SWAMY, R. N., *Surrey University Press*, pp. 134-170.

MEHTA, P. K. (1989), Pozzolanic and cementitious by-products in concrete, another look, Fly ash, Silica fume, Slag and other by-products in Concrete, edited by MALHOTRA, V. M., ACI SP 114, Vol. 1, pp. 1-44.

MEYERS, B. L. and SLATE, F. O. (1970), Creep and creep recovery of plain concrete as influenced by moisture conditions and associated variables, *Magazine of Concrete Research*, Vol. 22, No. 70, pp. 37-41.

MEYERS, B. L., SLATE, F. O. and WINTER, G. (1969), Relationship between time-dependent deformation and microcracking of plain concrete, *ACI Journal*, <u>Proceedings</u>, Vol. 66, No. 1, January, pp. 60-68.

MINDESS, S. (1984), Relationships between strength and microstructure for cement-based materials: an overview, <u>Very High Strength Cement-Based Materials</u>, edited by YOUNG, J. F., *Materials Research Society Symposia*, *Proceedings*, Vol. 42, pp. 53-68.

MINDESS, S. (1985), Relationships between strength and microstructure for cement-based materials: an overview, <u>Very High Strength Cement-Based Materials</u>. *Proceeding of Materials Research Society Symposium*, Vol. 42, edited by YOUNG, J. F., pp. 53-68.

MINDESS, S. (1994), Materials selection, proportioning and quality control, <u>High</u> <u>Performance Concretes and Applications</u>, edited by SHAH, S. P. and AHMAD, S. H., *Edward Arnold*, pp. 1-26.

MINDESS, S. and YOUNG, J. F. (1981), Concrete, Prentice-Hall, Inc., Englewood Cliffs, New Jersey 07632, 671 pp.

MORITA, S. and ADACHI, N. (1972), The stress-strain behaviour of concrete in the compression zone of flexural members, <u>Mechanical Behaviour of Materials</u>, <u>Proceedings of the International Conference on Mechanical Behaviour of Materials</u>, Vol. IV, The Society of Materials Science, Japan, pp. 162-171.

MÜLLER, H. S. and HILSDORF, H. K. (1990), Evaluation of the time dependent behaviour of concrete, *CEB Bulletin D'Information*, No. 199, 201 pp.

MÜLLER, H. S. and KÜTTNER, C. H. Creep of high performance concrete - Characteristics and code-type prediction model, *Proceedings of the Fourth International Symposium on Utilization of High-Strength/High-Performance Concrete*, Paris, France, Vol. 2, pp. 377-386.

NAGATAKI, S. and YONEKURA, A. (1982), Properties of drying shrinkage and creep of high strength concrete, *Transactions of the Japan Concrete Institute*, Vol. 4, pp. 223-235.

NEVILLE, A. M., DILGER, W. H. and BROOKS, J. J. (1983), Creep of plain & structural concrete, *Construction Press*, London and New York, 361 pp.

NEWMAN, K. (1968), Criteria for the Behaviour of Plain Concrete Under Complex States of Stress, <u>THE STRUCTURE OF CONCRETE</u> and its behaviour under load, *Proceedings of an International Conference*, London, September, editors: BROOKS, A. E. and NEWMAN, K., pp. 255-274.

NGAB, A. S., NILSON, A. H. and SLATE, F. O. (1981), Shrinkage and creep of high strength concrete, *ACI Journal*, *Proceedings*, Vol. 78, No. 4, July-August, pp. 255-259.

NGAB, A. S., SLATE, F. O. and NILSON, A. H. (1981a), Shrinkage and creep of high strength concrete, *ACI Journal*, <u>Proceedings</u>, Vol. 78, No. 4, July-August, pp. 255-261.

NGAB, A. S., SLATE, F. O. and NILSON, A. H. (1981b), Microcracking and time-dependent strains in high strength concrete, *ACI Journal*, <u>Proceedings</u>, Vol. 78, No. 4, July-August, pp. 262-268.

NIYOGI, A. K., HSU, P. and MEYERS, B. L. (1973), The influence of age at time of loading on basic and drying creep, *Cement and Concrete Research*, Vol. 3, pp. 633-644.

PARROT, L. J. (1969), The properties of high strength concrete, *Technical Report*, No. 42.417, Cement and Concrete Association, Wexham Springs, 12 pp.

PENTTALA, V. (1987), Mechanical properties of high strength concretes based on different binder combinations, <u>Utilization of High Strength Concrete</u>, *Proceedings of International Conference*, Stavanger, Norway, pp. 123-134.

PENTTALA, V. and RAUTANEN, T. (1990), Microporosity, creep, and shrinkage of high strength concretes, <u>Utilization of High Strength Concrete</u>, <u>Proceedings of the Second International Conference</u>, California, USA.

PERSSON, B. S. M. (1993), Basic creep of high-strength concrete at early ages, <u>Creep and Shrinkage of Concrete</u>, <u>Proceedings of the Fifth International RILEM Symposium</u>, Barcelona, pp. 523-528.

POPOVICS, S. (1970), A review of stress-strain relationships for concrete, *ACI Journal*, <u>Proceedings</u>, Vol. 67, No. 3, March, pp. 243-248.

POWERS, T. C. (1965), Mechanisms of shrinkage and reversible creep of hardened cement paste, <u>THE STRUCTURE OF CONCRETE</u> and its behaviour under load, *Proceedings of an International Conference*, London, September, editors: BROOKS, A. E. and NEWMAN, K., pp. 319-344.

POWERS, T. C. (1968), The thermodynamics of volume change and creep, *Materials and Constructions*, Vol. 1, pp. 487-507.

RASCH, C. (1962), Spannungs-Dehnungs-Linien des Betons und Spannungsverteilung in der Biegedruckzone bei Konstanter Dehngeschwindigkeit, *Deutscher Ausschuss für Stahlbeton*, Heft 154, Berlin.

REGOURD, M. M.- (1984), Microstructure of high strength cement paste systems, Very High Strength Cement-Based Materials, edited by YOUNG, J. F., Materials Research Society Symposia, Proceedings, Vol. 42, pp. 3-18.

REGOURD, M. M.- (1992), Microstructure of high performance concrete, <u>High</u> Performance Concrete - from material to structure, edited by MALIER, Y., *E&FN SPON*, pp. 3-13.

RICH, C. A. (1964), Discussion of the paper of STURMAN, SHAH and WINTER, Microcracking and inelastic behaviour of concrete, <u>Flexural Mechanics of Reinforced Concrete</u>, <u>Proceedings of the International Symposium</u>, Miami, Florida, November 10-12, ASCE-1965-50, ACI SP-12, pp. 496-498.

RILEM COMMISSION 42-CEA (1981), Properties of set concrete at early ages - state-of-the-art-report, *Materials and Structures*, Vol. 14, No. 84, pp. 399-450.

RUETZ, W. (1965), A hypothesis for the creep of hardened cement paste and the influence of simultaneous shrinkage, <u>THE STRUCTURE OF CONCRETE and its behaviour under load</u>, *Proceedings of an International Conference*, London, September, editors: BROOKS, A. E. and NEWMAN, K., pp. 365-387.

RÜSCH, H. (1960), Researches toward a general flexural theory for structural concrete, *ACI Journal*, <u>Proceedings</u>, Vol. 57, July, pp. 1-28.

RÜSCH, H. JUNGWIRTH, D. and HILSDORF, H. K. (1983), Creep and shrinkage - their effect on the behaviour of concrete structures, *Springer-Verlag*, 284 pp.

RÜSCH, H., SELL, R., RASCH, C., GRASSER, E., HUMMEL, A., WESCHE, K. and FLATTEN, H. (1968), Festigkeit und Verformung von unbewehrtem Beton unter konstanter Dauerlast, *Deutscher Ausschuss für Stahlbeton*, Heft 198, Berlin.

RUSSELL, H. G. and CORLEY, W. G. (1978), Time-dependent behaviour of columns in Water Tower Place, *Douglas McHenry International Symposium on Concrete and Concrete Structures*, ACI SP-55, pp. 347-373.

SARGIN, M. (1971), Stress-strain relationships for concrete and the analysis of structural concrete sections, *Study No. 4*, Solid Mechanics Division, University of Waterloo, Waterloo, Ontario, Canada.

SARGIN, M. and GHOSH, S. K. (1971), Effects of lateral reinforcement upon the strength and deformation properties of concrete, *Magazine of Concrete Research*, Vol. 23, No. 75-76, June-September, pp. 99-110.

- SARKAR, S. L. and AÏTCIN, P. C. (1987), Comparative study of the microstructures of normal and very high strength concrete, *Cement, Concrete and Aggregates*, CCAGDP, Vol. 9, No. 2, Winter, pp. 57-64.
- SARKER, S. L. (1992), High strength concrete and its microstructure, <u>Cement and Concrete Science & Technology</u>, <u>Progress in Cement and Concrete</u>, Vol. I, Part I, edited by GHOSH, S. N., *ABI Books Pvt. Ltd.*, pp. 381-415.
- SCHALLER, I., DE LARRARD, F., SUDRET, J. -P., ACKER, P. and LE ROY, R. (1992), Experimental monitoring of the Joigny bridge, <u>High Performance Concrete from material to structure</u>, edited by MALIER, Y., *E&FN SPON*, pp. 432-457.
- SELLEVOLD, E. J. (1987), The function of condensed silica fume in high strength concrete, <u>Utilization of High Strength Concrete</u>, <u>Proceedings of International Conference</u>, Stavanger, Norway, pp. 39-50.
- SELLEVOLD, E. J. and NILSEN, T. (1987), Condensed silica fume in concrete: a world review, <u>Supplementary Cementing Materials for Concrete</u>, edited by MALHOTRA, V. M., *CANMET/Canadian Government Publishing*, Chapter 3, pp. 167-243.
- SELLEVOLD, E. J. and RADJY, F. (1983), Condensed silica fume concrete: water demand and strength development, <u>Fly ash, Silica fume, Slag and other by-products in Concrete</u>, edited by MALHOTRA, V. M., *ACI SP 79*, pp. 677-694.
- SHAH, S. P. and CHANDRA, S. (1970), Fracture of concrete subjected to cyclic and sustained loading, *ACI Journal*, Proceedings, Vol. 67, No. 10, October, pp. 816-825.
- SHAH, S. P. and SLATE, F. O. (1965), Internal microcracking, mortar-aggregate bond and the stress-strain curve of concrete, <u>THE STRUCTURE OF CONCRETE</u> and its behaviour under <u>load</u>, *Proceedings of an International Conference*, London, September, editors: BROOKS, A. E. and NEWMAN, K., pp. 82-92.
- SHAH, S. P., GOKOZ, U. and ANSARI, F. (1981), An experimental technique for obtaining complete stress-strain curves for high strength concrete, *Cement, Concrete and Aggregates*, CCAGDP, Vol. 3, No. 1, Summer, pp. 21-27.

SHEN, J. H.(1992), Lineare und nichtlineare Theorie des Kriechens und der Relaxation von Beton unter Druckbeanspruchung, *Deutscher Ausschuss für Stahlbeton*, Heft 432, Berlin.

SHKOUKANI, H. and WALRAVEN, J. C. (1991), Sustained tensile strength of concrete, Structural Concrete, Proceedings of IABSE Colloquium, Stuttgart, Germany, pp. 725-729.

SICARD, V., FRANCOIS, R., RINGOT, E. and PONS, G. (1992), Influence of creep and shrinkage on cracking in high strength concrete, *Cement and Concrete Research*, Vol. 22, pp. 159-168.

SLATER, W. A. and LYSE, I. (1930), Compressive strength of concrete in flexure as determined from tests on reinforced beams, *ACI Journal*, <u>Proceedings</u>, Vol. 26, pp. 831-874.

SMADI, M. M. and SLATE, F. O. (1989), Microcracking of high and normal strength concretes under short- and long-term loading, *ACI Materials Journal*, Vol. 86, No. 2, March-April, pp. 117-127.

SMADI, M. M. and SLATE, F. O. (1989), Microcracking of high and normal strength concretes under short- and long-term loading, *ACI Materials Journal*, Vol. 86, No. 2, March-April, pp. 117-127.

SMADI, M. M., SLATE, F. O. and NILSON, A. H. (1985), High-, medium-, and low-strength concretes subject to sustained overloads - strains, strengths, and failure mechanisms, *ACI Journal*, <u>Proceedings</u>, Vol. 82, No. 5, September-October, pp. 657-664.

SMADI, M. M., SLATE, F. O. and Nilson, A. H. (1987), Shrinkage and creep of high-, medium-, and low-strength concretes, including overloads, *ACI Journal*, <u>Proceedings</u>, Vol. 84, No. 3, May-June, pp. 224-234.

SMERDA, Z. and KRISTEK, V. (1988), Creep and shrinkage of concrete elements and structures, *Elsevier*, 295 pp.

SMITH, R. G. (1960), The determination of the compressive stress-strain properties of concrete in flexure, *Magazine of Concrete Research*, Vol. 12, No. 36, November, pp. 165-170.

SMITH, R. G. and ORANGUN, C. O. (1969), Evaluation of the Stress-Strain Curve of Concrete in Flexure Using Method of Least Squares, *ACI Journal*, <u>Proceedings</u>, Vol. 66, No. 7, July, pp. 553-559.

SPARKS, P. R. and MENZIES, J. B. (1973), The effect of rate of loading upon the static and fatigue strengths of plain concrete in compression, *Magazine of Concrete Research*, Vol. 25, No. 83, June, pp. 73-80.

SPOONER, D. C. (1971), Stress-strain-time relationships for concrete, *Magazine of Concrete Research*, Vol. 23, No. 75-76, June-September, pp. 127-131.

SPOONER, D. C. (1972), The stress-strain relationship for hardened cement pastes in compression, *Magazine of Concrete Research*, Vol. 24, No. 79, June, pp. 85-92.

STREIT, W. (1991), Zeitabhängige Verformungen von Beton infolge hoher Druckbeanspruchungen, *Thesis*, Munich University of Technology, Germany, 124 pp.

STROEVEN, P. (1973), Some aspects of the micromechanics of concrete, *Thesis*, Delft University of Technology, The Netherlands, 323 pp.

STURMAN, G. M., SHAH, S. P. and WINTER, G. (1964), Microcracking and inelastic behaviour of concrete, <u>Flexural Mechanics of Reinforced Concrete</u>, <u>Proceedings of the International Symposium</u>, Miami, Florida, November 10-12, ASCE-1965-50, ACI SP-12, pp. 473-493.

STURMAN, G. M., SHAH, S. P. and WINTER, G. (1965), Effects of flexural strain gradients on microcracking and stress-strain behaviour of concrete, *ACI Journal*, <u>Proceedings</u>, Vol. 62, No. 7, July, pp. 805-822.

SWAMY, N. (1966), Discussion of the paper of STURMAN, SHAH and WINTER, Effects of flexural strain gradients on microcracking and stress-strain behaviour of concrete, *ACI Journal*, <u>Proceedings</u>, Vol. 63, No. 3, March, pp. 1717-1719.

TIMUSK, J. and GHOSH, R. S. (1991), Maturing creep of portland cement paste, *ACI Journal*, <u>Proceedings</u>, Vol. 68, No. 12, December, pp. 959-963.

WALRAVEN, J. C. and Han, N. (1991), Erfahrungen bei der Zusammensetzung von Beton mit hoher Festigkeit, *Symposium von Microsilica in der modernen Beton-technologie*, Konstanz, Deutschland, Elkem, pp. 405-413.

WALRAVEN, J. C., Han, N. and Stroband (1993), Report on various tests on concrete with high strength, CUR Commission C86 (in Dutch).

WALRAVEN, J. C. and SHEN, J. H. (1993), Non-linear creep: a general constitutive model, <u>Creep and Shrinkage of Concrete</u>, <u>Proceedings of the Fifth International RILEM Symposium</u>, Barcelona, pp. 213-218.

WARD, M. A. and COOK, D. J. (1969), The mechanism of tensile creep in concrete, *Magazine of Concrete Research*, Vol. 21, No. 68, September, pp. 151-158.

WATSTEIN, D. (1953), Effect of strain rate on the compressive strength and elastic properties of concrete, *ACI Journal*, Proceedings, Vol. 49, No. 8, April, pp. 729-744.

WISCHERS, G. von and DAHMS, J. (1977), Kriechen von frühbelastetem Beton mit hoher Anfangsfestigkeit, *Beton*, Vol. 27, No. 2+3, pp. 69-74, 104-108.

WITTMANN, F. H. (1982), Creep and shrinkage mechanism, <u>Creep and Shrinkage in Concrete Structures</u>, edited by BAZANT, Z. P. and WITTMANN, F. H., *John Wiley & Sons Ltd.*, pp. 129-161.

WOLSIEFER, J. (1984), Ultra high-strength field placeable concrete with silica fume admixture, *Concrete International*, Vol. 6, No. 4, April, pp. 25-31.

XI, Y. and JENNINGS, H. M. (1992), Relationships between microstructure and creep and shrinkage of cement paste, <u>Materials Science of Concrete III</u>, edited by SKALNY, J., *The American Ceramic Society, Inc.*, pp. 37-70.

YAMAMOTO, T. (1990), Creep and shrinkage of high-strength reinforced concrete columns, *Transactions of the Japan Concrete Institute*, Vol. 12, pp. 101-106.

YUE, L. and TAERWE, L. R. (1993), Empirical investigation of creep and shrinkage of high strength concrete, <u>Utilization of High Strength Concrete</u>, *Proceedings of the Third International Conference*, Lillehammer, Norway, Vol. 2, pp. 1263-1270.

Appendix **A**

General overview of the research program

In this appendix, a general overview of the experimental research program is given. On the basis of the variables adopted in tests, the program is generally divided into four series (R, S, C_n and C_o). The meaning of every symbol used in the table is fully described in *Chapter* 5

Table A-1 General overview of the research program in series R

(Rate sensitivity tests)

		Identifica	ition symbol		
				T0625	3
	H _{cg}			T0250	3
R		C	U	T0043	2
	N _{cg}			T0019	2
				T0002	2
				T0001	2
				L0500	2
				L0050	2
R	N _{cg}	С	U	L0010	2
				L0005	1
				L0001	1
				L2300	3
	Hcg			L0230	3
R		Т	U	L0023	3
	N _{cg}			L0008	3
		-		L0003	3
		_		L0001	3
R	H _{cg}	Т	U	SFL0230	4
	N _{og}			SFL0023	4
R	H _{cg}	С	υ	SRL0730	6
R	N _{cg}	С	U	SRL0730	3
Note *	strain	rate (0625 = 6.25	5 × 10 ⁻⁶ mm/s), T	-transverse, L-lor	ngitudinal

Table A-2 General overview of the research program in series R

(Rate sensitivity tests)

		Identificati	on symbol		Identification symbol									
				L2500	2									
R	H _{cg}	С	E0.075	L0250	2									
			E0.15	L0025	2									
				L0003	2									
				L10000	1									
				L0200	2									
R	H _{cg}	С	E0.15	L0034	2									
				L0002	2									
				L0001	1									
	_			L0250	3									
			E0.075	L0100	2									
R	N _{cg}	С		L0017	2									
			E0.15	L0008	2									
				L00008	2									
				L00005	2									
Note *		strain rate (0250	= 2.5 × 10 ⁻⁸ mm/	/s), L-longitudinal										

Table A-3 General overview of the research program in series R

(Rate sensitivity tests)

		Identificati	on symbol		
				L2300*	2
				L0230	2
				L0023	2
R	H _{cg}	т	E1/6	L0008	2
				L0003	2
				L0001	2
				L00001	1
				L2300	2
				L0230	2
R	N _{cg}	Т	E1/3	L0008	2
				L0003	2
				L0001	1
				L2300	3
			1	L0230	3
R	H _{cg}	т	E1/3	L0023	3
				L0008	3
		'		L0003	3
				L0001	3
Note *	S	train rate (2300 :	= 23.0 × 10 ⁻⁶ mm	/s), L-longitudina	

Table A-4 General overview of the research program in series S, C_n and C_e

(Sustained loading, creep at normal and early ages)

		Identificati	on symbol		
				75°	2
s	H _{cg}	С	U	85 _c	2
				95 _c	2
				15 _c	2
Cn	H _{cg}	С	U	35 _c	2
				50 _c	2
			-	50 _c	2
C _n	H _{cg}	С	υ	50 _v #	2
				50 _v #	2
	H _{cg}			30 _c	2
C _e -10	H _{gr}	С	U	50 _c	2
	H _{ls}			70 _c	2
	H _{cg}			30 _c	2
C _e -16	H _{gr}	С	U	50 _c	2
	H _{is}			70 _c	2
S	H _{cg}	С	υ	SRL0730	9
Cn	H _{cg}	С	U	SRL0730	9
C _n	H _{cg}		shrinkage		6
	H _{cg}				18
C _e -10	H_{gr}	С	U	SRL0730	18
	H _{Is}				18
C _e -10	H _{cg}				2
	H_{gr}		shrinkage		2
C _e -16	H _{is}				2
	H _{cg}				18
C _e -16	H_{gr}	С	U	SRL0730	18
	H _{is}				18
Note	*	stress level, # st	ep-wise variation	of sustained load	d

Appendix B Mix proportions of HSC and NSC

In this appendix, the mix proportions of HSC and NSC used in the four test series are respectively given in detail. All descriptions of the material used and other technical aspects are given in *Chapter 5*.

Table B-1 Mix proportions in test series R and S

(Rate sensitivity and sustained loading)

Mixture	Unit	нѕс	NSC	Note
Cement	kg/m ³	475	360	ENCI Portland Cement Class C
Silica fume	kg/m³	25	0	dry powder
W/(C+SF)	[0.30	0.50	water/(cement + silica fume)
Fine aggregate	kg/m³	718	726	0 - 4 mm
Coarse aggregate	kg/m³	1078	1090	4 - 16 mm
Superplasticizer:				Percentage of weight of cement
lignosulfonate-Na	%	0.2	,	with a little Na-gluconate
lignosulfonate	%	0.6	0.2	without Na-gluconate
Naphtalene	%	2.2-2.5	Ì	
Air content	%	1	1	****
Slump	mm	200	160	*****

Table B-2 Mix proportions in test series C_n and C_e

(Creep at normal and early ages)

Mixture	Unit	C _n H _{cg}	C₀Hcg	CeHgr	C _e His	Note
Cement	kg/m ³	475	475	475	475	ENCI Portland Cement C
Sílica fume	kg/m ³	25	25	25	25	dry powder
W/(C+SF)		0.30	0.30	0.30	0.50	water/(cement + silica fume)
Fine aggregate	kg/m ³	718	790	790	755	0 - 4 mm
Coarse aggregate	kg/m³	1078	1005	1005	1042	4 - 16 mm
Superplasticizer						
type I	kg/m³	14.25				lignosulfonate - Naphtalene
type II	kg/m³		14.25	14.25	14.25	Tillman OFP4
Air content	%	1	1.5	1.1	0.8	*****
Slump	mm	200	210	240	250	*****

Appendix **C**Experimental set-up

In this appendix, in addition to the figures shown in *Chapter* 5, the deformation measurements as well as the test rigs for the rest of test series are illustrated in figures and photos. Detailed explanations about the experimental set-up and the test procedures are given in *Chapter* 5.

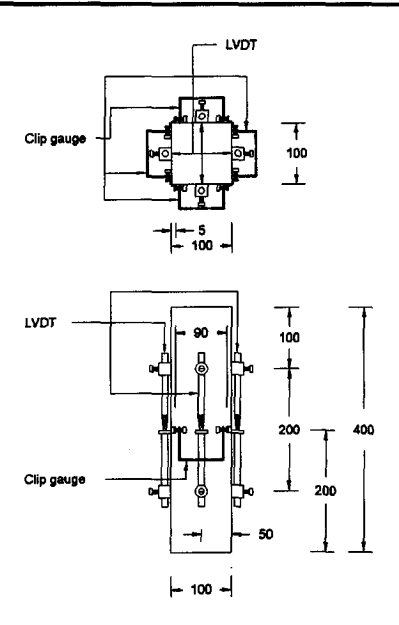


Fig. C.1 The deformation measurement set-up for RNCUL and SHCU test series.

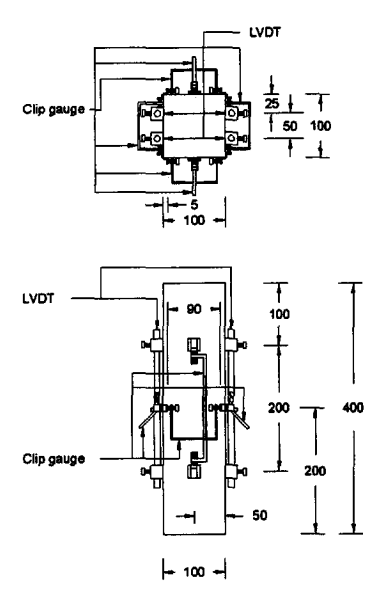


Fig. C.2 The deformation measurement set-up for RHCE and RNCE test series.

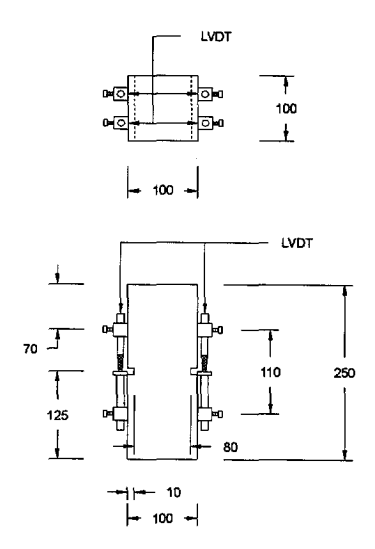


Fig. C.3 The deformation measurement set-up for RHTE and RNTE test series.

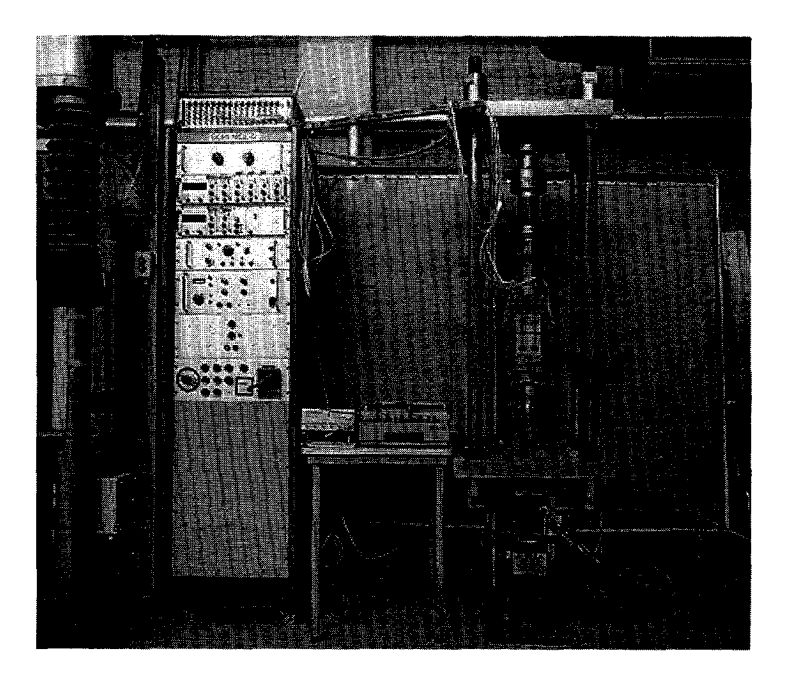


Fig. C.4 Test rig for RHTU, RNTU, RHTE and RNTE test series.



Fig. C.5 Test rig for C_nHCU test series.



Fig. C.6 The computer controlled automatic measuring system.

Appendix D Results of standard reference tests

In this appendix, the results of all standard reference tests for HSC and NSC in the four test series are listed. In addition, results of the statistical analysis are also given. The meaning of every combination of symbol listed in the table is fully described in *Chapter 5*.

Table D-1 Control tests for rate sensitivity experiments [RHCUSR and RNCUSR]

Control test	t _o	d∉ldt	$f_{cp}(t_0)$	$f_{cp}(t_0)/f_{cc}(t_0)$	& (¹	10 ⁻³)
No.	(days)	10 ⁻⁶ s ⁻¹	(N/mm²)		<i>Ec1</i> 0	€ctr0
RH _{cg} CUSRL-1	28	7.3	95.18	0.828	2.744	1.121
RH _{cg} CUSRL-2	28	7.3	97.49	0.848	2.897	0.933
RH _{cg} CUSRL-3	28	7.3	90.42	0.787	2.667	0.758
RH _{cg} CUSRL-4	35	7.3	94.31	0.821	2.802	1.000
RH _{cg} CUSRL-5	35	7.3	93.16	0.811	2.700	0.600
RH _{cg} CUSRL-6	35	7.3	91.14	0.775	2.701	0.829
RH _{cg} CUSRL-7	35	7.3	90.28	0.767	2.615	0.696
RH _{cg} CUSRL-8	35	7.3	95.32	0.824	2.852	1.075
RH _{cg} CUSRL-9	35	7.3	95.32	0.824	2.742	1.104
RN _{cg} CUSRL-1	28	7.3	27.39	0.641	1.009	0.288
RN _{cg} CUSRL-2	28	7.3	27.94	0.652	1.344	0.292
RN _{cg} CUSRL-3	35	7.3	29.95	0.714	1.449	0.721
RN _{cg} CUSRL-4	35	7.3	31,11	0.741	1.421	0.517
RN _{cg} CUSRL-5	35	7.3	29.92	0.758	1.507	0.479
RN _{cg} CUSRL-6	35	7.3	30.07	0.761	1.311	0.325

Table D-2 Control tests for rate sensitivity experiments (continued)

Control test	<i>d₅</i> /dt	Eci	μ	Evmex	σ _{mvs} /f _{cp}
No.	10 ⁻⁶ s ⁻¹	10 ³ N/mm ²		(10 ⁻³)	
RH _{cg} CUSRL-1	7.3	40.69	0.218	1.061	0.833
RH _{eg} CUSRL-2	7.3	40.82	0.179	1.688	0.989
RH _{cg} CUSRL-3	7.3	41.36	0.161	1.218	0.943
RH _{cg} CUSRL-4	7.3	40.48	0.225	1.095	0.918
RH _{cg} CUSRL-5	7.3	41.50	0.213	1.685	1.000
RH _{cg} CUSRL-6	7.3	38.18	0.243	1.078	0.932
RH _{cg} CUSRL-7	7.3	40.05	0.177	1.224	1.000
RH _{cg} CUSRL-8	7.3	40.22	0.220	1.059	0.874
RH∞CUSRL-9	7.3	40.51	0.154	1.129	0.846
RN _{cg} CUSRL-1	7.3	32.14	0.270	0.668	0.999
RN _{cg} CUSRL-2	7.3	30.54	0.226	0.771	0.976
RN _{cg} CUSRL-3	7.3	34.23	0.282	0.319	0.757
RN _{cg} CUSRL-4	7.3	34.40	0.207	0.566	0.916
RN₀gCUSRL-5	7.3	31.20	0.292	0.595	0.983
RN _∞ CUSRL-6	7.3	31.78	0.136	0.689	0.997

Table D-3 Control tests for sustained loading experiments in S series

Control test	t ₀	deldt	f _{cp28}	E _{ci}	£0
No.	(days)	10 ⁻⁶ s ⁻¹	(N/mm²)	(10 ³ N/mm ²)	(10 ⁻³)
SH _{cg} CUSR75 _c - 1	28	7.3	88.50	43.18	2.341
SH _{cg} CUSR75 _c - 2	28	7.3	86.89	40.90	2.422
SH _{cg} CUSR75 _c - 3	28	7.3	89.38	41.54	2.385
SH _{cg} CUSR85 _c - 1	28	7.3	99.93	44.07	2.607
SH _{cg} CUSR85 _c - 2	28	7.3	98.02	44.19	2.541
SH _{cg} CUSR85 _c - 3	28	7.3	100.7	43.23	2.578
SH _{cg} CUSR95 _c - 1	28	7.3	98.02	45.15	2.370
SH _{cg} CUSR95 _c - 2	28	7.3	98.61	43.85	2.519
SH _{cg} CUSR95 _c - 3	28	7.3	100.5	44.95	2.563

Table D-4 Control tests for creep constantly loaded at a normal age in C_nHCUSR_c series

Control test	t ₀	dεldt	f _{cp28}	E _{ci}	£0
No.	(days)	10 ⁻⁶ s ⁻¹	(N/mm²)	(10 ³ N/mm ²)	(10 ⁻³)
C _n H _{cg} CUSR15 _c - 1	28	7.3	102.1	43.60	2.696
C _n H _{cg} CUSR15 _c - 2	2,8	7.3	101.4	40.69	2.859
C _n H _{cg} CUSR15 _c - 3	28	7.3	97.14	40.79	2.548
C _n H _{cg} CUSR35 _c - 1	28	7.3	102.3	46.90	2.437
C _n H _{cg} CUSR35 _c - 2	28	7.3	102.6	43.88	2.593
C _n H _{eg} CUSR35 _c - 3	28	7.3	102.6	45.10	2.607
C _n H _{cg} CUSR50 _c - 1	28	7.3	94.36	45.57	2.267
C _n H _{cg} CUSR50 _c - 2	28	7.3	99.34	44.35	2.600
C _n H _{cg} CUSR50 _c - 3	28	7.3	98.75	43.46	2.526

Table D-5 Control tests for creep step-wisely loaded at a normal age in C_nHCUSR_v series

Control test	to	d <i>s</i> ldt	f _{cc28}	f _{cp28}	E _{ci}	ಏ
No.	(days)	10 ⁻⁸ s ⁻¹	(N/mm²)	(N/mm²)	(10 ³ N/mm ²)	(10 ⁻³)
C _n H _{cg} CUSR _v - 1	28	7.3	106.13	74.60	35.74	2.496
C _n H _{cg} CUSR _v - 2	28	7.3	104.96	76.06	36.09	2.590
C _n H _{cg} CUSR _v - 3	28	7.3	107.88	76.93	36.59	2.548
average	28	7.3	108.32	75.86	36.14	2.545
5D			1,200	0.961	0,349	0.038

Table D-6 Control tests for creep experiments loaded at an age of 10 hours in $C_e 10 H_{cg} CUSR$ series.

(HSC with crushed gravel)

Control test	t _o	dεldt	$f_{cc}(t_0)$	$f_{cp}(t_0)$	$E_c(t_0)$	ε ₀ (t ₀)
No.	(days)	10 ⁻⁶ s ⁻¹	(N/mm²)	(N/mm ²)	(10 ³ N/mm ²)	(10 ⁻³)
C _e 10H _{cg} CUSR-1	0.42	7.3	13.28	6.52	3.63	7.515
C _e 10H _{cg} CUSR-2	0.42	7.3	12.99	8.67	8.46	6.264
C _e 10H _{cg} CUSR-3	0.42	7.3	13.14	10.18	12.86	4.071
average	0.42	7.3	13.14	8.46	8.32	5.950
SĐ			0.118	1.502	3.769	1,423
C _e 10H _∞ CUSR-4	3	7.3	86.57	55.91	33.06	2.679
C _e 10H _{cg} CUSR-5	3	7.3	84.09	56.93	32.69	2.802
C _e 10H _{cg} CUSR-6	3	7.3	85.11	56.79	32.84	2.749
average	3	7.3	85.26	56 54	32.86	2.743
SD			1.018	0.451	0.152	0.050
C _e 10H _{cg} CUSR-7	7	7.3	95.91	63.07	35.54	2.822
C₀10Hℴ₀CUSR-8	7	7.3	95.47	63.36	34.22	2.866
C _e 10H _{cg} CUSR-9	7	7.3	95.33	64.09	34.77	2.732
average	7	7.3	95.57	63.51	34.84	2.807
SD			0.247	0.429	0.541	0.056
C _e 10H _{cg} CUSR-10	28	7.3	109.93	74.16	37.00	2.322
C _e 10H _{cg} CUSR-11	28	7.3	110.80	73.58	35.60	2.641
C _e 10H _{cg} CUSR-12	28	7.3	107.45	70.66	35.12	2.577
average	28	7.3	109.39	72.80	35.91	2.513
SD			1,419	1 532	0.798	0.138
C _e 10H _{cg} CUSR-13	90	7.3	115.62	79.42	37.04	2.784
C _e 10H _{cg} CUSR-14	90	7.3	110.36	83.50	38.98	2.564
C _e 10H _{cg} CUSR-15	90	7.3	111.39	81.31	38.08	2.527
average	90	7.3	112.46	81.41	38.08	2.625
SD			2,276	1 667	0.793	0.113
C _e 10H _{cg} CUSR-16	180	7.3	107.01	82.63	38.50	2.469
C _e 10H _{cg} CUSR-17	180	7.3	108.76	85.26	37.80	2.549
C _e 10H _{cg} CUSR-18	180	7.3	110.36	81.75	39.19	2.425
average	180	7.3	108.71	83.21	38.50	2.481
SĐ			1.368	1.491	0.567	0.051

Table D-7 Control tests for creep experiments loaded at an age of 10 hours in $C_e 10 H_{gr} CUSR$ series.

(HSC with granite)

			1		T	
Control test	to	dεidt	$f_{cc}(t_0)$	$f_{cp}(t_0)$	$E_c(t_0)$	$\varepsilon_0(t_0)$
No.	(days)	10 ⁻⁶ s ⁻¹	(N/mm ²)	(N/mm ²)	(10 ³ N/mm ²)	(10 ⁻³)
C _e 10H _{gr} CUSR-1	0.42	7.3	13.87	6.81	3.68	7.864
C _e 10H _{gr} CUSR-2	0.42	7.3	14.31	9.29	8.99	6.740
C _e 10H _{gr} CUSR-3	0.42	7.3	14.45	12.15	13.25	4.918
average	0.42	73	14.21	9.42	8.64	6.507
SD			0.247	2.182	3.915	1,214
C _e 10H _{gr} CUSR-4	3	7.3	82.92	54.01	31.45	2.476
C _e 10H _{gr} CUSR-5	3	7.3	80.00	55.47	32.15	2.579
C _e 10H _{gr} CUSR-6	3	7.3	83.65	54.16	31.17	2.462
average	3	7.3	82.19	54.55	31.59	2.506
SD			1.577	0.656	0.412	0.052
C _e 10H _{gr} CUSR-7	7	7.3	92.99	61.75	33.89	2.364
C _e 10H _{gr} CUSR-8	7	7.3	90.22	59.85	32.83	2.485
C _e 10H _{gr} CUSR-9	7	7.3	91.24	60.44	33.57	2.361
average	7	7.3	91.48	60.68	33.43	2.403
SD			1.144	0.794	0.444	0.058
C _e 10H _{gr} CUSR-10	28	7.3	104.23	72.26	34.86	2.623
C _e 10H _{gr} CUSR-11	28	7.3	102.77	70.37	35.46	2.476
C _e 10H _{gr} CUSR-12	28	7.3	101.46	71.39	35.81	2.542
average	28	7.3	102.82	71.34	35.38	2.547
SD			1.131	0.772	0 392	0.060
C _e 10H _{gr} CUSR-13	90	7.3	104.82	78.54	36.71	2.601
C _e 10H _{gr} CUSR-14	90	7.3	105.55	75.62	36.01	2.374
C _e 10H _{gr} CUSR-15	90	7.3	109.34	77.81	36.77	2.549
average	90	7.3	106.57	77 32	36.50	2.508
SD			1.981	1.241	0.345	0.097
C _e 10H _{gr} CUSR-16	180	7.3	108.47	79.42	35.46	2.828
C _e 10H _{gr} CUSR-17	180	7.3	107.15	80.00	35.50	2.637
C _e 10H _{gr} CUSR-18	180	7.3	110.51	81.75	35.57	2.864
average	180	7.3	108.71	80.39	35.51	2.778
SD			1.382	0.990	0.046	0.099
					V 0.70	u.usa

Table D-8 Control tests for creep experiments loaded at an age of 10 hours in C_010H_{11} CUSR series.

(HSC with limestone)

Control test	t _o	d <i>εld</i> t	$f_{cc}(t_0)$	$f_{cp}(t_0)$	$E_c(t_0)$	ε ₀ (t ₀)
No.		10 ⁻⁶ s ⁻¹	(N/mm ²)	(N/mm²)	(10 ³ N/mm ²)	(10 ⁻³)
	(days)					
C _e 10H _{is} CUSR-1	0.42	7.3	9.34	4.37	2.91	8.070
C _e 10H _{is} CUSR-2	0.42	7.3	9.34	5.72	7.36	5.364
C _e 10H _{is} CUSR-3	0.42	7.3	10.07	7.32	10.66	4.227
average	0.42	7.3	9.58	5.80	6.98	5.887
SD			0.344	1,206	3.176	1,612
C _e 10H _{Is} CUSR-4	3	7.3	69.20	45.84	40.27	1.800
C _e 10H _{is} CUSR-5	3	7.3	69.34	48.32	37.34	2.005
C _e 10H _{Is} CUSR-6	3	7.3	69.93	45.26	39.86	1.936
average	3	7.3	69.49	46.47	39.16	1.914
SD			0.316	1.327	1.295	0.085
C _e 10H _{Is} CUSR-7	7	7.3	79.56	52.70	38.74	2.112
C _e 10H _{Is} CUSR-8	7	7.3	77.66	56.20	40.29	1.963
C _e 10H _{Is} CUSR-9	7	7.3	76.06	52.70	35.70	1.868
average	7	7.3	77.76	53.87	38.24	1.981
SD			1,431	1.650	1 906	0.100
C _e 10H _{is} CUSR-10	28	7.3	88.76	63.80	41.97	1.919
C _e 10H _{is} CUSR-11	28	7.3	87.30	60.88	41.01	1.890
C _e 10H _{is} CUSR-12	28	7.3	89.34	61.90	39.26	1.978
average	28	7.3	88.47	62 19	40.75	1.929
SD			0.858	1 210	1 122	0.037
C _e 10H _{is} CUSR-13	90	7.3	91.09	64.82	38.62	1.978
C _e 10H _{is} CUSR-14	90	7.3	92.99	67.01	42.28	1.941
C _e 10H _{is} CUSR-15	90	7.3	92.99	66.13	40.04	1.993
average	90	7.3	92.36	65.99	40.31	1.971
SD			0.896	0.900	1.507	0.022
C _e 10H _{is} CUSR-16	180	7.3	92.26	66.42	43.71	2.000
C _e 10H _{is} CUSR-17	180	7.3	94.60	66.57	39.72	2.000
C _e 10H _{is} CUSR-18	180	7.3	94.89	66.42	43.71	2.000
average	180	7.3	93.92	66.47	42.38	2.000
SD		l	1,177	0.071	1.881	0.000
33		l	l	I	1	1

Table D-9 Control tests for creep experiments loaded at an age of 16 hours in $C_e 16 H_{cg} CUSR$ series.

(HSC with crushed gravel)

Control test	to	d <i>ɛld</i> t	f (t-)	5 (1)	<i>(</i> (4)	
No.	_	10 ⁻⁶ s ⁻¹	$f_{cc}(t_0)$	$f_{cp}(t_0)$	$E_c(t_0)$	$\varepsilon_0(t_0)$
	(days)		(N/mm²)	(N/mm²)	(10 ³ N/mm ²)	(10 ⁻³)
C _e 16H _{cg} CUSR-1	0.67	7.3	62.48	44.75	30.52	3.007
C _e 16H _{cg} CUSR-2	0.67	7.3	64.23	46.96	30.48	2.740
C _e 16H _{cg} CUSR-3	0.67	7.3	63.94	47.02	30.80	2.546
average	0.67	7.3	63.55	46.24	30.60	2.764
SD			0.766	1.056	0,142	0.189
C _e 16H _{cg} CUSR-4	3	7.3	97.37	69.64	36.39	2.767
C _e 16H _{cg} CUSR-5	3	7.3	97.23	68.61	36.63	2.676
C _e 16H _{cg} CUSR-6	3	7.3	96.79	69.93	35.93	2.864
average	3	7.3	97.13	69.39	36.32	2.769
SD			0.247	0.566	0.290	0.077
C _e 16H _{cg} CUSR-7	7	7.3	105.40	77.23	36.46	2.832
C _e 16H _{cg} CUSR-8	7	7.3	107.88	79.12	37.39	2.923
C _e 16H _{cg} CUSR-9	7	7.3	107.01	75.62	35.65	2.848
average	7	7.3	106.76	77 32	36.50	2.868
SD			1.027	1.430	0.711	0.040
C _e 16H _{cg} CUSR-10	28	7.3	120.73	87.88	37.84	2.700
C _e 16H _{cg} CUSR-11	28	7.3	117.96	88.32	36.35	2.819
C _e 16H _{cg} CUSR-12	28	7.3	120.00	85.84	36.93	2.733
average	28	7.3	119.56	87.35	37.04	2.751
SD			1.172	1.080	0.613	0.050
C _e 16H _{cg} CUSR-13	90	7.3	130.51	93.14	37.79	2.678
C _e 16H _{cg} CUSR-14	90	7.3	128.10	94.31	37.80	2.731
C _e 16H _{cg} CUSR-15	90	7.3	127.88	95.04	38.03	2.756
average	90	7.3	128.83	94 16	37.87	2.722
SD			1.191	0.783	0.111	0.033
C _e 16H _{cg} CUSR-16	180	7.3	128.61	98.39	38.90	2.639
C _e 16H _{cg} CUSR-17	180	7.3	129.20	95.04	38.43	2.656
C _e 16H _{cg} CUSR-18	180	7.3	129.93	97.66	37.65	2.690
average	180	7.3	129.25	97.03	38.33	2.662
SD			0.540	1 438	0.516	0.021
			V.000	1.700	V:410	U.UZ I

Table D-10 Control tests for creep experiments loaded at an age of 16 hours in $C_e 16H_{gr} CUSR$ series.

(HSC with granite)

Control test	t ₀	dεldt	$f_{cc}(t_0)$	$f_{cp}(t_0)$	$E_c(t_0)$	a.(t-)
	,	10 ⁻⁶ s ⁻¹			, ,	ε ₀ (t ₀)
No.	(days)		(N/mm ²)	(N/mm ²)	(10 ³ N/mm ²)	(10 ⁻³)
C _e 16H _{gr} CUSR-1	0.67	7.3	59.71	45.49	30.57	2.678
C _e 16H _{gr} CUSR-2	0.67	7.3	60.73	44.87	30.69	2.656
C _e 16H _{gr} CUSR-3	0.67	7.3	58.83	47.61	30.75	2.795
average	0.67	7.3	59.76	45.99	30.67	2.710
SD			0.776	1,173	0.075	0.061
C _e 16H _{gr} CUSR-4	3	7.3	92.41	66.57	35.06	2.722
C _e 16H _{gr} CUSR-5	3	7.3	92.41	66.86	34.74	2.630
C _e 16H _{gr} CUSR-6	3	7.3	92.70	67.15	33.17	2.896
average	3	7.3	92.51	66.86	34.32	2.749
SD			0.137	0.237	0.826	0,110
C _e 16H _{gr} CUSR-7	7	7.3	104.67	73.87	34.78	2.850
C _e 16H _{gr} CUSR-8	7	7.3	107.15	74.74	34.48	2.886
C _e 16H _{gr} CUSR-9	7	7.3	106.57	73.14	34.78	2.877
average	7	7,3	106.13	73 92	34 68	2.871
SD			1.059	0.654	0.141	0.015
C _e 16H _{gr} CUSR-10	28	7.3	120.00	83.50	35.71	2.505
C _e 16H _{gr} CUSR-11	28	7.3	120.58	82.92	37.06	2.386
C _e 16H _{gr} CUSR-12	28	7.3	119.42	83.94	34.92	2.619
average	28	7,3	120 00	83.45	35.90	2.503
SD			0.474	0.418	0.884	0.095
C _e 16H _{gr} CUSR-13	90	7.3	126.72	93.14	36.33	2.678
C _e 16H _{gr} CUSR-14	90	7.3	125.69	92.85	36.25	2.769
C _e 16H _{gr} CUSR-15	90	7.3	123.80	93.87	36.68	2.661
average	90	7.3	125.40	93.29	36.42	2.703
SD			1.209	0.429	0.187	0.047
C _e 16H _{gr} CUSR-16	180	7.3	127.01	94.16	35.31	2.929
C _e 16H _{gr} CUSR-17	180	7.3	125.84	96.20	36.56	2.777
C _e 16H _{gr} CUSR-18	180	7.3	126.86	88.18	35.21	2.636
average	180	73	126.57	92.85	35.69	2.781
SD			0.520	3.403	0.614	0.120
SU			U SZU	3.403	U.014	U. 12U

Table D-11 Control tests for creep experiments loaded at an age of 16 hours in $C_e16H_{1s}CUSR$ series.

(HSC with limestone)

Control test	t ₀	deldt	$f_{cc}(t_0)$	$f_{cp}(t_0)$	$E_c(t_0)$	$\varepsilon_0(t_0)$
No.	(days)	10 ⁻⁶ s ⁻¹	(N/mm²)	(N/mm²)	(10 ³ N/mm ²)	(10 ⁻³)
C _e 16H _{Is} CUSR-1	0.67	7.3	57.96	42.45	36.21	2.090
C _e 16H _{is} CUSR-2	0.67	7.3	59.85	44.45	37.62	2.097
C _e 16H _{is} CUSR-3	0.67	7.3	59.12	44.19	39.00	2.031
average	0.67	7.3	58.98	43,70	37.61	2.073
SD			0.778	0.888	1.139	0.030
C _e 16H _{Is} CUSR-4	3	7.3	90.80	63.21	40.77	2.304
C _e 16H _{Is} CUSR-5	3	7.3	88.91	63.21	42.58	2.214
C _e 16H _{Is} CUSR-6	3	7.3	91.53	64.53	42.34	2.139
average	3	7.3	90.41	63.65	41.90	2.219
SD			1.104	0.622	0.803	0.068
C _e 16H _{is} CUSR-7	7	7.3	99.85	70.07	42.29	2.223
C _e 16H _{is} CUSR-8	7	7.3	99.27	70.95	42.76	2.031
C _e 16H _{is} CUSR-9	7	7.3	98.69	70.37	41.87	2.033
average	7	7.3	99.27	70.46	42.31	2.096
SD			0.474	0.365	0.364	0.090
C _e 16H _{is} CUSR-10	28	7.3	109.34	80.15	43.73	2.168
C _e 16H _{ls} CUSR-11	28	7.3	111.68	78.10	44.05	2.126
Ce16HisCUSR-12	28	7.3	112.26	79.85	43.66	2.253
average	28	7.3	111 09	79.37	43.81	2.182
SD			1.262	0.904	0 170	0.053
C _e 16H _{is} CUSR-13	90	7.3	114.89	82.48	42.66	2.308
C _e 16H _{Is} CUSR-14	90	7.3	119.71	85.55	45.09	2.249
C _e 16H _{is} CUSR-15	90	7.3	117.81	83.94	44.02	2.203
average	90	7.3	117.47	83.99	43.92	2.253
SD			1.982	1.254	0.994	0.043
C _e 16H _{Is} CUSR-16	180	7.3	114.45	89.34	44.00	2.348
C _e 16H _{Is} CUSR-17	180	7.3	113.72	85.55	44.49	2.214
C _e 16H _{ls} CUSR-18	180	7.3	115.62	85.26	43.18	2.253
average	180	7.3	114.60	86.72	43.89	2.272
SD			0.783	1.859	0.540	0.056

Appendix **E**Test results of all series

In this appendix, the results of the four test series (R, S, C_n and C_e) are summarized in several tables. Besides, some statistic analysis are also included in the tables. All items used in these tables are fully described in *Chapter 5*.

Table E-1 Results in strain rate sensitivity tests for HSC under centric compression with transverse strain rate control (reference tests in Table D-1 and D-2)

Test	t ₀	(dε)√dt	<i>О</i> стах	σ _{cmax} /f _{cc28}	eo (°	10 ⁻³)
No.	(days)	(×10 ⁻⁶ s ⁻¹)	(N/mm ²)		€c/0	€ctr0
RH _{cg} CUT625-1	28	6.25	94.11	0.805	2.984	0.763
RH _∞ CUT625-2	28	6.25	93.84	0.803	3.028	0.821
RH∞CUT625-3	28	6.25	93.83	0.803	3.165	1.009
RH₀₀CUT250-1	28	2.50	90.51	0.775	3.117	0.968
RH _{og} CUT250-2	42	2.50	93.27	0.798	2.989	0.839
RH _{cg} CUT043-1	28	0.43	87.67	0.750	3.004	1.073
RH _{cg} CUT043-2	42	0.43	86.02	0.736	2.793	0.687
RH _{ag} CUT019-1	28	0.19	83.45	0.714	3.189	0.978
RH _{cg} CUT019-2	29	0.19	83.30	0.713	3.076	0.869
RH _{cg} CUT002-1	29	0.02	79.21	0.678	3,635	1.181
RH _{cg} CUT002-2	29	0.02	75.25	0.644	3.773	1.453
RH _{eg} CUT001-1	28	0.01	81.56	0.698	4.116	1.749
RH _{cg} CUT001-2	32	0.01	83.16	0.720	4.082	1.964

Table E-2 Results in strain rate sensitivity tests for HSC under centric compression with transverse strain rate control (reference tests in Table D-1 and D-2) [continued]

Test	$[(d\varepsilon)/dt]_i$	E _{ci}	μ	Eymax	σ _{mvs} l σ _{cmax}
No.	(10 ⁻⁶ s ⁻¹)	10 ³ N/mm ²		(10 ⁻³)	
RH₀gCUT625-1	38.50	38.73	0.169	1.528	0.947
RH _{cg} CUT625-2	37.60	36.65	0.163	1.509	0.984
RH _{cg} CUT625-3	39.30	36.55	0.173	1.485	0.949
RH _{cg} CUT250-1	13.90	36.47	0.196	1.449	0.963
RH _{cg} CUT250-2	14.40	38.12	0.179	1.427	0.951
RH _{cg} CUT043-1	2.30	36.72	0.173	1.292	0.886
RH _{cg} CUT043-2	2.10	36.53	0.179	1.419	1.000
RH _{cg} CUT019-1	1.20	36.41	0.169	1.431	0.930
RH _{cg} CUT019-2	1.10	36.49	0.173	1.431	0.954
RH _∞ CUT002-1	0.13	33.38	0.160	1.531	0.931
RH _∞ CUT002-2	0.11	34.22	0.171	1.407	0.913
RH _{cg} CUT001-1	0.08	34.73	0.171	1.530	0.940
RH _{cg} CUT001-2	0.06	36.14	0.233	1.439	0.915

Table E-3 Results in strain rate sensitivity tests for NSC under centric compression with transverse strain rate control (reference tests in Table D-1 and D-2)

Test	t ₀	(dε)₁/dt	<i>Остах</i>	σ _{cmax} /f _{cc28}	en (°	10 ⁻³)
No.	(days)	(×10 ⁻⁶ s ⁻¹)	(N/mm ²)		<i>Ec1</i> 0	Ect10
RN _{cg} CUT625-1	28	6.25	29.62	0.693	1.363	0.653
RN _{cg} CUT625-2	28	6.25	28.63	0.646	1.651	0.848
RN _{cg} CUT625-3	28	6.25	28.95	0.654	1.389	0.527
RN _{cg} CUT250-1	28	2.50	30.25	0.683	1.466	1.583
RN _{cg} CUT250-2	29	2.50	26.22	0.592	1.100	0.583
RN _{cg} CUT250-3	29	2.50	24.88	0.562	1.122	0.375
RN _{cg} CUT043-1	28	0.43	28.37	0.664	1.186	0.392
RN _{cg} CUT043-2	29	0.43	30.57	0.715	1.502	0.534
RN _{cg} CUT019-1	28	0.19	24.13	0.545	1.227	0.467
RN _{cg} CUT019-2	31	0.19	28.40	0.659	1.536	0.794
RN _{cg} CUT002-1	28	0.02	30.63	0.711	1.766	1.136
RN _{cg} CUT002-2	32	0.02	29.67	0.688	1.807	1.050
RN _{cg} CUT001-1	29	0.01	29.69	0.695	1.834	1.048
RN _{cg} CUT001-2	29	0.01	28.94	0.654	2.005	1.627

Table E-4 Results in strain rate sensitivity tests for NSC under centric compression with transverse strain rate control (reference tests in Table D-1 and D-2) [continued]

Test No.	[(<i>dɛ</i>)√ <i>dt</i>] _i (10 ⁻⁶ s ⁻¹)	<i>E_{ci}</i> 10 ³ N/mm ²	μ	<i>€vm</i> ax (10 ⁻³)	σ _{mvs} l σ _{cmax}
RN _{cg} CUT625-1	27.10	32.82	0.221	0.367	0.804
RN _{cg} CUT625-2	31.20	31.46	0.179	0.360	0.745
RN _{cg} CUT625-3	25.90	30.68	0.187	0.440	0.881
RN _{cg} CUT250-1	14.30	32.14	0.155	0.390	0.863
RN _{cg} CUT250-2	14.10	32.98	0.245	0.461	0.978
RN _{cg} CUT250-3	11.00	30.82	0.170	0.428	0.937
RN _{cg} CUT043-1	2.27	32.47	0.197	0.404	0.989
RN _{cg} CUT043-2	1.73	31.73	0.226	0.489	0.915
RN _{cg} CUT019-1	0.97	29.01	0.151	0.378	0.923
RN _{cg} CUT019-2	0.88	30.62	0.224	0.395	0.806
RN _{cg} CUT002-1	0.15	28.52	0.154	0.425	0.732
RN _{cg} CUT002-2	0.11	28.30	0.179	0.487	0.789
RN _{cg} CUT001-1	0.05	31.20	0.270	0.403	0.793
RN₀gCUT001-2	0.07	30.42	0.229	0.416	0.954

Table E-5 Results in strain rate sensitivity tests for NSC under centric compression with longitudinal strain rate control (reference tests in Table D-1 and D-2)

Test	t_0	(dɛ)√dt	<i>Остах</i>	σ _{cmex} /f _{cc28}	eo (*	10 ⁻³)
No,	(days)	(×10 ⁻⁶ s ⁻¹)	(N/mm ²)		Ec/0	€c#0
RN _{cg} CUL500-1	28	5.00	27.54	0.646	1.320	0.453
RN _{cg} CUL500-2	28	5.00	27.97	0.656	1.484	0.527
average	28	5.00	27.76	0.651	1.402	0.490
SD			0.215	0.005	0.082	0.037
RN _{cp} CUL050-1	28	0.50	28.14	0.660	1.500	****
RN _{cp} CUL050-2	31	0.50	29.31	0.698	1.569	0.715
average	29.5	0,50	28.73	0.679	1.535	0.715
SĐ	1.5		0.585	0.019	0.035	
RN _{cg} CUL010-1	30	0.10	27.61	0.648	1.639	0.563
RN _{cg} CUL010-2	31	0.10	27.59	0.647	1.614	0.510
average	30.5	0.10	27.60	0.648	1.627	0.537
SD	0.5		0.010	0.001	0.013	0.027
RN _{cg} CUL005-1	32	0.05	28.15	0.660	1.758	0.906
RN _{cg} CUL001-1	29	0.01	30.42	0.701	2.081	0.701

Table E-6 Results in strain rate sensitivity tests for NSC under centric compression with longitudinal strain rate control (reference tests in Table D-1 and D-2) [continued]

Test	$[(d\varepsilon)_t/dt]_i$	Eci	μ	€ _{vmax}	σ _{mvs} /σ _{cmax}
No.	(10 ⁻⁶ s ⁻¹)	10 ³ N/mm ²		(10 ⁻³)	
RN _{cg} CUL500-1	1.550	33.12	0.343	0.452	0.991
RN _{cg} CUL500-2	0.870	29.39	0.245	0.521	0.899
average	1.210	31.26	0.294	0.487	0.945
SD	0.340	1.865	0.049	0.035	0.046
RN _{cg} CUL050-1	****	31.77	****	****	****
RN _∞ CUL050-2	0.240	29.70	0.481	0.314	0.890
average	0.240	30.74	0.481	0.314	0.890
SD		1.035			
RN _{cg} CUL010-1	0.020	30.67	0.156	0.630	0.957
RN _{cg} CUL010-2	0.030	29.62	0.326	0.595	1.000
average.	0.025	30,15	0.241	0.613	0.979
SD	0.005	0.525	0.085	0.018	0.022
RN _{cg} CUL005-1	0.015	27.86	0.371	0.260	0.763
RN _{cg} CUL001-1	0.005	26.34	0.469	0.685	0.997

Table E-7 Results in strain rate sensitivity tests for HSC under centric tension with longitudinal strain rate control (reference tests in Table D-1 and D-2)

Test	t ₀	(dε)₁/dt	<i>σ</i> _{tmax}	E _t	€ro
No.	(days)	(10 ⁻⁶ s ⁻¹)	N/mm²	10 ³ N/mm ²	(10 ⁻³)
RH _{cg} TUL2300-1	32	23.0	4.37	48.48	0.107
RH _{cg} TUL2300-2	32	23.0	3.77	48.06	0.122
RH _{cp} TUL2300-3	32	23.0	3.79	33.38	0.134
average	32	23.0	3.98	43.31	0 121
SD			0.28	7.021	0.011
RH₀gTUL0230-1	28	2.30	4.73	42.53	0.129
RH _∞ TUL0230-2	28	2.30	4.91	38.41	0.152
RH _∞ TUL0230-3	28	2.30	4.19	47.69	0.122
average	28	2.30	4.61	42.88	0.134
SD			0.31	3.797	0.013
RH _{cg} TUL0023-1	28	0.23	4.20	34.31	0.151
RH _{cg} TUL0023-2	28	0.23	4.20	37.94	0.156
RH _{cg} TUL0023-3	32	0.23	4.53	38.47	0.141
average	30.7	0.23	4.31	36.91	0 149
SD	1.89		0.16	1,849	0.006
RH _{cg} TUL0008-1	32	0.08	4.26	41.52	0.118
RH _{cg} TUL0008-2	32	0.08	4.39	33.81	0.170
RH _{cg} TUL0008-3	33	0.08	4.14	26.30	0.202
average	32.3	0.08	4.26	33.88	0.163
SD	0.47		0.10	6.214	0.035
RH _{cg} TUL0003-1	29	0.03	4.39	32.14	0.148
RH _{cg} TUL0003-2	29	0.03	4.03	32.59	0.156
average	29	0.03	4.21	32.37	0 152
SD			0.18	0.225	0.004
RH₀gTUL0001-1	33	0.01	3.87	38.35	0.119
RH₀gTUL0001-2	34	0.01	4.38	25.53	0.190
average	33.5	0.01	4.13	31.94	0.155
SD	0.50		0.26	6 410	0.036

Table E-8 Results in strain rate sensitivity tests for NSC under centric tension with longitudinal strain rate control (reference tests in Table D-1 and D-2)

Test	t ₀	(dε)₁/dt	Otmax	E _t	€10
No.	(days)	(10 ⁻⁶ s ⁻¹)	N/mm²	10 ³ N/mm ²	(10 ⁻³)
RN _∞ TUL2300-1	34	23.0	2.69	28.13	0.117
RN _∞ TUL2300-2	34	23.0	2.31	32.65	0.086
RN _{og} TUL2300-3	34	23.0	2.16	30.95	0.078
average	34	23.0	2.39	30.58	0.094
SD			0.22	1.864	0.017
RN _∞ TUL0230-1	28	2.30	2.37	35.07	0.067
RN _∞ TUL0230-2	28	2.30	2.38	35.59	0.085
RN _∞ TUL0230-3	28	2.30	2.30	29.51	0.077
average	28	2.30	2.35	33.39	0.076
SD			0.04	2.752	0.007
RN _{cg} TUL0023-1	34	0.23	1.92	25.38	0.090
RN _{cg} TUL0023-2	37	0.23	1.84	26.23	0.092
RN₀gTUL0023-3	37	0.23	2.19	25.34	0.090
average	8	0.23	1.98	25.65	0.091
SD	1.41		0.15	0.410	0.001
RN _∞ TUL0008-1	37	0.08	2.56	25.11	0.115
RN⇔TUL0008-2	37	0.08	1.78	23.04	0.099
RN _{cg} TUL0008-3	38	0.08	2.64	31.40	0.083
average	37.3	0.08	2.33	26.52	0.099
SD	0.47		0.39	3.555	0.013
RN _{cg} TUL0003-1	28	0.03	2.34	31.32	0.085
RN _{cg} TUL0003-2	29	0.03	2.16	25.45	0.103
RN _{cg} TUL0003-3	30	0.03	2.09	19.73	0.140
average	29	0.03	2,20	25,50	0,109
SD	0.82		0.11	4.732	0.023
RN _{eg} TUL0001-1	28	0.01	2.01	26.05	0.113
RN _{eg} TUL0001-2	30	0.01	2.13	25.69	0.100
RN _{cg} TUL0001-3	31	0.01	1.74	26.10	0.106
average	29.7	0.01	1.96	25.95	0,106
SD	1.25		0.16	0.183	0.005

Table E-9 Results in strain rate sensitivity tests for HSC under eccentric compression (e/d = 0.075) with longitudinal strain rate control (reference tests in Table D-1 and D-2)

Test	t ₀	(dε)₁/dt	P _{max}	€0 (10 ⁻³)		ε _{cu} (10 ⁻³)	
No.	(days)	(×10 ⁻⁶ s ⁻¹)	(kN)	Ecc0	€ct0	Eccu	Ectu
RH _{cg} CE75L2500-1	28	25.00	809.6	3.244	1.384	3.545	0.853
RH _{cg} CE75L2500-2	28	25.00	813.6	3.343	1.342	****	****
RH _{cg} CE75L0250-1	28	2.500	801.6	3.468	1.468	4.935	0.502
RH _{cg} CE75L0250-2	28	2.500	801.6	3.325	1.368	3.690	0.431
RH ₀₉ CE75L0025-1	29	0.250	737.6	4.060	1.290	5.040	0.397
RH _∞ CE75L0025-2	29	0.250	761.6	3.959	1.561	4.655	0.873
RH _∞ CE75L0003-1	30	0.025	747.2	4.573	1.762	5.055	1.586
RH _{cg} CE75L0003-2	35	0.025	684.0	5.000	1.120	****	****

Table E-10 Results in strain rate sensitivity tests for HSC under eccentric compression (e/d = 0.15) with longitudinal strain rate control (reference tests in Table D-1 and D-2)

Test	t ₀	(dε)√dt	P _{mex}	బ (10 ⁻³)	Ecu (10 ⁻³)
No.	(days)	(×10 ⁻⁶ s ⁻¹)	(kN)	€ccQ	<i>€</i> c#0	Eccu	€ctu
RH _{cg} CE150L10000-1	32	100.0	620.0	3.580	-0.140	3.610	-0.122
RH _{cg} CE150L5000-1	35	50.00	620.0	3.710	-0.117	3.900	-0.253
RH _{cg} CE150L5000-2	35	50.00	566.4	2.330	0.090	****	****
RH _{cg} CE150L0500-1	32	5.000	596.8	4.120	-0.199	*****	****
RH _{cg} CE150L0500-2	40	5.000	638.4	3.520	0.083	5.300	-0.419
RH _{cg} CE150L0200-1	36	2.000	587.2	3.860	-0.211	3.980	-0.240
RH _{cg} CE150L0200-2	36	2.000	547.2	3.410	-0.204	****	*****
RH _{cg} CE150L0050-1	38	0.500	562.4	3.630	-0.286	7.070	-0.895
RH _{cg} CE150L0034-1	35	0.340	596.8	3.830	0.030	****	****
RH _{cg} CE150L0034-2	37	0.340	579.2	4.250	-0.293	8.140	-1.186
RH _{cg} CE150L0015-1	36	0.150	571.2	4.480	-0.502	5.860	-2.041
RH _{cg} CE150L0015-2	37	0.150	560.0	4.470	-0.519	4.630	-0.674
RH _∞ CE150L0005-1	38	0.050	568.0	4.995	-0.515	5.530	-0.731
RH _{cg} CE150L0001-1	32	0.010	609.6	6.490	-0.582	8.540	-1.742

Table E-11 Results in strain rate sensitivity tests for NSC under eccentric compression (e/d = 0.075) with longitudinal strain rate control (reference tests in Table D-1 and D-2)

Test	t _o	(dε)√dt	P _{max}	బ ('	10 ⁻³)	€cu (10 ⁻³)
No.	(days)	(×10 ⁻⁶ s ⁻¹)	(KN)	€cc0	Ect0	Есси	Ectu
RN _{eg} CE75L2500-1	37	2.500	280.0	2.110	0.746	6.876	-1.851
RN _{eg} CE75L2500-2	37	2.500	258.4	1.738	0.758	3.563	-0.800
RN _{cg} CE75L2500-3	37	2.500	272.0	1.865	0.564	6.238	-3.895
RN _{cg} CE75L1000-1	42	1.000	256.0	1.753	0.690	7.454	-3.345
RN _{cg} CE75L1000-2	43	1.000	256.8	1.744	0.903	6.909	-2.350
RN _{cg} CE75L0170-1	62	0.170	248.8	2.306	0.503	4.459	-0.755
RN _{cg} CE75L0075-1	34	0.075	248.0	2.319	0.561	6.710	-2.028
RN _∞ CE75L0075-2	35	0.075	256.8	2.336	0.729	7.410	-1.195
RN _∞ CE75L0008-1	43	0.008	292.0	2.850	1.318	6.429	-1.380
RN _{cg} CE75L0008-2	49	0.008	307.2	3.045	1.104	5.261	0.499
RN _{eg} CE75L0005-1	28	0.005	292.0	2.513	1.138	****	****
RN _{ég} CE75L0005-2	37	0.005	330.4	4.484	1.276	7.631	-1.113

Table E-12 Results in strain rate sensitivity tests for NSC under eccentric compression (e/d = 0.15) with longitudinal strain rate control (reference tests in Table D-1 and D-2)

Test	to	(dε)₁/dt	P _{max}	£0 (10 ⁻³)	ε _{cu} (10 ⁻³)	
No.	(days)	(×10 ⁻⁶ s ⁻¹)	(KN)	Ecc0	Ec.10	Eccu	Ectu
RN _{cg} CE150L2500-1	29	2.500	203.2	2.029	-0.098	5.539	-5.080
RN _{cg} CE150L2500-2	29	2.500	201.6	2.363	-0.159	5.144	-2.505
RN _{cg} CE150L2500-3	29	2.500	208.0	2.333	-0.260	4.783	-3.246
RN _{cg} CE150L1000-1	32	1.000	201.6	2.335	-0.218	7.040	-3.810
RN _{cg} CE150L1000-2	32	1.000	212.0	2.509	-0.245	7.353	-4.469
RN _{cg} CE150L0075-1	28	0.075	208.0	2.219	-0.065	****	****
RN _{cg} CE150L0075-2	29	0.075	205.6	2.805	-0.315	4.894	-1.559
RN _{cg} CE150L0050-1	30	0.050	226.4	2.849	-0.223	3.786	-2.210
RN _{eg} CE150L0050-2	32	0.050	218.4	3.171	-0.394	4.775	-1.511
RN _{eg} CE150L0008-1	30	0.008	257.6	4.550	-0.689	5.788	-1.469
RN _{cg} CE150L0005-1	35	0.005	238.4	3.535	-0.264	****	****

Table E-13 Results in strain rate sensitivity tests for HSC under eccentric tension (e/d = 1/6) with longitudinal strain rate control (reference tests in Table D-1 and D-2)

Test	t _o	(dε)₁/dt	P _{tmax}	<i>ε</i> ю ('	10 ⁻³)	ε _{tυ} (10 ⁻³	
No.	(days)	(×10 ⁻⁶ s ⁻¹)	(KN)	€#0	€tc0	Ettu	€tcu
RH _{cg} TE1/6L2300-1	41	23	27.45	0.230	-0.031	0.775	-0.293
RH _{cg} TE1/6L2300-2	41	23	25.10	0.216	-0.042	0.359	-0.122
RH _{cg} TE1/6L0230-1	30	2.3	27.95	0.220	-0.037	1.418	-0.526
RH _{cg} TE1/6L0230-2	30	2.3	26.50	0.164	0.004	1.316	-0.473
RH _{cg} TE1/6L0023-1	45	0.23	24.70	0.239	-0.045	0.466	-0.168
RH _{cg} TE1/6L0023-2	45	0.23	28.55	0.173	0.064	0.173	0.064
RH _{cg} TE1/6L0008-1	41	0.08	23.90	0.195	-0.018	0.448	-0.145
RH _{cg} TE1/6L0008-2	41	0.08	23.70	0.241	-0.014	0.425	-0.095
RH _{cg} TE1/6L0003-1	43	0.03	22.90	0.209	-0.043	0.495	-0.185
RH _{cg} TE1/6L0003-2	43	0.03	26.40	0.214	-0.014	0.543	-0.183
RH _{cg} TE1/6L0001-1	34	0.01	22.50	0.232	-0.042	0.623	-0.213
RH _∞ TE1/6L0001-2	35	0.01	20.75	0.139	-0.023	0.139	-0.023

Table E-14 Results in strain rate sensitivity tests for NSC under eccentric tension (e/d = 1/3) with longitudinal strain rate control (reference tests in Table D-1 and D-2)

Test	t _o	(dε)√dt	P _{tmax}	ε ₁₀ (10 ⁻³)		ε _{tu} (10 ⁻³)	
No.	(days)	(×10 ⁻⁶ s ⁻¹)	(KN)	€tt0	€tc0	Ettu	Etcu
RN _{cg} TE1/3L2300-1	31	23	13.85	0.148	-0.015	1.155	-0.158
RN _{cg} TE1/3L2300-2	31	23	14.75	0.148	-0.005	1.020	-0.139
RN _{c9} TE1/3L0230-1	28	2.3	17.70	0.132	-0.003	3.020	-0.360
RN _{cg} TE1/3L0230-2	31	2.3	12.50	0.170	-0.017	1.300	-0.146
RN _{cg} TE1/3L0008-1	30	0.08	14.35	0.134	0.002	0.134	0.002
RN _{cg} TE1/3L0008-2	30	0.08	12.75	0.186	-0.012	1.343	-0.251
RN _{cg} TE1/3L0003-1	28	0.03	18.85	0.123	0.003	1.832	-0.375
RN _{cg} TE1/3L0003-2	29	0.03	16.80	0.193	-0.005	2.270	-0.405
RN _{cg} TE1/3L0001-1	31	0.01	14.80	0.184	-0.010	1.811	-0.245

Table E-15 Results in strain rate sensitivity tests for HSC under eccentric tension (e/d = 1/3) with longitudinal strain rate control (reference tests in Table D-1 and D-2)

Test	t ₀	(dε)√dt	P _{tmax}	ειο (10 ⁻³)	ε _{tu} (10 ⁻³)
No.	(days)	(×10 ⁻⁶ s ⁻¹)	(KN)	EHO	Etc0	Ettu	€tcu
RH _∞ TE1/3L2300-1	35	23	20.75	0.291	-0.093	0.577	-0.208
RH _{cg} TE1/3L2300-2	35	23	22.45	0.264	-0.087	0.686	-0.258
RH _{cg} TE1/3L2300-3	35	23	23.85	0.282	-0.074	0.659	-0.220
RH _{og} TE1/3L0230-1	28	2.3	22.60	0.225	-0.070	0.689	-0.254
RH _{cg} TE1/3L0230-2	28	2.3	22.40	0.202	-0.062	0.670	-0.255
RH _{cg} TE1/3L0230-3	28	2.3	19.90	0.239	-0.075	0.714	-0.240
RH _{eg} TE1/3L0023-1	35	0.23	19.05	0.320	-0.110	0.618	-0.235
RH _{eg} TE1/3L0023-2	35	0.23	25.95	0.266	-0.068	0.743	-0.256
RH _{ep} TE1/3L0023-3	38	0.23	22.95	0.282	-0.086	0.755	-0.263
RH _{eg} TE1/3L0008-1	37	0.08	21.90	0.334	-0.111	0.793	-0.265
RH _{cg} TE1/3L0008-2	37	0.08	21.80	0.186	-0.030	0.448	-0.132
RH _{cg} TE1/3L0008-3	38	0.08	19.25	0.232	-0.057	0.386	-0.125
RH _{cg} TE1/3L0003-1	31	0.03	17.25	0.216	-0.071	0.907	-0.316
RH _{eg} TE1/3L0003-2	34	0.03	19.75	0.214	-0.065	0.695	-0.259
RH _{cg} TE1/3L0003-3	36	0.03	23.05	0.261	-0.072	0.723	-0.251
RH _{eg} TE1/3L0001-1	28	0.01	18.15	0.227	-0.055	0.995	-0.360
RH _{cg} TE1/3L0001-2	29	0.01	18.25	0.309	-0.087	0.868	-0.309
RH _{eg} TE1/3L0001-3	30	0.01	18.25	0.348	-0.110	0.893	-0.330

Table E-16 Results in strain rate sensitivity tests for HSC and NSC under centric tension (softening) with longitudinal strain rate control (reference tests in Table D-1 and D-2)

Test	t ₀	d∉ldt	G tmax	Et	<i>ε</i> ₁₀ (10 ⁻³)
No.	(days)	10 ⁻⁶ s ⁻¹	(N/mm²)	10 ³ N/mm ²	€tsh0	EtIO
RH _{cg} TUSFL0230-1	28	2.30	4.88	50.84	0.267	0.131
RH _{cg} TUSFL0230-2	28	2.30	4.65	47.40	0.262	0.139
RH _{cg} TUSFL0230-3	28	2.30	4.78	45.76	0.250	0.129
average	28	2.30	4.77	48.00	0.260	0.133
SD			0.09	2.117	0.007	0.004
RH _{cg} TUSFL0023-1	28	0.23	4.81	49.12	0.221	0.128
RH _{cg} TUSFL0023-2	29	0.23	3.96	47.47	0.273	0.126
RH _{cg} TUSFL0023-3	29	0.23	4.61	46,18	0.242	0.122
RH _{cg} TUSFL0023-4	29	0.23	4.69	47.50	0.239	0.126
average	29	0.23	4.52	47.57	0.244	0 126
SD			0.33	1.043	0.019	0.002
RN _{cg} TUSFL0230-1	28	2.30	2.12	27.15	0.190	0.101
RNcgTUSFL0230-2	28	2.30	2.35	29.76	0.193	0.102
RN _{cg} TUSFL0230-3	28	2.30	2.02	29.29	0.196	0.094
RN _{cg} TUSFL0230-4	28	2.30	2.23	30.14	0.168	0.089
average	28	2.30	2.18	29.09	0 187	0.097
SD			0,12	1.157	0.011	0.005
RN _{cg} TUSFL0023-1	29	0.23	1.82	31.55	0.188	0.087
RN _{cg} TUSFL0023-2	29	0.23	2.61	35.03	0.102	0.103
RN₀gTUSFL0023-3	29	0.23	2.14	30.92	0.231	0.104
RN _{cg} TUSFL0023-4	29	0.23	1.89	27.08	0.153	0.075
average	29	0.23	2.12	31.15	0.169	0.093
SD			0.31	2.821	0.047	0.012

Table E-17 Results in high sustained loading tests for HSC (reference tests in Table D-3)

Test	t ₀	$\sigma_c(t_0)/f_{cp28}$	t-t ₀	$\varepsilon_{ie}(t_0)$	(10 ⁻³)	€cu (10 ⁻³)
No.	(days)	at to	(hours)	Ecli	Ectri	Eclu	Ectru
SH∞ _S CU75 _c - 1	28	0.75	47.5*	1.911	0.454	3.161	0.992
SH _{cg} CU75 _c - 2	28	0.75	71.0*	1.923	0.495	3.186	1.017
SH _{cg} CU75 _c - 3	28	0.75	69.6*	1.831	0.386	3.018	0.797
average	28	0.75	62.7	1.888	0.445	3,122	0.935
SD			10.76	0.041	0.045	0.074	0.098
SH _{cg} CU85 _c - 1	28	0.85	0.68	2.379	0.575	2.803	0.826
SH _{cg} CU85 _c - 2	28	0.85	0.94	2.401	0.554	3.319	1.527
SH _∞ CU85₀ - 3	28	0.85	2.52	2.355	0.493	3.278	1.798
average	28	0.85	1.38	2.378	0.537	3.133	1.384
SĐ			0.81	0.019	0.039	0.234	0.409
SH _{cg} CU95 _c - 1	28	0.95	0.20	2.659	0.753	2.888	1.386
SH _{cg} CU95 _c - 2	28	0.95	0.21	2.424	0.689	2.520	0.723
SH _{cg} CU95 _c - 3	28	0.95	0.19	2.764	0.896	2.933	1.174
average	28	0.95	0.20	2.616	0.779	2.780	1.094
SD			0.008	0.142	0.087	0.185	0.276

^{*} Test were stoped deliberately

Table E-17 Results in high sustained loading tests for HSC (reference tests in Table D-3)[continued]

Test	f _{cp28}	(ds/dt)i	σ _{ci}	Eci
No.	(N/mm²)	10 ⁻⁶ s ⁻¹	(N/mm ²)	(10 ³ N/mm ²)
SH _{cg} CU75 _c - 1	85.3	4.35	64.0	35.1
SH _{cg} CU75 _c - 2	86.4	4.40	64.8	35.5
SH _{cg} CU75 _c - 3	86.3	4.35	64.7	36.4
average	86,0	4.37	64.5	35.7
50	0.50	0.02	0.36	0.54
SH _{cg} CU85 _c - 1	97.6	3.85	83.0	36.8
SH _{cg} CU85 _c - 2	98.9	3.98	84.1	36.9
SH _{cg} CU85 _c - 3	98.4	3.90	83.6	36.6
average	98.3	3.91	83.6	36.8
SD	0.54	0.05	0.45	0.12
SH _{cg} CU95 _c - 1	97.1	4.15	92.2	37.3
SH _{cg} CU95 _c - 2	97.1	4.09	92.2	37.1
SH _{cg} CU95 _c - 3	96.2	4.45	91.4	36.4
average	96.8	4.23	91.9	36.9
SD	0.42	0.16	0.38	0.39

Table E-19 Creep test results for HSC with a constant compressive loading applied at an age of 28 days (reference tests in Table D-4)

Test	to	$\sigma_c(t_0)/f_{cp28}$	t-t ₀	f _{cp28}	$\varepsilon_{sh}(t)$	$\varepsilon_c(t, t_0)$	$\varepsilon_{ie}(t_0)$
No.	(days)	at to	(days)	(N/mm²)	(10 ⁻³)	(10 ⁻³)	(10 ⁻³)
C _n H _{cg} CU15 _c - 1	28	0.15	216	100.2	0.234	0.690	0.293
C _n H _{cg} CU15 _c - 2	28	0.15	216	100.2	0.236	0.680	0.290
C _n H _{eg} CU35 _c - 1	28	0.35	210	102.5	0.263	1.455	0.758
C _n H _{cg} CU35 _c - 2	28	0.35	210	102.5	0.267	1.468	0.768
C _n H _{cg} CU50 _c - 1	28	0.50	203	97.48	0.247	1.958	1.013
C _n H _{cg} CU50 _c - 2	28	0.50	203	97.48	0.243	1.943	0.998

Table E-20 Creep test results for HSC with step-wise compressive loading applied at an age of 28 days (reference tests in Table D-5)

Test	t ₀	$\sigma_c(t_0)/f_{cp28}$	t-t ₀	f _{cp28}	$arepsilon_{sh}(t)$	$\varepsilon_c(t, t_0)$	$\varepsilon_{ie}(t_0)$
No.	(days)	at t ₀	(days)	(N/mm ²)	(10 ⁻³)	(10 ⁻³)	(10 ⁻³)
C _n H _{eg} CU12.5 _v - 1.1	28	0.125	12	75.86	0.029	0.309	0.205
C _n H _{cg} CU12.5 _v - 2.1	28	0.125	12	75.86	0.038	0.301	0.193
C _n H _{cg} CU12.5 _v - 1.2	40	0.250	11	75.86	0.048	0.643	0.219
C _n H _{cg} CU12.5 _v - 2.2	40	0.250	11	75.86	0.062	0.635	0.198
C _n H _{cg} CU12.5 _v - 1.3	51	0.375	11	75.86	0.067	0.996	0.204
C _n H _{cg} CU12.5 _v - 2.3	51	0.375	11	75.86	0.079	0.987	0.192
C _n H _{cg} CU12.5 _v - 1.4	62	0.500	11	75.86	0.074	1.349	0.200
C _n H _{cg} CU12.5 _v - 2.4	62	0.500	11	75.86	0.094	1.334	0.191
C _n H _{∞g} CU25, - 1.1	28	0.250	23	75.86	0.048	0.647	0.421
C _n H _{eg} CU25 _v - 2.1	28	0.250	23	75.86	0.060	0.658	0.434
C _n H _{eg} CU25 _v - 1.2	51	0.500	22	75.86	0.075	1.237	0.303
C _n H _{cg} CU25 _v - 2.2	51	0.500	22	75.86	0.094	1.366	0.385
C _n H _{cg} CU50 _v - 1	28	0.500	45	75.86	0.079	1.553	0.880
C _n H _{cg} CU50 _v - 2	28	0.500	45	75.86	0.094	1.421	0.805

Table E-21 Results of creep recovery tests for HSC step-wisely loaded at an age of 28 days and step-wisely unloaded at an age of 73 days (reference tests in Table D-5)

Test	to	$\sigma_c(t_0)/f_{cp28}$	t-t ₀	$\varepsilon_{sh}(t)$	$\varepsilon_c(t, t_0)$	$\varepsilon_{co}(t_0)$	$arepsilon_{irec}(t_0)$
No.	(days)	at to	(days)	(10 ⁻³)	(10 ⁻³)	(10 ⁻³)	(10 ⁻³)
C _n H _{cg} CU12.5 _v - 1.1	73	0.375	12	0.097	1.184	1.267	-0.150
C _n H _{cg} CU12.5 _v - 2.1	73	0.375	12	0.097	1.177	1.263	-0.142
C _n H _{cg} CU12.5 _v - 1.2	85	0.250	11	0.104	0.995	1.084	-0.184
C _n H _{cg} CU12.5 _v - 2.2	85	0.250	11	0.104	0.991	1.079	-0.178
C _n H _{cg} CU12.5 _v - 1.3	96	0.125	11	0.113	0.778	0.891	-0.209
C _n H _{cg} CU12.5 _v - 2.3	96	0.125	11	0.113	0.771	0.884	-0.205
C _n H _{cg} CU12.5 _v - 1.4	107	0.000	11	0.123	0.471	0.666	-0.264
C _n H _{cg} CU12.5 _v - 2.4	107	0.000	11	0.123	0.459	0.657	-0.258
C _n H _{cg} CU25 _v - 1.1	73	0.250	23	0.104	0.958	1.282	-0.366
C _n H _{eg} CU25 _v - 2.1	73	0.250	23	0.104	0.918	1.154	-0.281
C _n H _{eg} CU25 _v - 1.2	96	0.000	22	0.123	0.500	0.854	-0.398
C _n H _{dg} CU25 _v - 2.2	96	0.000	22	0.123	0.550	0.814	-0.376
C _n H _{cg} CU50 _v - 1	73	0.000	45	0.123	0.566	1.467	-0.860
C _n H _{og} CU50 _v - 2	73	0.000	45	0.123	0.501	1.399	-0.851

Table E-22 Results for HSC with crushed gravel in compressive creep tests at a loading age of 10 hours (reference tests in Table D-6)

Test	t _o	$\sigma_c(t_0)/f_{cp28}$	t-t _o	$f_{cp}(t_0)$	$\varepsilon_{sh}(t)$	$\varepsilon_c(t, t_0)$	$\varepsilon_{ie}(t_0)$
No.	(hours)	at to	(days)	(N/mm ²)	(10 ⁻³)	(10 ⁻³)	(10 ⁻³)
C _e 10H _{cg} CU30 _c - 1	10	0.30	90	8.46	0.520	0.965	0.155
C _e 10H _{cg} CU30 _c - 2	10	0.30	90	8.46	0.520	0.940	0.150
C _e 10H _{cg} CU50 _c - 1	10	0.50	90	8.46	0.520	1.350	0.460
C _e 10H _{cg} CU50 _c - 2	10	0.50	90	8.46	0.520	1.370	0.455
C _e 10H _{cg} CU70 _c - 1	10	0.70	90	8.46	0.520	1.405	0.565
C _e 10H _{cg} CU70 _c - 2	10	0.70	90	8.46	0.520	1.445	0.555

Table E-23 Results for HSC with granite in compressive creep tests at a loading age of 10 hours (reference tests in Table D-7)

Test No.	t ₀ (hours)	$\sigma_c(t_0)/f_{cp28}$ at t_0	t-t ₀ (days)	$f_{cp}(t_0)$ (N/mm ²)	$\varepsilon_{sh}(t)$ (10^{-3})	$\varepsilon_c(t, t_0)$ (10^{-3})	$\varepsilon_{ie}(t_0)$ (10^{-3})
	<u> </u>					<u> </u>	
C _e 10H _{gr} CU30 _c - 1	10	0.30	90	9.42	0.550	0.890	0.160
C _e 10H _{gr} CU30 _c - 2	10	0.30	90	9.42	0.550	0.910	0.150
C _e 10H _{gr} CU50 _c - 1	10	0.50	90	9.42	0.550	1.255	0.320
C _e 10H _{gr} CU50 _c - 2	10	0.50	90	9.42	0.550	1.250	0.320
C _e 10H _{gr} CU70 _c - 1	10	0.70	90	9.42	0.550	1.535	0.430
C _e 10H _{gr} CU70 _c - 2	10	0.70	90	9.42	0.550	1.555	0.400

Table E-24 Results for HSC with limeston in compressive creep tests at a loading age of 10 hours (reference tests in Table D-8)

Test No.	t ₀ (hours)	$\sigma_c(t_0)/f_{cp28}$ at t_0	t-t ₀ (days)	$f_{cp}(t_0)$ (N/mm ²)	ε _{sh} (t) (10 ⁻³)	$\varepsilon_c(t, t_0)$ (10^{-3})	$\varepsilon_{ie}(t_0)$ (10^{-3})
C _e 10H _{is} CU30 _c - 1	10	0.30	90	5.80	0.385	0.685	0.120
C _e 10H _{Is} CU30 _c - 2	10	0.30	90	5.80	0.385	0.705	0.120
C _e 10H _{Is} CU50 _c - 1	10	0.50	90	5.80	0.385	0.910	0.180
C _e 10H _{fs} CU50 _c - 2	10	0.50	90	5.80	0.385	0.930	0.185
C _e 10H _{Is} CU70 _c - 1	10	0.70	90	5.80	0.385	1,135	0.320
C _e 10H _{Is} CU70 _c - 2	10	0.70	90	5.80	0.385	1.105	0.265

Table E-25 Results for HSC with crushed gravel in compressive creep tests at a loading age of 16 hours (reference tests in Table D-9)

Test	to	$\sigma_c(t_0)/f_{cp28}$	t-t ₀	$f_{cp}(t_0)$	$arepsilon_{sh}(t)$	$\varepsilon_c(t, t_0)$	$\varepsilon_{ie}(t_0)$
No.	(hours)	at to	(days)	(N/mm²)	(10 ⁻³)	(10 ⁻³)	(10 ⁻³)
C _e 16H _{cg} CU30 _c - 1	16	0.30	90	46.4	0.410	1.630	0.485
C _e 16H _{cg} CU30 _c - 2	16	0.30	90	46.4	0.410	1.625	0.500
C _e 16H _{cg} CU50 _c - 1	16	0.50	90	46.4	0.410	2.325	0.860
C _e 16H _{cg} CU50 _c - 2	16	0.50	90	46.4	0.410	2.300	0.830
C _e 16H _{cg} CU70 _c - 1	16	0.70	90	46.4	0.410	3.200	1.300
C _e 16H _{cg} CU70 _c - 2	16	0.70	90	46.4	0.410	3.115	1.295

Table E-26 Results for HSC with granite in compressive creep tests at a loading age of 16 hours (reference tests in Table D-10)

Test	to	$\sigma_c(t_0)/f_{cp28}$	t-t ₀	$f_{cp}(t_0)$	$\varepsilon_{sh}(t)$	$\varepsilon_c(t, t_0)$	$\varepsilon_{ie}(t_0)$
No.	(hours)	at to	(days)	(N/mm ²)	(10 ⁻³)	(10 ⁻³)	(10 ⁻³)
C _e 16H _{gr} CU30 _c - 1	16	0.30	90	46.0	0.395	1.510	0.495
C _e 16H _{gr} CU30 _c - 2	16	0.30	90	46.0	0.385	1.505	0.475
C _e 16H _{gr} CU50 _c - 1	16	0.50	90	46.0	0.395	2.300	0.800
C _e 16H _{gr} CU50 _c - 2	16	0.50	90	46.0	0.385	2.315	0.820
C _e 16H _{gr} CU70 _c - 1	16	0.70	90	46.0	0.395	3.295	1.175
C _e 16H _{gr} CU70 _c - 2	16	0.70	90	46.0	0.385	3.480	1.275

Table E-27 Results for HSC with limestone in compressive creep tests at a loading age of 16 hours (reference tests in Table D-11)

Test No.	t ₀ (hours)	$\sigma_c(t_0)/f_{cp28}$ at t_0	<i>t-t</i> ₀ (days)	$f_{cp}(t_0)$ (N/mm ²)	$\varepsilon_{sh}(t)$ (10^{-3})	$\varepsilon_c(t, t_0)$ (10^{-3})	ε _{ie} (t ₀) (10 ⁻³)
C _e 16H _{is} CU30 _c - 1	16	0.30	90	43.7	0.330	1.250	0.360
C _e 16H _{is} CU30 _c - 2	16	0.30	90	43.7	0.340	1.180	0.350
C _e 16H _{is} CU50 _c - 1	16	0.50	90	43.7	0.330	1.925	0.600
C _e 16H _{is} CU50 _c - 2	16	0.50	90	43.7	0.340	2.075	0.620
C _e 16H _{Is} CU70 _c - 1	16	0.70	90	43.7	0.330	2.935	0.940
C _e 16H _{is} CU70 _c - 2	16	0.70	90	43.7	0.340	2.865	0.925

Table E-28 Results for HSC with crushed gravel in creep recovery tests at a loading age of 10 hours and a unloading age of 90 days (reference tests in Table D-6)

Test	t ₀	t-to	$\sigma_c(t_0)$	$\varepsilon_{sh}(t)$	$\varepsilon_c(t, t_0)$	$\varepsilon_{co}(t_0)$	$\varepsilon_{irec}(t_0)$
No.	(days)	(days)	(N/mm²)	(10 ⁻³)	(10 ⁻³)	(10 ⁻³)	(10 ⁻³)
C _e 10H _{c9} CU30 _c - 1	90	90	-2.54	0.579	0.945	0.965	-0.050
C _e 10H _{cg} CU30 _c - 2	90	90	-2.54	0.579	0.920	0.940	-0.055
C _e 10H _{cg} CU50 _c - 1	90	90	-4.23	0.579	1.265	1.350	-0.100
C _e 10H _{cg} CU50 _c - 2	90	90	-4.23	0.579	1.260	1.370	-0.120
C _e 10H _{cg} CU70 _c - 1	90	90	-5.92	0.579	1.255	1.405	-0.155
C _e 10H _{cg} CU70 _c - 2	90	90	-5.92	0.579	1.280	1.445	-0.165

Table E-29 Results for HSC with granite in creep recovery tests at a loading age of 10 hours and a unloading age of 90 days (reference tests in Table D-7)

Test No.	t ₀ (hours)	t-t ₀ (days)	$\sigma_c(t_0)$ (N/mm ²)	$\varepsilon_{sh}(t)$ (10^{-3})	$\varepsilon_c(t, t_0)$ (10^{-3})	$\varepsilon_{c\sigma}(t_0)$ (10 ⁻³)	$\varepsilon_{irec}(t_0)$ (10^{-3})
C _e 10H _{gr} CU30 _c - 1	90	90	-2.83	0.596	0.845	0.890	-0.075
C _e 10H _{gr} CU30 _c - 2	90	90	-2.83	0.596	0.860	0.910	-0.065
C _e 10H _{gr} CU50 _c - 1	90	90	-4.71	0.596	1.140	1.255	-0.130
C _e 10H _{gr} CU50 _c - 2	90	90	-4.71	0.596	1.130	1.250	-0.130
C _e 10H _{gr} CU70 _c - 1	90	90	-6.59	0.596	1.330	1.535	-0.190
C _e 10H _{gr} CU70 _c - 2	- 90	90	-6.59	0.596	1.375	1.555	-0.185

Table E-30 Results for HSC with limeston in creep recovery tests at a loading age of 10 hours and a unloading age of 90 days (reference tests in Table D-8)

Test	to	t-t ₀	$\sigma_c(t_0)$	$\varepsilon_{sh}(t)$	$\varepsilon_c(t, t_0)$	$\varepsilon_{co}(t_0)$	$\varepsilon_{irec}(t_0)$
No.	(hours)	(days)	(N/mm ²)	(10 ⁻³)	(10 ⁻³)	(10 ⁻³)	(10 ⁻³)
C _e 10H _{is} CU30 _c - 1	90	90	-1.74	0.423	0.670	0.685	-0.030
C _e 10H _{is} CU30 _c - 2	90	90	-1.74	0.423	0.685	0.705	-0.030
C _e 10H _{Is} CU50 _c - 1	90	. 90	-2.90	0.423	0.860	0.910	-0.055
C _e 10H _{Is} CU50 _c - 2	90	90	-2.90	0.423	0.875	0.930	-0.060
C _e 10H _{Is} CU70 _c - 1	90	90	-4.06	0.423	1.040	1.135	-0.090
C _e 10H _{Is} CU70 _c - 2	90	90	-4.06	0.423	1.025	1.105	-0.080

Table E-31 Results for HSC with crushed gravel in creep recovery tests at a loading age of 16 hours and a unloading age of 90 days (reference tests in Table D-9)

Test	t _o	t-t ₀	$\sigma_c(t_0)$	$\varepsilon_{sh}(t)$	$\varepsilon_c(t, t_0)$	$\varepsilon_{c\sigma}(t_0)$	$\varepsilon_{irec}(t_0)$
No.	(hours)	(days)	(N/mm²)	(10 ⁻³)	(10 ⁻³)	(10 ⁻³)	(10 ⁻³)
C _e 16H _{cg} CU30 _c - 1	90	90	-13.9	0.468	1.165	1.630	-0.405
C _e 16H _{cg} CU30 _c - 2	90	90	-13.9	0.468	1.145	1.625	-0.420
C _e 16H _{cg} CU50 _c - 1	90	90	-23.1	0.468	1.595	2.325	-0.545
C _e 16H _{cg} CU50 _c - 2	90	90	-23.1	0.468	1.605	2.300	-0.520
C _e 16H _{cg} CU70 _c - 1	90	90	-32.4	0.468	2.075	3.200	-0.780
C _e 16H _{cg} CU70 _c - 2	90	90	-32.4	0.468	2.240	3.115	-0.725

Table E-32 Results for HSC with granite in creep recovery tests at a loading age of 16 hours and a unloading age of 90 days (reference tests in Table D-10)

Test No.	t ₀ (hours)	<i>t-t</i> ₀ (days)	$\sigma_{c}(t_{0})$ (N/mm ²)	$\varepsilon_{sh}(t)$ (10^{-3})	$\varepsilon_c(t, t_0)$ (10^{-3})	$\varepsilon_{c\sigma}(t_0)$ (10^{-3})	ε _{irec} (t ₀) (10 ⁻³)
C _e 16H _{gr} CU30 _c - 1	90	90	-13.8	0.450	1.070	1.510	-0.345
C _e 16H _{gr} CU30 _c - 2	90	90	-13.8	0.450	1.045	1.505	-0.360
C _e 16H _{gr} CU50 _c - 1	90	90	-23.0	0.450	1.570	2.300	-0.525
C _e 16H _{gr} CU50 _c - 2	90	90	-23.0	0.450	1.595	2.315	-0.530
C _e 16H _{gr} CU70 _c - 1	90	90	-32.2	0.450	2.320	3.295	-0.785
C _e 16H _{gr} CU70 _c - 2	90	90	-32.2	0.450	2.225	3.480	-0.845

Table E-33 Results for HSC with limestone in creep recovery tests at a loading age of 16 hours and a unloading age of 90 days (reference tests in Table D-11)

Test No.	t ₀ (hours)	t-t ₀ (days)	$\sigma_c(t_0)$ (N/mm ²)	$\varepsilon_{sh}(t)$ (10^{-3})	$\varepsilon_c(t, t_0)$ (10 ⁻³)	$\varepsilon_{c\sigma}(t_0)$ (10 ⁻³)	$\varepsilon_{irec}(t_0)$ (10^{-3})
C _e 16H _{is} CU30 _c - 1	90	90	-13.1	0.381	0.875	1.250	-0.285
C _e 16H _{Is} CU30 _c - 2	90	90	-13.1	0.381	0.695	1.180	-0.180
C _e 16H _{is} CU50 _c - 1	90	90	-21.9	0.381	1.280	1.925	-0.480
C _e 16H _{Is} CU50 _c - 2	90	90	-21.9	0.381	1.430	2.075	-0.495
C _e 16H _{Is} CU70 _c - 1	90	90	-30.6	0.381	2.005	2.935	-0.680
C _e 16H _{is} CU70 _c - 2	90	90	-30.6	0.381	1.945	2.865	-0.685

Appendix **F**Results of experimental analysis

In this appendix, the results of experimental analysis on the basis of the test data obtained in four test series are shown. This forms a base for the discussions carried out in *Chapter 6* and *Chapter 7*. All items used in this appendix are described in *Chapter 5*.

Table F-1 Statistical analysis of results in strain rate sensitivity tests of HSC under centric compression with transverse strain rate control (reference tests in Table D-1 and D-2)

Test	Statistic	(dε)₁/dt	O _{cmax}	σ _{cmax} /f _{cc28}	ణ ('	10 ⁻³)
No.	item	(×10 ⁻⁶ s ⁻¹)	(N/mm²)		<i>Ec1</i> 0	Ec#0
RH₀gCUT0625	average	6.25	93.93	0.804	3.059	0.864
(3)	SD	0.00	0.130	0.001	0.077	0.105
RH _{cg} CUT0250	average	2.50	91.89	0.787	3.053	0.904
(2)	SD	0.00	1.380	0.011	0.064	0.064
RH _{cg} CUT0043	average	0.43	86.85	0.743	2.899	0.880
(2)	SD	0.00	0.825	0.007	0.105	0.193
RH _{cg} CUT0019	average	0.19	83.38	0.714	3.133	0.924
(2)	SD	0.00	0.075	0.000	0.056	0.055
RH _{cg} CUT0002	average	0.02	77.23	0.661	3.704	1.317
(2)	SD	0.00	1.980	0.017	0.069	0.136
RH _{bg} CUT0001	average	0.01	82.36	0.709	4.099	1.857
(2)	SD	0.00	0.800	0.011	0.017	0.107

Table F-2 Statistical analysis of results in strain rate sensitivity tests of HSC under centric compression with transverse strain rate control (reference tests in Table D-1 and D-2) [continued]

Test	Statistic	$[(d\varepsilon)_t/dt]_i$	Eci	μ	€ _{Vmax}	σ _{mvs} / σ _{cmax}
No.	item	(×10 ⁻⁶ s ⁻¹)	(GPa)		10 ⁻³	
RH _{cg} CUT0625	average	38.47	37.31	0.168	1.514	0.960
(3)	SD	0.694	1.005	0.004	0.021	0.017
RH _{cg} CUT0250	average	14.15	37.30	0.188	1.438	0.957
(2)	SD	0.250	0.825	0.009	0.011	0.006
RH _{cg} CUT0043	average	2.200	36.54	0.176	1.356	0.943
(2)	SD	0.100	0.185	0.003	0.063	0.057
RH _{cg} CUT0019	average	1.150	36.45	0.171	1.431	0.942
(2)	SD	0.050	0.040	0.002	0.000	0.012
RH _{cg} CUT0002	average	0.120	33.80	0.166	1.469	0.922
(2)	SD	0.010	0.420	0.006	0.062	0.009
RH _{cg} CUT0001	average	0.070	35.44	0.202	1.485	0.928
(2)	SD	0.010	0.705	0.031	0.045	0.013

Table F-3 Statistical analysis of results in strain rate sensitivity tests of NSC under centric compression with transverse strain rate control (reference tests in Table D-1 and D-2)

Test	Statistic	(dε)₁/dt	<i>Остах</i>	σ_{cmex}/f_{cc28}	s ₀ ('	10 ⁻³)
No.	item	(×10 ⁻⁶ s ⁻¹)	(N/mm²)		€cl0	€ctr0
RN _{cg} CUT0625	average	6.25	29.07	0.664	1.468	0.676
(3)	SD	0.00	0.412	0.021	0.130	0.132
RN₀gCUT0250	average	2.50	27.12	0.612	1.229	0.847
(3)	SD	0.00	2.282	0.051	0.168	0.527
RN _{cg} CUT0043	average	0.43	29.47	0.690	1.344	0.463
(2)	SD	0.00	1.100	0.025	0.158	0.071
RN _{cg} CUT0019	average	0.19	26.27	0.602	1.382	0.631
(2)	SD	0.00	2.135	0.057	0.154	0.163
RN _{cg} CUT0002	average	0.02	30.15	0.700	1.787	1.093
(2)	SD	0.00	0.480	0.011	0.020	0.043
RN₀gCUT0001	average	0.01	29.32	0.675	1.920	1.338
(2)	SD	0.00	0.375	0.020	0.086	0.289

Table F-4 Statistical analysis of results in strain rate sensitivity tests of NSC under centric compression with transverse strain rate control (reference tests in Table D-1 and D-2) [continued]

Test	Statistic	$[(d\varepsilon)_t/dt]_i$	Eci	μ	Evmax	σ _{mvs} l σ _{cmax}
No.	item	(×10 ⁻⁶ s ⁻¹)	(GPa)		10 ⁻³	
RN _{cg} CUT0625	average	28.07	31.65	0.196	0.389	0.810
(3)	SD	2.269	0.884	0.018	0.036	0.056
RN _{cg} CUT0250	average	13.13	31.98	0.190	0.426	0.926
(3)	SD	1.511	0.889	0.039	0.029	0.048
RN _{cg} CUT0043	average	2.000	32.10	0.212	0.447	0.952
(2)	SD	0.270	0.370	0.014	0.042	0.037
RN _{cg} CUT0019	average	0.930	29.82	0.188	0.387	0.865
(2)	SD	0.045	0.805	0.037	0.009	0.058
RN _{cg} CUT0002	average	0.130	28.41	0.167	0.456	0.761
(2)	SD	0.020	0.110	0.012	0.031	0.028
RN _{cg} CUT0001	average	0.060	30.81	0.250	0.410	0.874
(2)	SD	0.010	0.390	0.020	0.006	0.080

Table F-5 Statistical analysis of results in strain rate sensitivity tests of HSC under eccentric compression (e/d = 0.075) with longitudinal strain rate control (reference tests in Table D-1 and D-2)

Test	Statistic	(dɛ)√dt	P _{max}	£cc0	φ ₀ (10 ⁻⁵)	dφldt
No.	item	(×10 ⁻⁶ s ⁻¹)	(kN)	(10 ⁻³)	rad/mm	(10 ⁻⁸)
RH _{cg} CE75L2500	average	25.00	811.6	3.294	1.931	13.50
(2)	SD	0.000	2.000	0.050	0.071	0.020
RH _{cg} CE75L0250	average	2.500	801.6	3.397	1.979	1.330
(2)	SD	0.000	0.000	0.072	0.022	0.050
RH _{cg} CE75L0025	average	0.250	749.6	4.010	2.584	0.140
(2)	SD	0.000	12.00	0.051	0.186	0.010
RH _{cg} CE75L0003	average	0.025	747.2	4.787	3.391	0.016
(2)	SD	0.000	0.000	0.214	0.576	0.002

Table F-6 Statistical analysis of results in strain rate sensitivity tests of HSC under eccentric compression (e/d = 0.15) with longitudinal strain rate control (reference tests in Table D-1 and D-2)

Test	Statistic	(dε)√dt	P _{max}	€cc0	φ ₀ (10 ⁻⁵)	dφ/dt
No.	item	(×10 ⁻⁶ s ⁻¹)	(kN)	(10 ⁻³)	rad/mm	(10 ⁻⁸)
RH _{cg} CE150L1000	average	100.0	620.0	3.580	3.715	81.00
(1)	SD	0.000	0.000	0.000	0.000	0.000
RH _{cg} CE150L500	average	50.00	620.0	3.710	3.827	50.30
(2)	SD	0.000	0.000	0.000	0.000	0.000
RH _{cg} CE150L50	average	5.000	617.6	3.820	3.877	4.900
(2)	SD	0.000	20.80	0.300	0.445	0.200
RH _{cg} CE150L20	average	2.000	587.2	3.860	4.071	2.080
(2)	SD	0.000	0.000	0.000	0.000	0.000
RH _{cg} CE150L5	average	0.500	562.4	3.630	3,913	0.520
(1)	SD	0.000	0.000	0.000	0.000	0.000
RH _{cg} CE150L3.4	average	0.340	588.0	4.040	4.543	0.340
(2)	SD	0.000	8.800	0.210	0.000	0.000
RHcgCE150L1.5	average	0.150	565.6	4.475	4.887	0.160
(2)	SD	0.000	5.600	0.005	0.003	0.000
RH _{cg} CE150L0.5	average	0.050	568.0	4.995	5.510	0.050
(1)	SD	0.000	0.000	0.000	0.000	0.000
RH _{cg} CE150L0.1	average	0.010	609.6	6.490	7.072	0.010
(1)	SD	0.000	0.000	0.000	0.000	0.000

Table F-7 Statistical analysis of results in strain rate sensitivity tests of NSC under eccentric compression (e/d = 0.075) with longitudinal strain rate control (reference tests in Table D-1 and D-2)

Test	Statistic	(dε)₁/dt	P _{mex}	Ecc0	φ ₀ (10 ⁻⁵)	dφldt
No.	item	(×10 ⁻⁶ s ⁻¹)	(kN)	(10 ⁻³)	rad/mm	(10 ⁻⁸)
RN _{cg} CE75L2500	average	2.500	270.1	1.904	1.215	1.400
(3)	SD	0.000	8.916	0.154	0.168	0.141
RN _{cg} CE75L1000	average	1.000	256.4	1.749	0.952	0.400
(2)	SD	0.000	0.400	0.005	0.111	0.000
RN _{cg} CE75L0170	average	0.170	248.8	2.306	1.629	0.100
(1)	SD	0.000	0.000	0.000	0.000	0.000
RN _{cg} CE75L0075	average	0.075	252.4	2.328	1.650	0.050
(2)	SD	0.000	4.400	0.009	0.021	0.000
RN _{cg} CE75L0008	average	0.008	299.6	2.948	1.737	0.004
(2)	SD	0.000	7.600	0.098	0.205	0.001
RN _{cg} CE75L0005	average	0.005	330.4	4.484	3.208	0.003
(2)	SD	0.000	0.000	0.000	0.000	0.000

Table F-8 Statistical analysis of results in strain rate sensitivity tests of NSC under eccentric compression (e/d = 0.15) with longitudinal strain rate control (reference tests in Table D-1 and D-2)

Test	Statistic	(dε)√dt	P _{max}	£cc0	φ ₀ (10 ⁻⁵)	dφldt
No.	item	(×10 ⁻⁶ s ⁻¹)	(kN)	(10 ⁻³)	rad/mm	(10 ⁻⁸)
RN _{cg} CE150L2500	average	2,500	204.3	2.242	2.413	2.570
(3)	SD	0.000	2.719	0.151	0.205	0.060
RN _{cg} CE150L1000	average	1.000	206.8	2.422	2.653	1.050
(2)	SD	0.000	5.200	0.087	0.101	0.010
RN _{cg} CE150L0075	average	0.075	205.6	2.805	2.731	0.080
(2)	SD	0.000	0.000	0.000	0.000	0.000
RN _{cg} CE150L0050	average	0.050	222.4	2.950	3.273	0.060
(2)	SD	0.000	4.000	0.101	0.166	0.000
RN _{cg} CE150L0008	average	800.0	257.6	4.550	5.239	0.008
(1)	SD	0.000	0.000	0.000	0.000	0.000
RN _{cg} CE150L0005	average	0.005	238.4	3.535	3.799	0.005
(1)	SD	0.000	0.000	0.000	0.000	0.000

Table F-9 Statistical analysis of results in strain rate sensitivity tests of HSC under eccentric tension (e/d = 1/6) with longitudinal strain rate control (reference tests in Table D-1 and D-2)

Test	P _{tmax}	<i>E</i> ₈₀ (10 ⁻³)	х	σ _{ttm}	Ottc
No.	(kN)	€#O	Etc0	(mm)	(N/mm²)	(N/mm²)
RH _{cg} TE1/6L2300-1	27.45	0.230	-0.031	70.50	10.03	7.72
RH _{cg} TE1/6L2300-2	25.10	0.216	-0.042	66.98	10.95	7.06
RH _{cg} TE1/6L0230-1	27.95	0.220	-0.037	68.48	10.98	7.86
RH _{cg} TE1/6L0230-2	26.50	0.164	0.004	82.00	8.03	7.45
RH _{cg} TE1/6L0023-1	24.70	0.239	-0.045	67.32	10.37	6.95
RH _{cg} TE1/6L0023-2	28.55	0.173	0.064	126.9	6.76	8.03
RH _{cg} TE1/6L0008-1	23.90	0.195	-0.018	73.24	10.04	6.72
RH _{cg} TE1/6L00088-2	23.70	0.241	-0.014	75.61	7.57	6.67
RH _{cg} TE1/6L0003-1	22.90	0.209	-0.043	66.35	9.65	6.44
RH _{cg} TE1/6L0003-2	26.40	0.214	-0.014	75.09	8.54	7.43
RH _∞ TE1/6L0001-1	22.50	0.232	-0.042	67.74	9.84	6.33
RH _{cg} TE1/6L0001-2	20.75	0.139	-0.023	68.64	8.22	5.84

Table F-10 Statistical analysis of results in strain rate sensitivity tests of NSC under eccentric tension (e/d = 1/3) with longitudinal strain rate control (reference tests in Table D-1 and D-2)

Test	P _{tmex}	ε ₁₀ (10 ⁻³)		x	Ottm	Ottc
No.	(kN)	€#0	Etc0	(mm)	(N/mm²)	(N/mm²)
RN _{cg} TE1/3L2300-1	13.85	0.148	-0.015	72.64	4.99	6.06
RN _{cg} TE1/3L2300-2	14.75	0.148	-0.005	77.39	4.59	6.45
RN _{cg} TE1/3L0230-1	17.70	0.132	-0.003	78.22	5.34	7.74
RN _{cg} TE1/3L0230-2	12.50	0.170	-0.017	72.73	4.17	5.47
RN _∞ TE1/3L0008-1	14.35	0.134	0.002	81.21	4.09	6.28
RN _{cg} TE1/3L0008-2	12.75	0.186	-0.012	75.15	4.01	5.58
RN _{cg} TE1/3L0003-1	18.85	0.123	0.003	82.00	5.31	8.25
RN _{cg} TE1/3L0003-2	16.80	0.193	-0.005	77.98	5.10	7.35
RN _{cg} TE1/3L0001-1	14.80	0.184	-0.010	75.88	4.67	6.48

Table F-11 Statistical analysis of results in strain rate sensitivity tests of HSC under eccentric tension (e/d = 1/3) with longitudinal strain rate control (reference tests in Table D-1 and D-2)

Test	P _{tmax}	ε ₁₀ (10 ⁻³)		х	Ottm	σttc
No.	(kN)	Ett0	€tc0	(mm)	(N/mm ²)	(N/mm²)
RH _{cg} TE1/3L2300-1	20.75	0.291	-0.093	60.63	12.81	9.08
RH∞TE1/3L2300-2	22.45	0.264	-0.087	60.17	13.66	9.82
RH _{og} TE1/3L2300-3	23.85	0.282	-0.074	63.37	11.78	10.43
RH _{cg} TE1/3L0230-1	22.60	0.225	-0.070	61.02	12.60	9.89
RH _{cg} TE1/3L0230-2	22.40	0.202	-0.062	61.21	12.31	9.80
RH _{cg} TE1/3L0230-3	19.90	0.239	-0.075	60.89	11.45	8.71
RH _{cg} TE1/3L0023-1	19.05	0.320	-0.110	50.53	13.10	8.33
RH _{cg} TE1/3L0023-2	25.95	0.266	-0.068	63.71	12.77	11.35
RH _{cg} TE1/3L0023-3	22.95	0.282	-0.086	61.30	13.02	10.04
RH _{cg} TE1/3L0008-1	21.90	0.334	-0.111	60.04	13.99	9.58
RH _{cg} TE1/3L0008-2	21.80	0.186	-0.030	68.89	8.15	9.54
RH _{cg} TE1/3L0008-3	19.25	0.232	-0.057	64.22	8.87	8.42
RH _{cg} TE1/3L0003-1	17.25	0.216	-0.071	60.21	11.16	7.77
RH _{cg} TE1/3L0003-2	19.75	0.214	-0.065	61.36	10.81	8.64
RH _{cg} TE1/3L0003-3	23.05	0.261	-0.072	62.70	11.98	10.08
RH _{cg} TE1/3L0001-1	18.15	0.227	-0.055	64.40	8.57	7.94
RH _{cg} TE1/3L0001-2	18.25	0.309	-0.087	62.42	9.53	7.98
RH _{cg} TE1/3L0001-3	18.25	0.348	-0.110	60.79	10.70	7.98

Table F-12 Experimental analysis for HSC with crushed gravel in compressive creep tests at a loading age of 28 days (reference tests in Table D-4)

Test	Statistic	t-to	$\varepsilon_c(t, t_0)$	$\varepsilon_{sh}(t)$	$\varepsilon_{ie}(t_0)$	$\varepsilon_{cr}(t, t_0)$	<i>ф</i> 28	$C(t, t_0)$
No.	item	days	(10 ⁻³)	(10 ⁻³)	(10 ⁻³)	(10 ⁻³)		10 ⁻⁶
C _n H _{cg} CU15 _c	average	216	0.685	0.235	0.292	0.158	0.541	10.51
(2)	SD		0.005	0.001	0.002			
C _n H _{cg} CU35 _c	average	210	1.462	0.265	0.763	0.434	0.569	12.10
(2)	SD		0.007	0.002	0.005			
C₁HcgCU50c	average	203	1.951	0.245	1.006	0.700	0.696	14.36
(2)	SD		0.008	0.002	0.008			

Table F-13 Analysis for HSC in creep tests step-wisely loaded at an age of 28 days (see Table E-20)

Test	Statistic	t-t ₀	$\varepsilon_c(t, t_0)$	$\varepsilon_{sh}(t)$	$\varepsilon_{ie}(t_0)$	$\varepsilon_{cr}(t, t_0)$	\$ 28	$C(t, t_0)$
No.	item	days	(10 ⁻³)	(10 ⁻³)	(10 ⁻³)	(10 ⁻³)		10 ⁻⁶
C _n H _{cg} CU12.5 _v -1	average	12	0.305	0.034	0.199	0.072	0.274	7.59
(2)	SD		0.004	0.005	0.006			
C _n H _{cg} CU12.5 _v -2	average	11	0.639	0.055	0.209	0.070	0.267	7.38
(2)	SD		0.004	0.007	0.011			
C _n H _{cg} CU12.5 _v -3	average	11	0.992	0.073	0.198	0.082	0.313	8.65
(2)	SD		0.005	0.006	0.006			
C _n H _{cg} CU12.5 _v -4	average	11	1.342	0.084	0.196	0.070	0.267	7.38
(2)	SD		0.008	0.010	0.005			
C _n H _{cg} CU25 _v -1	average	23	0.653	0.054	0.428	0.171	0.326	9.02
(2)	SD		0.006	0.006	0.007			
C _n H _{cg} CU25 _v -2	average	22	1.302	0.085	0.344	0.220	0.419	11.60
(2)	SD		0.065	0.010	0.041			
C _n H _{cg} CU50 _v	average	45	1.487	0.087	0.843	0.557	.531	14.69
(2)	SD		0.066	0.008	0.038			

Table F-14 Analysis for HSC in creep recovery tests with step-wise unloading (see Table E-21)

Test	Statistic	t-t ₀	$\varepsilon_c(t, t_0)$	$\varepsilon_{sh}(t)$	$\varepsilon_{c\sigma}(t_0)$	$\varepsilon_{irec}(t_0)$	$\varepsilon_{rec}(t)$	Crec
No.	item	days	(10 ⁻³)	(10 ⁻³)	(10 ⁻³)	(10 ⁻³)	(10 ⁻³)	10 ⁻⁶
C _n H _{cg} CU12.5 _v -1	average	12	1.181	0.097	1.265	-0.146	-0.035	3.691
(2)	SD		0.004		0.002	0.004		
C _n H _{og} CU12.5 _v -2	average	11	0.993	0.104	1.082	-0.181	-0.012	1.265
(2)	SD		0.002		0.003	0.003		
C _n H _{cg} CU12.5 _v -3	average	11	0.775	0.113	0.888	-0.207	-0.019	2.004
(2)	SD		0.004		0.004	0.002		
C _n H _{cg} CU12.5 _v -4	average	11	0.465	0.123	0.662	-0.261	-0.059	6.222
(2)	SD		0.006		0.005	0.003		
C _n H _{eg} CU25 _v -1	average	23	0.938	0.104	1.218	-0.324	-0.060	3.164
(2)	SD		0.020		0.064	0.043		
C _n H _{og} CU25 _v -2	average	22	0.525	0.123	0.834	-0.387	-0.045	2.373
(2)	SD		0.025		0.020	0.011		
C _n H _{cg} CU50 _v	average	45	0.534	0.123	1.433	-0.856	-0.166	4.376
(2)	SD		0.033		0.034	0.005		

Table F-15 Analysis for HSC with crushed gravel in compressive creep tests at a loading age of 10 hours (see Tabel E-22)

Test No.	Statistic item	t-t₀ days	$\varepsilon_c(t, t_0)$ (10^{-3})	$\varepsilon_{sh}(t)$ (10 ⁻³)	$\varepsilon_{ie}(t_0)$ (10^{-3})	$\varepsilon_{cr}(t, t_0)$ (10^{-3})	фю	\$ 28	C(t, t ₀) 10 ⁻⁶
C _e 10H _{cg} CU30 _c	average	90	0.953	0.520	0.151	0.282	1.868	3.987	111.0
(2)	SD		0.013		0.003				
C _e 10H _{cg} CU50 _c	average	90	1.360	0.520	0.457	0.383	0.838	3.251	90.54
(2)	SD		0.010		0.003				
C _e 10H _{cg} CU70 _c	average	90	1.425	0.520	0.560	0.345	0.616	2.092	58.3
(2)	SD		0.020		0.005				

Table F-16 Analysis for HSC with granite in compressive creep tests at a loading age of 10 hours (see Table E-23)

Test	Statistic	t-t ₀	$\varepsilon_c(t, t_0)$	$\varepsilon_{sh}(t)$	$\varepsilon_{ie}(t_0)$	$\varepsilon_{cr}(t, t_0)$	<i>ф</i> 10	φ 28	C(t, t ₀)
No.	item	days	(10 ⁻³)	(10 ⁻³)	(10 ⁻³)	(10 ⁻³)			10 ⁻⁶
C _e 10H _{gr} CU30 _c	average	90	0.900	0.550	0.150	0.200	1.333	2.500	70.7
(2)	SD		0.010		0.005				
C _e 10H _{gr} CU50 _c	average	90	1.253	0.550	0.313	0.390	1.246	2.930	82.8
(2)	SD		0.003		0.000				
C _e 10H _{gr} CU70 _c	average	90	1.545	0.550	0.408	0.587	1.438	3.152	89.1
(2)	SD		0.010		0.015				

Table F-17 Analysis for HSC with limestone in compressive creep tests at a loading age of 10 hours (see Table E-24)

Test	Statistic	t-t ₀	$\varepsilon_c(t, t_0)$	$\varepsilon_{sh}(t)$	$\varepsilon_{ie}(t_0)$	$\varepsilon_{cr}(t, t_0)$	φ _t α	∲ 28	$C(t, t_0)$
No.	item	days	(10 ⁻³)	(10 ⁻³)	(10 ⁻³)	(10 ⁻³)			10 ⁻⁶
C _e 10H _{is} CU30 _c	average	90	0.695	0.385	0.115	0.195	1.696	4.567	112.1
(2)	SD		0.010		0.000				
C _e 10H _{is} CU50 _c	average	90	0.920	0.385	0.179	0.356	1.989	5.000	122.8
(2)	SD		0.010		0.003				
Ce10HisCU70c	average	90	1.120	0.385	0.288	0.447	1.552	4.487	110.1
(2)	SD		0.015		0.028				

Table F-18 Analysis for HSC with crushed gravel in compressive creep tests at a loading age of 16 hours (see Table E-25)

Test	Statistic	t-to	$\varepsilon_{c}(t, t_{0})$	$\varepsilon_{sh}(t)$	$\varepsilon_{ie}(t_0)$	$\varepsilon_{cr}(t, t_0)$	<i>ф</i> 10	\$ 28	C(t, t ₀)
No.	item	days	(10 ⁻³)	(10 ⁻³)	(10 ⁻³)	(10 ⁻³)			10 ⁻⁶
C _e 16H _{cg} CU30 _c	average	90	1.628	0.410	0.490	0.728	1.486	1.944	52.5
(2)	SD		0.003	0.000	0.008				
C _e 16H _{cg} CU50 _c	average	90	2.313	0.410	0.843	1.060	1.257	1.698	45.9
(2)	SD		0.013	0.000	0.015				
C _e 16H _{cg} CU70 _c	average	90	3.158	0.410	1.297	1.451	1.118	1.573	42.4
(2)	SD		0.043	0.000	0.003				

Table F-19 Analysis for HSC with granite in compressive creep tests at a loading age of 16 hours (see Table E-26)

Test	Statistic	t-t ₀	$\varepsilon_{\rm c}(t, t_0)$	$\varepsilon_{sh}(t)$	$\varepsilon_{ie}(t_0)$	$\varepsilon_{cr}(t, t_0)$	φ _t ο	<i>ф</i> 28	$C(t, t_0)$
No.	item	days	(10 ⁻³)	(10 ⁻³)	(10 ⁻³)	(10 ⁻³)			10 ⁻⁶
C _e 16H _{gr} CU30 _c	average	90	1.508	0.390	0.484	0.634	1.310	1.649	45.9
(2)	SD		0.003	0.005	0.010				
C _e 16H _{gr} CU50 _c	average	90	2.308	0.390	0.810	1.108	1.368	1.729	48.2
(2)	SD		0.008	0.005	0.010				
C _e 16H _{gr} CU70 _c	average	90	3.388	0.390	1.225	1.773	1.447	1.977	55.1
(2)	SD		0.093	0.005	0.050				

Table F-20 Analysis for HSC with limestone in compressive creep tests at a loading age of 16 hours (see Table E-27)

Test	Statistic	t-t ₀	$\varepsilon_{c}(t, t_{0})$	$\varepsilon_{sh}(t)$	$\varepsilon_{ie}(t_0)$	$\varepsilon_{cr}(t, t_0)$	фю	<i>ф</i> 28	$C(t, t_0)$
No.	item	days	(10 ⁻³)	(10 ⁻³)	(10 ⁻³)	(10 ⁻³)			10 ⁻⁶
C _e 16H _{is} CU30 _c	average	90	1.215	0.335	0.355	0.525	1.479	1.754	40.1
(2)	SD		0.035	0.005	0.005				
C _e 16H _{is} CU50 _c	average	90	2.000	0.335	0.609	1.056	1.734	2.117	48.3
(2)	SD		0.075	0.005	0.010				
C _e 16H _{is} CU70 _c	average	90	2.900	0.335	0.933	1.632	1.749	2.337	53.4
(2)	SD		0.035	0.005	0.008				

Table F-21 Analysis for HSC with crushed gravel in creep recovery tests at a loading age of 10 hours and a unloading age of 90 days (see Table E-28)

Test No.	Statistic item	$\varepsilon_c(t)$ (10^{-3})	$\varepsilon_c(t_0)$ (10 ⁻³)	$\varepsilon_{sh}(t)$ (10^{-3})	$\varepsilon_{irec}(t_0)$ (10^{-3})	ε _{rec} (t) (10 ⁻³)	Ered Ecr	С _{гес} (10 ⁻⁶)
C _e 10H _{cg} CU30 _c	average	0.933	0.953	0.579	-0.053	-0.026	0.092	10.24
(2)	SD	0.013	0.013	0.001	0.003			
C _e 10H _{cg} CU50 _c	average	1.263	1.360	0.579	-0.110	-0.046	0.120	10.88
(2)	SD	0.003	0.010	0.001	0.010			
C _e 10H _{cg} CU70 _c	average	1.268	1,425	0.579	-0.160	-0.056	0.162	9.46
(2)	SD	0.013	0.020	0.001	0.005			

Table F-22 Analysis for HSC with granite in creep recovery tests at a loading age of 10 hours and a unloading age of 90 days (see Table E-29)

Test No.	Statistic item	$\varepsilon_c(t)$ (10 ⁻³)	$\varepsilon_c(t_0)$ (10 ⁻³)	$\varepsilon_{sh}(t)$ (10^{-3})	$\varepsilon_{irec}(t_0)$ (10 ⁻³)	$\varepsilon_{rec}(t)$ (10 ⁻³)	Erecl Ecr	C _{rec} (10 ⁻⁸)
C _e 10H _{gr} CU30 _c	average	0.853	0.900	0.596	-0.070	-0.023	0.115	8.13
(2)	SD	0.008	0.010	0.001	0.005			
C _e 10H _{gr} CU50 _c	average	1.135	1.253	0.596	-0.130	-0.034	0.087	7.22
(2)	SD	0.005	0.003	0.001	0.000			
C _e 10H _{gr} CU70 _c	average	1.353	1.545	0.596	-0.188	-0.050	0.085	7.59
(2)	SD	0.023	0.010	0.001	0.003			

Table F-23 Analysis for HSC with limestone in creep recovery tests at a loading age of 10 hours and a unloading age of 90 days (see Table E-30)

Test	Statistic	$\varepsilon_c(t)$	$\varepsilon_c(t_0)$	$\varepsilon_{sh}(t)$	$\varepsilon_{irec}(t_0)$	$\varepsilon_{rec}(t)$	Erect Ecr	C _{rec}
No.	item	(10 ⁻³)	(10 ⁻³)	(10 ⁻³)	(10 ⁻³)	(10 ⁻³)		(10 ⁻⁶)
C _e 10H _{is} CU30 _c	average	0.678	0.695	0.423	-0.030	-0.025	0.128	14.37
(2)	SD	0.008	0.010	0.001	0.000			
C _e 10H _{Is} CU50 _c	average	0.868	0.920	0.423	-0.058	-0.032	0.090	11.03
(2)	SD	0.008	0.010	0.001	0.003			
C _e 10H _{Is} CU70 _c	average	1.033	1.120	0.423	-0.085	-0.040	0.090	9.85
(2)	SD	0.008	0.015	0.001	0.005			

Table F-24 Analysis for HSC with crushed gravel in creep recovery tests at a loading age of 16 hours and a unloading age of 90 days (see Table E-31)

Test	Statistic	$\varepsilon_c(t)$	$\varepsilon_c(t_0)$	$\varepsilon_{sh}(t)$	$\varepsilon_{irec}(t_0)$	$\varepsilon_{rec}(t)$	€red €cr	C _{rec}
No.	item	(10 ⁻³)	(10 ⁻³)	(10 ⁻³)	(10 ⁻³)	(10 ⁻³)		(10 ⁻⁶)
C _e 16H _{cg} CU30 _c	average	1.155	1.628	0.468	-0.413	-0.158	0.217	11.39
(2)	SD	0.010	0.003	0.001	0.008			
C _e 16H _{cg} CU50 _c	average	1.600	2.313	0.468	-0.533	-0.238	0.225	10.29
. (2)	SD	0.005	0.013	0.001	0.013			
C _e 16H _{cg} CU70 _c	average	2.158	3.158	0.468	-0.753	-0.305	0.210	9.42
(2)	SD	0.083	0.043	0.001	0.023			

Table F-25 Analysis for HSC with granite in creep recovery tests at a loading age of 16 hours and a unloading age of 90 days (see Table E-32)

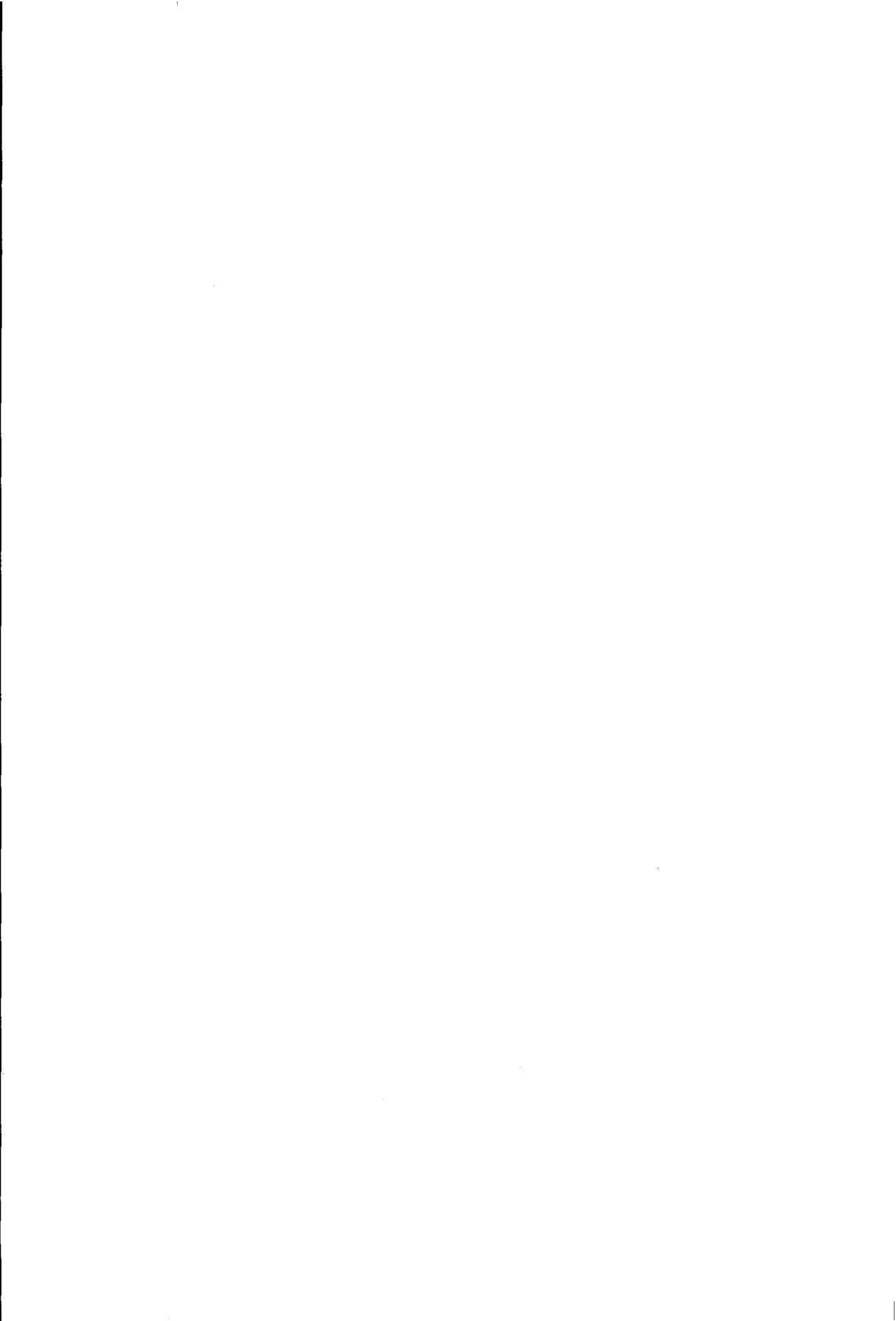
Test	Statistic	$\varepsilon_c(t)$	$\varepsilon_c(t_0)$	$\varepsilon_{sh}(t)$	$\varepsilon_{irec}(t_0)$	$\varepsilon_{rec}(t)$	Erecl Ecr	Crec
No.	item	(10 ⁻³)	(10 ⁻³)	(10 ⁻³)	(10 ⁻³)	(10 ⁻³)		(10 ⁻⁶)
C _e 16H _{gr} CU30 _c	average	1.058	1.508	0.450	-0.353	-0.157	0.248	11.38
(2)	SD	0.013	0.003	0.001	0.008			
C _e 16H _{gr} CU50 _c	average	1.583	2.308	0.450	-0.528	-0.257	0.232	11.17
(2)	SD	0.013	0.008	0.001	0.003			
C _e 16H _{gr} CU70 _c	average	2.273	3.388	0.450	-0.815	-0.360	0.203	11.18
(2)	SD	0.048	0.005	0.001	0.030			

Table F-26 Analysis for HSC with limestone in creep recovery tests at a loading age of 16 hours and a unloading age of 90 days (see Table E-33)

Test	Statistic	$\varepsilon_c(t)$	$\varepsilon_c(t_0)$	$\varepsilon_{sh}(t)$	$\varepsilon_{irec}(t_0)$	$\varepsilon_{rec}(t)$	Erec Ecr	Crec
No.	item	(10 ⁻³)	(10 ⁻³)	(10 ⁻³)	(10 ⁻³)	(10 ⁻³)		(10 ⁻⁶)
C _e 16H _{is} CU30 _c	average	0.785	1.215	0.381	-0.233	-0.243	0.463	18.54
(2)	SD	0.090	0.035	0.001	0.053			
C _e 16H _{is} CU50 _c	average	1.355	2.000	0.381	-0.488	-0.203	0.192	9.29
(2)	SD	0.075	0.075	0.001	0.008			
C _e 16H _{is} CU70 _c	average	1.975	2.900	0.381	-0.683	-0.288	0.176	9.41
(2)	SD	0.030	0.035	0.001	0.003			

Table F-27 Results for HSC and NSC in centric tensile softening tests (see Table E-16)

Statistical	dεldt	Otmex	Gr	E _t	lch
item	10 ⁻⁶ s ⁻¹	(N/mm²)	N/m	10 ³ N/mm ²	mm
		RH₀gTUS	FL25 (3)		
average	2.30	4.77	188	48.00	397
SD		0.09	20.1	2.117	
		RH _{cg} TUS	FL2.5 (4)		
average	0.23	4.52	173	47.57	403
SD		0.33	20.8	1.043	
		RN₀gTUS	SFL25 (4)		
average	2.30	2.18	107	29.09	665
SD		0.12	12.1	1.157	
		RN₀gTUS	FL2.5 (4)		
average	0.23	2.12	102	31.15	707
SD		0.31	15.0	2.821	



Samenvatting

Het tijdsafhankelijke gedrag van beton wordt zowel door interne als externe belastingen beïnvloed. Beton is een verouderingsgevoelig materiaal, dat wil zeggen dat zijn eigenschappen zich in de tijd ontwikkelen als gevolg van de doorlopende chemische reactie tussen cement en water (hydratatie), die wordt beïnvloed door temperatuur en relatieve vochtigheid. In vergelijking met andere belangrijke constructiematerialen, zoals staal en kunststoffen, vertoont beton een sterk verouderingseffect.

De tijdsafhankelijke eigenschappen van beton kunnen het constructiegedrag belangrijk beïnvloeden. In bepaalde opzichten zijn deze effecten ongewenst, terwijl ze in andere gevallen gunstig zijn. Aan de ene kant veroorzaakt een tijdsafhankelijke vervorming voorspanverliezen en een toename van vervormingen en doorbuigingen die de bruikbaarheid van een constructie verminderen. Daarnaast kan de reductie in sterkte het constructiedraagvermogen verminderen. Aan de andere kant kunnen tijdsafhankelijke vervormingen leiden tot een gunstige initiële spanningsverdeling die bewust door een opgelegde vervorming (bijvoorbeeld voorgebogen liggers) kan zijn geïntroduceerd. Een tijdsafhankelijke vervorming kan ook ongewenste spanningen in het beton beperken die veroorzaakt zijn door onbedoelde opgelegde vervormingen zoals zettingen van steunpunten, krimp en temperatuurgradiënten.

De laatste jaren heeft niet alleen de ontwikkeling en toepassing van hoge sterkte beton (HSB) een grote vlucht genomen, maar ook in onderzoek wordt meer en meer aandacht besteed aan de verschillen in fundamentele eigenschappen tussen HSB en normale sterkte beton (NSB). HSB wordt gekenmerkt door uitstekende mechanische eigenschappen zoals een hoge druksterkte, een hogere elasticiteitsmodulus en een hogere dichtheid (betere duurzaamheid).

De materiaalstructuur van HSB verschilt aanzienlijk van die van NSB. HSB heeft een onregelmatiger en meer gesloten poriestructuur, en een gelijkmatiger porieverdeling. Dit is, onder andere, een gevolg van de toevoeging van silica fume. De puzzolane reactie van dit materiaal leidt tot een betere hechting tussen toeslag en cementmatrix, tewijl de microdeeltjes ook als vulmiddel fungeren. Het overgangsgebied tussen de matrix en de toeslag, dat gewoonlijk grovere poriën en meer microscheuren bevat, wordt zeer dicht als gevolg van de aanwezigheid van silica fume. In HSB worden reeds vóór het belasten minder barsten en scheuren gevonden, wellicht als gevolg van de moeizame vochtuitwisseling tussen de kern en de uitwendige van het beton, hetgeen resulteert in minder drogingskrimp. Daarnaast draagt de sterkere hechting aan het grensvlak ook bij aan de vermindering van de grootte van en het aantal microscheuren.

Het hoofddoel van dit onderzoeksprogramma was om de kennis van het tijdsafhankelijke gedrag van HSB in het algemeen, te verbeteren. Op grond van een experimentele analyse werd meer inzicht verkregen over verschillende aspecten van de tijdsafhankelijke eigenschappen van HSB. De resultaten werden gebruikt om verbeterde formuleringen te ontwikkelen voor het tijdsafhankelijke gedrag van HSB.

Na het inleidende hoofdstuk van dit proefschrift wordt in Hoofdstuk 2 een algemene classificatie gegeven van het tijdsafhankelijke gedrag van beton. In dit hoofdstuk worden drie belangrijke aspecten van dit tijdsafhankelijke gedrag behandeld: de externe invloeden, de vervormingen van beton en de verouderingseffecten. Met betrekking tot de externe invloeden worden statische en kruipbelastingen beschouwd. De totale vervormingen onder externe belasting worden onderscheiden in tijdsafhankelijke (elastische) vervormingen, kruip en belastingonafhankelijke vervorming (krimp). Daar beton een verouderingsgevoelig materiaal is, moeten de bijdragen van het verouderingseffect aan de ontwikkeling van de betoneigenschappen, in het bijzonder aan sterkte en E-modulus, in beschouwing worden genomen wanneer het tijdsafhankelijke gedrag van beton wordt behandeld.

De studie van het tijdsafhankelijke gedrag van HSB dat in dit proefschrift wordt gepresenteerd omvat vier met elkaar verbonden fasen:

- literatuuronderzoek
- experimenteel onderzoeksprogramma
- theoretische modellering
- evaluatie

Een literatuuronderzoek naar het tijdsafhankelijke gedrag van beton onderworpen aan verschillende vervormingssnelheden en vervormingsgradiënten zowel onder druk- als trekbelasting wordt in Hoofdstuk 3 gepresenteerd. Het bereik van de vervormingssnelheid wordt meestal beperkt

tot het gebied tussen de zogenoemde statische en de kruipbelasting. Verschillende mechanische eigenschappen (zoals sterkte, vervorming, E-modulus, Poisson-getal, kritieke spanning, langeduur sterkte) worden als functie van de vervormingssnelheid uitvoerig besproken. Daarnaast wordt de invloed van de vervormingsgradiënt op het gedrag van beton besproken, waarbij de spanningsverdeling, de maximum spanning en de maximale vervorming van de uiterste vezel helangriike onderwerpen ziin. Het basismechanisme dat de gevoeligheid vervormingssnelheid veroorzaakt, is onderzocht. Verschillende mathematische modellen die ontwikkeld zijn om de spanning-rek relatie bij buiging te beoordelen, worden gepresenteerd. De meeste van de hier besproken artikelen hebben echter betrekking op normale sterkte beton, terwiil er slechts zelden artikelen over hoge sterkte beton op de literatuurlijst verschijnen. Omdat de materiaalstructuur van hoge sterkte beton afwijkt van die van normale sterkte beton worden ook enkele opmerkingen gemaakt met betrekking tot de gevoeligheid voor de vervormingssnelheid.

Op grond van het in Hoofdstuk 3 behandelde literatuuronderzoek kan worden geconcludeerd dat de materiaalstructuur een overheersende rol speelt ten aanzien van de gevoeligheid voor de vervormingssnelheid. De aantallen en grootten van de poriën, barsten (holten) en microscheuren in het beton bepalen de mate waarin de belastingssnelheid of de vervormingssnelheid het mechanische gedrag kan beïnvloeden. Het is duidelijk dat alle factoren die invloed hebben op de materiaalstructuur van beton (zoals de ouderdom van beton op het moment van beproeyen, de nabehandelingscondities, etc.) ook de gevoeligheid voor de vervormingssnelheid beïnvloeden. Tot nu toe is het een algemeen aanvaard uitgangspunt dat het tijdsafhankelijke gedrag van beton kan worden gerelateerd aan de aanwezigheid van vrij water in het beton. In de praktijk is vastgesteld dat de meeste betonconstructies vanaf een bepaalde diepte waterverzadigd blijven gedurende hun gebruiksduur. Uit de literatuurstudie wordt duidelijk dat een goed inzicht (begrip) van het fenomeen gevoeligheid van beton voor de vervormingssnelheid van belang is voor constructeurs. Wat betreft de materiaalstructuur heeft hoge sterkte beton in vergelijking met normale sterkte beton zijn eigen typische kenmerken. Hoge sterkte beton bezit een veel dichtere inwendige structuur, kleinere porieafmetingen, een gelijkmatiger porieverdeling en minder microscheuren zowel vóór als tijdens belasten. Het is daarom van essentieel belang om de mechanische eigenschappen van beton en het constructief gedrag van hoge sterkte beton in het bijzonder te begrijpen in relatie tot het probleem van de gevoeligheid voor de vervormingssnelheid voordat dit materiaal in de praktijk veilig kan worden toegepast.

Voor het tijdsafhankelijke gedrag van beton vormt kruip een van de belangrijkste aspecten. Kruip van beton is een complex fenomeen dat nog niet volledig kan worden verklaard waarin nog geen volledig inzicht bestaat. Voor het gedrag van betonconstructies heeft kruip een aanzienlijke invloed die zowel een toename van de doorbuiging veroorzaakt als de spanningsverdeling en voorspanverliezen beinvloedt. In hoofdstuk 4 wordt een literatuuronderzoek naar het kruipgedrag van beton onder drukbelasting beschreven. De factoren die kruip beïnvloeden, worden beknopt behandeld. De laatste kennis van het kruipmechanisme en verschillende uitvoerbare voorspellende modellen worden ook behandeld. In een latere fase van dit literatuuronderzoek wordt ook aandacht

besteed aan kruip van jong beton. Het onderzoek is uitgevoerd voor zowel normale als hoge sterkte beton, waarbij de nadruk ligt op hoge sterkte beton.

Het experimentele programma is onderverdeeld in vier series. Ieder van deze vier series heeft betrekking op verschillende parameters die relevant zijn voor het tijdsafhankelijke gedrag van hoge sterkte beton. In hoofdstuk 5 worden zowel de omvang van dit experimentele onderzoeksprogramma als de materialen, de uitvoering van de proeven, metingen, testprocedures uitvoerig beschreven. De experimentele resultaten worden gegeneraliseerd en uitgewerkt voor verdere analyse.

Het tijdsafhankeleijke gedrag van zowel HSB als NSB worden eerst bestudeerd door beton te belasten met verschillende vervormingssnelheden en vervormingsgradiënten. De in deze experimenten toegepaste vervormingssnelheden van belasten tot bezwijken variëren van enkele minuten tot enkele dagen. Zowel druk- als trekproeven zijn uitgevoerd, waarin naast centrische belasting ook excentrische belasting is beschouwd in combinatie met verschillende vervormingssnelheden.

Het tijdsafhankelijke gedrag van HSB was verder onderzocht door beton te onderwerpen aan een permanente constante spanning. In deze proeven waren de het spanningsniveau en de ouderdom bij het aanbrengen van de belasting de belangrijkste parameters; de belasting werd aangebracht zowel bij een ouderdom van 28 dagen als op jongere leeftijd. Daarnaast werden verschillende soorten toeslagmateriaal in de mengsels gebruikt om hun invloed op het tijdsafhankelijke gedrag te bestuderen. Krimp en kruipherstel waren eveneens in het onderzoek betrokken.

Op grond van de proefresultaten is in Hoofdstuk 6 een uitgebreide experimentele analyse uitgevoerd naar de gevoeligheid van HSB voor de vervormingssnelheid, de analyse concentreert zich op de invloed van de vervormingssnelheid en de vervormingsgradiënt op de fundamentele mechanische eigenschappen van hoge sterkte beton en normale sterkte beton (ter vergelijking) zowel onder druk- als onder trekbelasting. Uit de experimentele analyse is geconcludeerd dat HSB een grotere gevoeligheid voor de vervormingssnelheid vertoont dan NSB. Onder drukbelasting bij verschillende vervormingssnelheden ondervindt hoge sterkte beton een sterkere reductie van de maximale spanning dan normale sterkte beton wanneer de vervormingssnelheid vermindert. Andere mechanische eigenscahppen van HSB vertonen, in verschillende mate, een gevoeligheid voor de vervormingssnelheid. Er werd ook vastgesteld dat de aanwezigheid van een vervormingsgradiënt de gevoeligheid voor de vervormingssnelheid zou kunnen verminderen, zowel onder druk- als trekbelasting. De experimentele analyse maakt duidelijk dat de gevoeligheid voor de vervormingssnelheid van HSB onder trekbelasting minder duidelijk is dan onder drukbelasting.

In Hoofdstuk 7 werd een uitvoerige experimentele analyse uitgevoerd betreffende krimp en kruip van beton dat op normale en jonge leeftijd werd belast. Met betrekking tot de verschillende parameters is de experimentele analyse onderverdeeld in vier delen. In het eerste deel wordt de ontwikkeling van de sterkte en de E-modulus, die belangrijk zijn voor het tijdsafhankelijke gedrag

van beton dat op jonge leeftijd is belast, besproken. Vanwege de duidelijke relatie tussen krimp en kruip, wordt de in de experimenten waargenomen krimp in het tweede deel behandeld. De invloed van het soort toeslagmateriaal en de ouderdom waarop het beton wordt blootgesteld aan drogingskrimp werd onderzocht. In het derde deel wordt kruip van beton dat zowel op jonge als op normale leeftijd werd belst, geanalyseerd. De invloeden van het spanningsniveau en het soort toeslagmateriaal op kruip worden besproken. In het laatste deel wordt kruipherstel beschouwd. In alle vier delen worden de proefresultaten vergeleken met de voorspellingen die berekend zijn uit verschillende bestaande formuleringen. De vergelijkingen vormen een basis voor de verdere ontwikkeling van geschikte voorspellende formuleringen voor krimp en kruip van hoge sterkte beton dat op normale en jonge leeftijden wordt belast.

In het modelleringsstadium worden één kwalitatief en twee mathematische modellen voorgesteld. In Hoofdstuk 6 wordt de gevoeligheid van beton voor de vervormingssnelheid gemodelleerd op grond van het Stefan Effect (bekend in de fysica). Met behulp van dit voorgestelde model worden de in de experimenten waargenomen fenomenen kwantitatief geïnterpreteerd.

Om het tijdsafhankelijke gedrag van hoge sterkte beton onder een excentrische belasting te kunnen simuleren, is in Hoofdstuk 6 een mathematisch model ontwikkeld dat gebaseerd is op het idee van de beschadigde drukzone (CDZ) van Markeset (1993). Op grond van deze kennis van het tijdsafhankelijke gedrag van HSB in centrische proeven zijn verschillende parameters in dit model gebruikt om de invloeden van vervormingssnelheden en vervormingsgradiënten op de spanningsverdelingen in de drukzone te simuleren.

In hoofdstuk 8 wordt een gemodificeerd krimp- en kruipmodel afgeleid dat is gebaseerd op het bekende MC90 model. Om de ontwikkeling van sterkte en E-modulus van hoge sterkte beton te voorspellen als functie van de tijd zijn formuleringen opgesteld. Uitdrukkingen worden gegeven om krimp en kruip te berekenen, of op jonge of op normale leeftijden. Onder de aanname van kruiplineariteit kan het principe van superpositie worden toegepast om zowel de kruipvervorming voor wisselende spanningen als het kruipherstel te berekenen. Niet-lineariteit wordt expliciet in rekening gebracht.

Ten slotte zijn evaluaties van de drie voorgestelde modellen uitgevoerd. De experimentele waarnemingen worden in hoofdstuk 6 verklaard op grond van het kwalitatieve model dat het mechanisme van de gevoeligheid voor de vervormingssnelheid van beton beschrijft. Bij een hogere vervormingssnelheid wordt voor HSB onder drukbelasting een hogere poriewaterdruk opgebouwd ten gevolge van de kleinere porie-afmeting. Deze hogere poriewaterdruk vormt de belangrijkste bijdrage aan de verhindering van de longitudinale vervorming. Met het Stefan Effect kan de vertraagde ontwikkeling van de longitudinale vervorming worden verklaard. Tijdens de nabehandelingsperiode kan bovendien minder vrij water verdampen vanwege de moeilijkheid van de verplaatsing van vrij water door het beton. Bijgevolg is er meer vrij water beschikbaar om poriewaterdruk te doen ontstaan, waardoor het Stefan Effect tijdens belasten wordt vergroot. Bij een

lagere vervormingssnelheid zal het in de poriën onder spanning staande water voldoende tijd krijgen om door de kanalen (microscheuren en barsten) naar de onbelaste gebieden te stromen. Hierdoor wordt een relaxatie van de poriewaterdruk veroorzaakt; Bovendien wordt de door het Stefan Effect veroorzaakte tegenovergestelde kracht ook verminderd ten gevolge van een lagere vervormingssnelheid. Het beton neigt er daarom toe om sterktewaarden van de vaste fase aan te nemen. Hierbij wordt opgemerkt dat het Stefan-effect voor drukbelasting verschilt van dat voor trekbelasting. Onder trekbelasting is het effect van de vochtspanning minder dan onder drukbelasting.

Na de evaluaties is met betrekking tot de verificatie van het gemodificeerde CDZ model geconcludeerd dat door het introduceren van een uitbreiding om de gevoeligheid voor de vervormingssnelheid in rekening te brengen, het CDZ model kan worden toegepast om belastingvervorming relaties te simuleren voor excentrisch belaste prisma's bij verschillende opgelegde vervormingssnelheden en vervormingsgradiënten. De vergelijking tussen de resultaten van de numerieke berekening en de experimentele resultaten toont aan dat voor een goede voorspelling van de maximale belasting een vervormingssnelheid en e/d afhankelijke spanning-vervorming relatie noodzakelijk is. Wanneer een enkele spanning-vervorming relatie, die gebaseerd op centrische belastingproeven, onafhankelijk van de vervormingssnelheid, wordt toegepast - zoals in vele voorschriften - zullen de resultaten nooit erg nauwkeurig zijn.

De in Hoofdstuk 8 uitgevoerde evaluaties van MdMC90 tonen aan dat met een uitbreiding van de oorspronkelijke formulering van CEB-FIP Model Code 1990, waarbij uitdrukkingen voor kruip volgens Müller en Küttner (1996) in rekening worden gebracht, een uniforme formulering voor het voorspellen van het tijdsafhankelijke gedrag van HSB kan worden verkregen. Alle kenmerken van het originele model blijven aanwezig, dat wil zeggen dat het gemodificeerde MC90 nog steeds kan worden toegepast voor het voorspellen van het tijdsafhankelijke vervorming van NSB met dezelfde nauwkeurigheid. Daarnaast kan het worden gebruikt voor het voorspellen van krimp en kruip van NSB en HSB op jonge of normale leeftijden.

Een belangrijk punt van deze verificatie van MdMC90 is dat de onlangs door Müller en Küttner (1996) voorgestelde uitbreiding van MC90 ongeveer hetzelfde inhoudt als MdMC90 voor zover het kruip van HSB betreft dat op een leeftijd van 28 dagen wordt belast. Vanuit dit gezichtspunt is de verificatie van MdMC90 voor de kruip van HSB onder verschillende belastinggeschiedenissen (loading histories) ook geldig voor de onlangs voorgestelde uitbreiding van MC90. De belangrijkste aspecten van MdMC90 hebben echter betrekking op de mogelijkheid om de krimp en kruip van HSB op jonge leeftijden te voorspellen. Dit betekent ook dat MdMC90, zoals hier ontwikkeld, kan worden beschouwd als een verdere uitbreiding van de door Müller en Küttner (1996) voorgestelde gemodificeerde MC90 formulering.

Curriculum Vitae

Ningxu Han was born in Yinchuan, Ningxia, P. R. China, on June 25, 1960. He received the B.Sc. degree in structural engineering from Tongji University, Shanghai, P. R. China in February 1983. From February 1983 to February 1985 he was a structural engineer in Ningxia Architectural Design Institute, and was involved in the structural design and detailing of various types of projects such as office building, high-rise building. hospital, industrial building, theatre, school, etc. From 1985 to 1989 he became a lecturer and worked in the Department of Civil Engineering of Ningxia Institute of Technology. During this period, in addition to holding several lectures on reinforced concrete structure and prestressed concrete structure, structural safety, he was also engaged in research on the behaviour of reinforced concrete high-rise building in the seismic area. From 1989 to 1992, he was a researcher associated in Stevin Laboratory, Faculty of Civil Engineering, Delft University of Technology, where he was involved in the experimental program on the optimization of the mix proportion of high strength concrete and the effect of strain rate on the mechanical behaviour of high strength concrete. From April 1992 to April 1996, he became a Ph. D candidate in Stevin Laboratory, Delft University of Technology, working on the subject of time-dependent behaviour of high strength concrete. Since May 1996, he works as a senior engineer on concrete technology in Technologie & Engineering by, Strukton Group.